ABSTRACT

THE INVOLVEMENT OF CAP-INDEPENDENT mRNA TRANSLATION IN CELL FATE DECISIONS

By J. Kaitlin Morrison

July 2014

Director: Brett D. Keiper

DEPARTMENT OF BIOCHEMISTRY AND MOLECULAR BIOLOGY

During cell stress many biochemical processes are shut down. For example, global mRNA translation initiation is inhibited due to the disruption of the cap-dependent mRNA recruitment mechanism. One specific example of stress, apoptosis, results in activated caspases cleaving the translation initiation factor eIF4G. This cleavage disrupts cap-dependent mRNA translation initiation by removing the cap-binding domain. However, a specific subset of mRNAs can still be recruited for protein synthesis in a cap-independent manner by the residual initiation machinery. This selective recruitment of stress and apoptosis-related mRNAs promotes stress response and further induction of apoptosis. Many of these mRNAs contain internal ribosome entry sites (IRESes) that promote their enhanced translation during these conditions. Still other mRNAs have little dependence on the cap recognition mechanism. The expression of the encoded proteins, both anti- and pro-apoptotic, promote an initial period of attempted cell survival, then commitment to cell death when damage is extensive. This switch in mode of translation initiation and how it allows for selective mRNA translation is not well understood.

This study focuses on the utilization of cap-independent protein synthesis in the nematode worm, *C. elegans.* Due to their relative genetic simplicity, while maintaining molecular pathways found in higher organisms, and semi transparency that permits direct observation of cell fate decisions, *C. elegans* are the fitting *in vivo* model in which to study changes in translational regulation and how they affect cell fate. In this study we address the translational regulation of the stress and apoptosis-related mRNAs in *C. elegans: hsp-3* and *hsp-4* (BiP), *hif-1* (Hif-1), *cep-1* (p53), c*ed-9* (Bcl-2) and *ced-4* (Apaf-1) (mammalian homologues of *C. elegans* mRNAs are in parentheses). Altered translational efficiency of these messages was observed upon depletion of cap-dependent translation and induction of apoptosis within the *C. elegans* gonad. Our findings suggest a physiological link between the cap-independent mechanism and the enhanced translation of *hsp-3* and *ced-9.* This increase in the efficiency of translation may be integral to the stress response during the induction of physiological apoptosis. Further organism wide RNA-seq studies have begun to identify the entire population of mRNAs that rely highly on cap-dependent and independent translation. Development of this methodology, for detecting changes in translational efficiency on a global level, enables future follow-up studies to confirm additional mRNAs whose translation results in changes in cell fate decisions. Additionally, we carefully and specifically characterized *C. elegans ced-4* mRNA, the Apaf-1 homologue, and observed that its structure and mode of translation initiation differed from its mammalian homologue. *ced-4* mRNA translation illustrates one example of how selective translation in germ cells may differ from that observed in cultured mammalian cells responding to toxic treatments such as chemotherapy agents and hypoxia.

Networks of translational regulation are particularly important during germ cell development. The silencing of transcription, associated with chromosome condensation during meiosis, results in protein expression patterns that are dependent translational regulation. Genetic analysis shows that loss of key translational regulators leads to the onset of germ cell tumors within the *C. elegans* gonad. Cell growth and mitotic mRNAs typically rely highly on cap-dependent translation initiation in mammalian cell culture. Thus, we predicted that knockdown of cap-dependent translation would decrease expression of growth and mitotic proteins and result in a reversion of tumor phenotype. However, germ cell tumor progression was not grossly affected by knockdown of cap-associated eIF4G. The inability to revert this cell fate is most likely due to other regulators of translation at work in the germ line. Reversion of the tumor phenotype requires knockdown of multiple regulators of translation. Overall, our results indicate an important balance between cap-dependent and -independent translation initiation during stress and the affect of this balance on germ cell fate decisions.

THE INVOLVEMENT OF CAP-INDEPENDENT mRNA TRANSLATION IN CELL FATE DECISIONS

A DISSERTATION

Presented To

The Faculty of the Department of Biochemistry and Molecular Biology

East Carolina University

In Partial Fulfillment

Of the Requirements for the Degree

Doctor of Philosophy

by

J. Kaitlin Morrison

July 25, 2014

THE INVOLVEMENT OF CAP-INDEPENDENT mRNA TRANSLATION IN CELL FATE DECISIONS

by

J. Kaitlin Morrison

APPROVED BY:

DIRECTOR OF DISSERTATION:_____Brett D. Keiper_____

Brett D. Keiper, PhD

COMMITTEE MEMBER:_____Brian M. Shewchuk_____

Brian M. Shewchuk, PhD

COMMITTEE MEMBER:_____Ronald S. Johnson_____

Ronald S. Johnson, PhD

COMMITTEE MEMBER:_____David Rudel_____

David Rudel, PhD

CHAIR OF THE DEPARTMENT OF BIOCHEMISTRY AND MOLECULAR BIOLOGY:

_____Phillip H. Pekala_____

Phillip H. Pekala, PhD

DEAN OF THE GRADUATE SCHOOL:_____Paul J. Gemperline_____

Paul J. Gemperline, PhD

Dedication:

To my amazing parents for all their support over the last five years.

ACKNOWLDEGEMENTS

I would like to thank my family for all their love and continuous support over the last five years. I would not have even made it through comprehensive exams without my mom coming to Greenville to literally prevent my very old house from falling down on top of me. I would like to thank my father for his continued inspiration, perspective, high expectations for the scientific process and funny anecdotes. I would also like to thank my numerous friends for their continued support during graduate school. Linzy helped me to survive our first two years of graduate school with crazy late night study sessions with study breaks that always involved random discussions such as the best way to outrun an alligator. I would like to thank Beth, Reiko and Iñigo for their numerous emails, Skype dates, advice, memorable adventures and unwavering support. I would like to thank Liz, Adele, Christina and Julie for always brightening my day. Finally, I would like to thank LeAnna who is more like a sister than a best friend.

I would like to thank my numerous friends and colleagues at Brody School of Medicine during graduate school. Michelle always brought the fun to graduate school and is always willing to lend an ear to problems of science and life. Heather was always available for our pedicure therapy sessions. Nicole was the first person that I met at Brody and has been an amazing friend ever since. I would not have survived the last five years without martini Mondays and pottery Thursdays.

I would like to thank the entire Department of Biochemistry and Molecular Biology. I have appreciated the guidance and support over the last five years. I would like to thank Dr. Brett Keiper for accepting me into his lab and allowing me the freedom to explore this multi-faceted project. My time in his lab has developed me into the independent scientist

that I am today. I am indebted to all of the past and present members of the Keiper lab for their continued support. Thank you to Whitney who spent many of late nights trouble-shooting cloning with me and is always good for a laugh. Thank you to Melissa who came back to Greenville to teach me the proper way to inject worms. Mike, Fran and Vince have been incredibly supportive lab mates and good friends. Andrew and I have spent more time together over the last five years then I think either of us would like to admit working on our respective projects. I would have never completed the entirety of the work within this thesis without our Eminem inspired gradients or his careful instruction in all of the codes that Excel has to offer. Finally, I would like to thank my committee, Dr. Shewchuk, Dr. Johnson and Dr. Rudel, for their support and guidance during graduate school. Without the *hsp-3* paper that Dr. Shewchuk sent me several years ago my project would not contain one of its most interesting conclusions.

TABLE OF CONTENTS

LIST OF ABBREVIATIONS

4E-BP	eIF4E binding protein
act	actin
ANXA2	Annexin A2
Apaf-1	apoptotic protease activating factor
ATP	adenosine-5'-triphosphate
Bad	Bcl-2-associated death promoter
Bag	Bcl-2-associated athanogene
Bak	Bcl-2 homologous antagonist killer
Bax	Bcl-2-associated X protein
Bcl	B-cell lymphoma
BH	Bcl-2 homology domain
Bid	BH3 interacting-domain death agonist
BIM	BCL-2-like 11
BiP	binding immunoglobulin protein
Bmf	Bcl-2 modifying factor
BSA	bovine serum albumin
CARD	caspase recruitment domain
caspase	cysteine aspartate directed protease
CDK	cyclin-dependent kinase
cDNA	complementary DNA
CED	cell death defective
cep	C. elegans p53-like protein
CrPV	cricket paralysis virus
cRT-PCR	circularized reverse transcriptase-polymerase chain reaction
CSFV	classical swine fever virus
DAPI	4',6-diamidino-2-phenylindole
DAP5	death associated protein 5
DEPC	Diethylpyrocarbonate
DIC	differential interference contrast
DNA	deoxyribonucleic acid
DTC	distal tip cell
DTT	Dithiothreitol
EDTA	ethylenediaminetetraacetic acid
eIF	eukaryotic initiation factor
EMCV	encephalomyocarditis virus
ER	endoplasmic reticulum
Erk	extracellular signal-regulated kinase
EST	expressed sequence tag
Fas	fibroblast associated antigen
FBF	Fem-3 mRNA binding factor
fbxb	F-box B protein
fezf	FEZ family zinc finger protein
FBF	fibroblast growth factor

FPKM	fragments per kilobase of exon per million fragments
G1/G2	Gap 1/2
GDP	guanosine diphosphate
gfp	green fluorescent protein
GLD-1	Germ Line Development 1
GLP	abnormal germ line proliferation
gnrr	human Gonadotropin-Releasing hormone Receptor related
gpd/GAPDH	glyceraldehyde 3-phosphate dehydrogenase
GST	glutathione-S-transferase
GTP	guanosine triphosphate
HER2	human epidermal growth factor receptor 2
hif	hypoxia inducible factor
hlh	helix loop helix
hnRNP	heterogeneous ribonucleoprotein particle
HRV-2	human rhinovirus serotype 2
HSP	heat shock protein
IAP	inhibitor of apoptosis
IRES	internal ribosome entry site
IRS	insulin receptor substrate
ITAF	IRES trans-acting factor
JNK	c-JUN N-terminal kinase
LAG	Lin-12 and Glp-1 phenotype
M	Mitotic Phase
mesp	meiotic spindle
mex	Muscle Excess 3
Mnk-1	MAP kinase-interacting serine/threonie-protein kinase 1
MosSCI	mos1-mediated single copy insertion
mRNA	messenger ribonucleic acid
mRNP	messenger ribonucleoprotein
mTOR	mammalian target of rapamycin
NGM	nematode growth medium
Noxa	Phorbol-12-myristate-13-acetate-induced protein 1
NSAP1	heterogeneous nuclear ribonucleoprotein
ODC	ornithine decarboxylase
oma	oocyte maturation defective
p53	tumor suppressor p53
PABP	poly(A) binding protein
pal	posterior alae in males
PDK1	pyruvate dehydrogenase lipoamide kinase isozyme
PI3K	phosphatidylinositol 3-kinase
pie	pharynx and intestine in excess
PMSF	phenylmethylsulfonyl fluoride
PKB	protein kinase B
pos	posterior segregation
PTB	polypyrimidine tract binding protein
PTV-1	porcine teschovirus 1

Puma	p53-upregulated mediator of apoptosis
PVDF	polyvinylidene fluoride membrane
qPCR	quantitative reverse transcription polymerase chain reaction
RBP	RNA binding protein
Rheb	Ras homolog enriched in the brain
RNAi	RNA interference
RNA-seq	RNA Sequencing
RNasin	RNase Inhibitor
RNC	Ribonucleoside complex
RPA	RNase protection assay
rpl	Ribosomal Protein, large subunit
RT-PCR	reverse transcriptase-polymerase chain reaction
S	Synthesis Phase
SDS	sodium dodecyl sulfate
SL	splice leader
TAP	tobacco acid pyrophosphatase
TBE	Tris Borate EDTA
tRNA	transfer RNA
TSC	Tuberous sclerosis protein
TST	tris buffered saline with Tween
unc	Uncoordinated
unr	upstream of N-ras
UPR	unfolded protein response
UTP	uridine triphosphate
UTR	untranslated region
VEGF	vascular endothelial growth factor
XAF1	XIAP-associated factor 1
XIAP	X-linked inhibitor of apoptosis

LIST OF FIGURES

LIST OF TABLES

CHAPTER 1: LITERATURE REVIEW

The population of proteins present in a cell ultimately determines its identity; whether it is a neuron, an oocyte, a muscle or other cell type. Thus, regulation of protein synthesis is particularly important when determining cell fates. For example, deletion of two key translational regulators, Muscle Excess 3 (MEX-3) and defective in Germ Line Development 1 (GLD-1), in the *C. elegans* germ line results in formation of germ cell tumors that resemble human teratomas (Ciosk et al., 2006). In these tumors, germ cells transdifferentiate into somatic cell types such as muscle, neurons and gut (Ciosk et al., 2006). A broader understanding of translational control and how it leads to these cell fate decisions is needed to understand both normal development and aberrant fate decisions. In diseases such as cancer, with aberrant proliferation and dedifferentiation, and Parkinson's, with aberrant cellular suicide, understanding how translational regulation affects cell fate decisions is critical to developing targeted therapies.

Cell fate decisions are determined by translational control.

Growth and Proliferation. Translational control is particularly important to cell fate decisions during growth and proliferation. Four phases comprise the cell cycle: G1, S, G2 and M (Schafer, 1998). The first phase of the cell cycle, gap 1 (G1), is defined by cell growth prior to DNA replication in the synthesis (S) phase. During the second gap phase (G2), additional growth occurs before the cell division mitotic (M) phase. Progression through these phases is tightly regulated by cyclin association with serine/threonine cyclin-dependent kinases (CDKs) (Boonstra, 2003). The concentration of cyclins within cells is tightly regulated by the balance between protein synthesis and degradation, which is vital

for several of these progressions (Murray, 2004). Over-expression of translation initiation factors can thus result in over-expression of cyclins. For example, in NIH 3T3 cells over-expression of eukaryotic initiation factor 4E (eIF4E) results in enhanced translation of cyclin D1 mRNA and cell transformation (Rosenwald et al., 1993). eIF4E is one of the key translation initiation factors required for the cap-dependent mechanism of translation initiation. Switching the mode of translation initiation between cap-dependent and –independent translation is one of the key ways in which translation of mRNA populations can be regulated. Ironically, during the mitotic phase, protein synthesis is downregulated due to inhibition of the cap-dependent mechanism of protein translation. However, protein expression of cell cycle regulatory proteins, including ornithine decarboxylase (ODC), is essential for cell cycle progression (Fitzgerald and Semler, 2009). ODC is required for biosynthesis of polyamines, which are involved in mitotic spindle organization. To ensure cell cycle progression and completion of mitosis, ODC must be expressed during conditions that do not favor cap-dependent protein synthesis (Fitzgerald and Semler, 2009; Pyronnet et al., 2000). ODC relies on translational control via translation initiation to guarantee its high level of expression in the M phase. Although it is proposed to undergo mainly cap-dependent translation during the G1/S phase, it undergoes mainly cap-independent translation in the G2/M phase allowing for cell cycle progression (Fredlund et al., 1995; Pyronnet et al., 2000). This anecdote provides one example of the regulation of translation via the mechanism of translation initiation and how it affects the cell fate decision of proliferation.

Differentiation/Apoptosis. The fate decisions that accompany cell differentiation are also highly dependent on translational control. For example, during programmed cell death

(hereafter, apoptosis), the translation of specific subsets of proapoptotic proteins contributes to this cell fate differentiation decision. Knockdown of the cap-dependent translation initiation factor, eIF4G, in *C. elegans* leads to the induction of germ cell death (Contreras et al., 2008). This example, illustrates how the regulation of translation through the translation initiation mechanism results in a differentiation cell fate decision.

Cancer. One of the most frequently detected alterations in cancer is abnormal mRNA translation (Pandolfi, 2004). mRNAs with short unstructured 5' UTRs, such as actin, are translated readily under quiescent conditions (Graff et al., 2008; Lodish, 1974; Rhoads, 1993). However, long complex GC-rich 5' UTRs, which are difficult for ribosomes to scan, translate less efficiently (Graff et al., 2008). Enhanced cap-dependent translation initiation results in increased translation and thus expression of these highly structure and henceforth poorly translating mRNAs (Graff et al., 2008). The cap-dependent translation initiation mechanism requires mRNA cap recruitment through eIF4E binding (Sonenberg et al., 1978). Thus, Increasing the levels of eIF4E enhances the translation of mRNAs with complex 5' UTRs including cyclin D1, fibroblast growth factor (FGF) and matrix metalloprotease 9 (De Benedetti and Graff, 2004; Graff et al., 2008). Malignant proliferation in cancer may result, in part, from the increased translation of these highly structured, growth and cell cycle related mRNAs (De Benedetti and Graff, 2004). eIF4E is often overexpressed in breast, prostate, bladder, cervical and lung cancers and in head and neck carcinomas (Mamane et al., 2004). Additionally, overexpression of eIF4E is associated with an increased level of cancer recurrence and cancer-related death (Byrnes et al., 2006; Coleman et al., 2009; Flowers et al., 2009; Heikkinen et al., 2013; Holm et al., 2008; Li et al., 1998a; McClusky et al., 2005). Transgenic mice overexpressing eIF4E also have enhanced

tumor progression (Ruggero et al., 2004). A higher tumor grade, larger tumor size, negative estrogen receptor status, human epidermal growth factor receptor 2 (HER2) overexpression, positive p53 status, Cyclin E and Cyclin D1 expression are all correlated with tumors with higher eIF4E expression (Heikkinen et al., 2013). Thus, enhanced cap-dependent translation is associated with this tumorigenic cell fate. Other translation initiation factors are also overexpressed in cancer, such as eIF4GI in squamous cell lung carcinoma (Bauer et al., 2002). Full-length eIF4GI scaffolds eIF4E-bound mRNA and ribosomes to initiate cap-dependent translation (Morino et al., 2000). Its enhanced expression is also correlated with increased cap-dependent translation. Overall, over-expression of translation initiation factors leads to aberrant mRNA translation and changes patterns of protein expression.

Translational Control Changes During Stress: The Shift Toward Cap-Independent Translation

Cap-dependent translation initiation in mammals

Normal unstressed cells undergo translation initiation via cap-dependent and independent mechanisms. Translation initiation requires the recruitment of translation initiation factors (eIFs) and ribosomes to target mRNAs (reviewed in (Jackson et al., 2010)) (Figure 1.1). Initiation commences with the priming of ribosome for further initiation events by the association of eIF3 and eIF1A initiation factors with the 40S ribosome subunit (Passmore et al., 2007; Siridechadilok et al., 2005). Another initiation factor eIF2, a G-protein, associates with both guanosine triphosphate (GTP) and methionine bound tRNA forming the ternary complex. The ternary complex is responsible for recruitment of the first amino

Figure 1.1

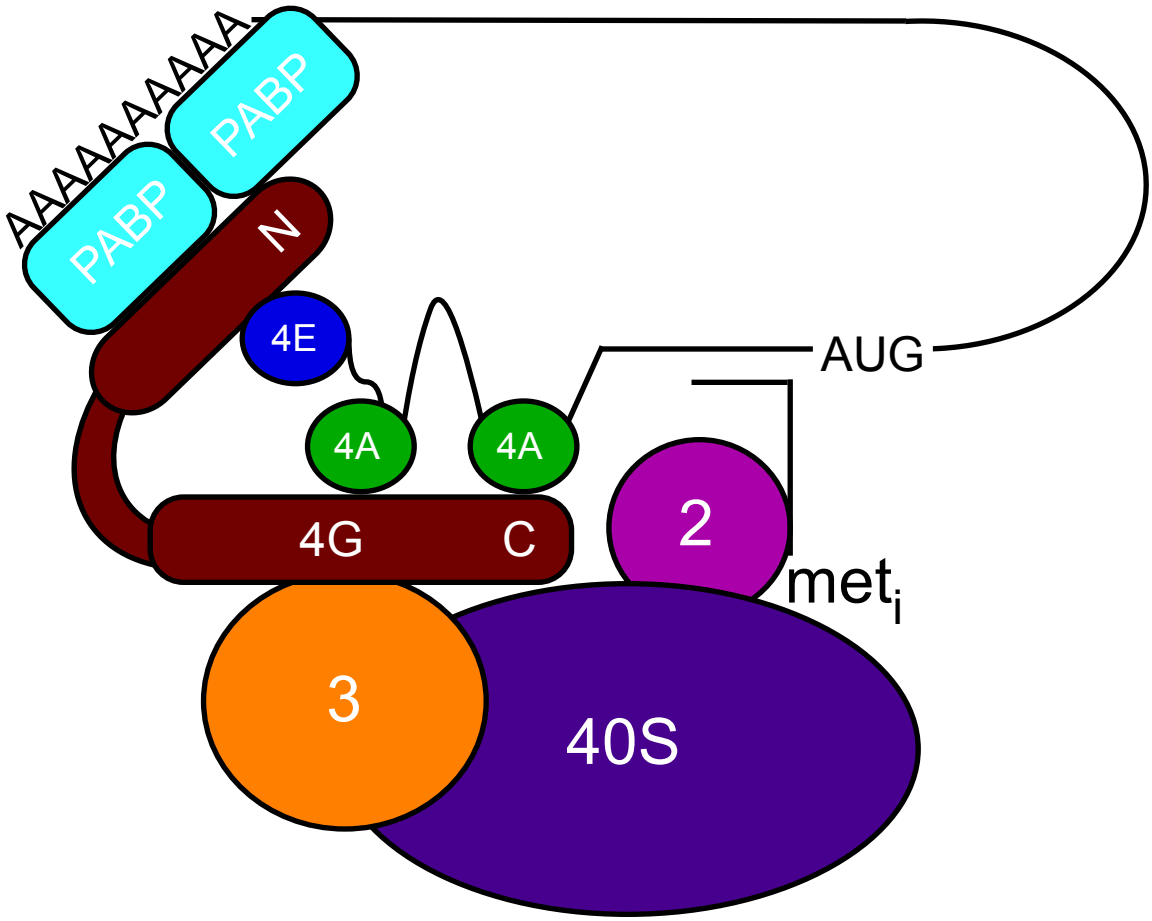

Figure 1.1 Schematic of the cap-dependent pre-initiation complex. This is a depiction of the committed step in cap-dependent translation initiation. eIFs are involved in the recruitment of mRNA to the ribosome for translation. eIF4E (blue) binds the mRNA cap and associates with eIF4G (maroon). eIF4G is a scaffolding complex that also associates with the poly(A) binding proteins (light blue), the ribosome binding factor, eIF3 (orange) and the RNA helicase eIF4A (green). By associating with the mRNA cap binding protein, eIF4E, and the poly(A) binding proteins allows for the circularization of mRNA and facilitates reinitiation events. Also depicted are the 40S subunit of the ribosome (purple) and the ternary complex, which is composed of eIF2 (pink) and Met-$tRNA_i^{Met}$.

acid-charged initiator tRNA to the ribosome to commence protein synthesis. The primed ribosome, ternary complex, eIF1, eIF1A and eIF3 then join together forming the 43S pre-initiation complex (Olsen et al., 2003). During cap-dependent translation, the eIF4 initiation factors are then responsible for mRNA recognition and recruitment to the 43S pre-initiation complex described above (Keiper et al., 1999). After mRNA reaches a length of about thirty nucleotides during transcription, 7-methylguanine is joined to the 5' end of the growing mRNA via 5'-5' triphosphate linkage (Furuichi et al., 1977; Shatkin, 1976). In cap-dependent recruitment, eIF4E binds the 7-methylguanosine mRNA cap and associates with the scaffolding protein, eIF4G (Lamphear et al., 1995; Sonenberg et al., 1978). The central region of eIF4G binds RNA helicase, eIF4A and 40S binding factor eIF3, effectively ushering mRNA to the ribosome for translation (Korneeva et al., 2000; Lamphear et al., 1995; Morino et al., 2000). The N-terminal domain of eIF4G also binds the Poly(A) binding proteins (PABP) effectively circularizing the mRNA and promoting additional rounds of translation initiation by the fully transited ribosomes (Imataka et al., 1998). Binding of initiation factors is cooperative and enhances the formation of pre-initiation complex on mRNAs. For example, eIF4A binding frequency is 2.4-fold increased in the presence of eIF3 (Korneeva et al., 2000). Additionally, eIF3 also stabilizes the binding of the ternary complex to the 40S pre-initiation complex thus promoting recruitment of Met-tRNA for protein synthesis (Korneeva et al., 2000). The association of eIF4F complex (eIF4A, eIF4B, eIF4E and eIF4G), mRNA and the 43S pre-initiation complex initiates mRNA scanning. Scanning continues until the complex, including the tRNA, recognizes the start codon (AUG) in the proper context and clamps down to form the 48S initiation complex. 48S formation is the committed step in protein synthesis. eIF5 joins allowing for GTP hydrolysis on eIF2, which

Figure 1.2

A

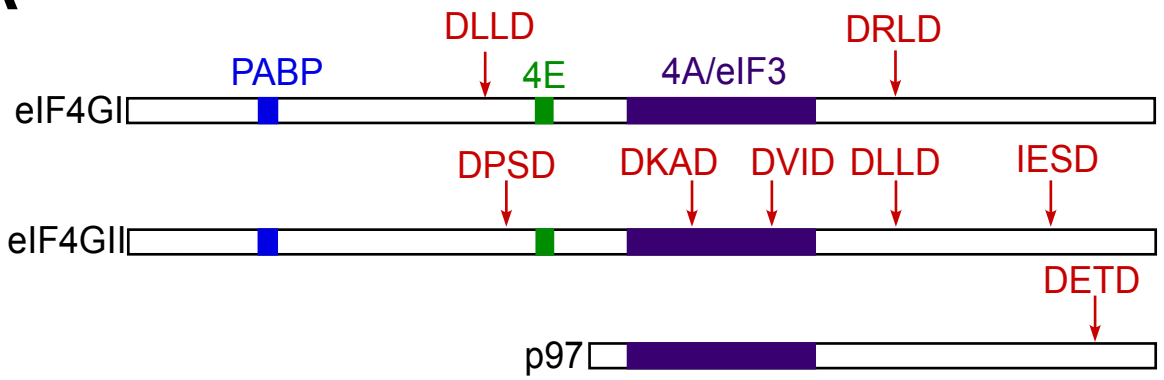
DLLD
DRLD
PABP
4E
4A/eIF3
eIF4GI
DPSD
DKAD
DVID
DLLD
IESD
eIF4GII
DETD
p97

B

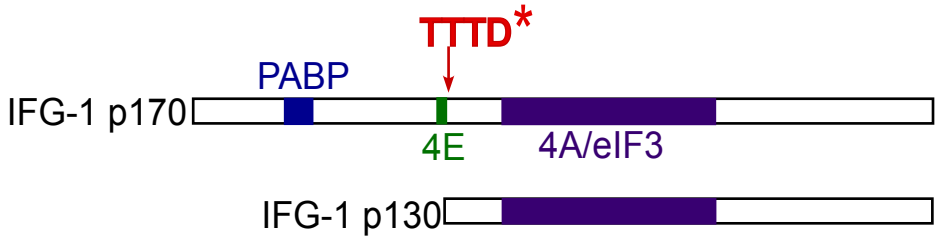
TTTD*
PABP
IFG-1 p170
4E
4A/eIF3
IFG-1 p130

Figure 1.2. Comparison of human and *C. elegans* eIF4G isoforms. (A) Diagram depicting cap-dependent (eIF4GI and eIF4GII) and independent (p97) eIF4G isoforms. The known caspase-3 processed sites within human eIF4GI, eIF4GII, and p97 isoforms are indicated. Relative positions of binding sites for major translation factor partners (PABP, eIF4E, and conserved eIF4A/eIF3 binding region) are also shown. The middle M-FAG region of eIF4GI is involved in cap-independent translation after caspase and viral cleavage. Caspase-cleavage results in eIF4GII degradation. p97 is cleaved leading to a p86 cleavage product that continues to translate mRNAs cap-independently. (B) *C. elegans* cap-dependent (p170) and cap-independent (p130) eIF4G isoforms. CED-3 cleavage site is indicated in red. Relative positions of binding sites for major translation factor partners (PABP, eIF4E, and conserved eIF4A/eIF3 binding region) are also shown.

results in dissociation of all eIF factors (Nanda et al., 2013). eIF5B then catalyzes the 60S subunit association (Lee et al., 2002). The outcome of this complicated initiation process is methionine bound tRNA in the ribosome P site. Translation elongation can then begin with the recognition of the second codon and the first peptide bond formation. Meanwhile, GDP is exchanged for GTP to recycle active eIF2 in a reaction catalyzed by eIF2B to allow continued rounds of translation initiation (Jennings et al., 2013).

Isoforms of eIF4G have differing potentials to initiate mRNA translation cap-dependently. Mammals have two genes encoding full-length eIF4G isoforms: eIF4GI and eIF4GII (Imataka and Sonenberg, 1997; Raught et al., 2000). Although both isoforms are broadly co-expressed, they are encoded by separate genes (Figure 1.2A) (Imataka and Sonenberg, 1997). eIF4GI and eIF4GII have three modular structural domains: an N-terminal domain that binds PABP and eIF4E, a C-terminal domain that binds eIF3 and eIF4A and a hinge region that links theses two domains (Imataka and Sonenberg, 1997). Thus, eIF4GI and eIF4GII are scaffolding proteins that are able to actively recruit mRNA to the ribosome for translation due to their association with both mRNA and ribosome binding proteins. eIF4GI and eIF4GII can also stimulate cap-dependent translation by recruiting Mnk1 to phosphorylate and activate eIF4E (Pyronnet et al., 1999) (Figure 1.3). The C-terminal region of eIF4GI and eIF4GII has domains that bind the serine/threonine kinase Mnk1, thus recruiting Mnk1 to activate eIF4E and stimulate cap-dependent protein synthesis (Figure 1.3) (Pyronnet et al., 1999; Waskiewicz et al., 1999). A third shorter eIF4G isoform encoded by a third gene, p97/DAP5/NAT1, is constitutively cap-independent (Imataka et al., 1997). p97 lacks the N-terminal domain that binds proteins that associate with the mRNA cap, eIF4E, and poly(A) tail, PABP (Imataka et al., 1997).

Figure 1.3

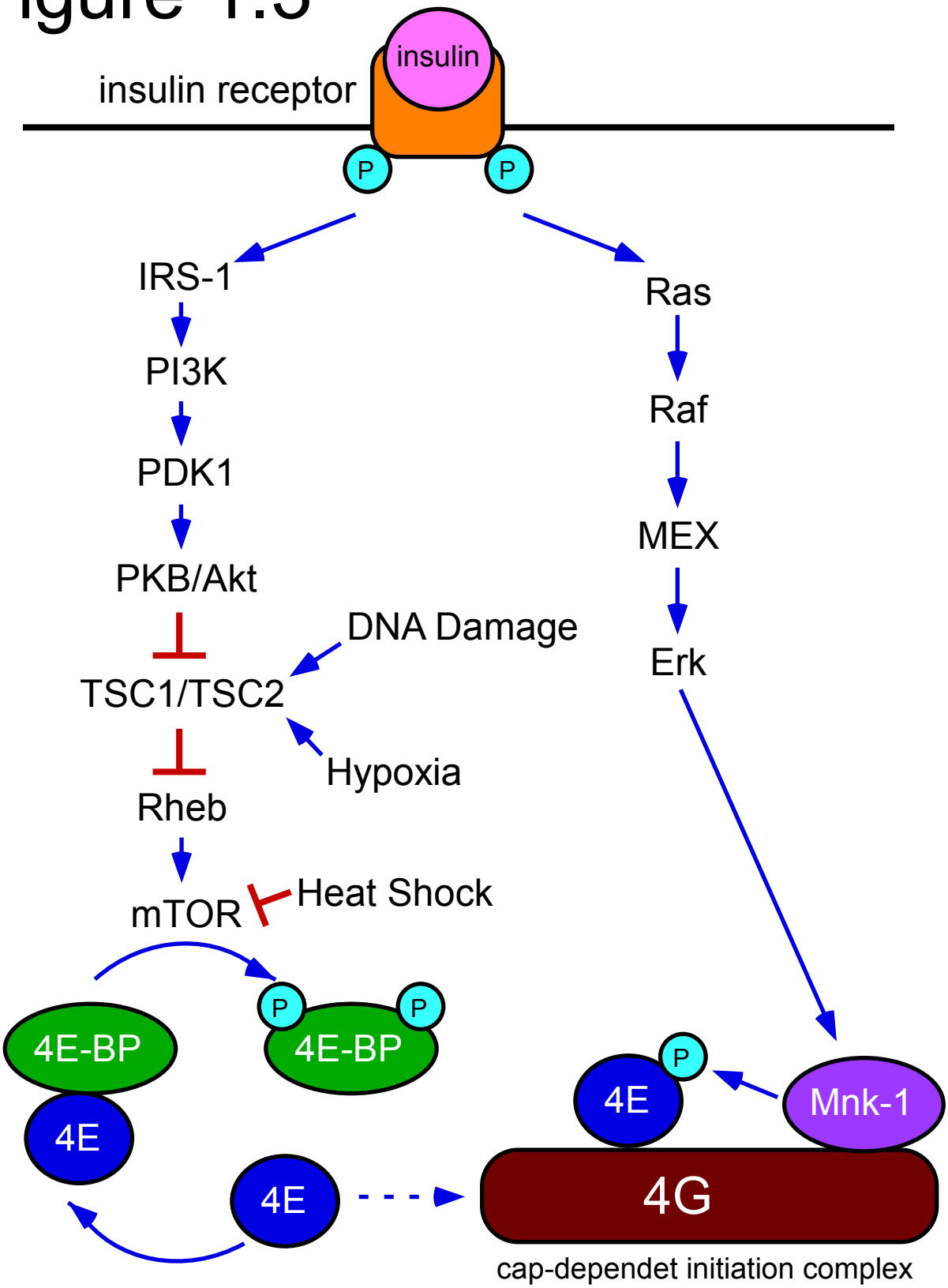
insulin
insulin receptor
P
P
IRS-1
PI3K
PDK1
PKB/Akt
DNA Damage
TSC1/TSC2
Hypoxia
Rheb
mTOR
Heat Shock
Ras
Raf
MEX
Erk
4E-BP
P
P
4E-BP
4E
4E
P
4E
Mnk-1
4G
cap-dependet initiation complex

Figure 1.3. Initiation of cap-independent translation through mTOR inhibition. Insulin signaling leads to the activation of mTOR and phosphorylation of 4E-BP leading to increased cap-dependent translation initiation. However, during stress, cap-dependent translation is inhibited through 4E-BP binding. Starvation, DNA damage, hypoxia and heat shock lead to inhibition of mTOR and decreased cap-dependent translation. Thus, these conditions favor the cap-independent translation initiation mechanism.

Instead, it contains only domains that bind ribosomes, eIF3 and eIF4A (Imataka et al., 1997). Thus, p97 is not able to recruit mRNAs cap-dependently and is not able to directly aid in mRNA circularization via the 3' poly(A) tail (Imataka et al., 1997). Additionally, during viral infection, viral protease 2A, and apoptosis, caspase-3, cleave eIF4G isoforms removing their cap-binding domains, creating a p97-like product (Haghighat et al., 1996; Marissen and Lloyd, 1998). Thus, cleavage inhibits the cap-dependent mechanism of mRNA translation in the cell (Haghighat et al., 1996; Marissen and Lloyd, 1998).

Cap-independent translation initiation in mammals

Cap-dependent translation is not, however, the only means by which proteins are synthesized. Many picornaviral mRNAs do not have 5' methyl caps, but are still very efficiently recruited to the ribosome for translation. This initiation of translation uses some, but not all, of the translation initiation factors. The central region of eIF4GI can bind eIF3, eIF4A and supports translation initiation despite the absence of cap-recognition (Pestova et al., 1996). Additionally, p97 is constitutively cap-independent due to the absence of an eIF4E-binding domain (Imataka et al., 1997). p97 mediated translation demonstrates that cap-independent translation initiation is not just a byproduct of eIF4G cleavage during viral infection and apoptosis, but occurs constitutively in healthy cells. mRNAs can be directly recruited to the ribosome independent of eIF4E using internal ribosome entry sites (IRESes) or other cap-independent means (Coldwell et al., 2000; Nevins et al., 2003). Although many scientists view IRES-based translation initiation and cap-independent protein synthesis as being synonymous, there are numerous precedents for heat shock protein mRNAs lacking IRESes yet still translating by cap-independent mechanisms. This

has been shown to occur in stressed mammalian cells, plant cells and in virus infected cells, although the mechanism by which heat shock mRNAs are initiated for translation is poorly understood (Dinkova et al., 2005; Joshi-Barve et al., 1992; Rhoads and Lamphear, 1995; Schneider, 1995).

Viral IRESes. IRESes were originally discovered in positive strand RNA viruses and allow for the translation of viral proteins after the down regulation of cap-dependent general cellular protein synthesis (Figure 1.4A-B) (Pelletier and Sonenberg, 1988). The transition to IRES-mediated translation is thought to lie at the heart of the "host synthesis takeover" by such RNA viruses. During viral infection, eIF4G isoforms are cleaved removing the eIF4E and PABP association domains necessary for cap-dependent mRNA recruitment and reinitiation events (Belsham et al., 2000; Haghighat et al., 1996). In this way, the viral infection results in the selective translation of its own mRNAs while inhibiting global translational efficiency of most cellular mRNAs. Many picornaviral mRNAs were also observed to lack the 5' cap necessary for cap-dependent protein recruitment and are thus constitutively translated cap-independently (Jang et al., 1990; Pelletier and Sonenberg, 1988). IRESes were first discovered in 1988 in poliovirus and encephalomyocarditis virus (EMCV) and these mRNA's IRESes served as the model for IRES characteristics for many years to come (Jang et al., 1990; Pelletier and Sonenberg, 1988). Poliovirus was observed to have an unusually long 5' UTR of about 750 nt and contained 7-8 AUGs within this 5' UTR (Pelletier and Sonenberg, 1988). Only three of the upstream AUGs were conserved in position and none of these AUGs result in conserved open reading frames (Pelletier and Sonenberg, 1988). The poliovirus IRES also has high degree of secondary structure and was naturally uncapped (Pelletier and Sonenberg, 1988). Rather, studies yielded pUp as the

Figure 1.4

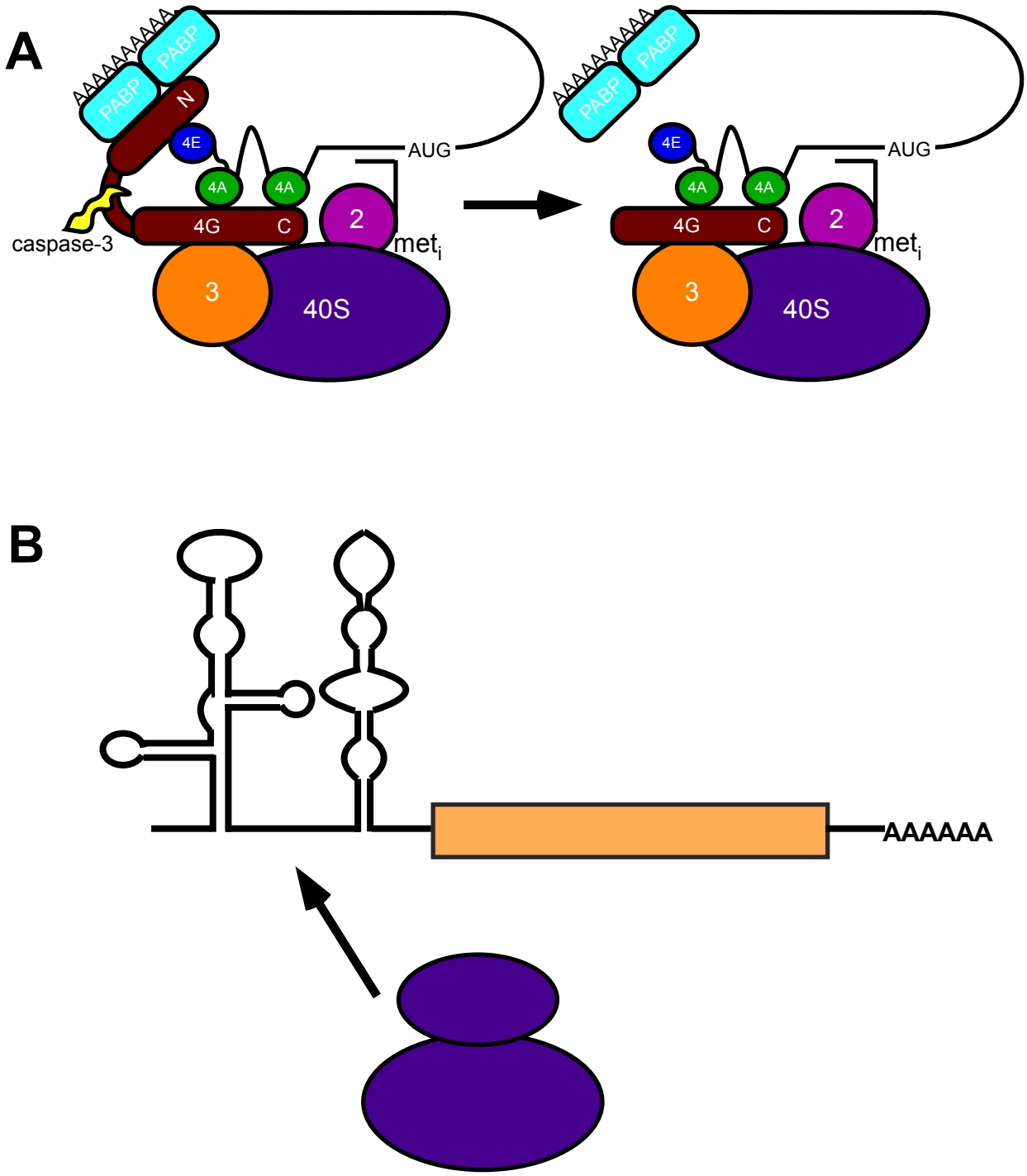
A
AAAAAAAAAA
PABP
PABP
N
4E
4A
4A
4G
C
2
3
40S
AUG
met$_i$
caspase-3
AAAAAAAAAA
PABP
PABP
4E
4A
4A
4G
C
2
3
40S
AUG
met$_i$
B
AAAAAA

Figure 1.4. Schematic of cap-independent translation initiation. (A) Depicts the cap-dependent translation initiation mechanism and the site of caspase cleavage. After caspase cleavage, translation initiates in a cap-independent manner, which does not involve the N-terminal region of eIF4G that binds to the PABPs and eIF4E. (B) Cartoon depicting internal ribosome entry of high secondary structure 5' UTR IRESes.

possible 5' terminus of poliovirus mRNA (Nomoto et al., 1976). Thus, these defining characteristics of the poliovirus (long 5' UTR, multiple AUGs, high secondary structure) became the recognized defining characteristics of IRESes.

Additional studies of viral IRESes showed that even with this relatively simplistic definition of an IRES, viral IRESes are quite diverse in these features. Thus, several groups began to divide viral IRESes into unique IRES classes based on secondary structure and dependence of other proteins for their translation initiation (reviewed in (Fitzgerald and Semler, 2009) and (Malys and McCarthy, 2011)). Structural classes termed I-IV were categorized based on maintained secondary structure and their dependence on certain initiation factors and IRES trans-acting factors (ITAFs). However, even with similar structures, the IRESes in similar classes were found to have differing requirements for IRES trans-acting factors (ITAFs) and translation initiation factors (Fitzgerald and Semler, 2009). Other attempts were made to characterize IRES elements solely by their dependence on factors for their translation initiation (Figure 1.5A-E) (Filbin and Kieft, 2009; Kieft, 2008; Malys and McCarthy, 2011). Type I IRESes require all of the canonical eIFs, except the cap-binding factor eIF4E, and may additionally require ITAFs for their translation initiation (Figure 1.4B) (Filbin and Kieft, 2009; Malys and McCarthy, 2011). Ribosome scanning occurs to identify their start codons (Malys and McCarthy, 2011). Examples of Type I IRESes include poliovirus and rhinovirus (Borman and Jackson, 1992; Jackson et al., 2010). Ribosomal scanning does not occur for Type II IRESes, which have an initiation codon that is located immediately after the 3' end of the IRES (Figure 1.4C) (Malys and McCarthy, 2011). These IRESes, which include EMCV, consequently do not require eIF1 and eIF1A initiation factors (Malys and McCarthy, 2011; Pestova et al., 1996).

Figure 1.5

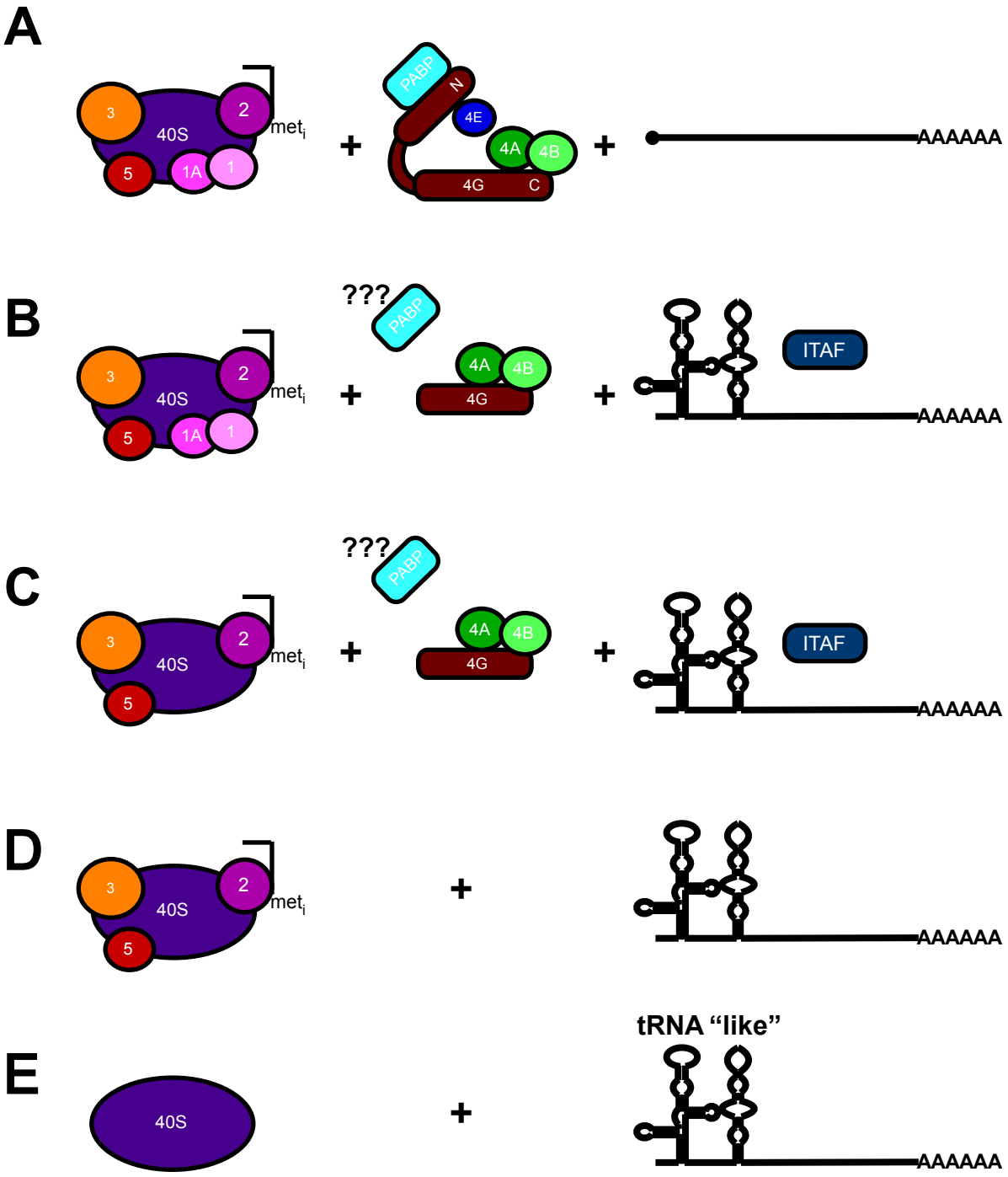
A
3
40S
2
met$_i$
5
1A
1
+
PABP
N
4E
4A
4B
4G
C
+
AAAAAA
B
3
40S
2
met$_i$
5
1A
1
+
???
PABP
4A
4B
4G
+
ITAF
AAAAAA
C
3
40S
2
met$_i$
5
+
???
PABP
4A
4B
4G
+
ITAF
AAAAAA
D
3
40S
2
met$_i$
5
+
AAAAAA
E
40S
+
tRNA "like"
AAAAAA

Figure 1.5. Proposed mechanisms of viral IRES-driven translation. A-E represent categorization of IRES elements on their dependence on translation initiation factors and ITAFs. (A) Initiation factors required for cap-dependent translation (B) Type I IRESes require all the canonical eIFs, except eIF4E, and may require additional ITAFs for their translation initiation. (C) Type II IRESes does not require eIF4E, eIF1 and eIF1A initiation factors, but require the other canonical translation initiation factors. (D) Type III IRESes do not require the eIF4F complex and associate directly with the ribosomal subunit at the initiation codon. They rely on eIF3, eIF2 and eIF5 for their initiation. (E) Type IV IRESes do not require any of the canonical eIFs or initiator tRNA.

Type III IRESes do not require the eIF4 complex at all and associate directly with the ribosomal subunit at the initiation codon (Figure 1.4D) (Filbin and Kieft, 2009; Malys and McCarthy, 2011). They solely rely on eIF3, eIF2 and eIF5 for their initiation (Malys and McCarthy, 2011). Examples of Type III IRESes include Hepatitis C, classical swine fever virus (CSFV) and porcine teschovirus 1 (PTV-1) (Pisarev et al., 2004; Rijnbrand et al., 1997; Tsukiyama-Kohara et al., 1992). The final group, Type IV, is perhaps the most novel and includes the very well studied cricket paralysis virus (CrPV) (Filbin and Kieft, 2009; Malys and McCarthy, 2011). CrPV does not require any of the canonical eIFs or initiator tRNA for its translation initiation. Instead, it appears to use its IRES' secondary and tertiary structure to recruit the ribosome directly to the IRES, perhaps by resembling tRNA (Figure 1.4E) (Jan et al., 2003; Jan and Sarnow, 2002; Pestova and Hellen, 2003; Pisarev et al., 2005; Schuler et al., 2006; Spahn et al., 2004; Wilson et al., 2000). Domain 3 of the CrPV IRES mimics the anticodon loop-codon interaction of tRNA and mRNA (Filbin and Kieft, 2009). Interestingly, the CrPV IRES can also bind directly to the pre-assembled 80S ribosomes directly (Pestova and Hellen, 2003; Pestova et al., 2004). The CrPV IRES has been described as perhaps beginning mRNA translation directly at the elongation phase. Overall, although the use of translation initiation factors and ITAFs may differ, viral IRESes use the cap-independent mechanism to translate viral mRNAs while eIF4G cleavage prevents translation of most cellular mRNAs. However, this transition to cap-independent translation promoting selective mRNA recruitment is not unique. A similar transition to the cap-independent mechanism promotes selective mRNA translation during cell stress (Pelletier and Sonenberg, 1988).

Cellular IRESes. IRESes are not just a phenomenon found in uncapped viral mRNAs. Despite having 5' caps, many cellular mRNAs encode IRES elements that allow for their cap-independent translation, even if they are also competent to initate by a cap-dependent mechanism. In fact, IRES-mediated translation is more resistant to physiological stress. As a result, many stress-related mRNAs have IRES elements in their 5' UTRs (Bornes et al., 2007; Coldwell et al., 2000; Henis-Korenblit et al., 2000; Thoma et al., 2004). Examples include mRNAs that encode growth factors, such as vascular endothelial growth factor (VEGF), the cell cycle progression protein, ODC, oncogene proteins, such as c-Myc, proapoptotic and antiapoptotic proteins, such as apoptotic protease activating factor (Apaf-1), and the cap-independent translation initiation factor, p97 (Bornes et al., 2007; Coldwell et al., 2000; Henis-Korenblit et al., 2000; Pyronnet et al., 2000; Thoma et al., 2004). Cellular IRESes are unable to be categorized similarly to viral IRESes due to their large secondary structure diversity. It is proposed that this diversity is the result of the need for regulation during multiple types of stress or cell fate decisions. Interestingly, a family of A-rich yeast IRESes have been shown to rely on PABP for their activity, once again demonstrating the diverse factor needs of different cellular IRESes (Gilbert et al., 2007).

ITAFs. One main question many scientists are addressing is how IRESes with opposing functions are translated at different time points during stress or under different stress conditions. One way in which IRES-mediated translation is regulated is via binding of ITAFs. ITAFs bind the IRES directly and can stimulate the cap-independent translation of the viral or cellular mRNA of interest. These factors also seem to be specific to the IRES of interest. The exact mechanism of how ITAFs promote the translation of IRES containing mRNAs is unknown, however these are several different proposed mechanisms for ITAF

utilization (Filbin and Kieft, 2009; Komar and Hatzoglou, 2011). Hypotheses include that the ITAFs remodel the secondary structure of the IRES allowing for it to have a higher or lower affinity for other components of the translation initiation apparatus (Filbin and Kieft, 2009; Komar and Hatzoglou, 2011). This allows the IRES to facilitate 80S formation without direct contact with the ribosome (Filbin and Kieft, 2009; Komar and Hatzoglou, 2011). Alternatively, the ITAFs could directly bind the ribosome and with help of other translation initiation factors recruit the ribosome to the target mRNA (Filbin and Kieft, 2009; Komar and Hatzoglou, 2011). A third possibility is that the ITAF could stabilize the IRES structure so that it can directly bind and recruit the ribosome (Filbin and Kieft, 2009; Komar and Hatzoglou, 2011). However, the possibilities may be entirely more complicated and be a combination of the above mechanisms contributing to the initiation of the target mRNA (Filbin and Kieft, 2009; Komar and Hatzoglou, 2011). The population of ITAFs that bind IRES elements differs depending on the target mRNA. For example, the Apaf-1 IRES is stimulated by Polypyrimidine tract binding protein (PTB) and upstream of N-ras (unr), whereas binding immunoglobulin protein (BiP) is stimulated by heterogeneous nuclear ribonucleoprotein (NSAP1) and La autoantigen (Cho et al., 2007; Kim et al., 2001; Mitchell et al., 2003). ITAFs not only act to promote IRES-driven translation, but they can also have inhibitory roles or differing roles that depend on the target mRNA of interest. For example, during human rhinovirus serotype 2 (HRV-2) infection hnRNP A1 re-localizes to the cytoplasm and promotes the translation of HRV-2 viral mRNA (Fitzgerald and Semler, 2009). However, hnRNP A1 is also re-localized to the nucleus during ultraviolet irradiation and inhibits the activity of the Apaf-1 IRES (Fitzgerald and Semler, 2009). ITAFs thus

regulate specific activation or deactivation of target mRNA IRES-mediated translation during different stress conditions.

Translation of heat shock proteins in the absence of IRES sequences. Many heat shock proteins including HSP 90, HSP 70, HSP 65 and HSP 27 are synthesized more efficiently after the knockdown of eIF4E (Joshi-Barve et al., 1992; Matsuura et al., 2008). Both pulse labeling and immunoprecipitation indicated HSP 90 and HSP 70 were synthesized at a faster rate during these cap-independent conditions (Joshi-Barve et al., 1992). Although the translational efficiency of the beforehand efficiently translated housekeeping mRNA actin decreased, HSP 90 and HSP 70 mRNA shifted from light to heavy polysomes indicating a substantial increase in translational efficiency, despite the knockdown of cap-dependent protein synthesis (Joshi-Barve et al., 1992). A simple explanation for this increase in translational efficiency of Hsp mRNAs would be the preferential translation of "strong" mRNAs with short, unstructured 5' UTRs (Lodish, 1974). However, despite increased translational efficiency after the knockdown of cap-dependent protein synthesis during heat shock, the translational efficiency of HSP 70 decreased during the cellular recovery phase from heat shock (Joshi-Barve et al., 1992). Thus, the HSP 70 mRNA is outcompeted for translation during recovery, contrasting with the "strong" mRNA definition (Joshi-Barve et al., 1992). No IRES has been found to account for HSP 70 cap-independent translation, despite extensive studies to characterize such an IRES sequence. Additionally, HSP 70 mRNA 5' UTR is highly unstructured, whereas the defining IRES characteristic is their long, highly structured 5' UTR (Lindquist and Petersen, 1990). IRES-mediated translation therefore is not the only cap-independent mechanism of translation initiation available in cells experiencing stress, cell death or viral infection.

Induction of cap-independent protein synthesis.

Viral infection leads to the activation of cap-independent protein synthesis due to eIF4G cleavage. As aforementioned, eIF4G isoform cleavage occurs during viral infection. Viruses hijack the host translation initiation machinery while simultaneously inhibiting translation of most host cellular mRNAs (Alvarez et al., 2003). Picornavirus encode protease 2A, which cleaves human eIF4G isoforms eIF4GI and eIF4GII (Lamphear et al., 1995). Protease 2A cleavage separates the cap-binding domain from the ribosome binding domain, thus preventing cap-dependent translation intiation and resulting in a dramatic shutdown of host cellular protein synthesis (Etchison et al., 1982; Krausslich et al., 1987; Lamphear et al., 1995). However, the central ribosome-binding domain is still able to support cap-independent translation (Aldabe et al., 1995; De Gregorio et al., 1999; Keiper and Rhoads, 1997; Leibowitz and Penman, 1971). Continued cap-independent translation sustains IRES-mediated viral mRNA and cellular mRNA translation initiation (Buchkovich et al., 2010; Jang and Wimmer, 1990; Tsukiyama-Kohara et al., 1992).

Apoptosis leads to the activation of cap-independent protein synthesis due to caspase cleavage. A specific example of when cap-independent translation contributes to protein expression patterns that determine cell fate is apoptosis. Apoptosis allows for the programmed removal of superfluous and damaged cells. For example, during development superfluous cells between the fingers commit cellular suicide to prevent webbing (Mori et al., 1995). Apoptosis is also important to remove cells after DNA damage, growth factor withdrawal and accumulation of misfolded proteins (Danial, 2007). For this reason, mutations in the apoptotic pathway are often informative markers for cancer. For example,

B-cell lymphoma 2 (BCL-2), an antiapoptotic signaling protein, was characterized as the defining oncogene in follicular lymphomas (Tsujimoto et al., 1985).

The eIF4G isoforms are targeted for cleavage by caspases as the result of apoptotic pathway activation. To initiate intrinsic apoptosis in human cells, an apoptotic signal/stressor results in the activation of BH3-only proteins such as Bim, Bid, Bad, Noxa and Puma (Danial, 2007). Activation can occur in several ways such as BID cleavage by caspase-8 (Li et al., 1998b), BAD phosphorylation (Datta et al., 2000), or PUMA transcriptional regulation by p53 (Chipuk et al., 2005). All of these modifications allow for the exposure of the BH3 domain and the interaction of this helical domain with the hydrophobic groove of their multidomain dimerization partners (Bcl-2 and Bcl-x_L) (Datta et al., 2000; Day et al., 2005; Hinds et al., 2003; Muchmore et al., 1996; Petros et al., 2001; Sattler et al., 1997). Activation of BH3-only proteins enables them to perturb the interaction between antiapoptotic (Bcl-2 and Bcl-x_L) and proapoptotic members (Bax and Bak) of the Bcl-2 family (Figure 1.6) (Datta et al., 2000; Kuwana et al., 2005; Petros et al., 2001; Sattler et al., 1997). This stimulates the release of proapoptotic Bax and Bak from antiapoptotic proteins, Bcl-2 and Bcl-x_L, allowing them to oligomerize forming a pore in the mitochondrial membrane (Dlugosz et al., 2006; Uren et al., 2007; Willis et al., 2005; Willis et al., 2007). BAK monomers, which are initially integrated in the mitochondrial outer membrane, oligomize and form endoplasmic reticulum (ER) and mitochondrial pores after BCL-2 inactivation (Karbowski et al., 2006; Wei et al., 2001). Pores in the ER membrane allow for calcium release (Szalai et al., 1999). Supraphysiologic calcium levels result in the opening of a large conductance channel in the inner membrane of the mitochondria, the permeability transition pore. The opened permeability transition pore results in swelling

Figure 1.6

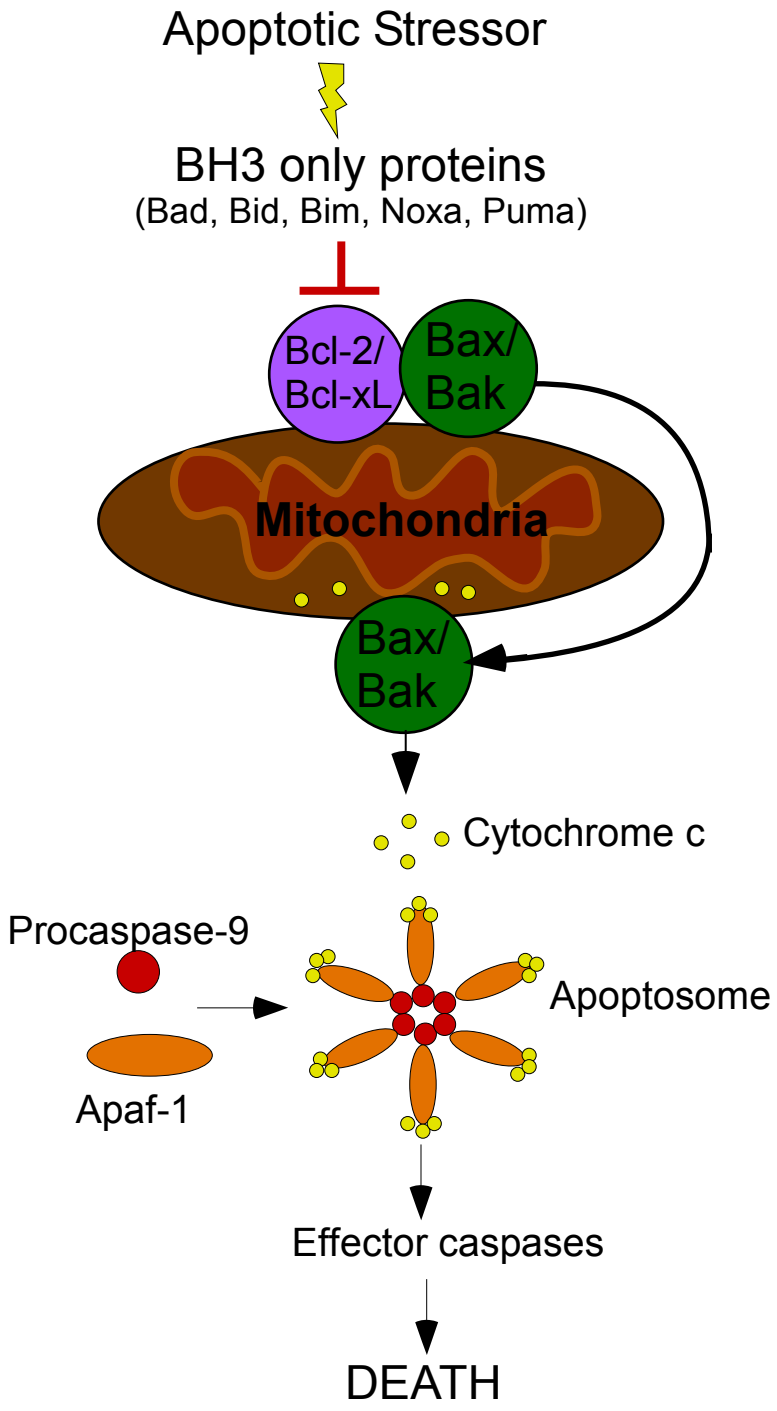
Apoptotic Stressor
BH3 only proteins
(Bad, Bid, Bim, Noxa, Puma)
Bcl-2/
Bcl-xL
Bax/
Bak
Mitochondria
Bax/
Bak
Cytochrome c
Procaspase-9
Apoptosome
Apaf-1
Effector caspases
DEATH

Figure 1.6. Human apoptotic pathway. The schematic represents the indirect activation model of the human intrinsic apoptotic pathway. Activation of BH3-only proteins such as Bim, Bid, Bad, Noxa and Puma enables these proteins to perturb antiapoptotic Bcl-2 and Bcl-x_L (Danial, 2007; Datta et al., 2000; Kuwana et al., 2005; Petros et al., 2001; Sattler et al., 1997). This leads to Bax and Bak oligomerization into a mitochondrial pore forming a pore (Dlugosz et al., 2006; Uren et al., 2007; Willis et al., 2005; Willis et al., 2007). Cytochrome c is released through the mitochondrial pore where it binds both Procaspase-9 and Apaf-1 to form the apoptosome (Li et al., 1997; Peng et al., 2006). Apoptosome formation leads to procaspase-9 activation (Nicholson et al., 1995). The active caspase then cleaves effecter procaspases, such as caspase-3 and caspase-7, resulting in their activation (Denault et al., 2006). These effecter caspases, in turn, degrade cellular machinery, such as the translation initiation proteins, leading to cell death (Marissen and Lloyd, 1998).

and rupture of the mitochondria (Szalai et al., 1999). Additionally, the proapoptotic protein BAX initially found in the cytosol of quiescent cells undergoes a three-dimensional structure change exposing its COOH-terminal tail from the hydrophobic BH1, BH2, BH3 cleft (Wolter et al., 1997). The structural reconfiguration results in BAX translocation to the mitochondria where it forms a mitochondrial pore (Annis et al., 2005; Kuwana et al., 2002; Wolter et al., 1997).

Mitochondrial pores allow for the release of cytochrome c into the cytoplasm where it binds both Procaspase-9 and Apaf-1 to form the apoptosome (Li et al., 1997; Peng et al., 2006). The oligomerization of Procaspase-9 and Apaf-1 is dependent on the presence of cytochrome c and ATP, most likely due to their binding exposing the caspase recruitment domain (CARD) in Apaf-1 allowing it to bind Procaspase-9 (Li et al., 1997). Oligomerization of the apoptosome components results in self-processing of the zymogene Procaspase-9 into its active caspase form (Nicholson et al., 1995). The active caspase then cleaves effecter procaspases, such as caspase-3 and caspase-7, resulting in their activation (Denault et al., 2006). These effector caspases, in turn, degrade cellular machinery, including transcription and translation factors, leading to cell death (Marissen and Lloyd, 1998).

Among the specific targets of activated caspase-3 are the eIF4G isoforms: eIF4GI, eIF4GII and p97 (Bushell et al., 1999; Marissen et al., 2000). Cleavage of the long isoforms (eIF4GI and II) removes the eIF4E and PABP domains, preventing their involvement in mRNA recruitment (Morino et al., 2000). The resulting central domain of eIF4GI (M-FAG/p76) continues to support translation in a cap-independent manner (Bushell et al., 1999). eIF4GII is degraded and does not have a known role in further translation (Nevins et al., 2003). The constitutively cap-independent eIF4G isoform, p97 is also cleaved to a

smaller p86 cleavage product (Henis-Korenblit et al., 2000). p86 associates with eIF3 and eIF4A and continues to support cap-independent translation (Henis-Korenblit et al., 2000; Nevins et al., 2003). Although the rate of protein synthesis in apoptotic cells is reduced to roughly 30-40%, the synthetic rate by p86 protein is selectively maintained (Nevins et al., 2003). Overall, translation initiation is still able to occur in a select subset of mRNAs via cap-independent translation after this caspase cleavage of the eIF4G family (Henis-Korenblit et al., 2000; Marissen and Lloyd, 1998; Nevins et al., 2003). Interestingly, not only does p86 (cleaved eIF4G p97) support translation of other proteins during apoptosis, p86 mediates its own cap-independent synthesis (Henis-Korenblit et al., 2000). Meanwhile, the translational activity of other products substantially decreases, as seen for ß-tubulin synthesis, whose activity was reduced by greater than 85% (Henis-Korenblit et al., 2000). The levels of p86 in apoptotic cells remain comparable to p97 levels in growing cells, while eIF4GI cleavage results in a low steady-state level of eIF4GI cleavage product (Henis-Korenblit et al., 2000). Thus, during apoptosis the proportion of eIF4G family members drastically changes.

Apoptosis-related IRES-driven mRNA translation. There are many apoptotic mRNAs, both proapoptotic and antiapoptotic, which contain IRES elements and are translated more efficiently during enhanced cap-independent translation. Examples of apoptotic IRES containing mRNAs include Bag-1, Bmf, p53, Apaf-1 and Bcl-2 (Coldwell et al., 2001; Coldwell et al., 2000; Dobbyn et al., 2008; Grespi et al.; Grover et al., 2008; Sherrill et al., 2004). The activation of these IRESes may require additional factors. For example, Apaf-1 requires polypyrimidine tract binding protein (PTB) and Upstream of N-ras (UNR) for its activation, allowing for Apaf-1 translation after eIF4G cleavage (Mitchell et al., 2001). In the

case of Apaf-1, its continued translation during apoptosis allows for a positive feedback loop resulting in continued apoptosis and greater eIF4G cleavage further promoting continued cap-independent translation.

4E-BP and cap-independent translation during heat shock, hypoxia, and other stress-related conditions. Cap-dependent translation can also be downregulated in a manner that does not require eIF4G cleavage through the activation of eIF4E Binding Protein (4E-BP) (Figure 1.3). Changes in 4E-BP sequestration of eIF4E are moderated through the phosphatidylinositol 3-kinases (PI3K)/mammalian target of rapamycin (mTOR) pathway. Insulin or other mitogens bind tyrosine kinase hormone receptors resulting in receptor autophosphorylation at tyrosine residues (Schmelzle and Hall, 2000). Activated tyrosine kinase receptor phosphorylates and activates IRS-1 leading to a signaling cascade that results in the inhibition of TSC1/TSC2 (tuberous sclerosis complex) complex (Backer et al., 1992; Gao and Pan, 2001; Myers et al., 1992; Potter et al., 2001). The TSC1/TSC2 complex is responsible for hydrolyzing guanosine triphosphate (GTP) to guanosine diphosphate (GDP) on Ras homolog enriched in the brain (Rheb) (Garami et al., 2003). Thus, TSC1/TSC2 inhibits Rheb during insulin stimulation (Garami et al., 2003). Rheb binds mTOR leading to its activation (Long et al., 2005). mTOR, in turn, phosphorylates and deactivates 4E-BP allowing eIF4E to associate with eIF4G and actively recruit mRNA to the ribosome via cap-association (Mamane et al., 2004). Thus, during periods of starvation where there is little insulin stimulation, cap-dependent translation is inhibited. Additionally, cellulr stress responses to amino acid starvation, heat shock, DNA damage and hypoxia all favor cap-independent conditions exerted through dephosphorylation of the eIF4E binding protein

(4E-BP) and in some cases cleavage of eIF4GI (Ma and Blenis, 2009; Tee and Proud, 2000; Tinton and Buc-Calderon, 1999; Vries et al., 1997).

Stress-related IRES-driven mRNA translation. Many stress related mRNAs are also translated cap-independently during stress. For example, the mammalian chaperone, BiP is encoded by an mRNA with a heat inducible IRES (Cho et al., 2007). Enhanced BiP expression allows recovery throughout the unfolded protein response (UPR) during heat shock. Similarly during hypoxia, mammalian cells upregulate cap-independent VEGF mRNA translation (Bornes et al., 2007). As a response to low oxygen availability, VEGF is able to stimulate angiogenesis, helping in organ recovery from hypoxia. DNA damage likewise leads to enhanced cap-independent translation of p53, BCL-2, XIAP and BAG-1 (Dobbyn et al., 2008; Grover et al., 2008; Gu et al., 2009; Sherrill et al., 2004). The induced translational expression of these proteins enables cells to recover from DNA damage and re-enter the cell cycle

Transient and Prolonged Stress lead to sequential cap-independent translation first of recovery and then of apoptosis-related mRNAs. If cell stress is transient the expression of these stress-related proteins provides the cell with the means to recover (reviewed in (Vaux, 1999)). However, if stress persists such that cells accumulate too much damage to recover, proapoptotic mRNAs are then translationally activated resulting in cell death. An example to illustrate the translation of these prosurvival mRNAs is XIAP, a member of the IAP family of antiapoptotic proteins that block the progression of apoptosis by binding to caspase-3, 7 and 9 and inhibiting their caspase activity (Lagace et al., 2001; Liston et al., 2003). XIAP has an IRES permitting its cap-independent translation after caspase-mediated cleavage of eIF4Gs and the dephosphorylation of 4E-BP (Holcik et al., 1999). Thus, after the

initial stress, XIAP can bind and inactivate caspases giving cells the opportunity to recover. Specifically, the XIAP IRES has been shown to be induced by transient cellular stresses such as anoxia, serum deprivation and low-dose gamma-irradiation (Holcik et al., 1999; Holcik et al., 2000; Nevins et al., 2003). The XIAP IRES is also activated by the presence of its ITAF, La autoantigen. La autoantigen undergoes dephosphorylation during Fas-induced apoptosis allowing for its relocalization to the cytoplasm where it may bind the XIAP IRES (Ohndorf et al., 2001). If stress persists, XIAP-associated factor 1 (XAF1) binds to XIAP and blocks its antiapoptotic activity, most likely by sequestering it to the nucleus (Liston et al., 2001). Proapoptotic IRESes may then be activated by their ITAFs during prolonged insult resulting in their cap-independent translation. For example, a PTB-containing complex is remodeled during apoptosis and relocates to the cytoplasm bound to the IRES of proapoptotic Apaf-1 (King et al., 2014). hnRNPA1, which inhibits Apaf-1 IRES-mediate translation, relocalizes to the nucleus during apoptosis (King et al., 2014). Relocation relieves Apaf-1 IRES-mediated translation inhibition (King et al., 2014). IRES mediated translation of XIAP and Apaf-1 mRNAs provides a clear example of cap-independent regulation resulting in changes in protein expression that results in attempted recovery or after prolonged insult cellular suicide.

Translational control links heat shock and apoptosis

Translational control comprises part of a weighted fate decision of recovery versus apoptosis for cells submitted to external stresses or naturally fated for elimination. There is a similar link between ER stress and apoptosis (Lin et al., 2007). ER stress not only activates the unfolded protein response (UPR) through c-Jun N-terminal kinase (JNK), it

eventually also activates an apoptotic response by phosphorylating and inactivating Bcl-2 (Lin et al., 2007; Yamamoto et al., 1999). JNK also phosphorylates BH3-only proteins (e.g. Bad) activating them to further promote apoptosis (Yu et al., 2004). ER stress and apoptosis, in turn, promote cap-independent translation through 4E-BP activation and caspase cleavage of eIF4G, respectively. BiP and Bcl-2 expression are then enhanced via IRES-mediated translation (Sherrill et al., 2004; Yang and Sarnow, 1997). BiP expression leads to renewed proper protein folding and BCL-2 expression prevents apoptosis resulting in a recovery period (Lin et al., 2007). Expression of BiP and Bcl-2 therefore contributes to fate decisions that assess cumulative cell damage following the disruption of normal protein synthesis. Overall, cap-independent translation provides a means to respond to prevailing hazardous conditions by selectively enhancing translational efficiency of mRNAs that will influence decisions in recovery or demise.

Alternative splicing of apoptotic mRNAs and its effect on cell fate

In addition to translation control, alternative splicing has been shown to play a role in cell fate decisions to live or die. Many of the pro- and antiapoptotic pre-mRNAs are alternatively spliced, including Fas, Bcl-2 , Bcl-w, Bax, Bim, Caspase-1, Caspase-2, Caspase-3, Caspase-6, Caspase-7 and Caspase-10 (Alnemri, 1997; Alnemri et al., 1995; Cascino et al., 1995; Fernandes-Alnemri et al., 1995a; Fernandes-Alnemri et al., 1995b; Gibson et al., 1996; O'Connor et al., 1998; Oltvai et al., 1993; Tsujimoto and Croce, 1986; Wang et al., 1994). Within the Bcl-2 protein family there are more than twenty members. Of those members most have at least two isoforms. Frequently the isoforms have opposing functions. One example of this change is the alterations in splicing of the Bcl-x gene (Boise

et al., 1993). The Bcl-x gene has two alternatively spliced mRNA variants that encode proteins of opposing apoptotic functions; Bcl-x_S is proapoptotic while Bcl-x_L is antiapoptotic (Boise et al., 1993). Not only does Bcl-x_L function in the apoptotic pathway to prevent apoptosis, it can also interact with Apaf-1 to inhibit the activation of caspases and promotes tumor cell invasion (Du et al., 2007; Hu et al., 1998). On the other hand, Bcl-x_S can selectively induce apoptosis, even in tumor cells (Dole et al., 1996). Splicing changes for these transcripts have been shown to result from the induction DNA damage, leading to an increase in the levels of the antiapoptotic transcript (Revil et al., 2007; Shkreta et al., 2008; Shkreta et al.). Thus, changes in splicing patterns in this example and many more have been associated with the altered fate decisions in cells and in phenotypes leading to death or cancer. Apaf-1 mRNA is also alternatively spliced with four splice variants, two of which are missing a WD-40 repeat required for the response to cytochrome c and activation of Procaspase-9 (Benedict et al., 2000; Saleh et al., 1999). Apaf-1 lacking a WD-40 repeat does not appear to be a negative regulator of apoptosome activation, but instead may be an activator or bind another cofactor with a similar function to cytochrome c (Benedict et al., 2000). This demonstrates once again how there can be alternative functions due to splice variant proteins. Interestingly, the pattern of Apaf-1 mRNA splicing has been shown to differ in cancer cells as opposed to normally proliferating cells (Benedict et al., 2000; Saleh et al., 1999; Zou et al., 1999). Additional Apaf-1 mRNA, with the proper number WD-40 repeats, was detected in cancer cell lines including HeLa and 293T cells, although the effect of this alternative splicing on cell fate has yet to be determined (Benedict et al., 2000; Zou et al., 1997). Overall, this demonstrates how changes in splicing patterns can change the

overall fate of the cell, whether it is to push the cell towards suicide or promote proliferation/cancer phenotypes.

C. elegans as an in vivo model to study regulation of translation

The nematode *C. elegans* provides a versatile model system in which to study the complex mechanism of translation initiation and its regulation. *C. elegans* are easy to work with; a fast growing organism within which genetic changes can be observed phenotypically over multiple generations in a relatively short period of time. *C. elegans* are semitransparent allowing for direct observation of cell fate decisions within a living organism. The invariant progression of the 959 developing somatic cells, including 131 cells that commit apoptosis, is well documented providing a known background for genetic analysis (Sulston and Horvitz, 1977; Sulston et al., 1983). About a thousand germ cells inhabit the reproductive tract and a subset of these too undergo apoptotic progression (Gumienny et al., 1999). *C. elegans* was also the first multicellular eukaryote with a completely sequenced genome and have provided a relatively simple developmental animal model to modify genetically. The reproductive tract (germ line) of the worms is particularly suited to studying protein synthesis, cell proliferation, differentiation and apoptotis. Stem cell fate decisions in the *C. elegans* germ line are regulated primarily by mRNA translational control (Kimble and Crittenden, 2007). All germ cells entering meiosis experience chromosome condensation that correlates with suppressed transcription (Figure 1.7). Therefore, changes in protein expression, leading to cell fate decisions, result from translational regulation of stored mRNAs. Mitotic cells from the distal tip progress linearly through a transition zone and then enter meiosis (Figure 1.7) (Gumienny et al., 1999). As these germ cells progress

Figure 1.7

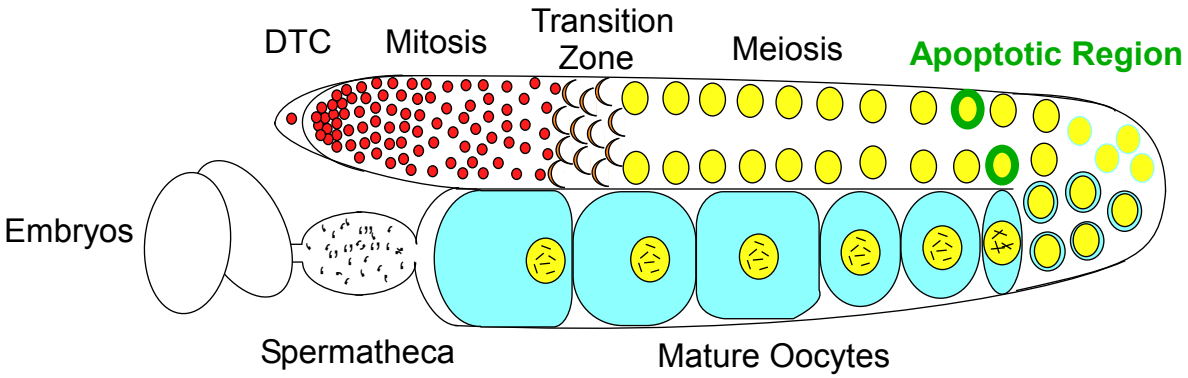
DTC
Mitosis
Transition Zone
Meiosis
Apoptotic Region
Embryos
Spermatheca
Mature Oocytes

Figure 1.7. *C. elegans* gonad as a model system. In the *C. elegans* gonad, cells progress through mitosis from the distal tip progressing through a transition zone and entering meiosis (Gumienny et al., 1999). During meiosis there is condensation of chromosomes, which correlates with suppressed transcription. Therefore, stem cell fate decisions are regulated primarily by mRNA translational control (Kimble and Crittenden, 2007). Cells progress to the bend in the gonad where 50% of the oocytes are naturally fated to commit cellular suicide. These cells are believed to act like the nurse cells of higher-level organism providing extra cytoplasmic components, ribosomes, mRNA and mitochondria to their maturing sibling oocytes (Gumienny et al., 1999).

through mitosis and the initial stages of meiosis I, they have semi-enclosed cellular membranes in the form of a syncitium resulting in a shared cytoplasm (Gumienny et al., 1999; Hansen et al., 2004). The syncitium contains a shared pool of maternal mRNAs whose selective translation gives rise to critical developmental proteins that determine germ cell fate. One vital cell fate decision, for developing germ cells, is the choice between apoptosis and continued maturation. The apoptotic pathway was initially elucidated genetically in *C. elegans* by Horwitz and Hengartner (Hengartner et al., 1992; Hengartner and Horvitz, 1994; Xue et al., 1996; Zhou et al., 2001). These discoveries lead to the delineation of the conserved apoptotic pathway in humans. Thus, *C. elegans* are the ideal simple model to study the apoptotic mechanism in conjunction with the regulation of translation that is also found in more complex organisms.

eIFs in C. elegans

C. elegans have two major isoforms of eIF4G, denoted IFG-1 p170 and IFG-1 p130 that are encoded by the same *ifg-1* gene (Figure 1.2B) (Contreras et al., 2008). IFG-1 p170, much like the longer mammalian eIF4G isoforms, binds to m7GTP-sepharose columns and is thus able to associate with the mRNA cap binding proteins, eIF4E isoforms IFE-1-5 (Amiri et al., 2001; Contreras et al., 2008; Dinkova et al., 2005; Henderson et al., 2009; Keiper et al., 2000). Conversely, IFG-1 p130 is reminiscent of p97 and is constitutively cap-independent (Contreras et al., 2008). Both IFG-1 p170 and p130 have domains that are predicted to associate with eIF3, eIF4A, ribosomes and MNK-1 (Contreras et al., 2008). Thus, cap-dependent translation appears to result from the translation initiation complexes

assembled on IFG-1 p170, while IFG-1 p130 is only involved in complexes directing cap-independent translation (Contreras et al., 2011; Contreras et al., 2008).

The C. elegans conserved apoptotic pathway also leads to cap-independent translation.

The apoptotic pathway is conserved in *C. elegans* and allows for the programmed removal of superfluous cells during development (Figure 1.8). Apoptosis also occurs naturally in a substantial fraction of germ cells. In the adult gonad about 50% of cells produced from the stem cells at the distal tip never become mature oocytes, but are instead removed as germ cell corpses (Gumienny et al., 1999). In the gonad, as in somatic organs, the *C. elegans* Bcl-2 homolog, CED-9, inhibits CED-4, the Apaf-1 homolog, function during normal growth and development (Chinnaiyan et al., 1997b; Hengartner et al., 1992; Hengartner and Horvitz, 1994; Yang et al., 1998; Zou et al., 1997). However, as the cells reach the end of pachytene a substantial subset commit themselves to cellular suicide (Gumienny et al., 1999). These cells are thought to act in a similar manner to nurse cells of higher-level organisms providing extra cytoplasmic RNAs, proteins, organelles and other components needed by the cells that reach maturity (Gumienny et al., 1999). In germ cells destined to die, the function of CED-4 in the apoptotic region is no longer inhibited by CED-9 and as a result activates the cell death machinery (Chinnaiyan et al., 1997a). CED-4 binds the procaspase CED-3, forming the apoptosome. Apoptosome formation initiates CED-3 self-cleavage and activation in the presence of ATP (Chinnaiyan et al., 1997a; Chinnaiyan et al., 1997b; Yang et al., 1998; Yuan et al., 1993). CED-3 cleaves cellular machinery resulting in cell death. Much like the mammalian system, one of the specific targets of CED-3 is the translation initiation factor eIF4G (IFG-1) leading to cap-independent protein synthesis (Contreras et

Figure 1.8

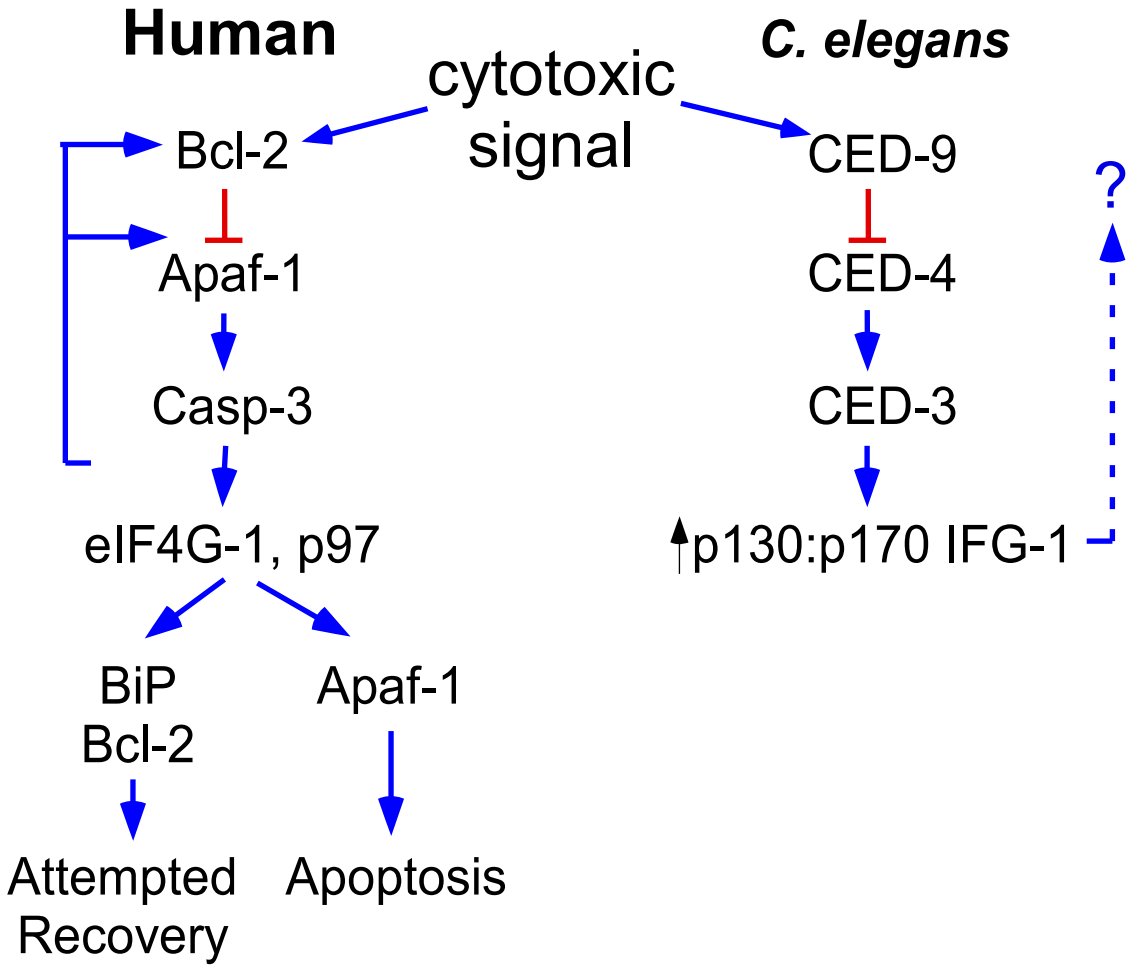
Human
C. elegans
cytotoxic signal
Bcl-2
Apaf-1
Casp-3
eIF4G-1, p97
BiP
Bcl-2
Apaf-1
Attempted Recovery
Apoptosis
CED-9
CED-4
CED-3
p130:p170 IFG-1
?

Figure 1.8. Comparison of the human and *C. elegans* apoptotic pathways. The Bcl-2 homologue (CED-9) inhibits CED-4 (Apaf-1) activation. CED-4 binds CED-3 forming the apoptosome leading to CED-3 self-cleavage. CED-3 cleaves eIF4G isoforms (IFG-1 p130 and p170) leading to the induction of cap-independent protein synthesis.

al., 2011). These cells are then recognized by CED-1, a receptor on the surface of the gonad sheath, as a result of the phosphatidyl serine configuration on the surface of the apoptotic cells (Zhou et al., 2001). The resulting corpses are then engulfed and eliminated from the gonad.

C. elegans IFG-1, much like human eIF4G, is a target for caspases during apoptosis (Contreras et al., 2011). The *C. elegans* caspase, CED-3, cleaves IFG-1 p170 and p130 at the canonical TTTD site and, in the case of p170, removes the cap-association domain (Contreras et al., 2011). Unlike mammals, no known homologue of 4E-BP has been identified in nematodes. This absence indicates that the only known mechanism to initiate cap-independent translation in *C. elegans* is caspase cleavage of IFG-1. It should be noted that IFG-1 p170 expression is important for many other stages of worm fertility and growth (Contreras et al., 2011). RNAi knockdown of p170 resulted in few late stage oocytes and few viable embryos (Contreras et al., 2011). RNAi targeting both IFG-1 p170 and p130 resulted not only in preventing germ cell development but also results in stunted somatic growth of the worms, similar to the genetic null phenotype caused by a gene deletion (Contreras et al., 2008). These results indicate the importance of cap-dependent translation for normal growth and development. Enhanced cap-independent translation in worms, however, appears to correlate with the induction of apoptosis, particularly in germ cells (Contreras et al., 2011; Contreras et al., 2008). These observations indicate that IFG-1 p170 may be associated with translation of mRNAs encoding proteins with functions in growth and maturation, while IFG-1 p130 preferentially translates stress and apoptosis-related mRNAs.

Alternative Splicing in C. elegans.

The mRNA of the *C. elegans* homologue of Apaf-1, CED-4, undergoes alternative splicing like its mammalian homologue (Shaham and Horvitz, 1996). CED-4 has two known splice variants, CED-4L and CED-4S that differ in the splicing of exon 3 and exon 4 (Shaham and Horvitz, 1996). CED-4S is the well-characterized variant involved in the induction of apoptosis, whereas CED-4L has been shown to have a lesser known antiapoptotic activity (Shaham and Horvitz, 1996). *C. elegans* mRNAs, unlike most mammalian mRNAs, have an additional level of splicing complexity due to mRNAs containing operons and thus intergenic regions that must be spliced away. A large number of apoptotic mRNAs (*ced-2, ced-4, ced-6, ced-9, ced-10 and ced-12)* are found in such operons (Blumenthal et al., 2002) (Spieth et al., 1993) (Blumenthal and Spieth, 1996). . This leads to the question of whether alternative splicing of pre-mRNA plays a role in the onset of apoptosis (Blumenthal et al., 2002; Blumenthal and Spieth, 1996; Spieth et al., 1993). Briefly, there are three types of non-canonical trans-splicing of operon primary transcripts in *C. elegans*: SL1 trans-splicing, SL2 trans-splicing and SL1-type trans-splicing (Figure 1.9). SL1 trans-splicing usually occurs on the first gene in an operon removing the outron and replacing it with an SL1 splice leader in a similar mechanism to cis-splicing of introns (Figure 1.9A-B). SL2 trans-splicing occurs for downstream genes in an operon (Figure 1.9C). Poly(A) cleavage results in an upstream mRNA that is no longer part of the remaining downstream pre-mRNA with the intergenic region still attached (Liu et al., 2003). The remaining 3' pre-mRNA rapidly undergoes a trans-splicing event leading to removal of the intergenic region and inclusion of SL2 splice leader sequence at the 5' end. SL2 splicing is undergone by apoptotic mRNAs such as *ced-4* (Liu et al., 2003). The final type of splicing that occurs is SL1-type trans-

Figure 1.9

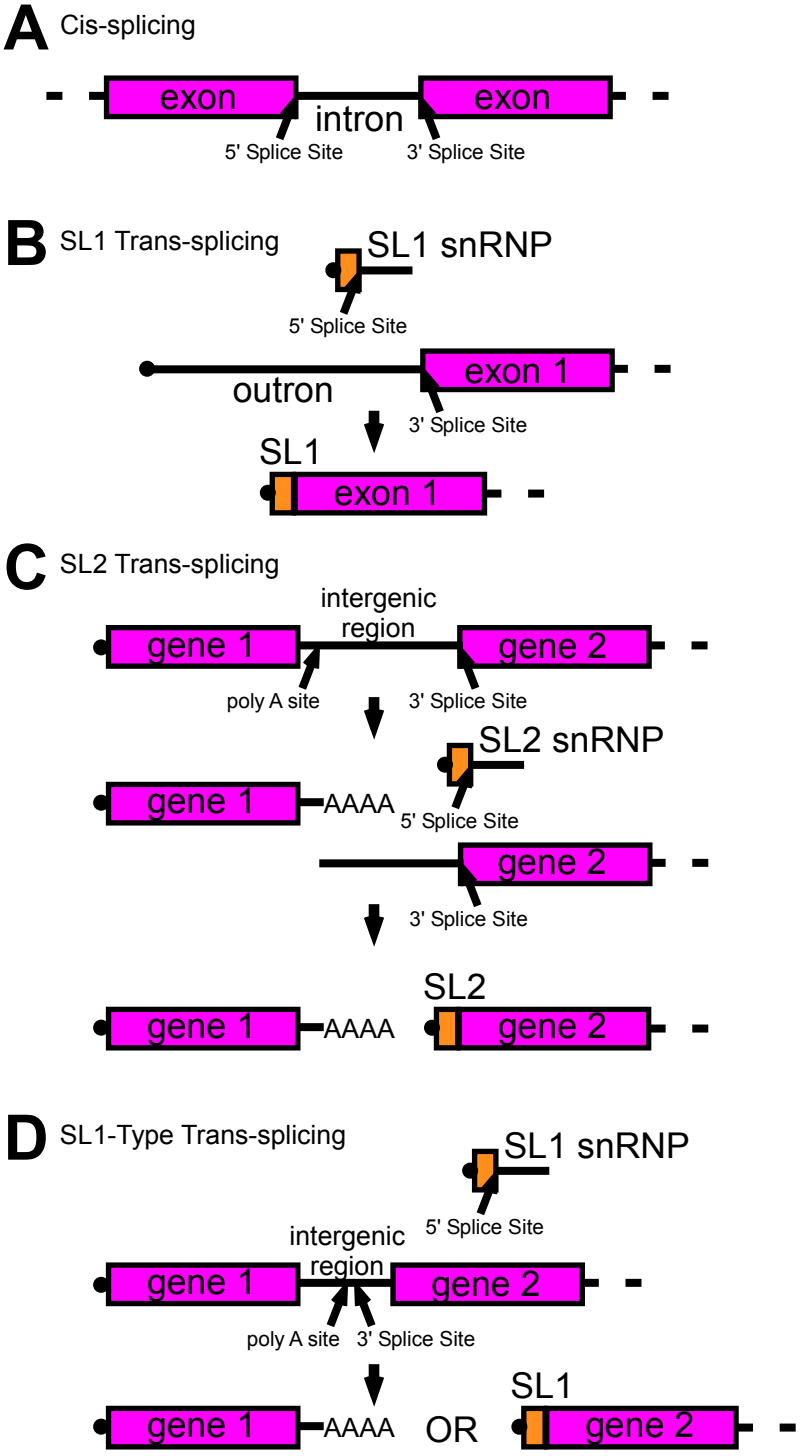
A Cis-splicing
exon
intron
exon
5' Splice Site
3' Splice Site
B SL1 Trans-splicing
SL1 snRNP
5' Splice Site
outron
exon 1
3' Splice Site
SL1
exon 1
C SL2 Trans-splicing
intergenic region
gene 1
gene 2
poly A site
3' Splice Site
SL2 snRNP
gene 1
AAAA
5' Splice Site
gene 2
3' Splice Site
SL2
gene 1
AAAA
gene 2
D SL1-Type Trans-splicing
SL1 snRNP
5' Splice Site
intergenic region
gene 1
gene 2
poly A site
3' Splice Site
SL1
gene 1
AAAA
OR
gene 2

Figure 1.9. Trans-splicing of *C. elegans* polycistronic mRNAs. (A) Schematic representing cis-splicing of introns. (B) Schematic representing SL1 trans-splicing. SL1 splicing usually occurs on the first gene in an operon removing a 5' outron. (C) Schematic representing SL2 trans-splicing. SL2 trans-splicing occurs for downstream genes in an operon. (D) Schematic representing SL1-type trans-splicing. SL1-type splicing results in only one mature mRNA species.

splicing, which occurs to make mature *ced-9* mRNA (Figure 1.9D) (Williams et al., 1999). In this type of splicing, only one mature mRNA results and there is no intergenic region (Williams et al., 1999). The polyadenylation/cleavage results in degradation of the downstream mRNA or the SL1 splicing of the second mRNA results in destruction of the upstream mRNA's resident polyadenylation site (Williams et al., 1999). During stress (heat shock, cold shock, hypoxia, chemical toxicity), all splicing events occur less efficiently and there is a change in splicing patterns (Liu et al., 2003). The Blumenthal lab reported that during stress, particularly heat shock, inefficient SL2 trans-splicing occurred resulting in new mRNAs variants (Liu et al., 2003). In this situation, 3' cleavage of the upstream gene occurrs, however the SL2 trans-splicing that results in a 5'-capped downstream mRNA was inhibited (Liu et al., 2003). This inhibition results in an uncapped mRNA that contains 5' outron sequence (Liu et al., 2003). Therefore, alternative splicing, such as outron inclusion or even early intron bypass, may result in mRNAs with altered translation initiation character particularly due to change in the 5' UTR sequence.

C. elegans as a convenient model to study the dysregulation of translation and cancer.

During oogenesis in the *C. elegans* gonad there is silencing of germ cell transcription that is correlated with chromosome condensation (Seydoux et al., 1996). Overall changes in protein synthesis are therefore the result of translational regulation of the accumulated pool of stored maternal mRNAs. Oncogenesis is also characterized by translational control, much like the *C. elegans* gonad, making the gonad a useful model to better understand how changes in translational control contribute to cell fate. It has been observed by several labs that deletion of key translational regulators results in germ cell tumor progression in the *C.*

elegans gonad. For example, loss of a key translational repressor protein, GLD-1, results in dedifferentiation germ cells and the onset of a germ cell tumor (Jones and Schedl, 1995).

By elucidating the changes in mRNA translation initiation that might drive a cell's fate to die, we can better understand which genes could be targeted in mammalian cancers to cause these same changes in fate decision from proliferation to death. Many characteristics of *C. elegans* make them a versatile model to study cancer research include: a completely characterized and invariant cell lineage, semitransparency of the whole organism, allowing for direct observation of all individual cell fates, a system of genetics that is well established, and genes and pathways involved in cancer are highly conserved. *C. elegans* also have less genetic redundancies, however orthologues of the cell cycle proteins are well conserved in mammals (reviewed in (Kirienko et al., 2010; Sulston and Horvitz, 1977; Sulston et al., 1983)). Research in worms has allowed for the study of anything from cell migration/metastasis to cell cycle control, to neural networks, to fertility, to longevity, to cell death and cell cycle control (Kirienko et al., 2010). Overall, studies in *C. elegans* can enable a more comprehensive molecular-genetic understanding of dysregulated pathways that lead to cancer.

CHAPTER 2: INDUCTION OF CAP-INDEPENDENT BiP (*hsp-3)* AND Bcl-2 (*ced-9*) TRANSLATION IN RESPONSE TO eIF4G (IFG-1) DEPLETION IN *C. ELEGANS**

*** Morrison JK, Friday AJ, Henderson MA, Hao E, Keiper BD. Induction of cap-independent BiP (hsp-3) and Bcl-2 (ced-9) translation in response to eIF4G (IFG-1) depletion in C. elegans. Translation 2014; 2:e28935; http://dx.doi.org/10.4161/trla.28935**

Introduction

Stem cell fate decisions in the *C. elegans* germ line are regulated primarily by mRNA translational control (Kimble and Crittenden, 2007). All germ cells entering meiosis experience chromosome condensation that correlates with suppressed transcription. Therefore, changes in protein expression, leading to cell fate decisions, result from translational regulation of stored mRNAs. One vital fate decision for developing germ cells is the decision between apoptosis and continued maturation. During *C. elegans* oogenesis, nearly half of the progenitor cell population is naturally fated for death before reaching maturity (Gumienny et al., 1999). These cells contribute cytoplasmic contents (mRNAs, ribosomes, mitochondria) and nutrients to the maturing sibling oocytes (Gumienny et al., 1999). The dying oocytes are thought to perform a similar role to nurse cells in the ovaries of higher animals. Thus, oogenesis in worms provides a versatile model to study the role of protein synthesis regulation in an unusual cell fate decision to differentiate naturally toward apoptosis.

The translation initiation complex selects mRNAs for protein synthesis. Initiation factor eIF4G provides a scaffold for the assembly of other initiation factors and ribosomes on recruited mRNAs (Imataka et al., 1998; Lamphear et al., 1995). In mammals there are three eIF4G isoforms: eIF4GI, eIF4GII and p97 (Gradi et al., 1998; Imataka et al., 1997). eIF4GI and eIF4GII contain binding domains for eIF4E, which binds to the mRNA cap, eIF3

and eIF4A, which associate with the 40S subunit of the ribosome, and poly(A) binding proteins (PABP) (Imataka et al., 1998; Lamphear et al., 1995; Morino et al., 2000). These domains promote the recruitment of mRNA to the ribosome for translation (Keiper et al., 1999). Caspase-3 cleaves eIF4GI and eIF4GII during apoptosis removing their eIF4E and PABP binding domains preventing their involvement in translation initiation (Bushell et al., 1999; Henis-Korenblit et al., 2000; Marissen and Lloyd, 1998; Morino et al., 2000; Pestova et al., 1996). eIF4GII becomes degraded and plays no further role in protein synthesis (Marissen et al., 2000). However, translation initiation still occurs on a select subset of mRNAs via cap-independent translation (Nevins et al., 2003). Cleaved eIF4GI, and its cap-independent paralog, p97, are known to bind directly to mRNA, often via internal ribosome entry sites (IRESes) (Henis-Korenblit et al., 2000; Nevins et al., 2003). This association allows cleaved eIF4GI and p97 to recruit a specific population of mRNAs for translation during stress (Henis-Korenblit et al., 2000; Nevins et al., 2003). We have previously shown in *C. elegans* that CED-3 (caspase) cleavage of IFG-1 p170 (eIF4GI) during apoptosis removes its cap-associated domain much like the mammalian ortholog (Contreras et al., 2011). After cleavage, cap-independent initiation allows cleaved IFG-1 p170 (not cap-associated) and IFG-1 p130 (constitutively not cap-associated) to recruit mRNAs for translation (Contreras et al., 2008). Unlike in mammalian cells, only these two eIF4G forms are found in *C. elegans* and are encoded by a single *ifg-1* gene. Thus, we are investigating changes in translation initiation that result from the differential usage of IFG-1 p170, IFG-1 p130 and their caspase cleaved products. IFG-1 cleavage may allow for the differential expression of proteins determining whether the oocyte matures or succumbs to apoptosis. Importantly, we have previously demonstrated that the IFG-1 p170 loss is not merely the

cell's attempt to shut down all protein synthesis, leading to inevitable cell death. Instead, our epistasis experiments revealed that the disruption of cap-dependent translation acts as an upstream effector of cellular suicide acting through the apoptotic (*ced*) signaling pathway (Contreras et al., 2011). Our model proposes that changes in protein expression, resulting from eIF4G cleavage, are an integral part of apoptotic cell fate decisions.

eIF4G cleavage results in a change in the population of mRNAs being translated. Among these target mRNAs are both pro- and anti-apoptotic mRNAs. mRNAs involved in cell cycle progression or cell growth are typically cap-dependent and thus disadvantaged, halting further growth and proliferation (De Benedetti and Graff, 2004). Some mRNAs that encode stress-response proteins continue to translate cap-independently via IRESes. Such proteins provide the cell with an opportunity to recover from an apoptotic fate (Holcik and Sonenberg, 2005). An example of an anti-apoptotic protein whose mRNA translates via an IRES is Binding immunoglobulin Protein (BiP) (Yang and Sarnow, 1997). BiP is a chaperone protein located in the endoplasmic reticulum (ER) that facilitates protein folding and promotes recovery from heat shock and ER stress (Lee, 2005). Another example mRNA, Bcl-2, is also translated via an IRES and prevents apoptosome formation (Sherrill et al., 2004). The enrichment of anti-apoptotic proteins such as BiP and Bcl-2 during stress conditions presents cells with the means to recover and escape the apoptotic fate. Conversely, a second subset of mRNAs containing IRESes encode apoptotic proteins such as Apaf-1 (Coldwell et al., 2000). Apaf-1 drives further cell death by promoting apoptosome formation resulting in caspase activation (Coldwell et al., 2000). Dynamic regulation of cap-independent translation of pro- and anti-apoptotic mRNAs may cause protein expression patterns that determine the germ cell's differentiation decision.

Our research addresses the protein synthetic mechanism regulating germ cell fates in the *C. elegans* model system. The induction of cap-independent translation and its involvement in the natural apoptotic cell fate decision has yet to be studied in a natively differentiating cell lineage. In this study we address the physiological translational control of cap-independent mRNAs. Importantly, our findings show that regulation of some apoptotic mRNAs in this whole organism system differs from observations in cultured mammalian cells. Cap-independent conditions enhance the translational efficiency of some, but not all, *C. elegans* homologues of known mammalian IRES-containing mRNAs. At least one mRNA that lacks a 5' IRES (*hsp-3*) is upregulated by cap-independent translation. Moreover, selective translation in germ cells differs from the cap-independent translation observed in cultured mammalian cells responding to toxic treatments such as chemotherapy agents and hypoxia.

Results

A splicing defect increases the proportion of non-cap-associated (p130) to cap-associated (p170) IFG-1 isoforms. Caspase-mediated cleavage of eIF4GI (IFG-1) during apoptosis increases the ratio of the non-cap-associated IFG-1 p130-like cleavage products to the cap-associated p170 (Contreras et al., 2011). This change in ratio may decrease the efficiency of translation of cap-dependent mRNAs and enhance the translation of cap-independent mRNAs. In order to study how this change in ratio of IFG-1 isoforms alters the translation of specific mRNAs *in vivo*, we developed a *C. elegans* mutant strain with a 2.5-fold increase in the p130:p170 IFG-1 ratio (Figure 2.1D). The change in isoform proportion is caused by a splicing defect in *ifg-1* intron 5 that results from a Mos transposon insertion

at an intron-exon junction (Figure 2.1A). Mis-spliced *ifg-1::mos* mRNAs retain most or all of the Mos transposon sequence (Figure 2.1B). These mRNAs also have multiple termination codons in all reading frames that will result in nonfunctional truncated N-terminal IFG-1 upon expression (Figure 2.1C). Truncated proteins are not detected by western blot and are likely degraded (Figure 2.1D and data not shown). A small proportion of p170 *ifg-1* mRNA (34% of total) properly splices out the Mos sequence (Figure 2.1B). Properly spliced p130 and p170 mRNAs are translated into functional proteins. However, the overall protein abundance of both IFG-1 isoforms is diminished by 30% (Figure 2.1D). Western blotting to detect both the p170 and p130 shows that loss of p170 protein expression (to 38% of wild type levels) accounts for nearly all of the decrease. This reduction is likely due to the more rapid turnover of N-terminally extended eIF4G forms and was confirmed using an N-terminal IFG-1 antibody (data not shown) (Keiper et al., 1999). As a viable mutant worm strain, *ifg-1::mos* worms are therefore an appropriate whole animal model in which to address how suppression of cap-associated p170 alters the translational efficiency of specific mRNAs.

***ifg-1::mos* and *ced-9ts* mutant strains exhibit marked increases in germ line apoptosis.** Previous experiments demonstrated that RNAi knockdown of cap-associated p170 induced germ cell apoptosis (Contreras et al., 2008). Therefore, we addressed whether the reduced p170 protein abundance in the *ifg-1::mos* strain lead to a similar induction of germ cell apoptosis. To observe and count apoptotic corpses in the gonad, *ifg-1::mos* was crossed into a CED-1::GFP-expressing strain. CED-1::GFP is expressed by somatic sheath cells that surround the germ cells in the gonad. Sheath cells invade and

Figure 2.1

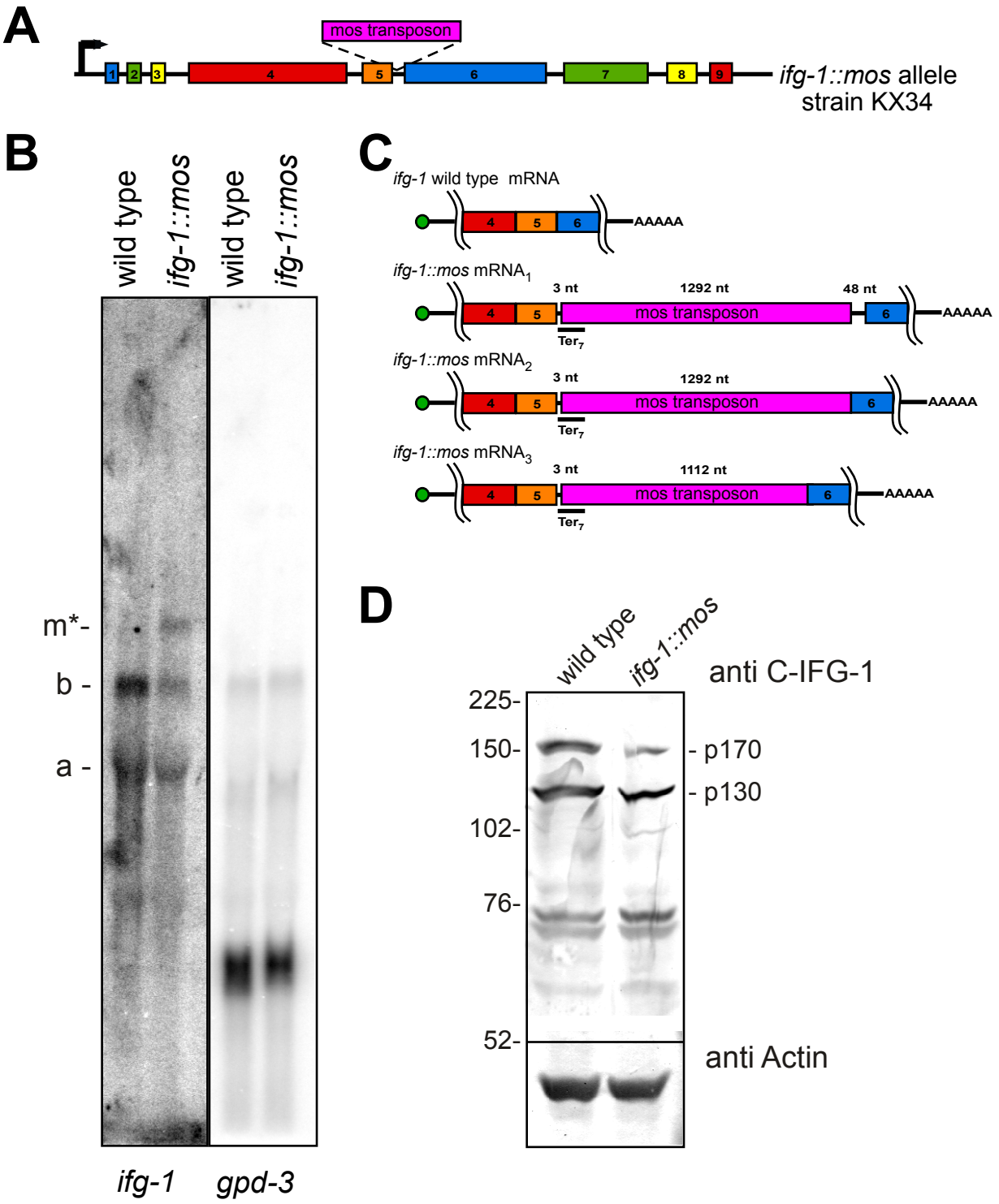
A
mos transposon
1
2
3
4
5
6
7
8
9
ifg-1::mos allele
strain KX34
B
wild type
ifg-1::mos
wild type
ifg-1::mos
m*-
b -
a -
ifg-1
gpd-3
C
ifg-1 wild type mRNA
AAAAA
ifg-1::mos mRNA1
3 nt
1292 nt
48 nt
mos transposon
Ter7
ifg-1::mos mRNA2
3 nt
1292 nt
mos transposon
Ter7
ifg-1::mos mRNA3
3 nt
1112 nt
mos transposon
Ter7
D
wild type
ifg-1::mos
anti C-IFG-1
225-
150-
102-
76-
52-
- p170
- p130
anti Actin

Figure 2.1. A splicing defect increases the proportion of non-cap-associated (p130) to cap-associated (p170) IFG-1 (eIF4G) isoforms. (A) Diagram depicting the Mos transposon insert in the *ifg-1* gene. The Mos transposon is inserted at 3 bp downstream of the exon-intron 5 junction. The strain was outcrossed 5 times to ensure the absence of additional mutations.(B) northern blot hybridization depicts *ifg-1* message populations. Northern blotting of wild type mRNA displays mRNAs of 2500 nt (a) and 4500 nt (b) indicative of p130 and p170 variants. To control for RNA loading, the blot was stripped and reprobed for *gpd-3* RNA. Full-length p170 mRNA (4500 nt) was reduced by 42% and an additional mRNA variant (m*) at approximately 6000 nt was detected in the *ifg-1::mos* strain that accounted for 17% of all *ifg-1* mRNAs. The ratio of p130:p170 mRNA increased 2-fold as p130 mRNA and the total *ifg-1* mRNA amounts changed little relative to *gpd-3* mRNA. (C) Diagrams representing the four partially spliced variants of *ifg-1* mRNA due to the Mos transposon insertion. These splice variants were characterized by RT-PCR and sequencing. All three Mos-containing mRNAs encode nonsense codons in all three reading frames. (D) Western Blot for IFG-1 using the central antibody that detects both the p170 and p130 isoforms. Wild type worms express equal amounts of each IFG-1 isoform (p130:p170 ratio is 1.2), whereas the *ifg-1::mos* strain p130 abundance is 3.1-fold higher than p170. IFG-1 p170 consistently shows a much greater reduction, likely due to its instability. In the *ifg-1::mos* strain the total amount of IFG-1 expression is also reduced 30% in comparison to the wild type strain. Western blotting for actin was used as a loading control.

engulf the dying oocyte and CED-1::GFP fluorescence allows for real time visualization of this process (Zhou et al., 2001). The progression of germ cell apoptosis was measured by counting GFP-decorated oocytes in synchronized late larval to young adult *ifg-1::mos* and wild type worms over a 48-hour period (Figure 2.2A). Small numbers of germ cell corpses begin to accumulate in both strains as their gonads mature from the larval (L3) stage to the adult stage. This is followed by a steady and significant increase in apoptotic corpses (to an average of 13-15) in *ifg-1::mos* hermaphrodites in the young adult stages (24-48 hours). By contrast, the steady state number of apoptotic germ cells levels off at about 6 hours after wild type worms reach adulthood. The increase in apoptosis in the *ifg-1::mos* strain indicates that depleting IFG-1 p170 relative to p130 results in increased germ cell apoptosis.

From our previous work and the experiments of others we know that depletion of IFG-1 and CED-9 induces germ cell apoptosis (Contreras et al., 2011; Hengartner et al., 1992). Thus, we decided to utilize both of these strains to investigate germ line translational control. We compared germ line apoptosis observed in the *ifg-1::mos* strain to a strain with a temperature sensitive defect in the anti-apoptotic protein CED-9 (Bcl-2). Loss of CED-9 enables apoptosome formation leading to caspase activation and eventual cell death in both somatic and germ cells (Chinnaiyan et al., 1997b; Pourkarimi et al., 2012). The *ced-9ts* strain showed a significant increase in apoptotic corpses in the young adult stages (24-48 hours) that mirrored the changes observed in the *ifg-1::mos* strain. Importantly, the activation of the caspase, CED-3, in the *ced-9ts* strain causes IFG-1 p170 cleavage to a p130-like product, perhaps promoting a similar outcome to the *ifg-1::mos* allele (Contreras et al., 2011). Thus, the *ced-9ts* strain similarly allows us to observe how

Figure 2.2

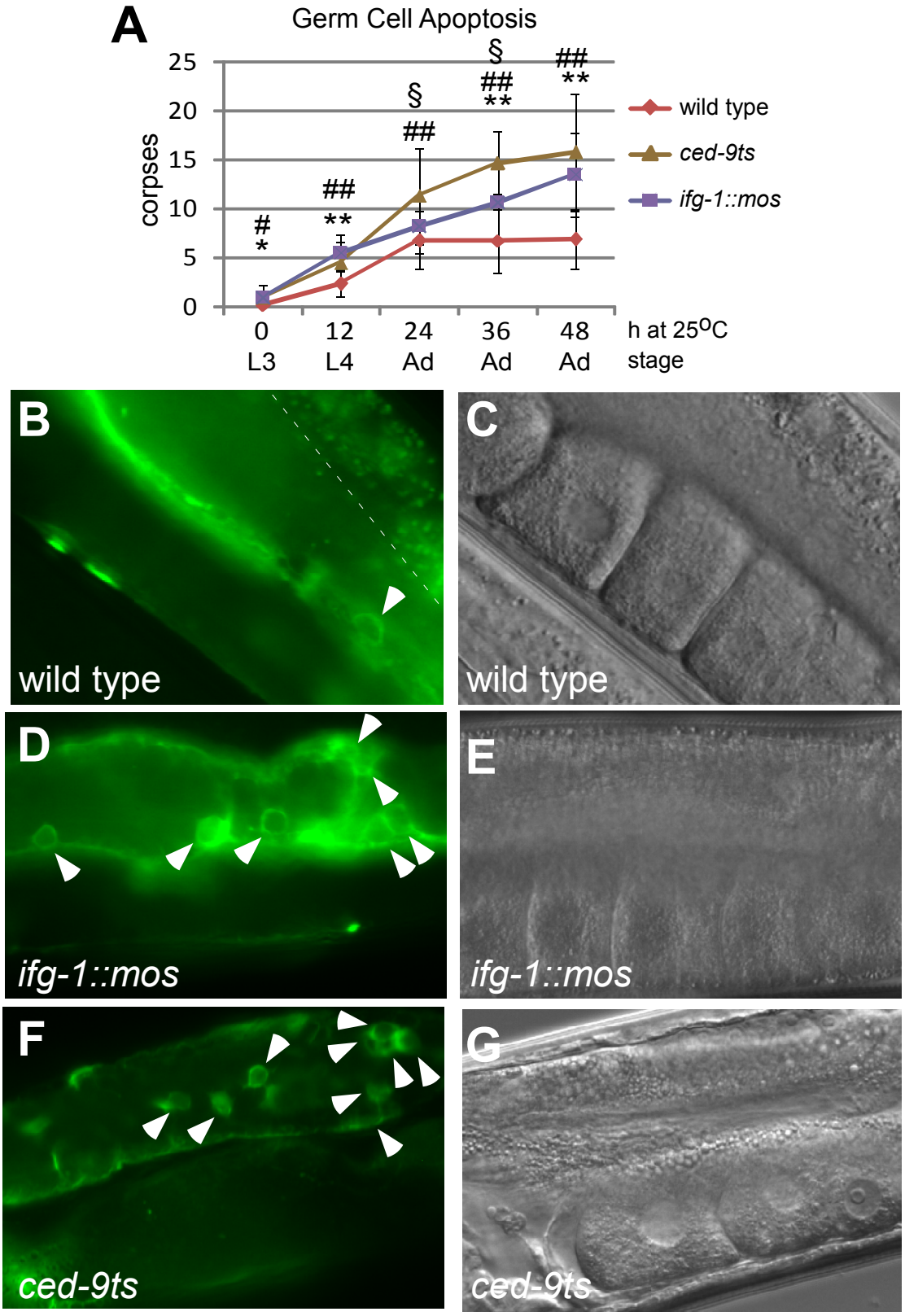
A
Germ Cell Apoptosis
corpses
25
20
15
10
5
0
0
L3
12
L4
24
Ad
36
Ad
48
Ad
h at 25°C
stage
wild type
ced-9ts
ifg-1::mos
B
wild type
C
wild type
D
ifg-1::mos
E
ifg-1::mos
F
ced-9ts
G
ced-9ts

Figure 2.2. *ifg-1::mos* transgenic lines exhibit a marked increase in apoptotic corpses in the germ line. (A) A graph depicting CED-1::GFP decorated corpses in the wild type, *ifg-1::mos*, and *ced-9ts* strains over time. There is an initial increase in apoptosis in all of the strain as they mature from the L3 larval stage, in which sperm fills the gonad and there is little to no apoptosis. During the L4 larval stage oocytes begin to progress through the gonad and the level of constitutive apoptosis increases. The level of apoptosis within the adult wild type gonad remains constant over time. However, the levels of apoptosis in the *ifg-1::mos* and c*ed-9ts* lines continue to increase during the adult stage. **ifg-1::mos* significantly different from wild type strain $p<0.05$, ** $p<0.001$, # *ced-9ts* significantly different from the wild type strain $p<0.01$, ## $p<0.001$, § *ifg-1::mos* significantly different from c*ed-9ts* strain $p<0.001$. (B and C) Fluorescence and DIC image of wild type, *ifg-1::mos* (D and E) and *ced-9ts* (F and G) strains expressing the CED-1::GFP apoptotic marker after 24 hours at 25°C. DIC images confirm normal growth and differentiation of oocytes within the gonads of mutant strains.

physiological changes in the relative p130: p170 representation may affect translation initiation. The gonads of adult worms of both *ifg-1::mos* and *ced-9ts* strains showed visually obvious increases in the prevalence of germ cell corpses (Figure 2.2B, 2.2D and 2.2F). Importantly, all strains showed normally developed gonads with a typical linear progression of developing germ cells that mature into oocytes (Figure 2.2C, 2.2E and 2.2G). The strains displayed no other marked morphological defects.

The *ifg-1::mos* strain displays decreased fertility and embryo viability. The prevalence of apoptosis among germ cells is expected to result in a decrease in the number of viable oocytes reaching maturity. However, it is unclear if surviving oocytes are themselves fully competent to develop as embryos upon fertilization. To correlate the increase in germ cell apoptosis with a decrease in *ifg-1::mos* fertility, we followed egg laying in wild type and *ifg-1::mos* hermaphrodites. Simultaneously, we monitored the course of development to address any subsequent developmental defects in the *ifg-1::mos* hermaphrodites. We found only a modest decrease in the number of total eggs laid by the *ifg-1::mos* worms at 25°C (Data not shown). The wild type strain laid about 228 eggs per hermaphrodite mother, whereas the *ifg-1::mos* strain laid about 148 eggs. The more significant effect of depleting cap-associated IFG-1 p170 was substantial embryonic lethality and arrest in early larval development. The majority of wild type eggs mature into L3 or L4 larvae by 48 hours (Data not shown). By comparison, less than a third of *ifg-1::mos* eggs are able to enter larval development and these arrest at larval L1/L2 stages. By 96 hours only 11 of those larvae (just under 7% of all eggs laid) reached maturity as adults. In comparison, over 191 wild type eggs (84%) developed into fertile adult offspring. Diminished fecundity is not an

anomaly. Similar results were seen previously with the *ifg-1*(ok1211) null worms and IFG-1 p170 RNAi. We previously observed both embryonic lethality and L2 larval arrest when IFG-1 function was disrupted (Contreras et al., 2008). L2 larval arrest is the terminal phenotype of *ifg-1*(ok1211) null worms. Embryonic lethality and the induction of apoptosis were observed upon IFG-1 p170 knockdown due to RNAi. These data suggest that depletion of cap-associated IFG-1 p170 promotes cap-independent translation in the gonad and subsequent apoptosis leading to a corresponding reduction in fertility. Our findings also suggest two other critical developmental steps rely on sufficient IFG-1 activity; progression through embryogenesis and the growth that accompanies early larval development.

***hsp-3* mRNA is translated more efficiently when cap-associated IFG-1 p170 is depleted.** The *ifg-1::mos* and *ced-9ts* strains provided the opportunity to study how changes in the representation of the IFG-1 can affect the recruitment of target mRNAs for translation. Recently, Li, et al. identified an IRES in the 5' UTR of extended transcripts of the *C. elegans hsp-3* mRNA. This IRES allowed *hsp-3* mRNA to be translated cap-independently, much like its mammalian homologue BiP (Li and Wang, 2012; Yang and Sarnow, 1997). In human cell lines, the *BiP* mRNA IRES allows for enhanced BiP expression during heat shock, facilitating cellular recovery by chaperoning protein folding (Cho et al., 2007). We investigated the translational control of *hsp-3* mRNA after depletion of cap-associated IFG-1 p170 and following induction of apoptosis via the *ced-9ts/Bcl-2* mutation. Polysome profiling was used to observe changes in translational efficiency of *hsp-3* mRNA and the ubiquitously expressed *gpd-3* (GAPDH) mRNA as a control. Worm lysates from the wild

Figure 2.3

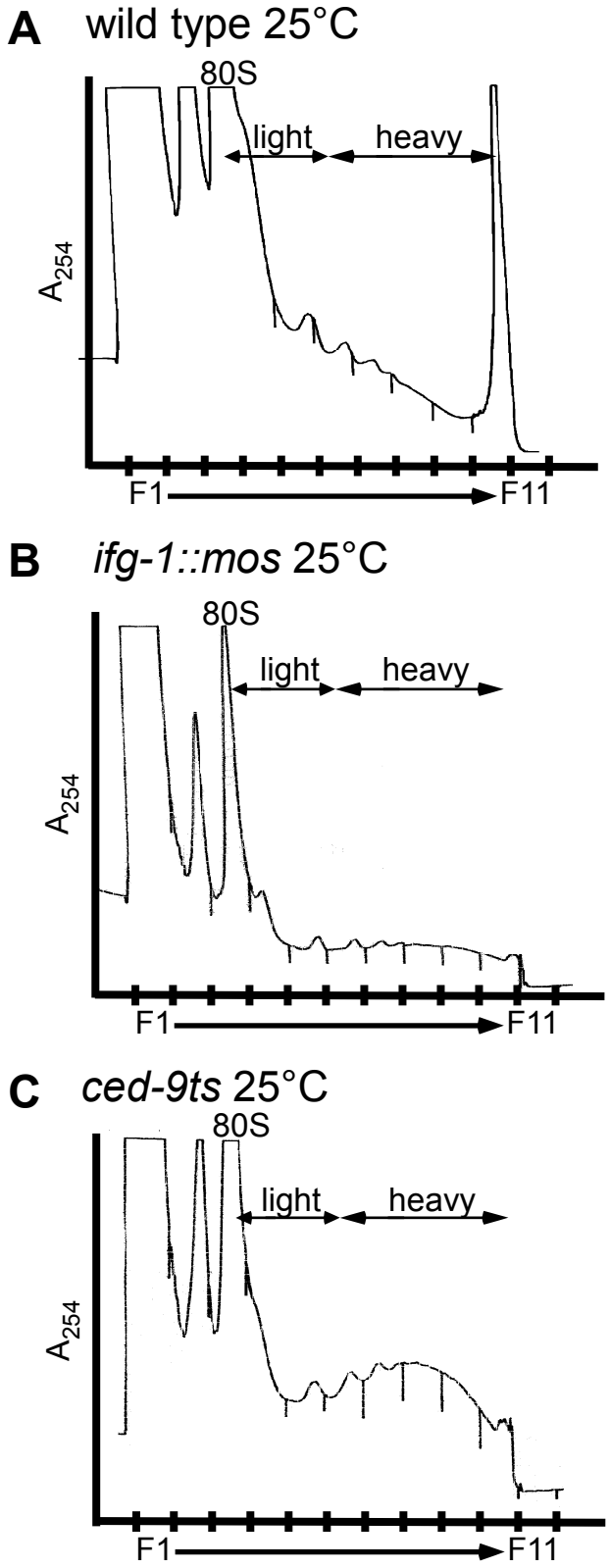
A wild type 25°C
80S
light
heavy
A254
F1
F11
B ifg-1::mos 25°C
80S
light
heavy
A254
F1
F11
C ced-9ts 25°C
80S
light
heavy
A254
F1
F11

Figure 2.3. Polysome profiles from sucrose gradients with continuous monitoring of absorbance at 254nm. During sucrose gradient fractionation of worm lysates from wild type (A), *ifg-1::mos* (B) and *ced-9ts* (C) strains absorbance was measured at 254nm. These gradients represent 1 of 4 biological replicates of wild type and *ced-9ts* strains and 1 of 2 biological replicates of the *ifg-1::mos* strain. The profiles of biological replicates closely resemble one another and confirm the observed changes in translational efficiency.

type, *ifg-1::mos*, and *ced-9ts* (Figure 2.3A-C) strains were fractionated on sucrose gradients to resolve polyribosomal complexes. mRNAs were quantified across the gradient by quantitative real-time PCR (qPCR) to monitor changes in their mRNA distributions that reflect the number of bound ribosomes. The percentage of each specific mRNA represented in each fraction was calculated to determine the translational activity of the target mRNA. Induction of apoptosis was monitored in each strain by visualizing corpses (Figure 2.2A-G) in order to correlate increased apoptosis with changes in the efficiency of translation of target messages (Figure 2.4A-B). As expected, *gpd-3* mRNA was translated efficiently in the wild type strain. A modest decrease in the translational efficiency of *gpd-3* was detected in the *ifg-1::mos* strain indicated by the leftward shift in the mRNA distribution. *gpd-3*, however, still translated pretty efficiently on heavy polysomes (Figure 2.4A). This modest decrease in translation was not unexpected in the *ifg-1::mos* strain where reduced levels of both IFG-1 isoforms are found. When the function of Bcl-2 was abrogated in the *ced-9ts* strain, the distribution of *gpd-3* mRNA among polysomes broadened, but the median of the message distribution mirrored that of the wild type strain (Figure 2.4B). These data demonstrate that the *gpd-3* mRNA remains relatively efficiently translated under both conditions that trigger IFG-1 p170 depletion/cleavage and apoptosis.

The translational efficiency of *hsp-3* was similarly measured by polysome loading to determine if reduced p170 levels, due to the *ifg-1* splicing defect (*ifg-1::mos*) or cleavage during apoptosis (*ced-9ts*), altered its translation. Both the *ifg-1::mos* and *ced-9ts* strains showed consistent, modest increases in *hsp-3* mRNA translational efficiency (Figure 2.4C-D). This increase is significant due to the overall shift of the mRNA density into the more efficiently translating fractions near the bottom of the gradient. It should be noted that

Figure 2.4

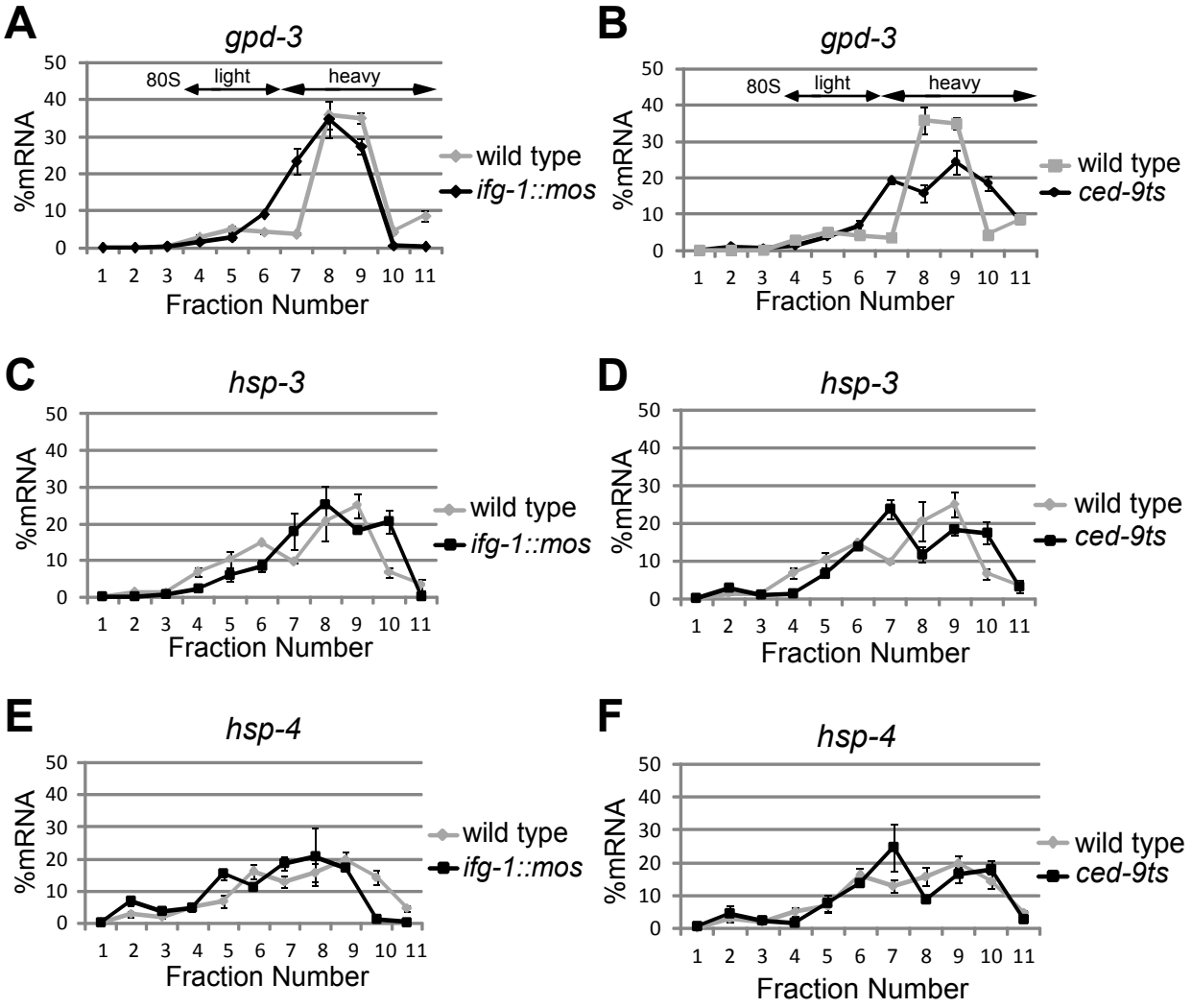
A
gpd-3
80S
light
heavy
%mRNA
Fraction Number
wild type
ifg-1::mos
B
gpd-3
80S
light
heavy
%mRNA
Fraction Number
wild type
ced-9ts
C
hsp-3
%mRNA
Fraction Number
wild type
ifg-1::mos
D
hsp-3
%mRNA
Fraction Number
wild type
ced-9ts
E
hsp-4
%mRNA
Fraction Number
wild type
ifg-1::mos
F
hsp-4
%mRNA
Fraction Number
wild type
ced-9ts

Figure 2.4. *hsp-3* mRNA is translated more efficiently after the reduction of cap-associated p170 abundance. RNA distributions quantified by qPCR in each gradient fraction indicate changes in translational efficiency of *gpd-3* in the *ifg-1::mos* (A) and *ced-9ts* (B) strains in comparison to the wild type strains. The percent mRNA was quantified by calculating the amount of a specific target mRNA in each fraction then dividing by the total amount of that mRNA across the entire gradient and multiplying by 100. qPCR quantified RNA distributions indicating changes in the translational efficiency of *hsp-3* in the *ifg-1::mos* (C) and *ced-9ts* (D) strains in comparison to the wild type strain. Changes in translational efficiency of *hsp-4* in the *ifg-1::mos* (E) and c*ed-9ts* (F) strains are indicated by qPCR quantification of gradient fractions. All qPCR results from the *ced-9ts* strain were confirmed in four biological replicates and *ifg-1::mos* strain in biological duplicates.

polysome resolution is non-linear on sucrose gradients. Shifts in position near the top of the gradient (fractions 4-7) represent increases of one or two ribosomes bound. However, equivalent shifts at the bottom of the gradient (fractions 8-11), as are observed for *hsp-3* mRNA (especially noting shifts in fraction 10), represent a much larger addition of bound ribosomes and therefore a much greater increase in translational efficiency. *hsp-3* mRNA also becomes depleted from light polysomes as additional ribosomes bind and increase the message's representation in the heavy polysome regions of the gradient. The change in translational efficiency was confirmed in biological replicates with similar curves that depicted the same increase in translational efficiency. The authenticity of mRNA sedimentation due to ribosome association was confirmed by pretreatment with EDTA prior to centrifugation to release *hsp-3* (and other) mRNAs from ribosomes (data not shown). Most importantly, *hsp-3* translates more efficiently under stress and pro-apoptotic conditions that inhibit the translation of most other cellular mRNAs. Increased ribosome association, indicative of enhanced initiation rate, occurred despite decreases in the cap-associated eIF4 complex. This provides a correlation between enhanced *hsp-3* translation and cap-independent translation conditions.

Expressed sequence tags (ESTs) reveal a rare (1 in 300), longer *hsp-3* mRNA variant that has IRES characteristics in the extended 5' UTR. However, the increase in translational efficiency of bulk *hsp-3* mRNA most likely is not the result of an IRES in the 5' UTR. Mapping the 5' end of the *hsp-3* mRNA by RNase protection assay (RPA) using an antisense probe covering all of the mature mRNA forms was performed on RNA from wild type, *ifg-1::mos, ced-9ts* and wild type temperature stressed worms (Figure 2.5A). A full length, 5'-extended mRNA was not detected (Figure 2.5B). However, two short mRNAs indicative of about a 25

nucleotide 5' UTR were found. RNA quality was confirmed by RPA using a 3' UTR *act-1* probe. When detecting the translational efficiency of *hsp-3* mRNA using qPCR, we used internal primers designed to detect all *hsp-3* populations, so it is unlikely the overall translational efficiency would be affected by a minor extended mRNA population, if present. Thus, although *hsp-3* is translated more efficiently after the depletion of IFG-1 p170, this increase in translational efficiency is not due in large part to the upstream IRES sequence.

Another BiP homologue mRNA, *hsp-4,* has little change in translational efficiency during cap-independent conditions. BiP has two *C. elegans* homologues HSP-3 and HSP-4 (Heschl and Baillie, 1990). Both homologues are localized to the ER as chaperones involved in stress response to heat shock (Heschl and Baillie, 1989). Unlike *hsp-3,* however, which is constitutively transcribed, *hsp-4* mRNA levels are almost undetectable during non-stressed conditions (Heschl and Baillie, 1990). The *hsp-4* gene becomes transcriptionally activated with the onset of stress (Heschl and Baillie, 1990). Although *hsp-3* and *hsp-4* mRNA coding regions share 70% nucleotide identity, *hsp-3* has conserved sequences in its 5' UTR not present in *hsp-4* (Heschl and Baillie, 1989, 1990). These sequences are conserved among several distant nematode species and even in rats (Heschl and Baillie, 1989). *hsp-4* mRNA also lacks most of the defined IRES region of *hsp-3* mRNA. Given the strong homology between these mRNAs but differences in 5' leader sequences, we sought to determine if *hsp-4* mRNA behaves similarly or differently from *hsp-3* mRNA upon depletion of IFG-1 p170. We observed that *hsp-4* mRNA translational efficiency changed in a way that mirrored changes in *gpd-3* mRNA distribution. There was a slight decrease in the efficiency

Figure 2.5

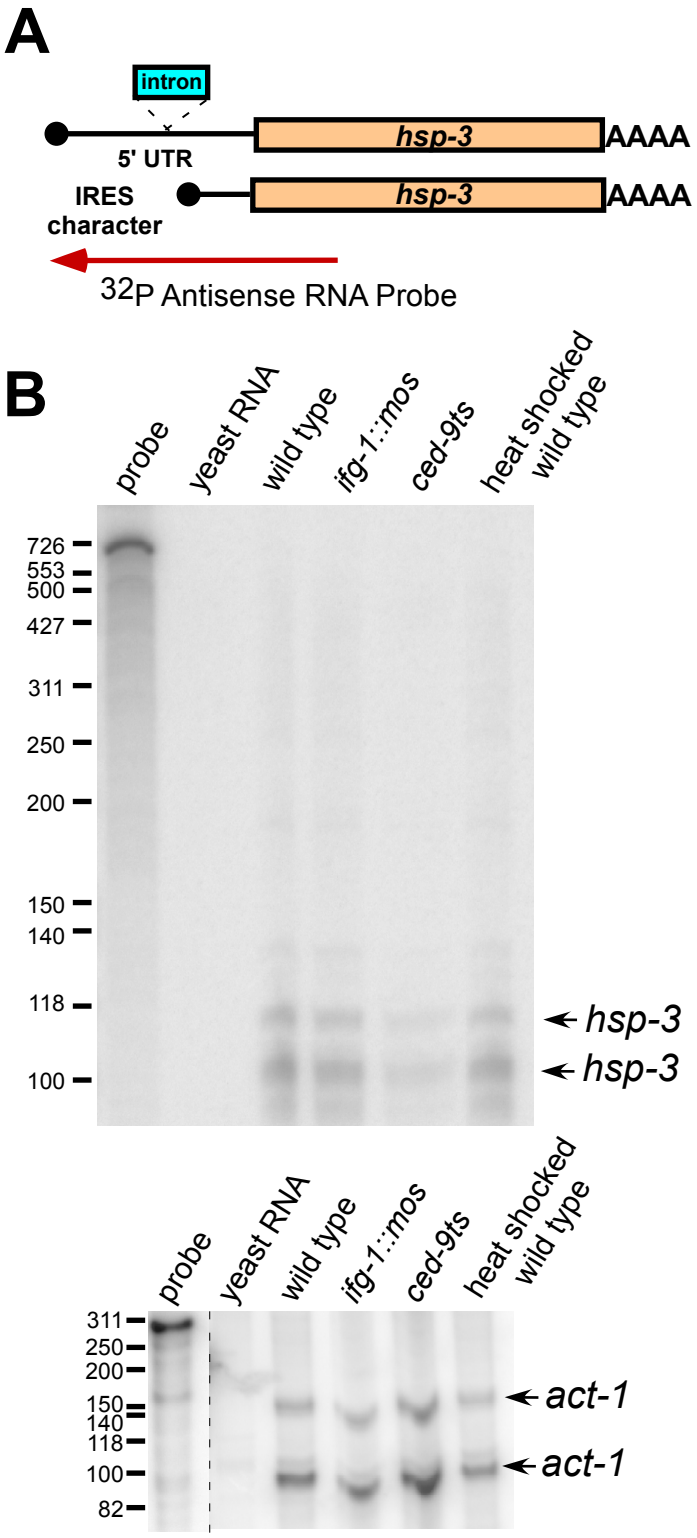
A
intron
hsp-3
AAAA
5' UTR
IRES
character
hsp-3
AAAA
32P Antisense RNA Probe
B
probe
yeast RNA
wild type
ifg-1::mos
ced-9ts
heat shocked
wild type
726
553
500
427
311
250
200
150
140
118
100
hsp-3
hsp-3
probe
yeast RNA
wild type
ifg-1::mos
ced-9ts
heat shocked
wild type
311
250
200
150
140
118
100
82
act-1
act-1

Figure 2.5. 5' UTR of extended *hsp-3* mRNA is not detected in total *C. elegans* RNA. (A) Diagram indicating the coverage of the *hsp-3* mRNA probe. The arrow indicates the RPA probe extending upstream from exon 1 and covering all potential mRNA variants. (B) RNase Protection Assays were conducted by hybridizing the 5' probe to total mRNA in wild type, *ced-9ts, ifg-1::mos* and wild type heat shocked strains. The arrows indicate the two detected *hsp-3* mRNA 5' variants. Control RNase Protection Assay detecting *act-1* mRNA is shown to demonstrate RNA quality.

of *hsp-4* translation in the *ifg-1::mos* strain (Figure 2.4E) and no change in *ced-9ts* worms (Figure 2.4F) relative to wild type. The slight decrease suggests that *hsp-3* mRNA has a greater capacity to undergo cap-independent translation, although both messages maintain relatively efficient translation after the knockdown of IFG-1 p170. Thus, while *hsp-3* is stress-regulated at the level of translation, *hsp-4* may only be regulated by transcriptional control.

Bcl-2 homologue mRNA, *ced-9*, is translated more efficiently upon cleavage of IFG-1 p170, but not upon genetic depletion. mRNA encoding B-cell lymphoma 2 (Bcl-2), an anti-apoptotic regulator in the apoptotic pathway, is translated cap-independently via an IRES during mammalian apoptosis (Sherrill et al., 2004). We assayed the translational control of the *C. elegans* Bcl-2 homologue, *ced-9*, by polysome resolution. In wild type worms, *ced-9* mRNA is distributed bimodally (Figure 2.6A and 2.6B). The majority of the mRNA resides in the medium-sized polysomes, while a lesser portion is broadly associated among very light polysomes. Following the induction of apoptosis in *ced-9ts* mutant worms, *ced-9* mRNA from both populations becomes translated more efficiently (Figure 2.6B). Like *hsp-3* mRNA, the heavier peak of *ced-9* mRNA moves near the bottom of the gradient from fraction 9 to fraction 10 indicating a substantial increase in the number of bound ribosomes and an increase in the efficiency of translation. Some *ced-9* mRNA also mobilizes from the non-translating or very light polysome region into the moderately translating region (from fractions 4-5 into fraction 7). The *ced-9ts* strain undergoes loss of CED-9 function due to a point mutation in *ced-9* mRNA. This mutation did not result in changes in *ced-9* mRNA accumulation nor directly enhanced *ced-9* mRNA translation. Rather the

Figure 2.6

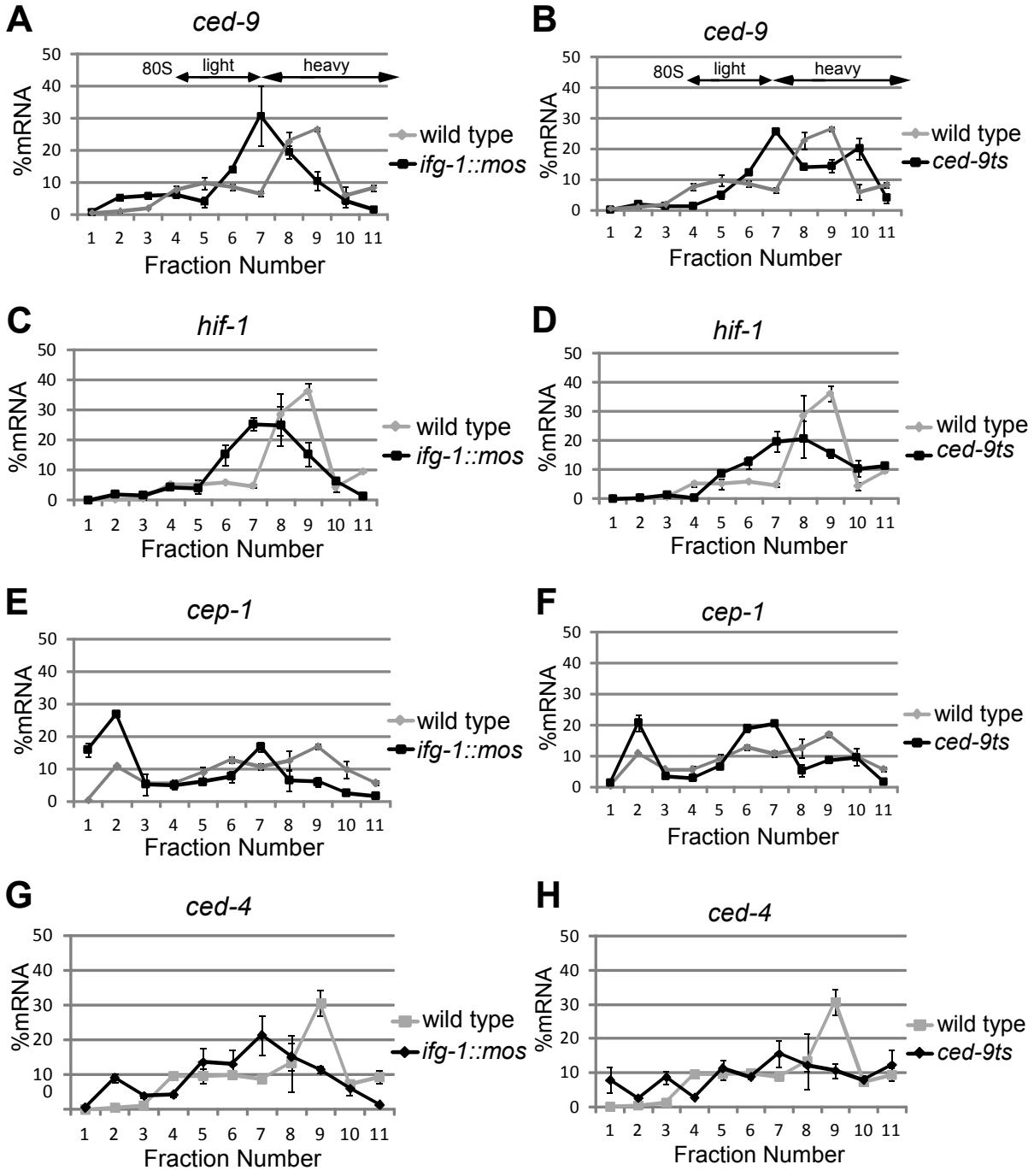
A
ced-9
80S
light
heavy
%mRNA
Fraction Number
wild type
ifg-1::mos
B
ced-9
80S
light
heavy
%mRNA
Fraction Number
wild type
ced-9ts
C
hif-1
%mRNA
Fraction Number
wild type
ifg-1::mos
D
hif-1
%mRNA
Fraction Number
wild type
ced-9ts
E
cep-1
%mRNA
Fraction Number
wild type
ifg-1::mos
F
cep-1
%mRNA
Fraction Number
wild type
ced-9ts
G
ced-4
%mRNA
Fraction Number
wild type
ifg-1::mos
H
ced-4
%mRNA
Fraction Number
wild type
ced-9ts

Figure 2.6. Other stress and apoptotic mRNAs, *ced-9* (Bcl-2), *hif-1* (HIF-1), *cep-1* (p53) and *ced-4* (Apaf-1) have differing abilities to be translated after depletion of cap-associated IFG-1 p170. RNA distributions were quantified by qPCR in wild type, *ifg-1::mos*, and *ced-9ts* strains from polysome profiles depicted in Figure 2.3. These gradients represent 1 of 4 biological replicates of wild type and *ced-9ts* strains and 1 of 2 biological replicates of the *ifg-1::mos* strain. Changes efficiency of *ced-9* mRNA translation was determined in *ifg-1::mos* (A) and *ced-9ts* (B) strains in comparison to the wild type strain. RNA distributions quantified by qPCR indicating changes in translational efficiency of *hif-1* in the *ifg-1::mos* (C) and *ced-9ts* (D) strains in comparison to the wild type strains. qPCR quantified RNA distributions indicating changes in the translational efficiency of *cep-1* in the *ifg-1::mos* (E) and *ced-9ts* (F) strains in comparison to the wild type strain. Changes in efficiency of total c*ed-4* mRNA translation were determined in *ifg-1::mos* (G) and *ced-9ts* (H) strains in comparison to the wild type strain. All qPCR data was confirmed in biological duplicates.

changes in the efficiency of translation resulted from the induction of apoptosis. Thus, *ced-9* in the whole worm was translated similarly to its mammalian homologue during apoptotic stress. Conversely, *ced-9* mRNA translation was not enhanced by IFG-1 depletion in the *ifg-1::mos* strain (Figure 2.6A). It is possible that the decrease in both IFG-1 p170 and p130 in this strain is suboptimal for *ced-9* mRNA initiation. CED-9 has both pro- and anti-apoptotic functions in *C. elegans* making it an interesting candidate for translational control during apoptosis (Galvin et al., 2011). Overall, these results suggest that cleavage of IFG-1 p170, resulting in increased p130-like products, may differ translationally from genetic IFG-1 depletion, resulting in decreased expression of both p170 and p130.

Other stress and apoptotic mRNAs, *hif-1* (HIF-1) and *cep-1* (p53), have decreased translational efficiency upon depletion of IFG-1 p170. Mammalian hypoxia inducible factor 1 (*hif-1*) is a transcription factor that promotes cell survival during hypoxia (Keith and Simon, 2007). HIF-1 mRNA is translated efficiently under cap-independent conditions during hypoxia in mammalian cell lines (Lang et al., 2002). p53 mRNA, encoding a key regulator of DNA damage-induced apoptosis, is translated via an IRES (Weingarten-Gabbay et al., 2013). We investigated whether *C. elegans hif-1* (HIF-1) and *cep-1* (p53) mRNAs are also translated more efficiently in *ifg-1::mos* and *ced-9ts* worms. Contrary to expectations, decreases in p170 due to the *ifg-1* splicing defect (Figure 2.6C and 2.6E) or its cleavage during apoptosis (Figure 2.6D and 2.6F) lead to a decrease in *hif-1* and *cep-1* mRNA translational efficiency. In both cases the *hif-1* and *cep-1* mRNAs move from very heavy polysomal loading to medium-sized polysomes or, in the case of *cep-1* mRNA off polysomes entirely. This decreased efficiency indicates that *hif-1* and *cep-1* mRNAs require the cap-

associated IFG-1 p170 for efficient translation. Thus, despite the importance of HIF-1 and p53 mRNAs during stress conditions in mammalian cell lines, these mRNA do not have a selective translational advantage during stress and/or apoptosis in *C. elegans*.

***ced-4* (Apaf-1) mRNA translation is not induced by IFG-1 p170 depletion.** An IRES in the 5' UTR of mammalian Apaf-1 allows for its synthesis after the induction of cap-independent translation (Coldwell et al., 2000). We previously observed that RNAi knockdown of IFG-1 p170 not only increased the number of germ cell corpses, but also induced the appearance of punctate CED-4 (Apaf-1) structures typical of apoptosome formation in dying oocytes (Contreras et al., 2008). Together these data lead us to investigate whether *C. elegans* c*ed-4* mRNA also encodes an IRES promoting its cap-independent translation. Due to its integral role in the apoptosome and potential IRES characteristics in its 5' UTR (see Figure 2.7), we expected that the translational efficiency of *ced-4* mRNA to increase after IFG-1 p170 depletion. Contrary to our predictions, *ced-4* mRNA underwent a significant decrease in translational efficiency in both the *ifg-1::mos* (Figure 2.6G) and *ced-9ts* (Figure 2.6H) strains. Not only does c*ed-4* message shift to regions in the gradient containing fewer ribosomes, a portion of the mRNA leaves the polysomal region entirely. Thus, the induction of apoptosis and cap-independent conditions inhibit translation initiation of *ced-4* mRNA. As this result was inconsistent with the IRES-mediated translation of mammalian Apaf-1, it was necessary to carefully characterize the 5' structure of *ced-4* mRNA to see if such sequences were present in *C. elegans* mRNA.

Figure 2.7

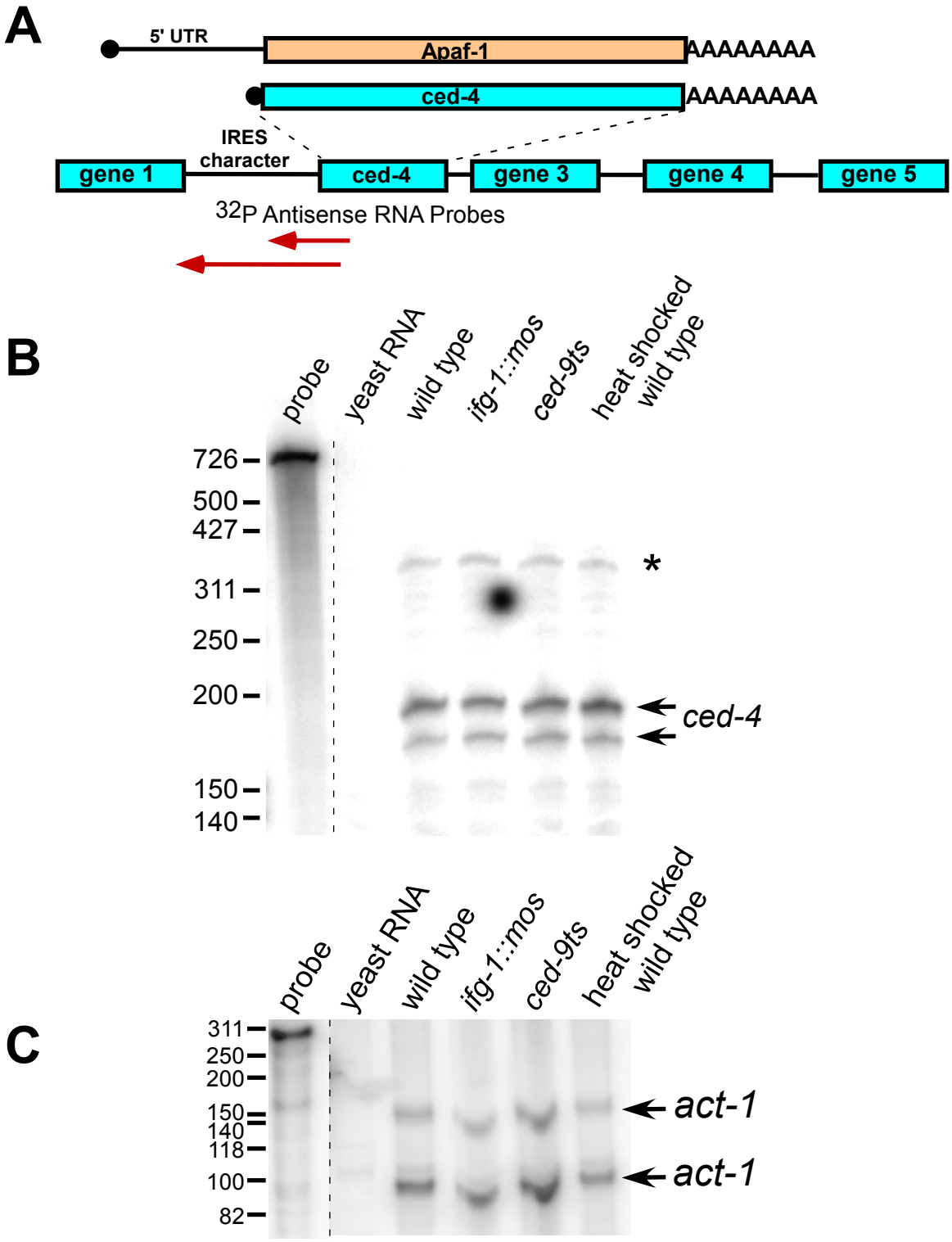
A
5' UTR
Apaf-1
AAAAAAAA
ced-4
AAAAAAAA
IRES
character
gene 1
ced-4
gene 3
gene 4
gene 5
32P Antisense RNA Probes
B
probe
yeast RNA
wild type
ifg-1::mos
ced-9ts
heat shocked
wild type
726
500
427
311
250
200
150
140
*
ced-4
C
probe
yeast RNA
wild type
ifg-1::mos
ced-9ts
heat shocked
wild type
311
250
200
150
140
118
100
82
act-1
act-1

Figure 2.7. *ced-4* mRNA structure and mode of translation differs from that of Apaf-1 mRNA. (A) Diagram comparing *C. elegans* c*ed-4* and mammalian Apaf-1 mRNAs. *ced-4* is the second gene in an operon with a canonical trans-splice splice site adjacent to its translation start site leaving no encoded 5' UTR. However, the intergenic region upstream of this splice site has sequence typical of an IRES, such as polypyrimidine tracts and multiple AUG start sites. The arrow indicates the RPA probe extending upstream from exon 1 into the intergenic region. The probe was used to attempt to detect extended c*ed-4* message variants. (B) RNase Protection Assays were conducted by hybridizing the 5' probe to total mRNA in wild type, *ced-9ts*, *ifg-1::mos* and wild type heat shocked strains. The arrows indicate the SL2 trans-spliced message variant. A band consistent with extended *ced-4* mRNA that could not be confirmed with longer *ced-4* mRNA probe or other characterization methods (*). (C) Control RNase Protection Assay detecting *act-1* mRNA is shown to demonstrate RNA quality.

***ced-4* mRNA lacks the extended 5' UTR containing an IRES that is present in Apaf-1 mRNA.** We hypothesized that some or all of the conserved intergenic region upstream of the *ced-4* translation start site could be present in mature *ced-4* mRNA. This region contains sequences characteristic of a putative IRES (Figure 2.7A) that may allow the mRNA to be translated after the knockdown of cap-associated IFG-1 p170. To detect 5' extended *ced-4* mRNA variants, we again performed RNase protection assays (RPAs) on RNA isolated from wild type, *ifg-1::mos*, *ced-9ts* and wild type heat shocked (Figure 2.7B) worms using a radiolabeled probe that extended from exon 1 upstream into the intergenic region. Two protected fragments indicative of standard SL2 trans-spliced mRNA that lacked putative IRES sequence were detected in all RNA populations. We did observe a larger band consistent with a longer mRNA variant (*). However, in attempts to confirm this mRNA variant using an RNA probe that extended through the entire intergenic region, we never observed a longer RNA variant (Figure 3.5A). Additionally, the putative extended mRNA was never detected in polysomal or poly(A) RNA (see Chapter 3). RNA quality was confirmed using an RNase Protection Assay of *act-1* mRNA (Figure 2.7C). As final confirmation of the absence of 5' extended (IRES) c*ed-4* mRNA forms, we performed RT-PCR on circularized, end-ligated mRNA using diverging primers in exon 8 and exon 1 (Figure 2.8A). This procedure amplified the ligated junction between the decapped 5' end and poly(A) tail. Only clones beginning with SL2 splice leader sequence adjacent to the start codon were observed (Figure 2.8B). No sequences indicative of a 5' extended *ced-4* mRNA variant were ever found. Therefore, *ced-4* mRNA does not encode a 5' IRES as does its mammalian counterpart. Two 3' UTR variants for *ced-4* mRNA were characterized, including 219 and 257 nt past the termination codon, suggesting alternate polyadenylation

Figure 2.8

A

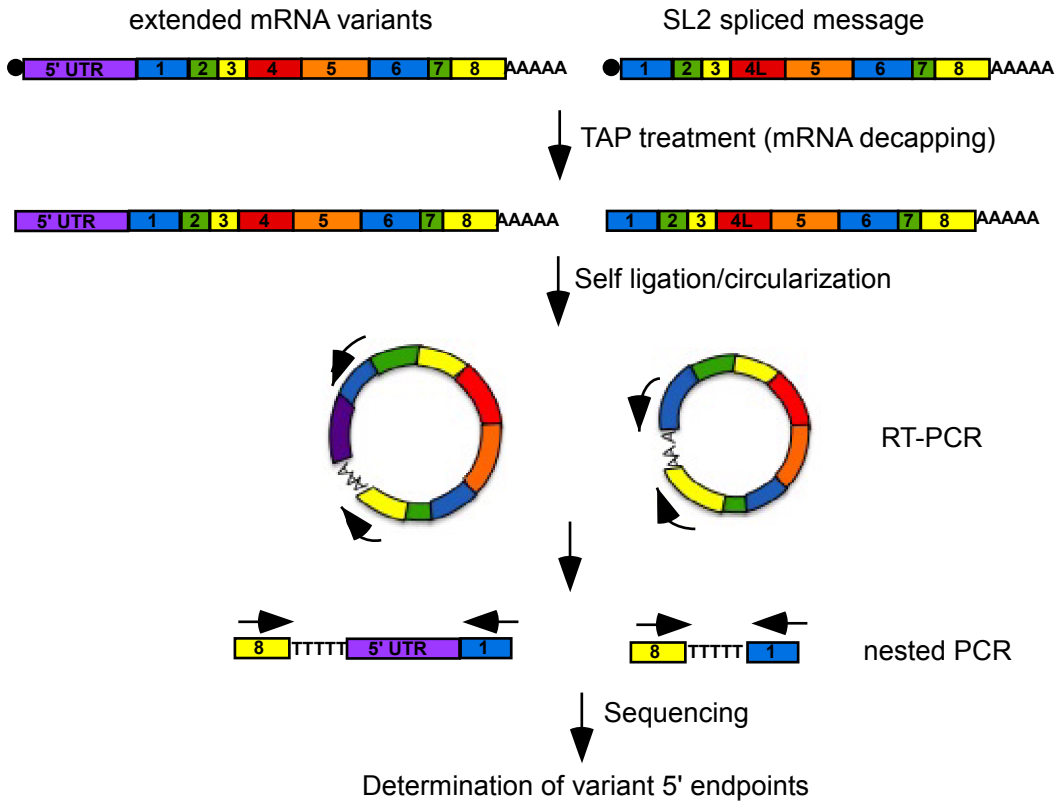
extended mRNA variants
SL2 spliced message
5' UTR
1
2
3
4
5
6
7
8
AAAAA
4L
TAP treatment (mRNA decapping)
Self ligation/circularization
RT-PCR
TTTTT
nested PCR
Sequencing
Determination of variant 5' endpoints

B

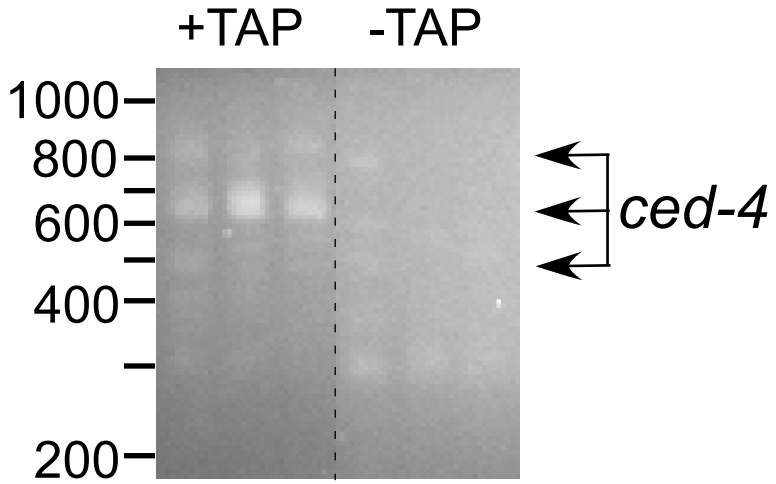
+TAP
-TAP
1000
800
600
400
200
ced-4

Figure 2.8. Verification of *ced-4* mRNA endpoints by circularized RT-PCR. (A) Schematic representing cRT-PCR strategy and possible outcomes. (B) Total messenger RNA was isolated from *C. elegans* wild type worms. These mRNAs were decapped using TAP to allow T4 ligation of the 5' end and the poly(A) tail of mRNAs. cDNA across the junction was then synthesized. An additional nested PCR was performed and the resulting cDNA amplifications were subcloned and sequenced. Agarose gel electrophoresis of nested PCR across the ligated junction is shown. Extended mRNA variants differed due to poly(A) tail size and alternative 3' end points.

sites. The lack of a *ced-4* IRES suggests translational regulation of Apaf-1 mRNA differs during nematode apoptosis compared to stressed mammalian cells.

Discussion

Normal cells and tissues utilize both cap-dependent and cap-independent mechanisms of translation initiation to recruit cellular mRNAs (Gilbert, 2010; Komar et al., 2012; Malys and McCarthy, 2011). The relative amount of the cap-independent contribution varies in quiescent, dividing and differentiating cells. It varies as well in response to stress, apoptosis and viral infection (Contreras et al., 2008; Keiper and Rhoads, 1997). The contribution is usually dictated by isoforms of eIF4G and their proteolytic cleavage (Contreras et al., 2008; Keiper and Rhoads, 1997). In this study we demonstrated a physiological link between levels of cap-associated eIF4G (IFG-1 p170) and translational control of cell death and chaperone mRNAs in whole worms when responding to apoptosis and translational stress. These studies demonstrate that cap-independent translation can play a role in the natural apoptotic cell fate decision in healthy, whole organisms and their natively differentiating cell lineage (e.g. germ cells). Genetic depletion of a key translation initiation factor (IFG-1 p170), or its cleavage during *ced-9ts*-induced apoptosis, caused a subset of mRNAs to increase in translational efficiency. This illustrates that these mRNAs may utilize cleaved IFG-1 p170 or constitutively non-cap associated p130 for their initiation. Conditions that produced enhanced cap-independent initiation favored more efficient translation of *C. elegans hsp-3* (BiP) mRNA *in vivo.* As demonstrated, these conditions may be either genetic depletion of IFG-1 p170 (eIF4G) or CED-9 (Bcl-2) inactivation that leads to IFG-1 p170 cleavage by CED-3 (caspase). Ultimately, the

translational mechanism may be identical. These data are consistent with translational enhancement of the mammalian BiP mRNA after the induction of cap-independent protein synthesis (Buchkovich et al., 2010). The mammalian BiP is translated cap-independently via an IRES sequence in its 5' UTR (Koong et al., 1994). Although Li et al. demonstrated enhanced expression of a downstream cistron from the *hsp-3* putative 5' UTR in a bicistronic transgenic reporter, our RNase protection mapping of *hsp-3* mRNA 5' ends indicates that all of the detectable *hsp-3* transcripts have short (~25 nt) 5' UTRs that lack the purported IRES (Li and Wang, 2012). The sequence used by Li et al. to drive bicistronic expression also contained an intron sequence that is spliced out of the single known, extended *hsp-3* expressed sequence tag (WormBase, 2007). The *hsp-3* upstream intron has been reported to contain enhancer elements and a TATA box that appear to promote transcription initiation from the start site that we have mapped (Heschl and Baillie, 1989, 1990). Our data indicate that short *hsp-3* mRNAs translate efficiently cap-independently and their cap-independent translation is not dependent on the purported IRES. There are numerous precedents showing heat shock protein mRNAs that lack IRESes still translate by cap-independent mechanisms in stressed mammalian and plant cells, and in virus infected cells (Dinkova et al., 2005; Joshi-Barve et al., 1992; Rhoads and Lamphear, 1995; Schneider, 1995). *C. elegans hsp-3* mRNA is clearly one of these cap-and IRES-independent mRNAs. The translational efficiency of *ced-9* (Bcl-2) mRNA also increased after CED-9 inactivation. The disruption of Bcl-2 function in living worms allowed us to look at physiologically induced change in IFG-1 isoform representation leading to enhanced *ced-9* mRNA translation (producing an inactive protein). These experiments illustrate the importance of

eIF4G (IFG-1 p170 and p130) isoform representation in selecting mRNAs for translation in response to stressors to the organism.

It is notable that the differences in mRNA translational efficiency were observed as changes in polysomal mRNA distribution in total worm lysates. Certainly apoptotic or stressor stimuli in individual cell types or tissues would lead to more robust recruitment of unique mRNAs for translation than we document here. Most likely the changes we observed in translational efficiency were muted due to the large number of somatic and germ cells not undergoing apoptosis. We expect, then, that changes in translational efficiency within individual cells result in large changes in protein synthesis that may determine their differentiated vs. apoptotic state. Clearly, the changes in translation initiation were robust enough to enhance germ cell apoptosis and decrease fecundity. The number of germ cell corpses increased to a level equivalent to that observed when the apoptotic pathway was directly affected. As expected, increased apoptosis decreased the fertility of *ifg-1::mos* adult hermaphrodites. We also observed that constricting cap-dependent translation resulted in a high level of embryonic lethality and arrested larval development. The multiple developmental arrests support our previous findings on the importance of cap-dependent protein synthesis to normal worm development (Contreras et al., 2011; Henderson et al., 2009).

Several putative cap-independent IRES mRNAs did not respond similarly to cap-independent conditions in whole worms. Although HIF-1, Apaf-1 and p53 mRNAs are reported to translate cap-independently in mammalian cell culture via IRES sequences, we did not observe similar translational enhancement in *C. elegans*. Instead, *C. elegans* homologues of these mRNAs translated less efficiently when cap-associated IFG-1 p170

was depleted. *hif-1* (HIF-1)*, cep-1* (p53), and *ced-4* (Apaf-1) mRNAs were markedly absent from heavy polysomes suggesting they were at a disadvantage for initiation (Figure 2.9). In several cases the *C. elegans* homologue mRNAs differs significantly from the mammalian counterpart. In particular, unlike its mammalian homologue Apaf-1, c*ed-4* was shown by mapping to lack a 5' IRES sequence and translated poorly in both *ifg-1::mos* and *ced-9ts* genetic backgrounds (Coldwell et al., 2000). We previously observed that the RNAi knockdown of IFG-1 p170 led to the accumulation of punctate CED-4 structures typical of apoptosomes in apoptosing germ cells. (Contreras et al., 2008) The current study suggests their appearance of CED-4 structures was probably not due to new synthesis, but may have resulted from enhanced protein stability and the accumulation of CED-4 into easily detected foci on apoptosomes. More importantly, our data point out clear differences between protein synthetic regulation of stress and cell death proteins such as Apaf-1, p53 and HIF-1 in whole animals versus cells in culture. Such observations suggest that both organism and physiological context may greatly alter expected protein synthetic regulation.

We propose a model that relates protein synthesis to the apoptotic pathway in normal development and physiological stress (Figure 2.10). In this model, the translation machinery is itself responsible for the selection of mRNAs during times of stress. This allows a cell to initially attempt recovery before committing itself to cellular suicide. Cell death signals initiates apoptosis by preventing CED-9 (Bcl-2) from inhibiting the activity of CED-4 (Apaf-1) (Hengartner and Horvitz, 1994; Pourkarimi et al., 2012; Zou et al., 1997). In our experiments the genetic loss of CED-9 (Bcl-2) function allows precocious activation of CED-4 (Apaf-1). CED-4 binds procaspase CED-3 forming the apoptosome (Chinnaiyan et al., 1997a; Nicholson et al., 1995). Apoptosome formation initiates autocatalysis and activation

Figure 2.9

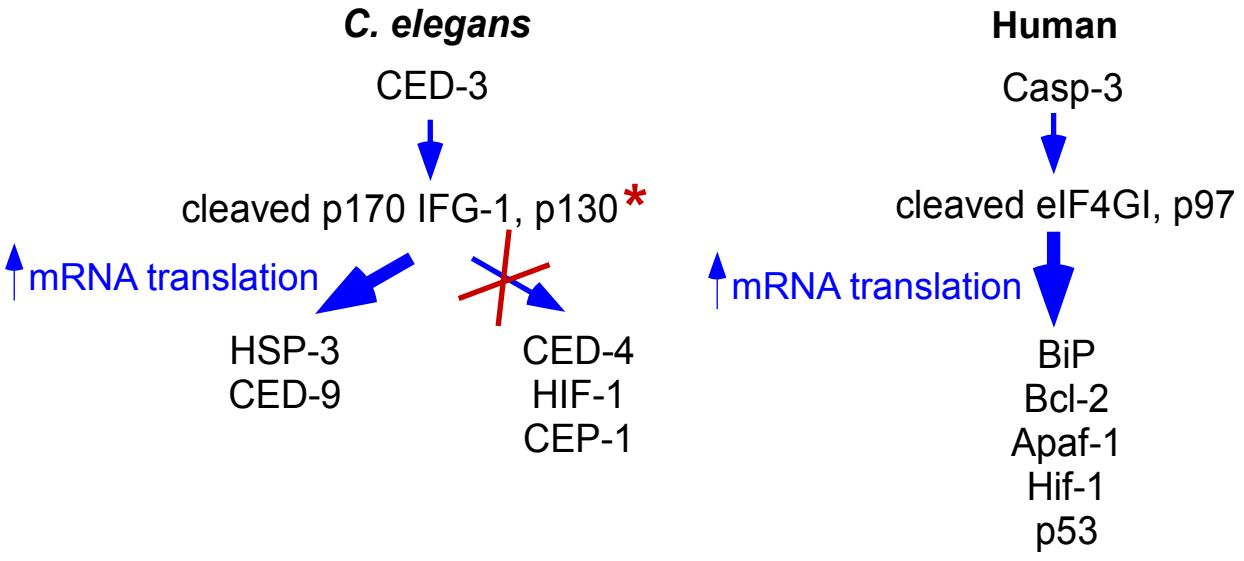
C. elegans
CED-3
cleaved p170 IFG-1, p130*
mRNA translation
HSP-3
CED-9
CED-4
HIF-1
CEP-1
Human
Casp-3
cleaved eIF4GI, p97
mRNA translation
BiP
Bcl-2
Apaf-1
Hif-1
p53

Figure 2.9. Model comparing the translational efficiencies of *C. elegans* and mammalian stress related mRNAs. Wide width arrows indicate the increased translational efficiency of *C. elegans hsp-3* and *ced-9* mRNAs and human BiP, Bcl-2, Apaf-1, Hif-1 and p53. The decreased translational efficiency of other *C. elegans* mRNAs, *ced-4, hif-1* and *cep-1,* is shown by an "x." * indicates the genetic manipulation of the *ifg-1::mos* strain.

of CED-3 (Chinnaiyan et al., 1997a; Li et al., 1997). Active CED-3 then cleaves IFG-1(eIF4G) separating the PABP and eIF4E-binding domains from the region that associates with the ribosome (Contreras et al., 2011). This prevents utilization of the mRNA cap or poly(A) for mRNA recruitment to the ribosome. Instead, it promotes cap-independent mRNA initiation through the ribosome-binding portion of IFG-1 p130 or the p130-like cleavage product of p170 (Contreras et al., 2011). Cap-independent translation of mRNAs (either containing or lacking IRESes) allows for the expression first of proteins involved in attempted recovery, then subsequently those that ensure the apoptotic fate. One such non-IRES mRNA translationally enhanced during the initial phase is *hsp-3* (BiP). This chaperone protein is thought to promote protein refolding under stress conditions (Lee, 2005). CED-9 (Bcl-2) synthesis is also enhanced and may also be involved in the recovery phase. Since CED-9 is an integral member of the apoptotic pathway, the induction of cap-independent translation may result in a feedback loop that prevents further apoptosis. Interestingly, some cap-independent products switch roles to promote apoptosis at later times if recovery has not been accomplished. Genetic evidence shows that CED-9 may be one of these proteins with an initial role in cellular survival followed by a later role in cell death (Galvin et al., 2011). In mammalian cells, a similar initial attempt at recovery involves the sequential use of first anti-apoptotic and then pro-apoptotic IRESes for translation control during progressive stress conditions (Holcik and Sonenberg, 2005). In both cases, regulated cap-independent translation mediates the switch.

We are discovering that the interplay of cap-dependent and -independent translation during development may provide a means to selectively enhance translational efficiency of mRNAs that influence cell fate decisions. Germ cells in particular must rely on

Figure 2.10

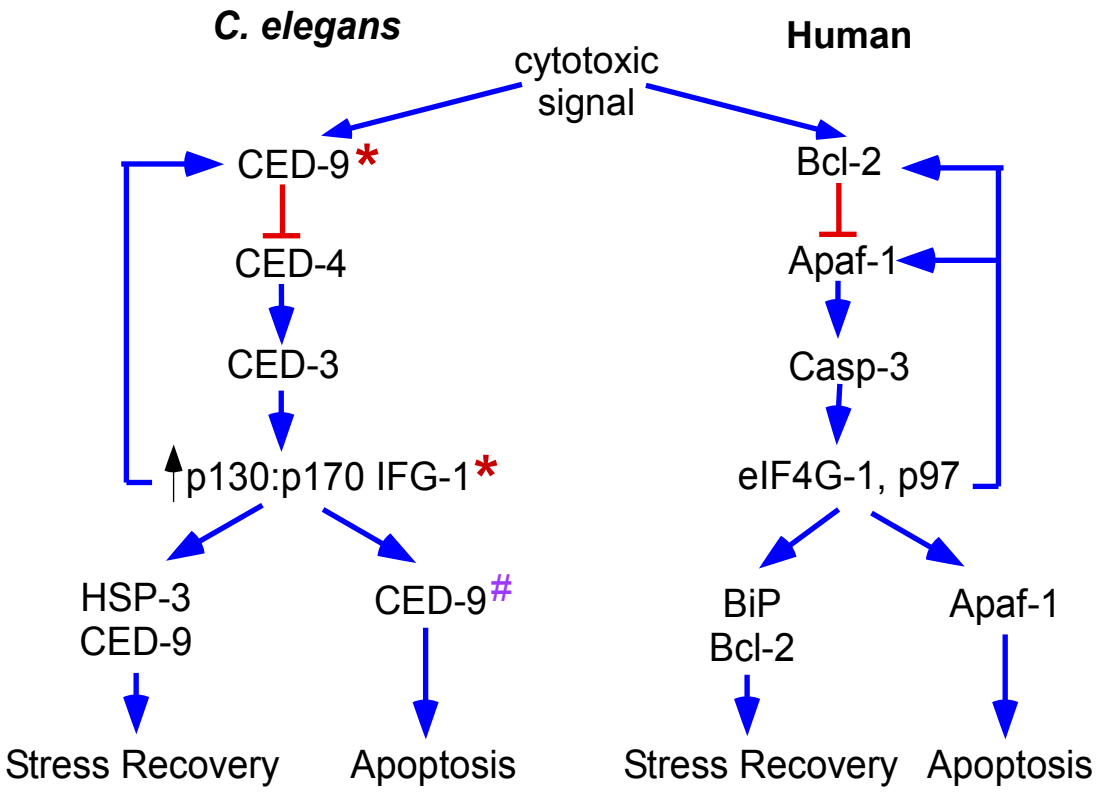
C. elegans
Human
cytotoxic signal
CED-9*
CED-4
CED-3
p130:p170 IFG-1*
HSP-3
CED-9
CED-9#
Stress Recovery
Apoptosis
Bcl-2
Apaf-1
Casp-3
eIF4G-1, p97
BiP
Bcl-2
Apaf-1
Stress Recovery
Apoptosis

Figure 2.10. Model for the induction of cap-independent translation of stress-related mRNAs during apoptosis. The induction of apoptosis in humans leads to the activation of caspases and cleavage of the cap-dependent translation initiation factor eIF4GI and constitutively cap-independent translation initiation factor p97. This cleavage leads to the induction of cap-independent protein synthesis. As a result, the translational efficiency is increased for pro- and anti-apoptotic messages such as pro-apoptotic Apaf-1 and recovery mRNAs Bcl-2 and BiP. The translation of Bcl-2 and BiP promotes periods of cellular recovery from stress. Subsequent translation of Apaf-1 leads to cellular suicide. In the *C. elegans* gonad, apoptosis activated caspase, CED-3 leads to *C. elegans* eIF4GI (IFG-1 p170) and p97 (IFG-1 p130) cleavage. This cleavage leads to an increase in p130-driven translation of stress-related mRNAs *hsp-3* and *ced-9.* * indicates that genetic manipulation in the *ifg-1::mos* and c*ed-9ts* strains leads to the induction of cap-independent protein synthesis. # indicates a proapoptotic function for CED-9 (Galvin et al., 2011).

translational regulation of stored maternal mRNAs for their maturation. Alternatively, germ cells undergo apoptosis inducing translation initiation factor IFG-1 (eIF4G) cleavage. At the threshold of that decision, cap-independent synthesis of anti-apoptotic CED-9 and HSP-3 may suppress germ cell apoptosis and allow most cells to mature into oocytes.

CHAPTER 3: CHARACTERIZATION OF *ced-4* mRNA STRUCTURE AND TRANSLATIONAL EFFICIENCY AFTER DEPLETION OF CAP-DEPENDENT PROTEIN SYNTHESIS

Introduction

Apoptosis results in activation of caspases that cleave the translation initiation machinery resulting in enhanced cap-independent mRNA translation (See Chapter 1). Apoptotic stressors, such as DNA damage, activate members of the BH3-only family of proteins resulting in a signaling cascade that leads to caspase activation (Huang and Strasser, 2000). The BH3-only proteins perturb the antiapoptotic function of mitochondrial membrane proteins Bcl-2 and Bcl-xL (Danial, 2007). This perturbation results in the activation of proapoptotic proteins such as Bax and Bak (as reviewed in (Danial, 2007). Bax and Bak homodimerize to form a pore in the mitochondrial membrane resulting in the release of cytochrome c (Desagher et al., 1999; Wei et al., 2000). Cytochrome c and ATP are essential for the activation of Apaf-1 to assemble the apoptosome. This dependence is most likely due to the requirement of cytochrome c and ATP binding to expose Apaf-1's caspase recruitment domain (CARD), which allows Apaf-1 to recruit procaspase-9 (Li et al., 1997). Cytochrome c, Apaf-1 and regulatory procaspase-9 join together to form the apoptosome (Li et al., 1997). Apoptosome formation brings into close proximity the procaspase-9 proteins and results in their subsequent cleavage and activation (Renatus et al., 2001). The activated caspase-9 then cleaves the effector procaspase, procaspase-3, which in turn cleaves other substrate proteins in the cell resulting in cell death (Li et al., 1997).

One target of caspase-3 is isoforms of the translation initiation factor eIF4G (eIF4GI, eIF4GII and p97) (Bushell et al., 1999; Marissen et al., 2000). eIF4G cleavage removes the

eIF4E and PABP-binding domain from eIF4GI, preventing the involvement of these facilitator proteins in mRNA recruitment (5' and 3' end coordination) to the ribosome (Morino et al., 2000). However, the central portion of eIF4GI is still intact and becomes involved in translation initiation that is independent of cap-recruitment. eIF4GII cleavage by caspase 3, in contrast, results in its degradation and eIF4GII does not have a known role in further translation initiation (Nevins et al., 2003). The constitutively cap-independent eIF4G isoform, p97 is also cleaved, but is likewise still able to support cap-independent translation initiation, much like the central portion of eIF4GI (Henis-Korenblit et al., 2000). Thus, after caspase activation translation initiation is still able to occur on a select subset of mRNAs via cap-independent translation initiation facilitated by cleaved eIF4GI and p97 (Henis-Korenblit et al., 2000; Marissen and Lloyd, 1998; Nevins et al., 2003).

Genetic studies in *C. elegans* initially elucidated the apoptotic mechanism that is highly conserved in humans (Hengartner et al., 1992; Hengartner and Horvitz, 1994; Xue et al., 1996; Zhou et al., 2001). Thus, *C. elegans* is the ideal simplified model to study the apoptotic mechanism found in more complex organisms. Apoptosis is prevalent within *C. elegans* embryonic and larval development, where 131 of the 1090 total somatic cells undergo cellular suicide (Sulston and Horvitz, 1977; Sulston et al., 1983). Additionally, in the adult gonad, about 50% of cells produced by stem cells at the distal tip undergo apoptosis and thus never become mature oocytes (Gumienny et al., 1999). These germ cells are believed to perform a similar function to vertebrate nurse cells providing extra cytoplasm and other components needed by the gametes that reach maturity (Gumienny et al., 1999). Similar to the aforementioned mammalian apoptotic pathway, the function of CED-4 (Apaf-1) during apoptosis is no longer inhibited by CED-9 (Bcl-2), allowing CED-4 to

act as an activator of the cell death machinery (Chinnaiyan et al., 1997b; Pourkarimi et al., 2012). CED-4 binds the procaspase CED-3, forming the apoptosome, initiating CED-3 self-cleavage and activation in the presence of ATP (Chinnaiyan et al., 1997a; Gumienny et al., 1999; Yang et al., 1998; Yuan et al., 1993). Also, similar to mammalian cells, the activation of apoptosis in *C. elegans* leads to the cleavage of the translation initiation factor, IFG-1 (eIF4G) (Contreras et al., 2011; Marissen and Lloyd, 1998). The single *C. elegans* eIF4G, IFG-1, has two isoforms, p170 and p130, that are derived from the same gene (Contreras et al., 2011). Both isoforms are cleaved by CED-3 during apoptosis (Contreras et al., 2011) (Figure 3). The cleavage separates IFG-1 p170's predicted PABP and eIF4E binding domains from the domains that associate with the ribosome (Contreras et al., 2011). This prevents the active recruitment of the mRNA to the ribosome thorugh cap and poly(A) interactions. IFG-1 p130 is also cleaved by CED-3 (Contreras et al., 2011). However, IFG-1 p130 is constitutively cap-independent, much like mammalian p97, and does not contain the eIF4E and PABP binding domains (Contreras et al., 2008). After digestion by CED-3, translation initiation is still able to occur on a select subset of cap-independent mRNAs facilitated by cleaved IFG-1 p170 and p130 (Morrison, 2014).

Human Apaf-1 has been specifically demonstrated to translate cap-independently via an internal ribosome entry site (IRES) after the initiation of apoptosis (Coldwell et al., 2000). Apaf-1 mRNA has a long, G-C rich, with extensive secondary structure 5' UTR that acts as an IRES sequence (Mitchell et al., 2001). This IRES sequence is active in many transformed human cell culture lines including human cervical carcinoma (HeLA), human liver carcinoma (HepG2), human breast carcinoma (MCF7), human embryonic kidney (HK293) and human lung (MRC5) (Mitchell et al., 2001). However, the Apaf-1 IRES also

requires IRES transacting factors (ITAFs) for its efficient translation initiation (Mitchell et al., 2001). In rabbit reticuloctye lysates IRES-mediated Apaf-1 translation was enhanced by polypyrimidine tract binding protein (PTB) and upstream of N-ras (unr) (Mitchell et al., 2001). It has been demonstrated that the binding of these ITAFs leads to a change in the three dimensional structure of the Apaf-1 IRES, which is proposed to facilitate 48S complex assembly (Mitchell et al., 2003).

In this study we compared the mRNA structure of *C. elegans ced-4* mRNA to its mammalian homologue Apaf-1 in an effort to compare their mechanisms of translation initiation. Although Apaf-1 was noted to have an extended 5' UTR containing an IRES, *ced-4* mRNA structure predicted from known cDNAs did not include a long 5' UTR with putative IRES characteristics. Previous studies in our lab illustrated that the induction of cap-independent protein synthesis occurred after IFG-1 cleavage during apoptosis (Contreras et al., 2011). CED-4 protein simultaneously collected in punctate apoptosome-like structures (Contreras et al., 2008). However, in these studies we found that translation of *ced-4* mRNA decreased during induced apoptosis in *C. elegans*. Importantly, our data delineated some clear differences in the protein synthetic regulation of *ced-4* mRNA during apoptosis in comparison to its mammalian homologue, Apaf-1.

Results

***ced-4* polycistronic mRNA contains IRES characteristics similar to Apaf-1 mRNA.** The 5' UTR region of Apaf-1 contains an IRES that promotes cap-independent translation of a downstream cistronic in a bicistronic plasmid (Coldwell et al., 2000). Apaf-1 has a 578 nucleotide long 5' UTR with IRES characteristics such as high GC content (67%) and

multiple upstream AUG codons (2) (Coldwell et al., 2000). Thus, we wanted to investigate whether the mRNA encoding the *C. elegans* homologue of Apaf-1, CED-4, had a similar IRES-mediated mechanism of translation initiation during apoptosis. The presence of such a mechanism would allow a novel *in vivo* study of cap-independent IRES-mediated translation in a whole animal model that is also amenable to genetic investigations. ESTs compiled for *ced-4* transcripts show that *it* has only two known mRNA variants that both contain an SL2 leader trans-spliced directly to the AUG start codon. Trans-splicing leaves only a 22 nucleotide splice leader sequence as the residual 5' UTR in the identified *ced-4* mRNA variants. However, *ced-4* pre-mRNA is polycistronic transcript leaving the possibility that alternative splicing at that junction could result in other 5' extended mRNA variants (Figure 3.1A) (Blumenthal et al., 2002; Spieth et al., 1993). *ced-4* is the second gene in an operon, a gene cluster transcribed from a distal 5' promoter upstream of the cluster, with an inordinately long intergenic region of 540 bp between *ced-4* and the upstream cistron (Blumenthal et al., 2002; Spieth et al., 1993). Much like mammalian Apaf-1, *ced-4* pre-mRNA has polypyrimidine stretches and has multiple AUG codons in the intergenic region (Figure 3.1B). The sequence upstream of *ced-4* also has a high degree of secondary structure typical of known mammalian IRES sequences (Figure 3.1C). We predicted that if any of these similar sequences were maintained via alternative splicing of *ced-4* mRNA, that *ced-4* mRNA may also translate cap-independently via an IRES. Inclusion of this 5' outron sequence may also result from inefficient SL2 trans-splicing during stress (Liu et al., 2003). The Blumenthal lab has reported that during stress, particularly heat shock, 3' cleavage and polyadenylation of the upstream gene's mRNA may not be followed by SL2 splicing of the downstream gene's mRNA in the operon transcript (Liu et al., 2003). Thus, aberrant

Figure 3.1

A

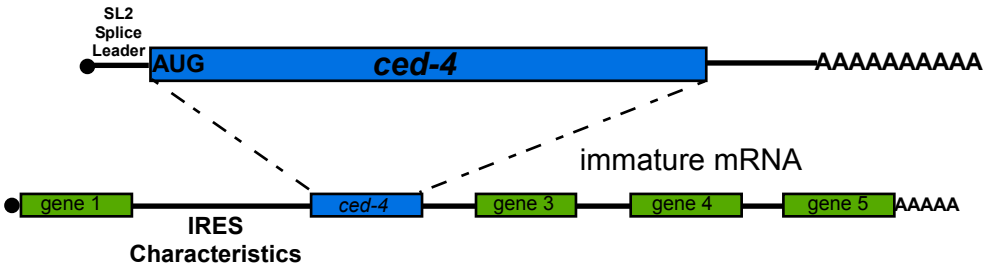

B

```
     F26A1.1 gene                                   ced-4 430s
  1  ATGTACTGTT TTTGTATTTG AATATTGTAT TACAGGGTTG GGATTCTCGG CAAATATCAG CGACAGTGGA AGATTTAGAA GAAGGACGTG TGACAATCAC

101  TAAGCAAAGA GGAAAGGATA AAGGATTGTG ATATTTCACT GTTTTACTCA TTCGCTTTTT AAATAAGAAC TATATGCCGA TTTGCCGATA TATTTTTGTT
                                                 pA
201  TATTAGGCCT CTCACATTCC TGTACAATGT TTCTACCAAA TAAACTGCAT TTTTATCTGA AAATTCGAAT TTATTTTTGT CTACTTTTTA CTCGTTGCAT
                                                                      ***
301  TCGAGATCAG CATATCTTCC GGTCTATTTA TATTCAACGA TTTTTATAAA TTAGTACTCC TTCATGTTTA ATTTCATTTT ATCTGTAAGC TTTACTGTAT
                                                                                                      ced-4 886s
                                        ***                                 ***                 ***
401  TTTTTTAAAA TCTTTCTTGC TTCTATCTGA TTATACAATG TTCTTTACTC ATTTTCAAGG TATTTTTATG CCTCACAATT TATGCACATT TCGGGCTTGG
                                ***                     ***                                 *  **
501  AGATTTATCC TCTATATTAC ATGCCTGTTT TTTTAAAGGA TATAATGTTT AACAAATAAT TTTTTATCAA TGCTATTGTA TATTCTCCAG CTAACCGTTG
                                                                                          Met1
     ced-4 1003s                                                                    SL2                ced-4 gene
601  TTTCGAAAAC ATCACCTAGC ATTTTAAAAT TCACAAAATC TTGCTTCCTT ATAATCAAGA AGATTTTTCA GATGCTCTGC GAAATCGAAT GCCGCGCTTT
                                ced-4 92a
701  GAGCACGGCA CACACGAGGC TCATCCACGA CTTTGAACCA CGTGACGCAT TGACTTATTT AGAAGGCAAA AACATTTTCA CAGAAGATCA TTCTGAACTT
                886s RPA end point      ced-4 200a      430s RPA end point
801  ATCAGTAAAA TGTCAACTCG CCTCGAGAGG ATCGCCAATT TTCTTCGAAT CTATCGACGT CAAGCTTCTG AACTTGGACC ACTCATCGAC TTTTTCAACT
                        ced-4 288a
901  ACAACAATCA AAGTCACCTT GCTGATTTCC TCGAAGACTA CATCGATTTT GCGATAAATG AGCCAGATCT ACTTCGTCCA GTAGTGATTG CTCCACAATT
```

C

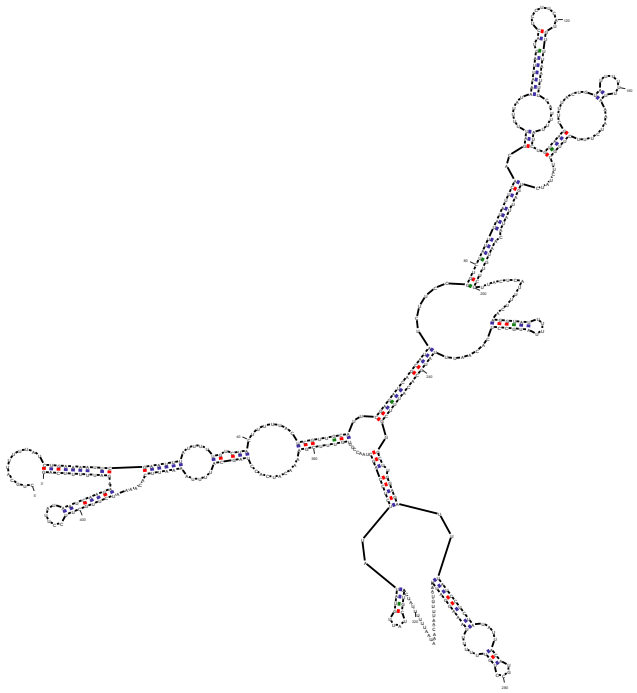

Figure 3.1. Schematic of *ced-4* polycistronic mRNA 5' intergenic region. (A) Schematic of known *ced-4* mRNA variant and *ced-4* polycistronic mRNA. (B) *ced-4* intergenic sequence. *ced-4* coding region (blue) and upstream gene F26A1.1 (gene) are separated by an abnormally long intergenic region. The polyadenylation site of the upstream gene (pA) and *ced-4* initiation codon (Met1) are used to highlight the beginning and end of the outron sequence. The intergenic sequence has many IRES characteristics including polypyrimidine stretches (bold), multiple upstream AUGs (***) and high secondary structure (C). RPA end points (purple) and primer binding sites (orange) are indicated .

splicing during stress results in an uncapped mRNA that contained 5' outron sequence (Liu et al., 2003). It is then conceivable that during stress conditions a new *ced-4* mRNA variant, containing the aforementioned IRES characteristics in its extended 5' UTR, may result from inefficient SL2 trans-splicing.

PCR analysis of *ced-4* mRNA structure did not reveal full-length alternative 5' endpoints. To determine if *ced-4* mRNA had alternative 5' endpoints containing some of the upstream intergenic region, with IRES characteristics, we performed extensive analysis of the 5' end of *ced-4* mRNA. We analyzed the 5' endpoints not only in the wild type strain, but also in a strain with enhanced cap-independent translation initiation due to a depletion in the cap-dependent IFG-1 isoform, p170 (Morrison, 2014). This cap-independent strain (*ifg-1::mos*) allowed us to determine if the *ced-4* mRNA variant representation changed during conditions that promote apoptosis and cap-independent synthesis. Furthermore, we also analyzed *ced-4* mRNA variants during temperature stressed conditions where inefficient trans-splicing may occur (Liu et al., 2003). Northern blot analysis of *ced-4* mRNA was inconclusive when it came to assessing alternative 5' endpoints (Figure 3.2). However, systematic PCR analysis using primers within the intergenic region and downstream *ced-4* sequence revealed the absence of mature spliced message that extended through the entire intergenic region (Figure 3.3A). Using a primer set located 186 bp upstream of the AUG start site and a downstream primer in exon 6, we were unable to prime any extended mature mRNA variants in either wild type, temperature stressed wild type or temperature stressed *ifg-1::mos* worms (Figure 3.3B). Only contaminating DNA could be amplified using this primer set (data not shown). However, PCR using a primer located only 69 bp

Figure 3.2

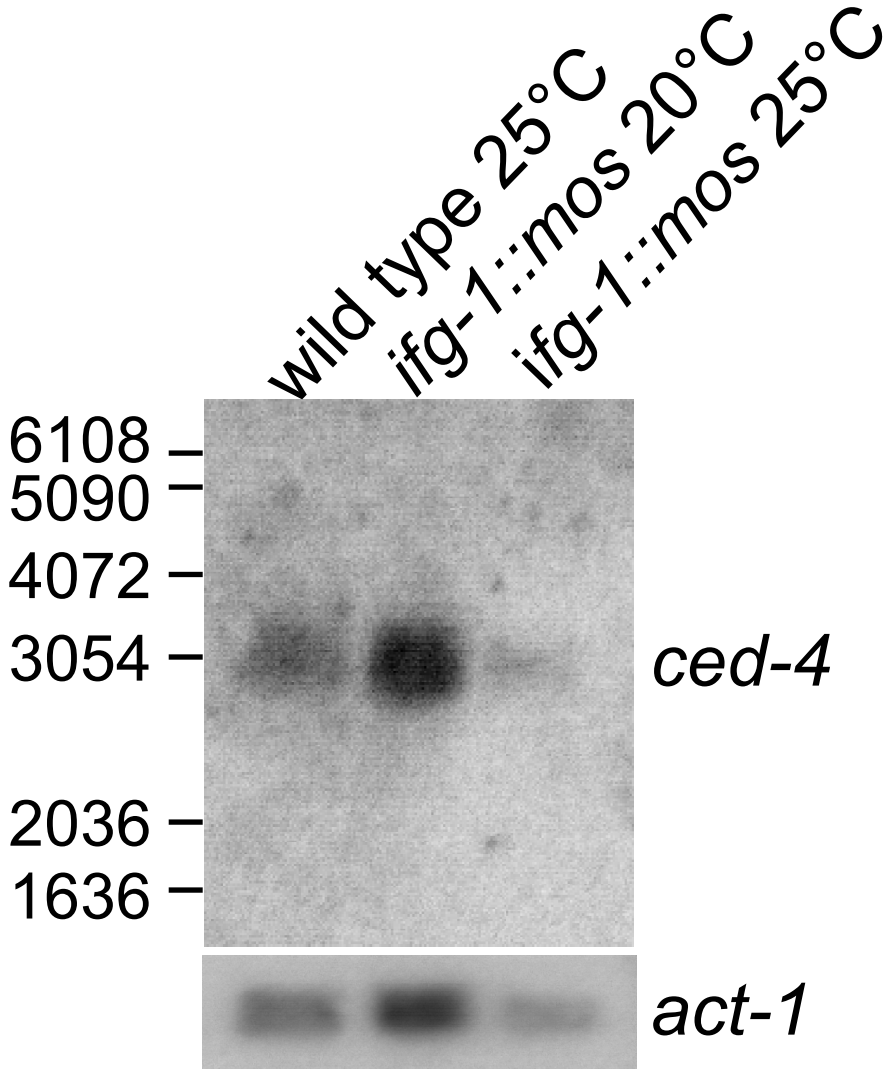
wild type 25°C
ifg-1::mos 20°C
ifg-1::mos 25°C
6108
5090
4072
3054
2036
1636
ced-4
act-1

Figure 3.2. *ced-4* mRNA Northern Blot inconclusive for 5' extended mRNA variants. Northern blot on wild type, *ifg-1::mos* and *ifg-1::mos* temperature stressed RNA extracts with *ced-4* and *act-1* probes. Detection of extended 5' mRNA variants is inclusive.

upstream of the AUG start site with the downstream primer in exon 6 amplified mRNAs encoding both *ced-4* isoforms, CED-4S and CED-4L. The 5'-extended mRNA was amplified from wild type, temperature stressed wild type and temperature stressed *ifg-1::mos* strains (Figure 3.3C). These mRNAs were fully spliced through the primed exon 6 suggesting they were derived from fully mature *ced-4* mRNAs. It is formally possible, though, that amplified products may be from mid-splicing messages that are only spliced through exon 6. To confirm or refute the absence of extended mRNA variants of at least 186 bp, we performed a second PCR with a second primer set (886s primer and a downstream primer in exon 3 (Figure 3.3D)). A full-length fully-spliced *ced-4* mRNA variant was not amplified in the wild type, wild type temperature stressed or *ifg-1::mos* temperature stressed strains. Again, a partially spliced *ced-4* mRNA was amplified in the *ifg-1::mos* temperature stressed strain. This mRNA variant had intron 1 spliced out, but intron 2 was not removed from the message. All PCR-characterized amplified message variants are summarized in Figure 3.3E and compared to the *ced-4* operon. To determine if the 69 bp extended *ced-4* mRNA variant detected (or other thus far undetected mRNA variants) were the result of alternative trans-splicing, we performed PCR amplification using primers for the SL1 and SL2 splice leader sequences (Figure 3.4). Although the initial round PCR amplified what appeared to be extended alternatively spliced 5' mRNA variants using the SL1 primer, nested PCR amplified only the previously known *ced-4* mRNA with a trans-splice site lacking 5' extended mRNA sequence. The previously detected 69 bp *ced-4* extended mRNA variant could not be confirmed by any of our follow-up PCR approaches. If it does represent a mature mRNA variant, it likely does not arise from alternative SL trans-splicing.

Figure 3.3

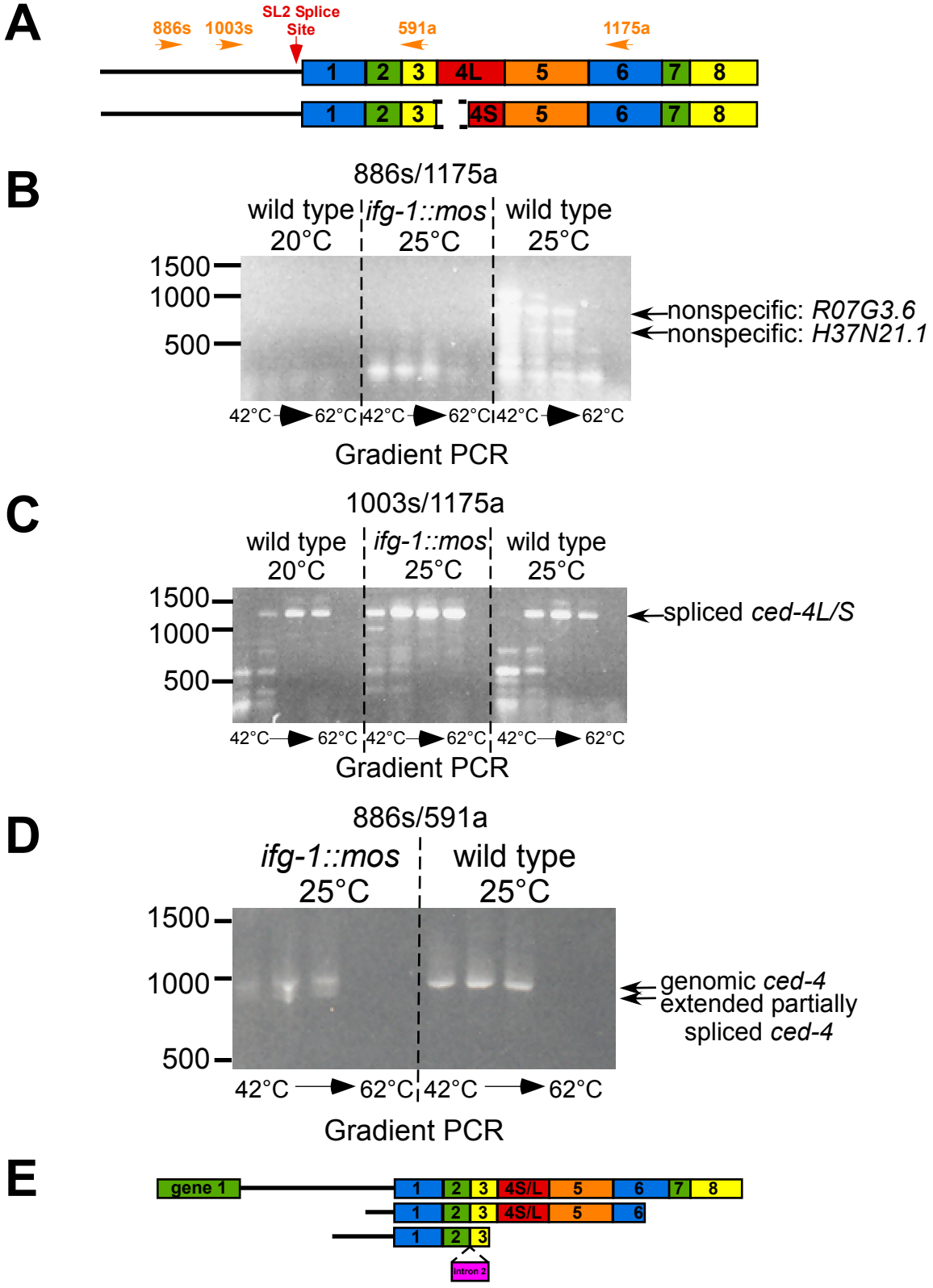
A
886s
1003s
SL2 Splice Site
591a
1175a
1
2
3
4L
5
6
7
8
1
2
3
4S
5
6
7
8
B
886s/1175a
wild type 20°C
ifg-1::mos 25°C
wild type 25°C
1500
1000
500
nonspecific: R07G3.6
nonspecific: H37N21.1
42°C
62°C
42°C
62°C
42°C
62°C
Gradient PCR
C
1003s/1175a
wild type 20°C
ifg-1::mos 25°C
wild type 25°C
1500
1000
500
spliced ced-4L/S
42°C
62°C
42°C
62°C
42°C
62°C
Gradient PCR
D
886s/591a
ifg-1::mos 25°C
wild type 25°C
1500
1000
500
genomic ced-4
extended partially spliced ced-4
42°C
62°C
42°C
62°C
Gradient PCR
E
gene 1
1
2
3
4S/L
5
6
7
8
1
2
3
4S/L
5
6
1
2
3
intron 2

Figure 3.3. Full-length upstream intergenic region not amplified during systematic *ced-4* mRNA PCR. (A) Schematic depicting the location of priming sites on *ced-4S* and *ced-4L* splice variants. (B) Gradient PCR amplification (42˚C to 62˚C) using 886s and 1175a primer set. Only two nonspecific amplification products (R07G3.6 and H37N21.1) were detected. (C) Gradient PCR amplification (42˚C to 62˚C) using 1003s and 1175a primer set. Spliced *ced-4S* and *ced-4L* variants were detected. (D) Gradient PCR amplification (42˚C to 62˚C) using 886s and 591a primer set. Only genomic *ced-4* and an extended partially spliced *ced-4* amplification product was detected. (E) Schematic representing amplified *ced-4* products.

Figure 3.4

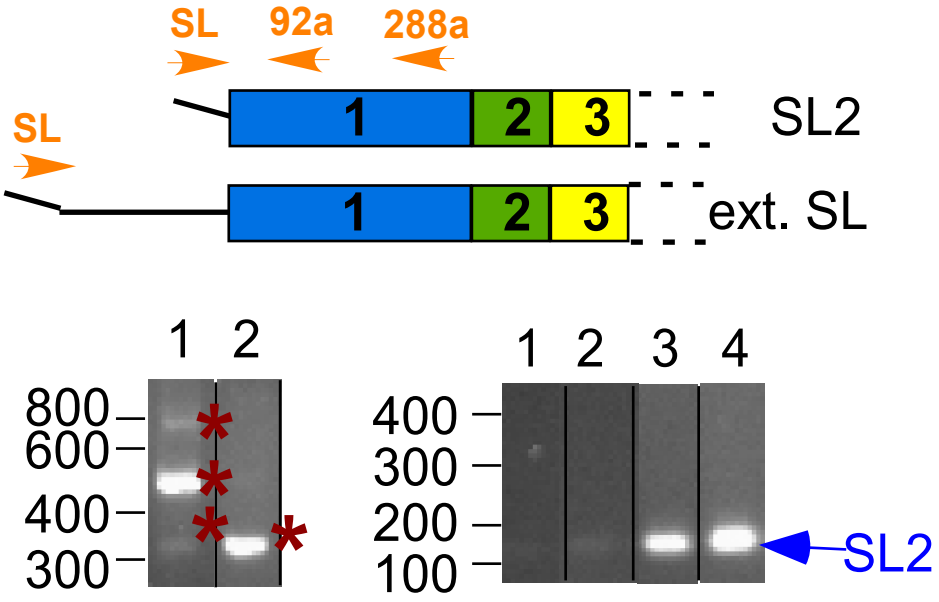
SL
92a
288a
SL
1
2
3
SL2
1
2
3
ext. SL
1 2
800
600
400
300
1 2 3 4
400
300
200
100
SL2

Figure 3.4. *ced-4* alternative splice variants not amplified using splice leader primers. Schematic of SL2 trans-spliced *ced-4* mRNA with primers indicated by orange arrows. Schematic of the proposed extended *ced-4* mRNA variant from alternative splicing. Primary PCR using the SL1 primer amplified 3 PCR products (*), two of which appeared to be extended. Nested PCR only amplified a product consistent with the known SL2 splice variant. PCR SL2 splice leader sequences indicated no extended mRNA variants. Only the known SL2 splice variant was detected (indicated by the arrow).

Further 5' analysis using RNase Protection to detect 5' extended mRNA variants. To more conclusively determine if *ced-4* mRNA contained some of the intergenic region containing IRES characteristics, we performed RPAs using two probes, one that extended from exon 1 into the 3' end of the upstream gene and one that extended from exon 1 into the intergenic region to the 886s primer site (186 bp upstream). These RPA probes were used to analyze RNA from wild type, *ced-9ts* and *ifg-1::mos* strains grown during normal and temperature stressed conditions (Figure 3.5A). The *ced-9ts* strain used in these experiments has a temperature sensitive decrease in CED-9 function leading to the induction of apoptosis (Hengartner et al., 1992). We previously demonstrated that apoptosis induced by the *ced-9ts* lesion leads to the activation of CED-3 that cleaves IFG-1 p170 removing its cap-binding domain and leading to the initiation of cap-independent mRNA translation (Contreras et al., 2011). The *ced-9ts* strain was used in a similar manner to the *ifg-1::mos* strain to confirm that neither means to cause IFG-1 p170 depletion changes the prevalence of a potential cap-independent *ced-4* mRNA variants. The two bands protected in the RPA were indicative of sizes representing the known shorter 5' endpoint of *ced-4* mRNA and the 3' end of the upstream gene in the operon. We did not observe protection of any 5' extended mRNA variants. We created a second, independent probe to confirm longer protected fragments were the result of 3' protection of the upstream gene in the operon. These assays confirmed that the larger protected mRNA bands were derived from the 3' end of the upstream gene rather than from *ced-4* mRNA (see Chapter 2 Figure 2.7). A RPA using a probe to protect *act-1* mRNA was also performed to ensure equal loading, RNA quality and to quantify the protected mRNA variants (Figure 3.5B). Quantification of protected *ced-4* variants and upstream operon gene revealed that

Figure 3.5

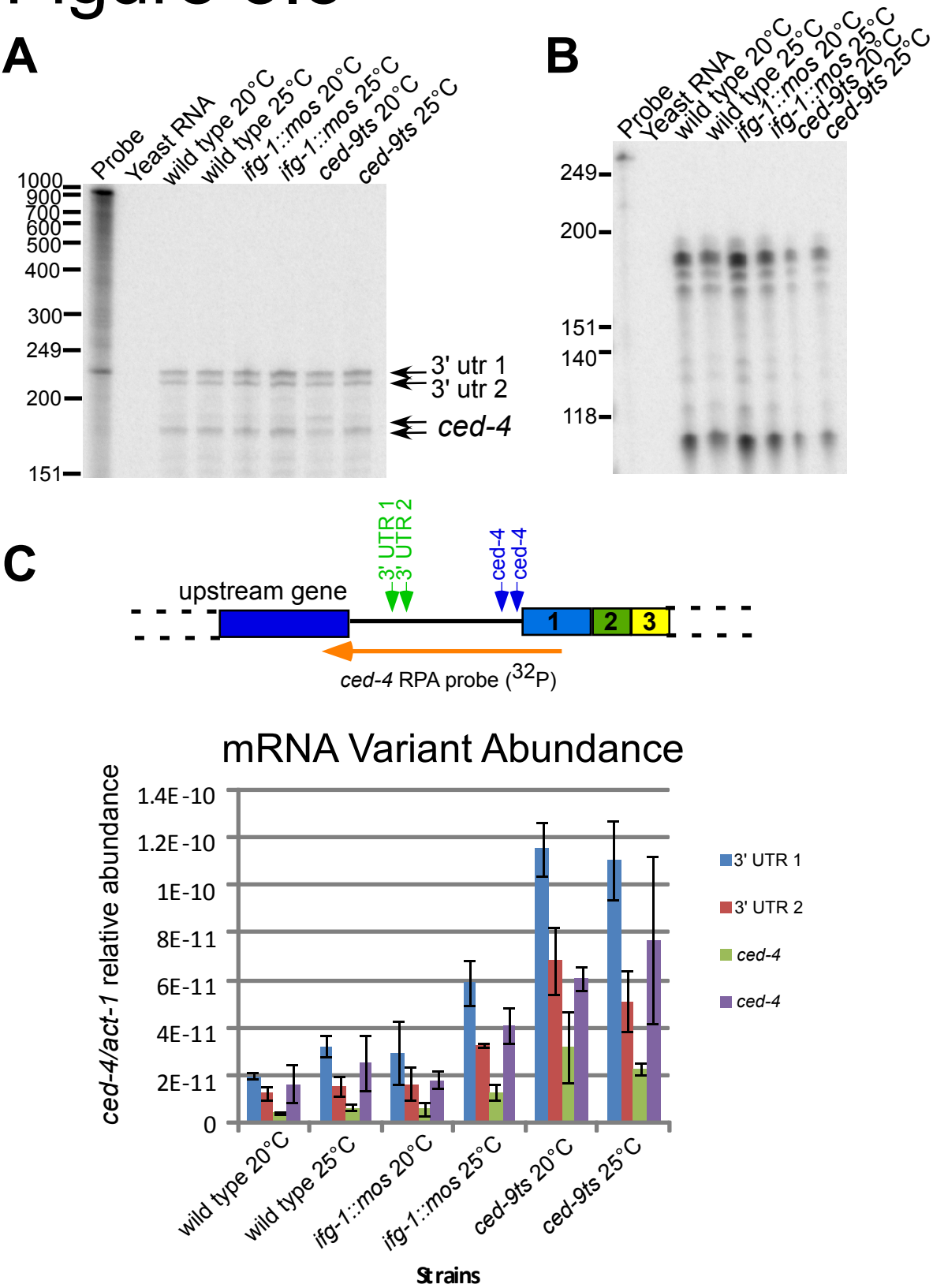
A
Probe
Yeast RNA
wild type 20°C
wild type 25°C
ifg-1::mos 20°C
ifg-1::mos 25°C
ced-9ts 20°C
ced-9ts 25°C
1000
900
700
600
500
400
300
249
200
151
3' utr 1
3' utr 2
ced-4
B
Probe
Yeast RNA
wild type 20°C
wild type 25°C
ifg-1::mos 20°C
ifg-1::mos 25°C
ced-9ts 20°C
ced-9ts 25°C
249
200
151
140
118
C
upstream gene
3' UTR 1
3' UTR 2
ced-4
ced-4
1
2
3
ced-4 RPA probe (32P)
mRNA Variant Abundance
ced-4/act-1 relative abundance
1.4E-10
1.2E-10
1E-10
8E-11
6E-11
4E-11
2E-11
0
3' UTR 1
3' UTR 2
ced-4
ced-4
wild type 20°C
wild type 25°C
ifg-1::mos 20°C
ifg-1::mos 25°C
ced-9ts 20°C
ced-9ts 25°C
Strains

Figure 3.5. 5' extended variants of *ced-4* mRNA are not detected via RNase protection assays. (A) RNase Protection Assay using a probe spanning the entire intergenic region. RPAs were conducted by hybridizing the probe to total mRNA in wild type, wild type temperature stressed, *ced-9ts*, *ced-9ts* temperature stressed, *ifg-1::mos* and *ifg-1::mos* temperature stressed worms. Arrows indicate the detected *ced-4* 5' end points. The 3′ UTR of the upstream gene was also protected as indicated by the specified arrows. (B) Control RNase Protection Assay detecting *act-1* mRNA is shown to demonstrate RNA quality. (C) mRNA abundance of the *ced-4* and the upstream gene was determined by calculating the signal volume normalized to *act-1* signal volume. Diagram depicts *ced-4* and upstream 3' UTR end points.

although there seemed to be more total operon mRNA in strains with depleted IFG-1 p170, there was no change in the ratio of the upstream gene's mRNA to *ced-4* mRNA (Figure 3.5C). There was also no change in the polyadenylation site usage of the upstream gene in the cap-independent strains or upon temperature stress.

As a positive control for the ability of the RPA probe to protect full length extended mRNA variants, we conducted the same assay using a control *in vitro* transcribed *ced-4* mRNA (Figure 3.6A). The control RNA extended from 186 bp upstream of the AUG start site into exon 1. The control RNA's 5' extended *ced-4* sequence was protected by the *ced-4* probe RPA probe (Figure 3.6B). This confirmed the ability of the probe to protect full-length *ced-4* mRNA sequences. Varied concentrations of positive control RNA ranging from 1ng to 1pg were then doped into total extracted mRNA from wild type worms. The total amount of endogenous protected *ced-4* mRNA variants were then compared to protected control RNA to confirm that the extended mRNA could be detected in the same physiological concentration range as the shorter endogenous *ced-4* mRNA variants (Figure 3.6C). These data confirmed the sensitivity of our RPA using the *ced-4* probe to protect any extended mRNA variants the in the same concentration range as shorter mRNA variants. These data suggest that if such a 5' extended *ced-4* mRNA is produced from endogenous RNA processing, it must be in substantially lower abundance than the detected shorter forms. To confirm that the absence of longer protected *ced-4* mRNA variants, we also performed RPAs on isolated enriched poly(A) RNA from wild type worms (data not shown). Even after enrichment, there were no detected 5' extended *ced-4* mRNA variants. Detection of *act-1* mRNA was used to confirm mRNA quality and equal loading in the poly(A) RNA experiments (data not shown).

Figure 3.6

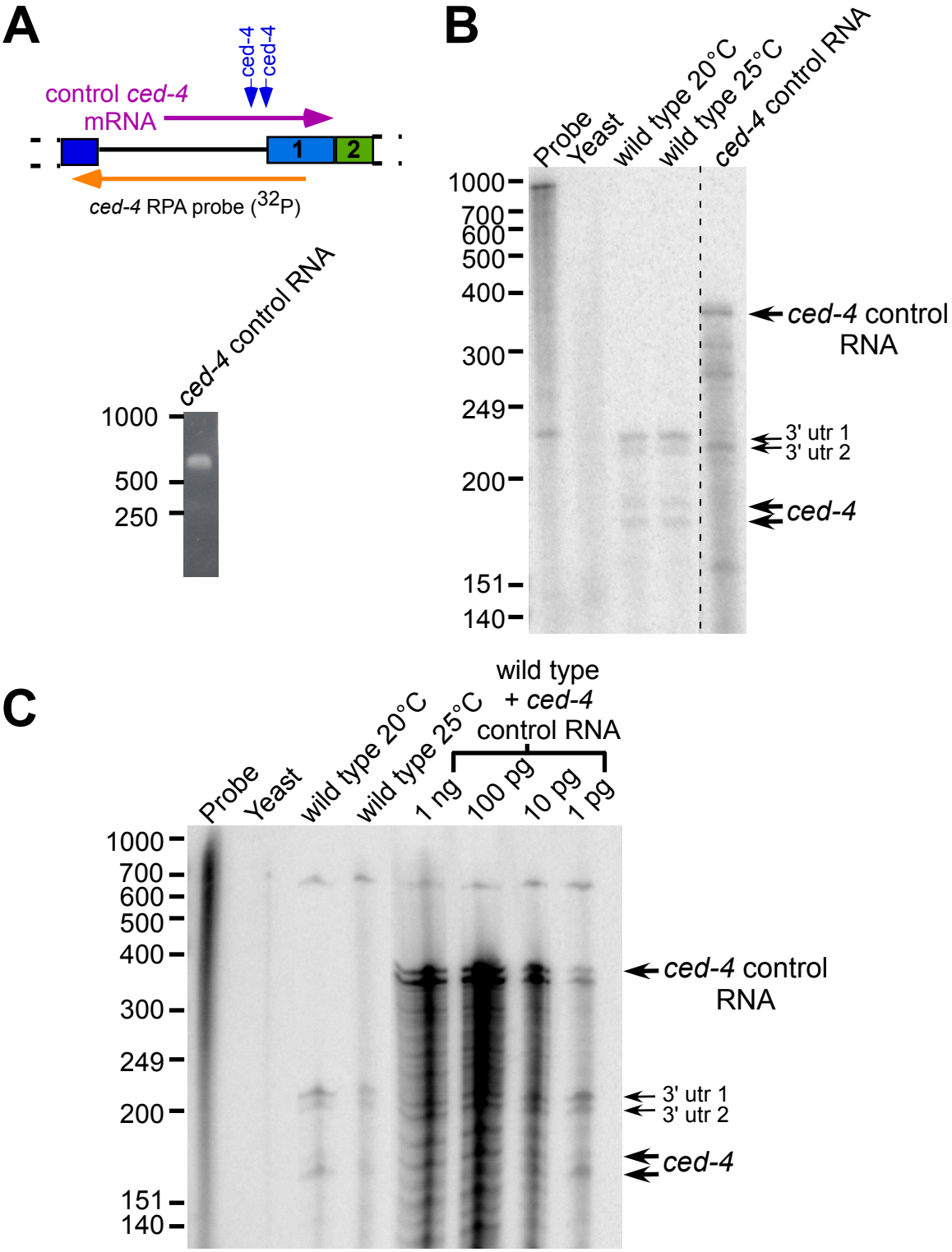
A
ced-4
ced-4
control ced-4
mRNA
1
2
ced-4 RPA probe (32P)
ced-4 control RNA
1000
500
250
B
Probe
Yeast
wild type 20°C
wild type 25°C
ced-4 control RNA
1000
700
600
500
400
300
249
200
151
140
ced-4 control
RNA
3' utr 1
3' utr 2
ced-4
C
Probe
Yeast
wild type 20°C
wild type 25°C
wild type
+ ced-4
control RNA
1 ng
100 pg
10 pg
1 pg
1000
700
600
500
400
300
249
200
151
140
ced-4 control
RNA
3' utr 1
3' utr 2
ced-4

Figure 3.6. Control *ced-4* mRNA confirms RPA probe integrity and ability to detect putative extended *ced-4* mRNA variants. (A) Schematic indicating *ced-4* upstream intergenic region. *ced-4* RPA probe (orange) extends the length of the entire intergenic region. A control *ced-4* mRNA (purple) extends 186 base pairs into the intergenic region. Control RNA run on a agarose gel and stained with ethidium bromide to demonstrate RNA quality. (B) RPA using *ced-4* probe on wild type and wild type temperature stressed worms. Protection products were compared to a RPA on *ced-4* control RNA. *ced-4* control RNA was protected by the *ced-4* RPA probe indicating the probe's ability to detect extended *ced-4* mRNA variants. (C) RPA using *ced-4* probe on wild type and wild type temperature stressed worms. These RPAs were compared to RPAs performed on wild type RNA doped with varying amounts of *ced-4* control RNA. The detection of control RNA was equivalent to protection of shorter mRNA variants found in the worm extracts, indicating that the absence of protected extended *ced-4* mRNA variants was not due to an inability to detect the extended variants at a similar signal volume as the shorter mRNA variants.

To determine which of the *ced-4* mRNA variants become actively translated on ribosomes, we performed RPAs on isolated polysome gradient fractions (Figure 3.7). Worm lysates from temperature stressed wild type and *ifg-1::mos* strains were fractionated on sucrose gradients to resolve polyribosomal complexes. RPAs were then performed on each gradient fraction in order to determine each of the *ced-4* mRNA variants translational efficiency. Across the sucrose gradient there were no detected extended mRNA variants. Additionally, the induction of enhanced cap-independent translation in the *ifg-1::mos* strain did not cause the detected shorter *ced-4* mRNA variants (spliced directly at the AUG) to translate more efficiently (Figure 3.7A and 3.7B). Curiously, the upstream gene whose 3' end is detected by the extended probe translates more efficiently in the *ifg-1::mos* strain. The upstream gene shifts from the moderately efficiently translating region of the gradient into the heavy polysomes. The identitiy of a protein encoded by this upstream mRNA is not known, nor is its significance to apoptosis. Northern blots to detect *act-1* mRNA on each gradient fraction in the wild type and *ifg-1::mos* strains was used as a control for mRNA quality and efficient global translation.

***ced-4* mRNA is not translated more efficiently after the depletion of cap-associated IFG-1 p170.** Although we did not observe any 5' extended *ced-4* mRNA variants, the canonical *ced-4* mRNA could still be translated cap-independently like its mammalian homologue. It has long been known that many heat shock protein mRNAs lack 5' IRESes, and encode very short 5' UTRs but are still translated cap-independently (Dinkova et al., 2005; Joshi-Barve et al., 1992; Rhoads and Lamphear, 1995; Schneider, 1995). Our previous experiments showed that a knockdown of IFG-1 p170 using RNAi resulted not only in an

Figure 3.7

A

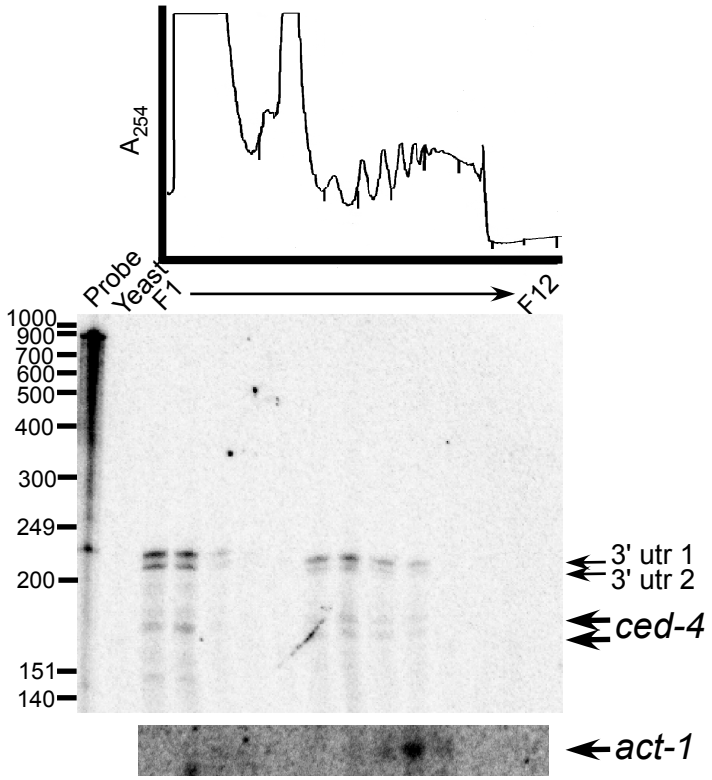
A254
Probe
Yeast
F1
F12
1000
900
700
600
500
400
300
249
200
151
140
3' utr 1
3' utr 2
ced-4
act-1

B

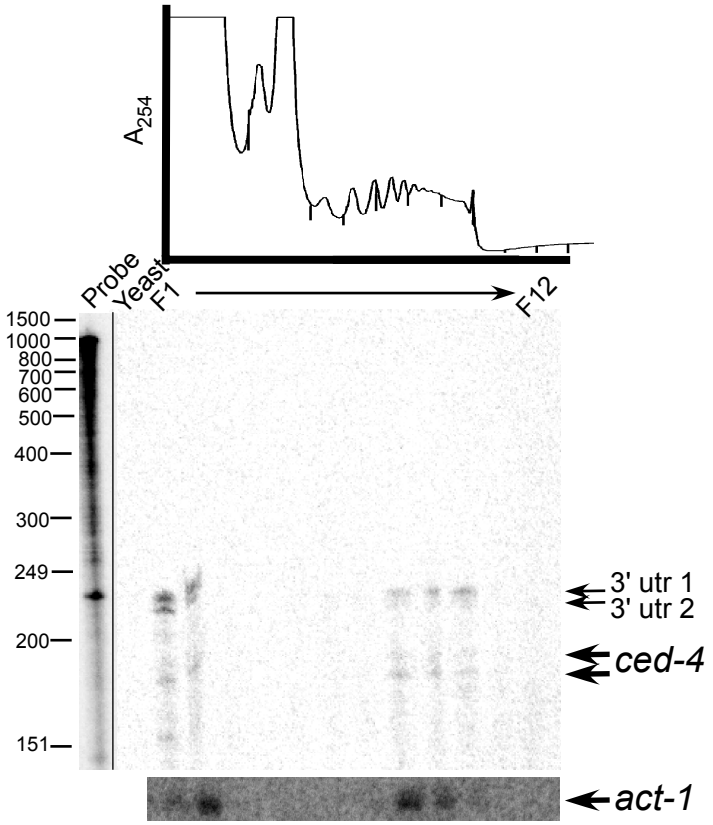
A254
Probe
Yeast
F1
F12
1500
1000
800
700
600
500
400
300
249
200
151
3' utr 1
3' utr 2
ced-4
act-1

Figure 3.7. Extended *ced-4* variants not detected on polyribosomes. During sucrose gradient fractionation of worm lysates from wild type (A) and *ifg-1::mos* (B) absorbance was measured at 254nm. RPAs were performed using the *ced-4* probe on each gradient fraction of the wild type and *ifg-1::mos* strain. Arrows indicate the detected *ced-4* 5' end points. The 3′ UTR of the upstream gene was also protected as indicated by the specified arrows. No extended *ced-4* mRNA variants were found in the nonpolysomal or polysomal regions. *ced-4* mRNA was not translated more efficiently in the cap-independent strain as indicated by gradient fraction localization. Northern blots with an *act-1* probe were performed on each gradient fraction to demonstrate RNA quality. A slight decreased in *act-1* translational efficiency was detected.

increase in apoptosis within the *C. elegans* gonad, but also induced the expression of punctate CED-4 structures typical of apoptosome formation (Contreras et al., 2008). Together these data led us to investigate whether c*ed-4* mRNA is translated cap-independently even without using a 5' IRES. Due to its integral role in cell death and the cleavage of cap-associated IFG-1 p170 during apoptosis, we expected the translational efficiency of *ced-4* mRNA to increase under cap-independent/apoptotic conditions. Sucrose gradient fractionation was performed on wild type, *ifg-1::mos* and *ced-9ts* strains (Chapter 2 Figure 2.3). Real time quantitative PCR (qPCR) was performed on each gradient fraction in order to determine the percent representation of the mRNA in each gradient fraction and determine the mRNA's translational efficiency. However, our previous findings (Chapter 2) showed that for the total poulation of *ced-4* mRNA variants, their translational efficiency decreased during proapoptotic conditions (Chapter 2 Figure 2.5G and Figure 2.5H) (Morrison, 2014). In this study we focused on the specific mRNA translational efficiency of each known *ced-4* mRNA variants (Figure 3.8A). There are two known splice variants of *ced-4* mRNA, anti-apoptotic *ced-4L* and pro-apoptotic *ced-4S* (Shaham and Horvitz, 1996). Only CED-4S is involved in apoptosome formation. We designed c*ed-4S*-specific primers to assess its unique translational efficiency. First we assessed if there was an overall change in *ced-4S* mRNA representation in our cap-independent and apoptotic strains in comparison to the wild type strain (Figure 3.8B). There was no significant change in *ced-4S* mRNA representation in the *ifg-1::mos* and *ced-9ts* strains in comparison to the wild type. We then assessed the change in translational efficiency of *ced-4S* in worms with an increased dependence on cap-independent translation. We found that the efficiency of translation of c*ed-4S* mRNA decreases in a manner very similar to the total *ced-4* mRNA population in

Figure 3.8

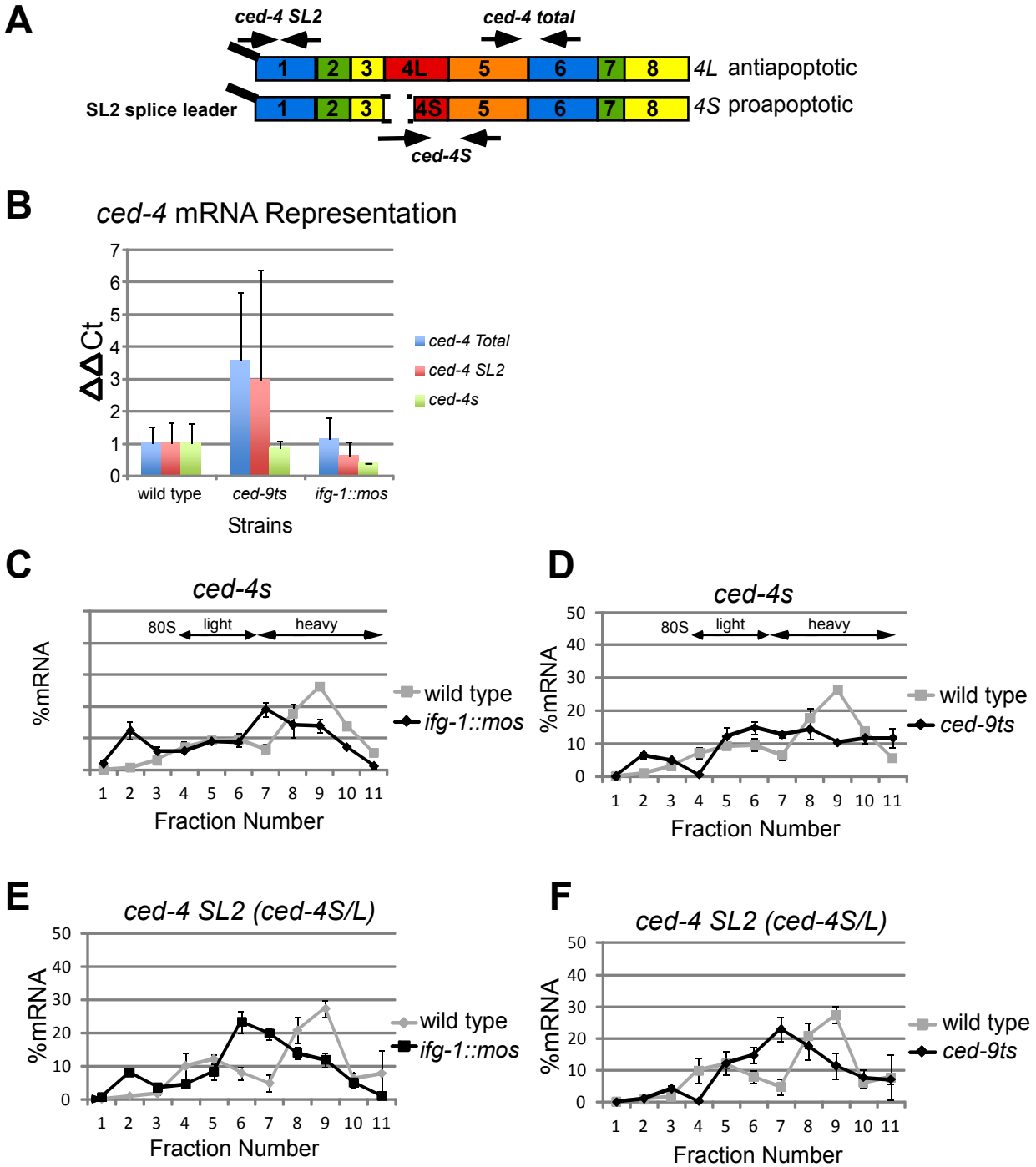
A
ced-4 SL2
ced-4 total
1
2
3
4L
5
6
7
8
4L antiapoptotic
SL2 splice leader
1
2
3
4S
5
6
7
8
4S proapoptotic
ced-4S
B
ced-4 mRNA Representation
ΔΔCt
ced-4 Total
ced-4 SL2
ced-4s
wild type
ced-9ts
ifg-1::mos
Strains
C
ced-4s
80S
light
heavy
%mRNA
wild type
ifg-1::mos
Fraction Number
D
ced-4s
80S
light
heavy
%mRNA
wild type
ced-9ts
Fraction Number
E
ced-4 SL2 (ced-4S/L)
%mRNA
wild type
ifg-1::mos
Fraction Number
F
ced-4 SL2 (ced-4S/L)
%mRNA
wild type
ced-9ts
Fraction Number

Figure 3.8. *ced-4* mRNA variants are translated less efficiently after the induction of cap-independent protein synthesis. (A) Schematic of *ced-4S* and *ced-4L* mRNA with qPCR primers pairs (indicated by black arrows). (B) qPCR of total *ced-4* mRNA, SL2-spliced *ced-4* and proapoptotic *ced-4S* of total RNA extracts from wild type, *ced-9ts* and *ifg-1::mos* strains. There is no significant change in *ced-4* splice variant representation in the *ced-9ts* and *ifg-1::mos* strains. RNA distributions were quantified by qPCR in wild type, *ifg-1::mos*, and *ced-9ts* strains from polysome profiles depicted in Figure 2.3. These gradients represent 1 of 4 biological replicates of wild type and *ced-9ts* strains and 1 of 2 biological replicates of the *ifg-1::mos* strain. Changes efficiency of *ced-4S* mRNA translation was determined in *ifg-1::mos* (C) and *ced-9ts* (D) strains in comparison to the wild type strain. RNA distributions quantified by qPCR indicating changes in translational efficiency of *ced-4 SL2* in the *ifg-1::mos* (E) and *ced-9ts* (F) strains in comparison to the wild type strains.

both the *ifg-1::mos* (Figure 3.8C) and *ced-9ts* (Figure 3.8D) strains (Morrison, 2014). Unfortunately, *ced-4L* mRNA was undetectable by our methods using qPCR on the gradient fractions (data not shown). These data indicate that even the pro-apoptotic *ced-4* mRNA variant experiences decreased translational efficiency during apoptosis and cap-independent synthesis.

As described above, the SL2 trans-spliced c*ed-4* variant mRNA does not contain a potential 5' UTR IRES and as a result should translate cap-dependently. To assess the translational efficiency of SL2 trans-spliced *ced-4* mRNA, we designed *SL2-ced-4* specific primers. We, once again, quantified the target mRNA in total RNA from *ifg-1::mos* and *ced-9ts* worms (Figure 3.8B). There was no significant change in SL2 spliced *ced-4* mRNA representation that could result in increased mRNA translation solely due to increased message availability to the ribosome. Our data also demonstrated that the SL2 trans-spliced *ced-4* variant underwent a similar loss of translational activity in the *ifg-1::mos* (Figure 3.8E) and *ced-9ts* (Figure 3.8F) strains. In summary, decreases in c*ed-4* mRNA translation were consistent for all known spliced variants and indicate that *ced-4* mRNA does not utilize cap-independent translation in *C. elegans*.

Discussion

Initiation of apoptosis in mammals leads to activation of BH3 only proteins, which perturb BCL-2 antiapoptotic activity (Huang and Strasser, 2000). This prevention of BCL-2 antiapoptotic activity leads to Bax/Bak pore formation in the mitochondrial membrane and results in the release of cytochrome c into the cytosol (Figure 3.9) (Desagher et al., 1999; Wei et al., 2000). Cytochrome c, Apaf-1 and caspase-9 then form the apoptosome, which

Figure 3.9

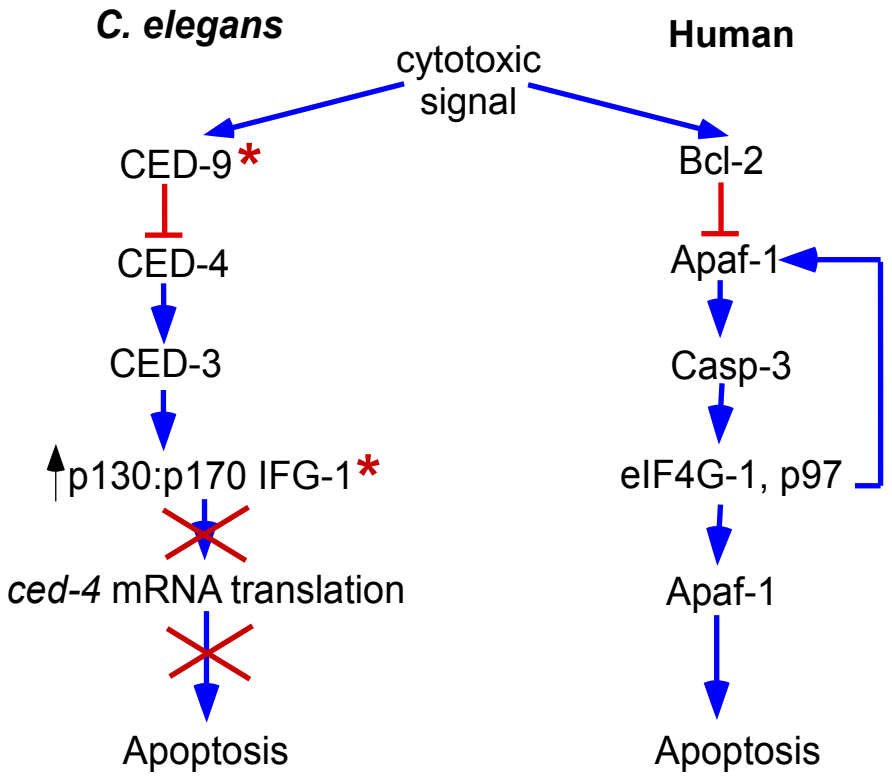
C. elegans
Human
cytotoxic signal
CED-9*
Bcl-2
CED-4
Apaf-1
CED-3
Casp-3
p130:p170 IFG-1*
eIF4G-1, p97
ced-4 mRNA translation
Apaf-1
Apoptosis
Apoptosis

Figure 3.9. Translation of *ced-4* mRNA differs from its mammalian homologue, Apaf-1 mRNA. Apaf-1 translational efficiency in increased during apoptosis due to activation of cap-independent translation initiation. Caspases cleave the cap-dependent eIF4GI removing its cap-binding domain preventing further cap-dependent translation initiation. The constitutively cap-independent eIF4G isoform, p97, is also cleaved by p97. The cleavage of these translation initiation factors leads to enhanced Apaf-1 expression. Although apoptosis in *C. elegans* also leads to the induction of apoptosis, activation of caspase (CED-3) and eIF4G cleavage (IFG-1 p170 and p130), the Apaf-1 homologue (CED-4) is not translated more efficiently. * indicates that genetic manipulation in the *ifg-1::mos* and c*ed-9ts* strains leads to the induction of cap-independent protein synthesis.

allows for the activation of procaspase to its active caspase form (Li et al., 1997). Activated caspases then cleave cellular machinery leading to the death of the cell. Targets of the activated caspases include the eIF4GI, eIF4GII and p97 translation initiation factors (Bushell et al., 1999; Marissen et al., 2000). Cleavage of eIF4GI leads to an increase in cap-independent translation as a result of the eIF4E and PABP domain being cleaved away from the ribosome association domain (Morino et al., 2000). The ribosome association domain is still able to conduct translation initiation that is not dependent on the mRNA cap (Morino et al., 2000). A specific pool of mRNAs are not dependent on cap-association for their recruitment to the ribosome for translation. One example of a cap-independent mRNA with an IRES sequence is Apaf-1 (Coldwell et al., 2000). IRES-mediated translation allows for continued expression of Apaf-1 protein after the shut down of cap-dependent protein synthesis (Coldwell et al., 2000). Apaf-1 expression drives further apoptosis and complete eIF4G cleavage. In this study we have demonstrated a key point of divergence in the transaltional regulation of the *C. elegans* apoptotic pathway. We were unable to detect a 5' IRES in *ced-4* mRNA that would allow for its enhanced translation after IFG-1 cleavage in *C. elegans.* Additionally, *ced-4* mRNA translation was not enhanced upon induction of cap-independent translation activity *in vivo*. Thus, overall the regulation of translation of apoptotic mRNAs and the ability to feedback into the pathway through CED-4/Apaf-1 is not conserved in our proposed model (Figure 3.9).

Extensive characterization of the 5' endpoint of *ced-4* mRNA did not reveal an extended 5' UTR region. The intergenic region with IRES characteristics was not found in mature mRNA variants via RPAs of total RNA, poly(A) RNA or actively translating mRNA. By RT-PCR we were unable to amplify mature fully-spliced messages with a 5' UTR of more

than 69 bp. Although the 69 bp mRNA was amplified and sequenced to show a fully-spliced *ced-4* mRNA variant through exon 6, we were unable to confirm this message variant via other PCR methods. We were also unable to confirm that this message was fully mature due to the amplification not extending over all intron-exon junctions. The fact that a 69 bp extended *ced-4* mRNA was not detected by RPA may suggest that this message was an immature mRNA variant. SL PCR to identify alternative splicing leading to other mRNA variants, only amplified the known SL2-spliced mRNA variant. Overall, our extensive 5' characterization failed to identify a reliably detected 5' extended mRNA variants. Thus we conclude that the *ced-4* mRNA structure differs from the human Apaf-1 mRNA structure. This difference in mRNA structure results in a differing mechanism of translation initiation after eIF4G cleavage during apoptosis, due to the absence of a 5' IRES sequence.

Although the mammalian and *C. elegans* apoptotic pathways are closely conserved, the upregulation of Apaf-1 expression due to its cap-independent synthesis is not a conserved feature (Figure 3.9). Not only were we unable to identify an IRES sequence in the 5' UTR of *ced-4,* we were also unable to observe an increase in the translational efficiency of *ced-4* mRNA after IFG-1 p170 depletion. The depletion of IFG-1 p170 in the *ifg-1::mos* strain did not result in an increase in *ced-4* mRNA translational efficiency as we had previously observed with the *hsp-3* cap-independent mRNA (Morrison, 2014). Additionally, *ced-9ts* induced IFG-1 p170 cleavage, did not result in an increase of *ced-4* mRNA translational efficiency. These studies indicate *ced-4* mRNA translation is not maintained after the depletion of the cap-dependent translation factor IFG-1 p170 and suggest that the mode of translation of *ced-4* mRNA differs from Apaf-1. Additionally, these findings also suggest an alternative interpretation of previous observations that CED-4 punctate

structures increased in germ cells undergoing apoptosis in worms depleted of IFG-1 p170 (Contreras et al., 2011). We now conclude that this was not due to an increase in CED-4 protein synthesis, but instead resulted from either changes in protein localization or stabilization during apoptosis.

Our data delineates clear differences between the protein synthetic regulation of Apaf-1 mRNA in *C. elegans* whole worms and humans cell culture. Increased flux through the apoptotic pathway in *C. elegans* in the absence of increased CED-4 protein accumulation most likely results the increased expression of other proapoptotic proteins or a decrease in expression of antiapoptotic proteins.

CHAPTER 4: DEPLETION OF THE CAP-DEPENDENT IFG-1 (eIF4G) ISOFORM IN *C. ELEGANS* DOES NOT AFFECT GERM CELL TUMOR PROGRESSION

Introduction

Within the *C. elegans* germ line the fate of stem cells is regulated primarily by mRNA translational control (Kimble and Crittenden, 2007). Germ cells progress linearly from the distal tip proximally through mitosis into a transition zone and then into meiosis. The cell fate decisions leading to this meiotic progression are the result of networks of translational control (Figure 4.1A). At the distal end of the *C. elegans* gonad is a somatic distal tip cell (DTC), which is essential for the maintenance of the stem cell population (Crittenden et al., 1994; Henderson et al., 1994; Tax et al., 1994). The DTC expresses LAG-2, which binds to the GLP-1/Notch receptor that is expressed on the cell surface of germ cells (Figure 4.1B) (Crittenden et al., 1994; Henderson et al., 1994; Tax et al., 1994). LAG-2 binding the GLP-1 receptor results in cleavage of its intracellular receptor domain (Christensen et al., 1996; Kovall, 2008). The cleaved product then translocates to the nucleus and promotes mitosis and prevents precocious meiotic gene expression (Christensen et al., 1996; Kovall, 2008). One protein whose expression is enhanced by GLP-1 signalling is FBF-2, which is essential for inhibiting meiosis and maintaining the stem cell niche (Crittenden et al., 2002; Lamont et al., 2004). FBF-2 inhibits meiotic genes by binding to the 3' UTR of their mRNAs and inhibiting their translation (Bernstein et al., 2005). Examples of FBF targets include *gld-1* and *gld-3* mRNAs, which themselves encode translational regulators that promote the transition to meiosis (Crittenden et al., 2002; Eckmann et al., 2004). GLD-3 promotes meiosis by associating with the poly(A) polymerase, GLD-2, that lengthens the poly(A) tails

Figure 4.1

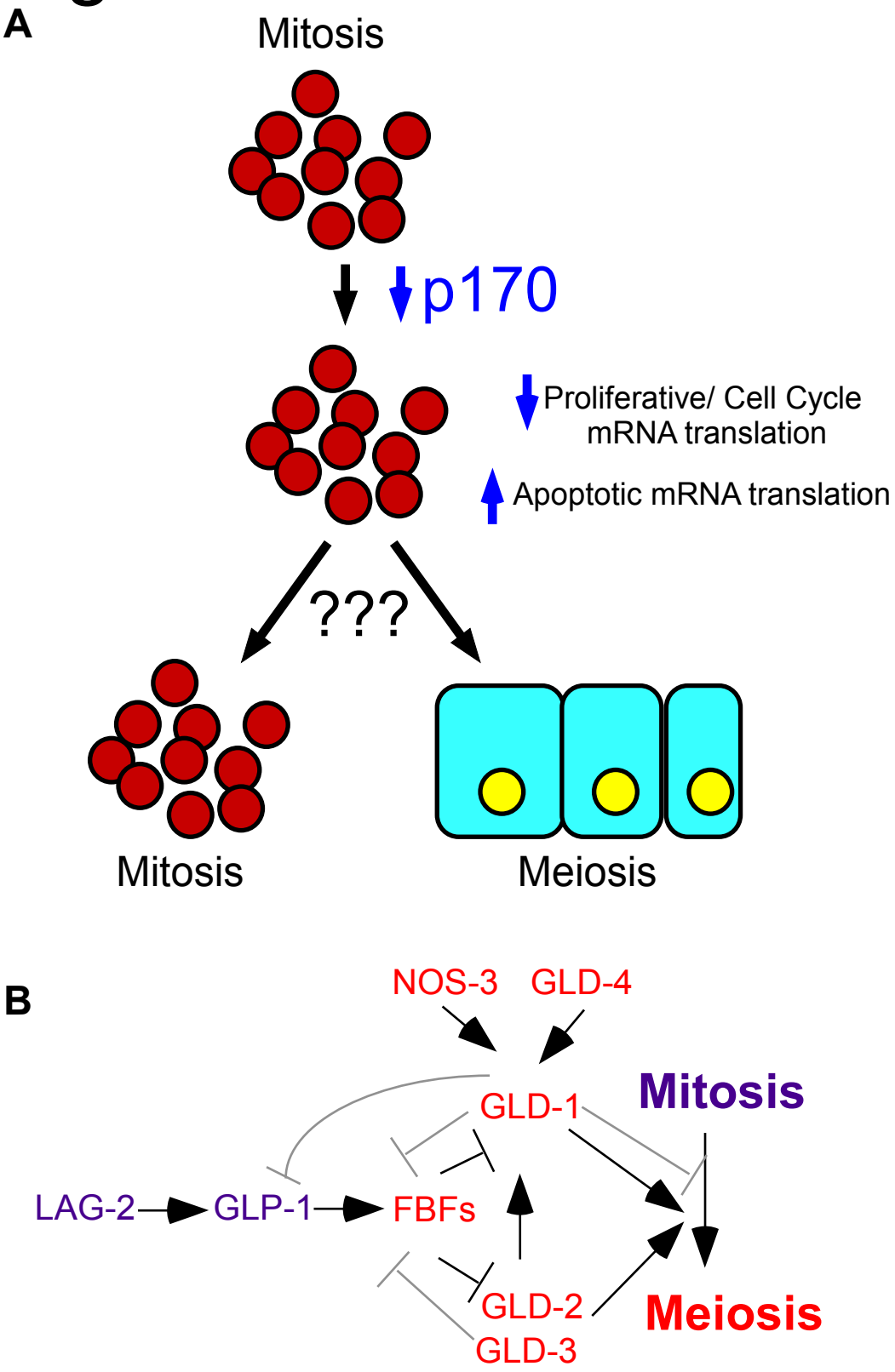
A
Mitosis
p170
Proliferative/ Cell Cycle
mRNA translation
Apoptotic mRNA translation
???
Mitosis
Meiosis
B
NOS-3
GLD-4
GLD-1
Mitosis
LAG-2
GLP-1
FBFs
GLD-2
GLD-3
Meiosis

Figure 4.1. Model depicting known translational regulation in germ cell tumors. (A) Model illustrating our hypothesis that as a result of IFG-1 p170 knockdown the mitotic cell fate decision will change to meiosis. Knockdown of p170 results in decreased translation of proliferative and cell cycle related mRNAs and increased translation of apoptotic mRNAs in mammals. (B) Schematic depicting translational regulation involved in the mitosis to meiosis cell fate decision. LAG-2 stimulates the GLP-1 receptor leads to FBF expression. FBF inhibits the translation and expression of GLD-1, GLD-2 and GLD-3. The GLD family members are key translational regulators of genes involved in the mitosis to meiosis cell fate decision.

of targeted messages increasing their stability and translational efficiency (Eckmann et al., 2004; Eckmann et al., 2002). GLD-1, on the other hand, is a translational repressor that prevents the translation of mitotic mRNAs, allowing for the cells to enter meiosis (Jones and Schedl, 1995; Lee and Schedl, 2001). GLD-1 is even further regulated translationally by NOS-3, which perturbs the FBF inhibition of GLD-1, and GLD-4, another poly(A) polymerase that acts on *gld-1* mRNA (Hansen et al., 2004; Kraemer et al., 1999; Schmid et al., 2009). GLD-1, in turn, represses GLP-1 upon its expression, further committing the germ cells to meiosis (Farley and Ryder, 2012). Thus, a complex network of translational regulators governs the mitosis to meiosis transition, suggesting this differentiation step should be highly sensitive to disruptions in translation initiation activity.

As a result of replicative immortality and maintenance of pluripotency of germ cells, the *C. elegans* germ line is a versatile model to study mechanisms that govern cell fate decisions. Likewise, this system is useful in assessing how dysregulation of translational control can result in the formation of germ cell tumors. In this study we focus on two different types of germ cell tumors that result from the disruption of key translational regulators: *glp-1(ar202)* and *gld-1* (Figure 4.2A-C). *glp-1(ar202)* worms have a single base pair missense mutation (G529E) that results in proximal germ cell tumor and a penetrating distal germ cell tumor, at later time points, after a 25˚C temperature shift (Pepper et al., 2003). These tumors result from a population of mitotic germ cells that fail to differentiate and continue to mitotically divide (Pepper et al., 2003). Conversely, the other strain [gld-1(q485) I/hT2 [bli-4(e937) let-?(q782) qIs48] (I;III); fem-1(hc17)] lacking GLD-1 develops germ cell tumors that initially enter meiosis before dedifferentiating back to mitosis (Francis et al., 1995a; Francis et al., 1995b). The loss of GLD-1 prevents suppression of GLP-

Figure 4.2

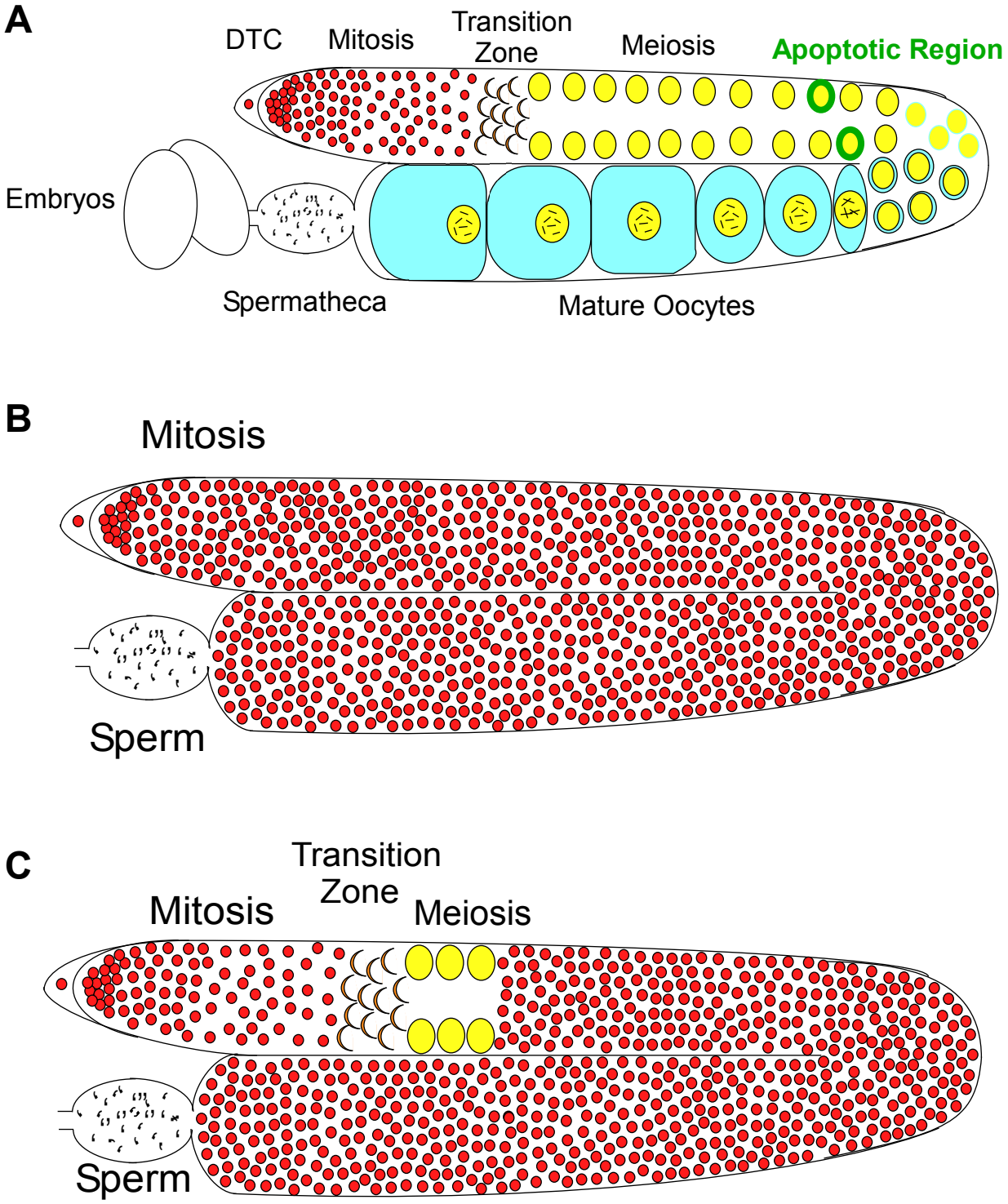
A
DTC
Mitosis
Transition Zone
Meiosis
Apoptotic Region
Embryos
Spermatheca
Mature Oocytes
B
Mitosis
Sperm
C
Transition Zone
Mitosis
Meiosis
Sperm

Figure 4.2. Model depicting mitotic and dedifferentiated germ cell tumors compared to the wild type gonad. (A) Schematic representing the wild type gonad. (B) Schematic representing a mitotic germ cell tumor resulting from a gain-of-function mutation in *glp-1.* (C) Schematic representing a dedifferentiated germ cell tumor from a *gld-1* loss-of-function strain.

1 and mitosis, while also allowing unrestricted translation of meiotic mRNAs that should be repressed (Francis et al., 1995b) (Francis et al., 1995a).

There are two primary mechanisms of translation initiation: cap-dependent translation and cap-independent translation. During cap-dependent translation, mRNA is recruited to the scaffolding protein, IFG-1 p170 (eIF4G), by the cap-binding protein, IFE (eIF4E) (Contreras et al., 2008; Imataka et al., 1998; Lamphear et al., 1995). IFG-1 p170 has binding domains for IFEs, ribosome binding and PABPs (Contreras et al., 2011; Contreras et al., 2008; Imataka et al., 1998; Lamphear et al., 1995; Morino et al., 2000). Thus, IFEs and IFG-1 p170 collectively recruit mRNA to the ribosome for translation (Keiper et al., 1999). In contrast, cap-independent translation does not rely on IFE recruitment of mRNA to IFG-1 p170 (Nevins et al., 2003). Instead, *C. elegans* express a second eIF4G isoform, IFG-1 p130, that is constitutively cap-independent due to its inability to associate with cap-binding proteins (Contreras et al., 2008). Cap-independent translation is prevalent during apoptosis when CED-3 (caspase) cleaves IFG-1 isoforms removing the IFE and PABP binding domains from IFG-1 p170 (Contreras et al., 2011). In mammalian cells, cap-independent translation is also enhanced when suppressed mTOR signaling results in the dephosphorylation of 4E binding protein (4E-BP) resulting in it sequestering eIF4E, preventing eIF4G association (Ma and Blenis, 2009; Tee and Proud, 2000; Tinton and Buc-Calderon, 1999; Vries et al., 1997). A similar mechanism of cap-independent translation, through 4E-BP sequestration, has yet to be identified in *C. elegans.* mRNAs involved in cell cycle progression or cell growth, such as cyclin D1 are typically highly cap-dependent and thus disadvantaged upon the switch (De Benedetti and Graff, 2004). Further growth and cell cycle progressions are thus halted. However, mRNAs that encode proteins involved in

stress response and apoptosis are translated more efficiently allowing cellular recovery or programmed cell death (Coldwell et al., 2000).

Enhanced cap-dependent translation due to over-expression of eIF4E and eIF4G results in accelerated cellular growth, tumorigenesis and malignant translation of mammalian cells (Fukuchi-Shimogori et al., 1997; Lazaris-Karatzas et al., 1990). This transformation is due, in part, to the enhanced translation of cap-dependent cell cycle mRNAs (De Benedetti and Graff, 2004). Conversely, enhanced cap-independent translation, as we have previously reported in *C. elegans* due to the RNAi knockdown of the cap-dependent IFG-1 p170, results in the induction of apoptosis (Contreras et al., 2011; Contreras et al., 2008). Thus, in this study we attempt to knockdown cap-dependent translation using RNAi targeted against IFG-1 p170 to determine if changes in the mode of translation affect *C. elegans* germ cell tumor fate decisions (Figure 4.3A). We hypothesized that the decrease in cap-dependent translation might prevent translation of proliferative and cell cycle mRNAs and simultaneous increased translation of apoptotic mRNAs resulting in alternative cell fate decisions of proliferative germ line tumor cells (Figure 4.1A). It is possible that suppressing protein synthetic events that drive mitosis would cause germ cell tumor cells to arrest. Alternatively, enhancing protein synthetic events that promote apoptosis might even cause tumor cell death. However, our results indicate that solely changing the relative amounts of cap-dependent to cap-independent translation in *C. elegans* germ cell tumor animals did not result in changes in germ cell tumor fate in the P0 generation of worms.

Results

Knockdown of cap-dependent IFG-1 p170 induces germ cell apoptosis. To phenotypically confirm the depletion of IFG-1 p170 by RNAi in live worms, we assayed the production of germ cell corpses. As previously described, RNAi against the 5' end of the longest *ifg-1* mRNA was used to selectively deplete cap-dependent IFG-1 p170 (Figure 4.3A) (Contreras et al., 2008). IFG-1 p170 RNAi-expressing bacteria were fed to wild type worms expressing CED-1::GFP. CED-1 is a lipoprotein transmembrane receptor found in the gonad sheath. It recognizes apoptosing cells allowing the sheath cells to invade and engulf dying oocytes. Thus, CED-1::GFP allows for the real-time visualization of the engulfment process and allows observation of the number of cells actively undergoing apoptosis (Zhou et al., 2001). Under the identical conditions used in the germ cell tumor strains, selective depletion of IFG-1 p170 significantly increased germ cell apoptotic corpses in wild type worms when compared to worms feed IFG-1 p170 RNAi (Figure 4.3C,E). The overall linear progression and differentiation of residual germ cells within the gonad, however, did not change (Figure 4.3B,D). As previously described, IFG-1 p170 RNAi also lead to a decrease in fertility (Contreras et al., 2008). The gonad morphology also overall deteriorated due to the large number of apoptotic cells. Interestingly, gonad deterioration seems to be specific to the IFG-1 defect. Similar gonad deterioration was not observed when germ cell apoptosis was alternatively induced by knockdown of the antiapoptotic protein, CED-9 (data not shown).

Knockdown of IFG-1 p170 does not change germ cell tumor progression in *glp-1 gf* worms. Previous experiment in both *C. elegans* whole worms and human cell lines have demonstrated that decreases in eIF4G cap-dependent isoform representation increased

Figure 4.3

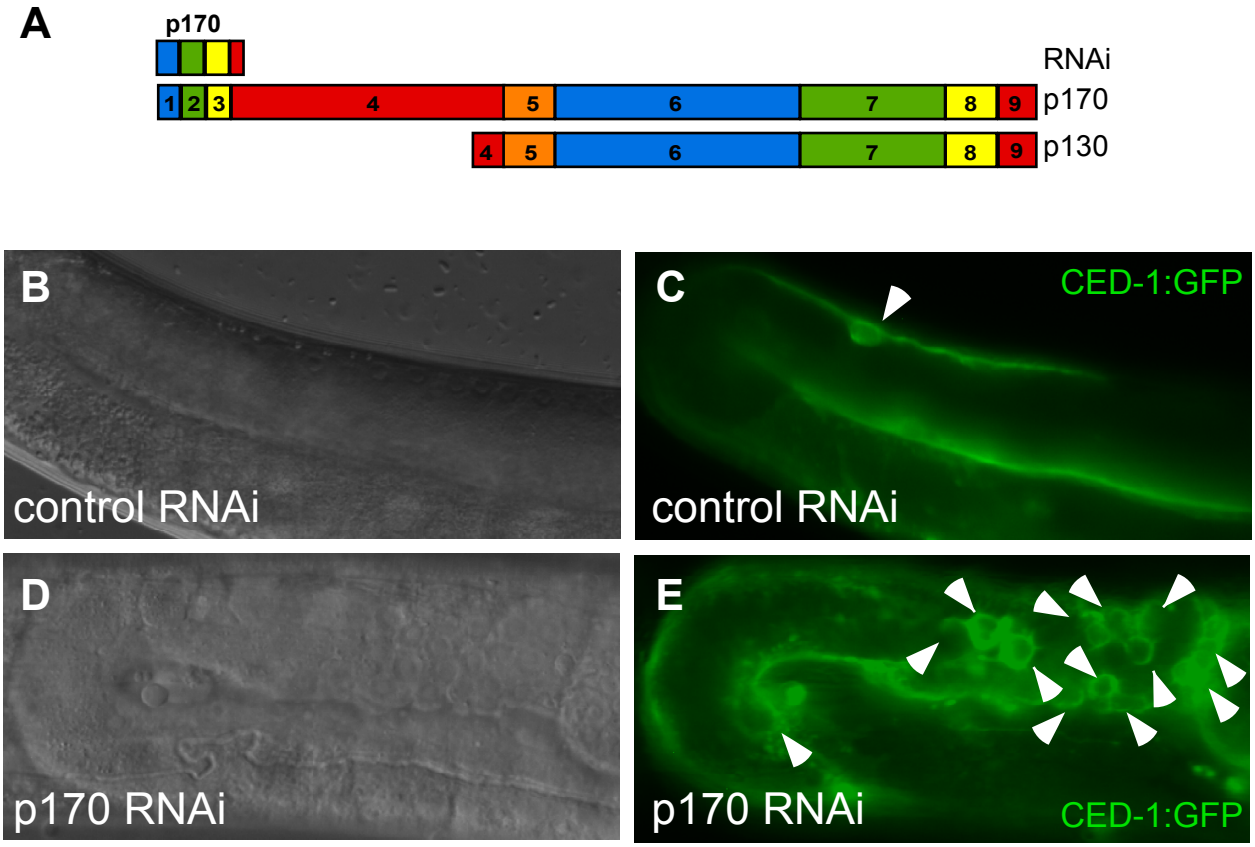
A
p170
RNAi
1
2
3
4
5
6
7
8
9
p170
4
5
6
7
8
9
p130
B
control RNAi
C
CED-1:GFP
control RNAi
D
p170 RNAi
E
p170 RNAi
CED-1:GFP

Figure 4.3. Suppression of cap-dependent translation induces germ cell apoptosis in the wild type gonad. (A) Schematic of *ifg-1 p170* and *p130* mRNA variants and RNAi target to *ifg-1 p170*. Fluorescence and DIC images of wild type, CED-1::GFP, expressing control RNAi (B-C) and *ifg-1 p170* RNAi (D-F) fed worms.

mRNA translation of both pro- and antiapoptotic mRNAs while subsequently decreasing mRNA translation of cell cycle mRNAs (Coldwell et al., 2000; De Benedetti and Graff, 2004; Henis-Korenblit et al., 2000; Imataka et al., 1997; Morrison, 2014). We hypothesized that changing the protein synthetic mechanism in tumorous germ cells in *C. elegans,* to rely more heavily on cap-independent initiation, would result in new protein expression patterns leading to reversion of the tumor phenotype. Therefore, we oberseved germ cell progression after IFG-1 p170 depletion in wild type germ lines and germ cell tumor worm strains using DAPI staining and immunofluorescence of phophohistone H3. The former clearly identifies germ cells at various stages of meiotic differentiation by chromosome morphology. The latter identifies cells actively undergoing mitosis and is used to estimate mitotic index. We anticipated that the proposed changes in protein expression would lead to a restored normal progression of germ cells. In the wild type strain fed either control or IFG-1 p170 RNAi there was normal germ cell progression from mitosis, through the transition zone and into meiosis where germ cell arrested in the M-phase of meiosis I (Figure 4.4A-D). DAPI staining of control RNAi treated worms confirmed proper packing of meiotic nuclei as cells entered meiosis and nuclei condensed into six bivalent chromosomes during subsequent diakinesis (Figure 4.4B). The progression of mitotic and meiotic nuclei did not change after IFG-1 p170 RNAi treatment (Figure 4.4D). This was not unexpected in the P0 generation of RNAi fed worms. It should be noted that in the F1 generation IFG-1 p170 RNAi results in normal meiotic and mitotic nuclei, however during diplotene stages chromosome condensation did not occur (Contreras et al., 2008). The *glp-1(ar202)* strain fed control RNAi had a proximal germ tumor and a penetrating distal germ cell tumor due to germ cells failing to exit mitosis (Figure 4.4E). DAPI staining confirmed

Figure 4.4

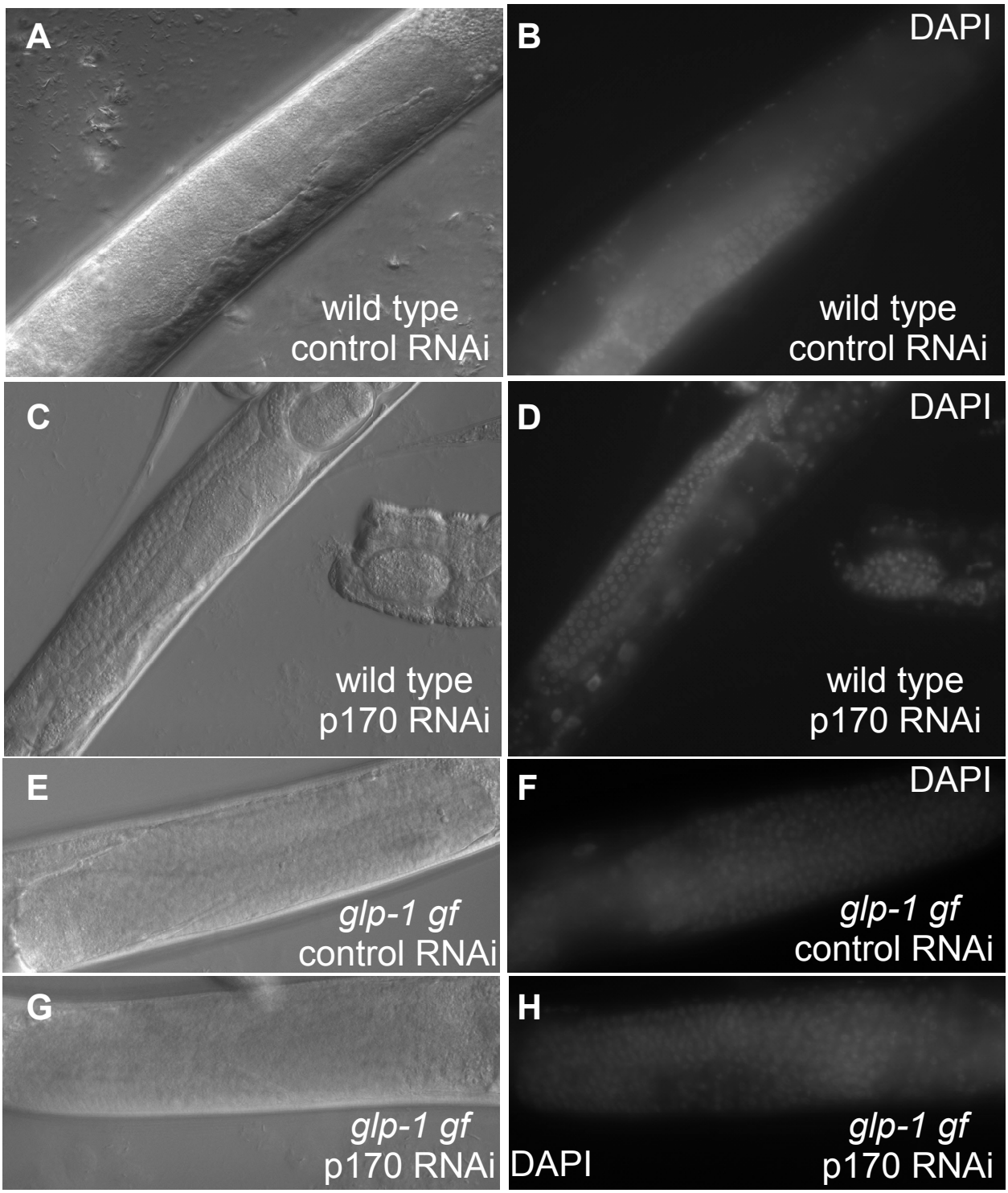
A
wild type
control RNAi
B
DAPI
wild type
control RNAi
C
wild type
p170 RNAi
D
DAPI
wild type
p170 RNAi
E
glp-1 gf
control RNAi
F
DAPI
glp-1 gf
control RNAi
G
glp-1 gf
p170 RNAi
H
DAPI
glp-1 gf
p170 RNAi

Figure 4.4. Depletion of cap-dependent protein synthesis does not affect the mitotic cell fate decision in *glp-1* gain-of-function germ cell tumors. DIC and DAPI images of wild type control RNAi (A-B) and *ifg-1 p170* RNAi (C-D) feed worms. DIC and DAPI images of *glp-1* gain-of-function control RNAi (E-F) and *ifg-1 p170* RNAi (G-H) feed worms.

densely packed mitotic nuclei throughout (Figure 4.4F). The observed progression of mitotic germ cells did not change in IFG-1 p170 RNAi fed worms (Figure 4.4G). We did not observe any mature oocytes or meiotically differentiated germ cells in the *glp-1* strain adult worms. Additionally, we observed densely packed mitotic nuclei extending throughout the gonad in both proximal and penetrating distal tumors (Figure 4.4H).

The extent of mitosis does not change after IFG-1 p170 knockdown in the *glp-1* strain. Although we did not observe a reversion of the tumorous phenotype in the *glp-1* strain after the knockdown of IFG-1 p170, we predicted that the changes in protein expression might still decrease the extent of mitosis in the *glp-1* strain. This could result from a decrease in the expression of proteins related to cell cycle progression as previously observed in mammalian cell culture. To observe changes in the extent of mitosis we dissected gonads from RNAi-treated worms and immunostained these gonads with an antibody against phospho-histone H3. This immunostaining illuminates germ cells in the M phase of both mitosis and meiosis. Immunostaining of wild type worms fed control RNAi revealed several cells undergoing M phase mitosis near the distal tip of the gonad (Figure 4.5A-C). Additionally, at the proximal end of the gonad, the mature oocytes were arrested in M-phase meiosis as evident by their six condensed bivalent chromosomes. Overlay of phospho-histone H3 immunostaining with DAPI indicated phopho-H3 immunostaining was specific to DNA in M-phase cells (Figure 4.5B-C). We observed similar staining patterns in wild type worms feed IFG-1 p170 RNAi, indicating no change in the extent of mitosis due to knockdown of IFG-1 p170 (Figure 4.5D-F). We did observe, however, a decrease in the number of mature oocytes after IFG-1 p170 knockdown. This decrease was expected based

Figure 4.5

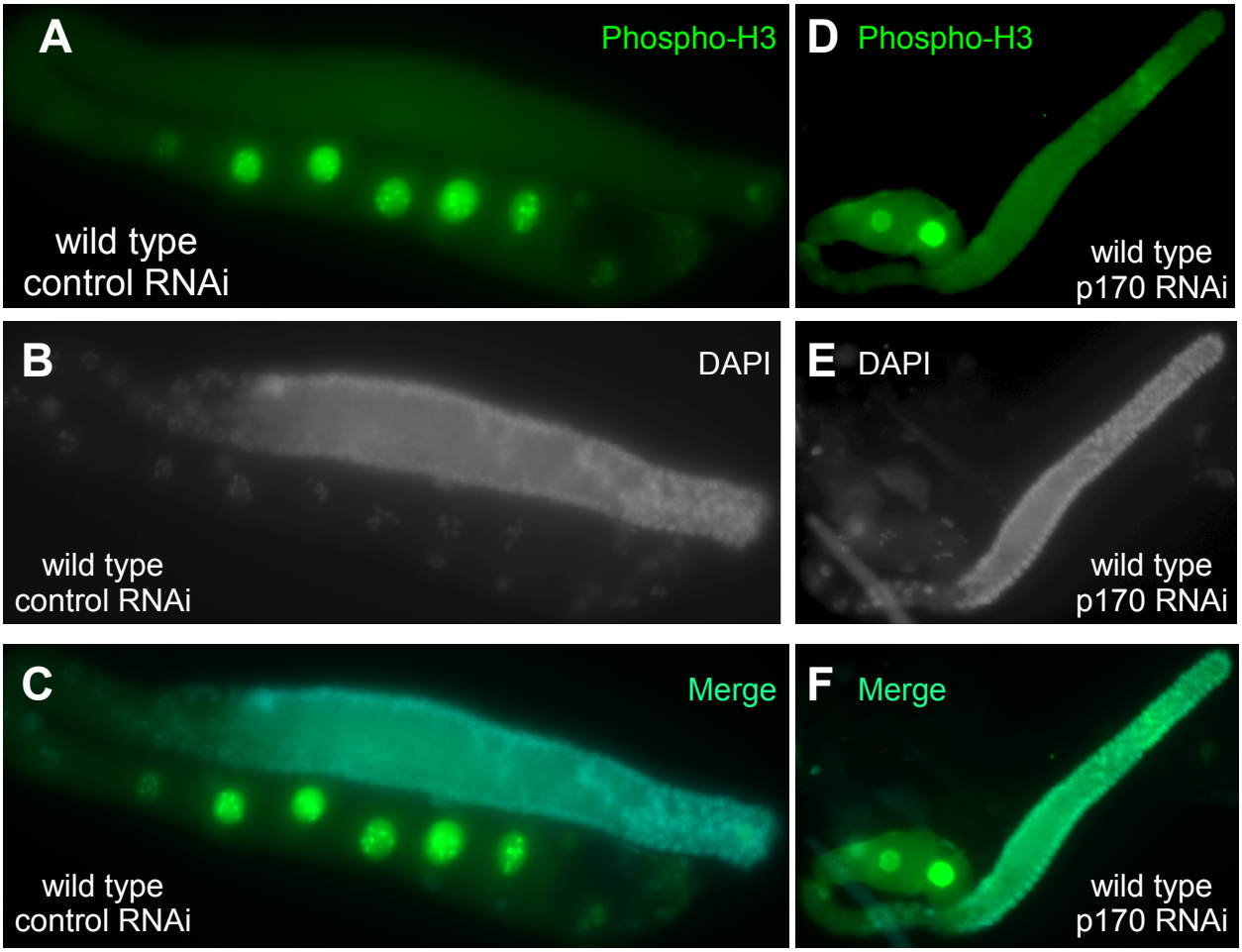
A
Phospho-H3
wild type
control RNAi
D
Phospho-H3
wild type
p170 RNAi
B
DAPI
wild type
control RNAi
E
DAPI
wild type
p170 RNAi
C
Merge
wild type
control RNAi
F
Merge
wild type
p170 RNAi

Figure 4.5. Population of mitotic germ cells does not change in wild type gonads after the depletion of cap-associated IFG-1 p170. Phospho-histone immunostaining, DAPI and overlayed images of wild type control RNAi (A-C) and *ifg-1 p170* RNAi (D-F) feed worms. DIC images confirm normal growth and differentiation of oocytes within the gonads of RNAi feed worms.

on previous experiments revealing reduced fertility (Contreras et al., 2008). Once again, phospho-histone H3 immunostaining was specific, demonstrated by its colocalization with DNA (Figure 4.5E-F). Overall, these finding demonstrate that in wild type worms there was no change in the extent of mitosis after the knockdown of IFG-1 p170.

We next addressed whether knockdown of IFG-1 p170 would result in a reduction of the extensive mitosis in *glp-1* tumorous germ lines. Phospho-histone H3 immunostaining revealed a large number of cells in M phase mitosis in the *glp-1* strain (Figure 4.6A-C). These cells were particularly concentrated in the proximal end of the gonad in the mitotic proximal tumor (Figure 4.6A). We did observe in a number of gonads without a completely penetrating distal germ cell tumor. In these several smaller oocytes arrested in M-phase meiosis in the region between the proximal and distal germ cell tumors were observed (Figure 4.6A). However, most gonads had completely penetrating distal germ cell tumors. DAPI staining colocalization demonstrated the specificity of Phospho-histone H3 immunostaining (Figure 4.6B-C). The extent of mitosis did not change due to the knockdown of IFG-1 p170 (Figure 4.6D-F). A large number of cells undergoing mitosis in the *glp-1* strain were still observed after the knockdown of IFG-1 p170 (Figure 4.6D). Once again, the M-phase mitotic cells were mostly concentrated in the proximal germ cell tumor. Occasionally, we also observed meiotic M-phase germ cells in the region between the proximal and distal germ cell tumors as were previously observed after control RNAi feeding. Most *glp-1* tumors, however, had penetrating distal germ cell tumors. The specificity of phospho-histone H3 staining was once again confirmed by DAPI overlay (Figure 4.6E-F).

Figure 4.6

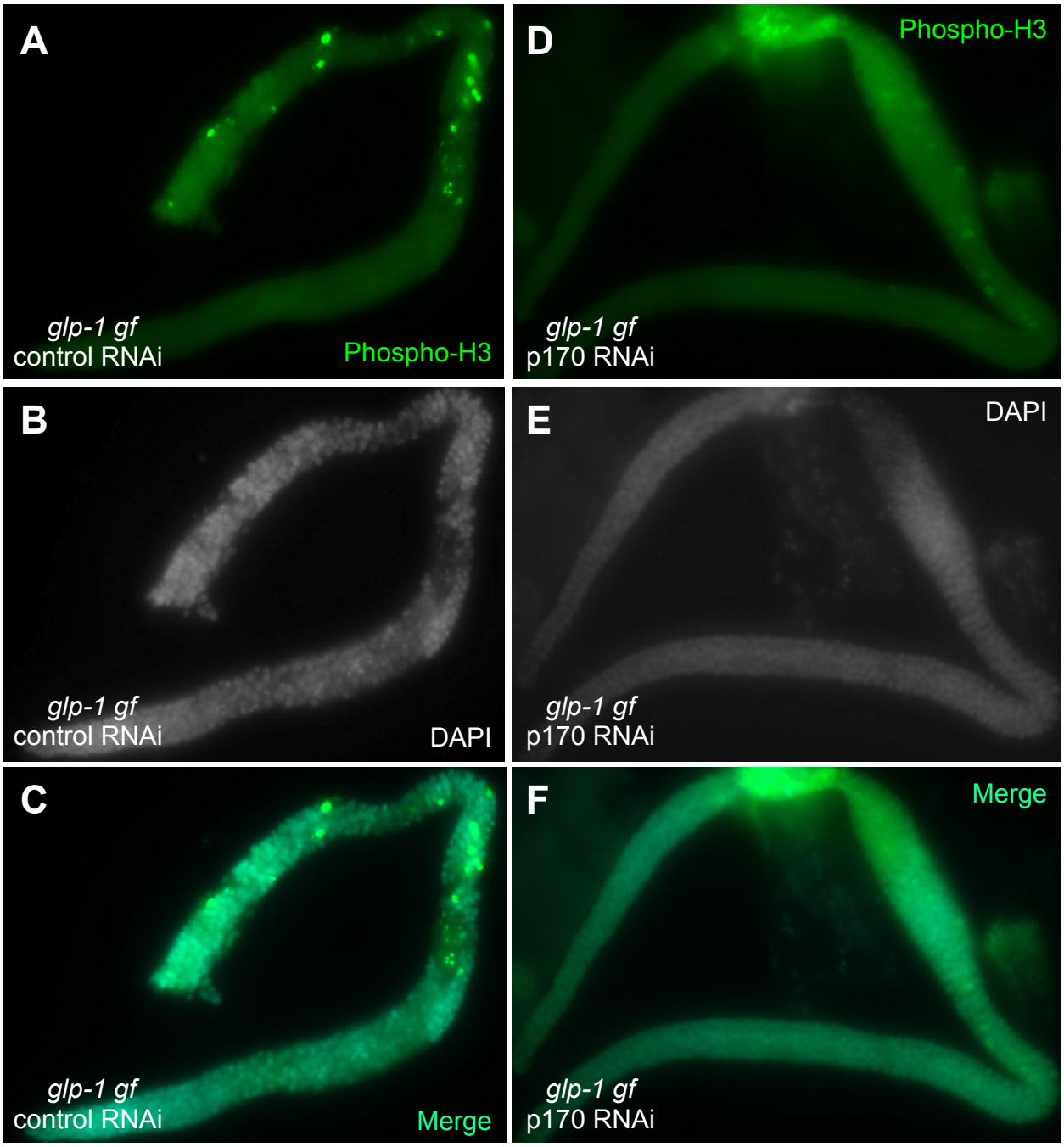
A
glp-1 gf
control RNAi
Phospho-H3
D
Phospho-H3
glp-1 gf
p170 RNAi
B
glp-1 gf
control RNAi
DAPI
E
DAPI
glp-1 gf
p170 RNAi
C
glp-1 gf
control RNAi
Merge
F
Merge
glp-1 gf
p170 RNAi

Figure 4.6. Population of mitotic germ cells does not change in *glp-1* gain-of-function germ cell tumors after the depletion of cap-associated IFG-1 p170. Phospho-histone immunostaining, DAPI and overlayed images of *glp-1* gain-of-function control RNAi (A-C) and *ifg-1 p170* RNAi (D-F) feed worms. DIC images confirm normal growth and differentiation of oocytes within the gonads of RNAi feed worms.

Knockdown of IFG-1 p170 does not alter germ cell tumor progression in dedifferentiated *gld-1lf* germ cell tumors. The *gld-1* loss of function strain differs from the *glp-1* strain in that germ cells initially enter meiosis and then dedifferentiate back into mitosis. This difference in tumor formation and the differences in translational regulator expression (GLP-1 now properly expressed, GLD-1 now absent) may result in different sensitivity to IFG-1 p170 knockdown. Control RNAi treated *gld-1* worms had dedifferentiated germ cell tumors (Figure 4.7A-B). The germ cells entered meiosis and then reverted back into mitosis resulting in a gonad filled with mitotic germ cells (Figure 4.7A). DAPI staining revealed the condensed mitotic nuclei extending through the entirety of the gonad to the proximal end vulva (Figure 4.7B). Neither the morphology nor the extent of germ cell tumor progression changed after the knockdown of IFG-1 p170 in the *gld-1* strain (Figure 4.7C-D). In this strain, no cells progressed normally through the gonad to give rise to mature oocytes (Figure 4.7C). Additionally, DAPI staining revealed densely packed mitotic nuclei extending throughout the gonad (Figure 4.7D).

The extent of mitosis does not change after IFG-1 p170 knockdown in the dedifferentiated *gld-1* tumor strain. Phospho-histone H3 immunostaining of *gld-1* worms demonstrated a large number of M phase mitotic cells found throughout the entire gonad as expected for the tumorous germ line (Figure 4.8A-C). Phospho-histone H3 staining was shown to colocalize with DNA (Figure 4.8B-C). Knockdown of IFG-1 p170 did not reduce the number of cells in M phase mitosis in the *gld-1* strain (Figure 4.8D). A large number of cells dispersed throughout the gonad are found in M phase mitosis in this

Figure 4.7

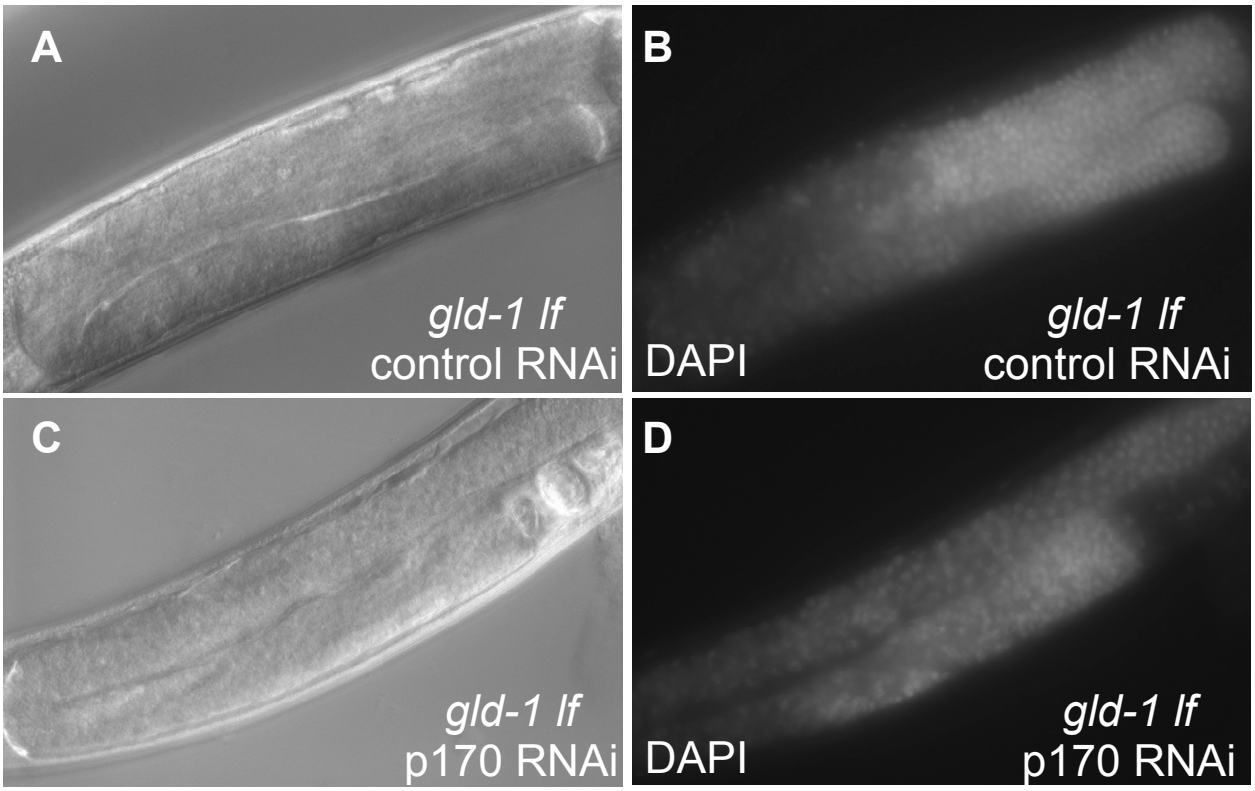
A
gld-1 lf
control RNAi
B
DAPI
gld-1 lf
control RNAi
C
gld-1 lf
p170 RNAi
D
DAPI
gld-1 lf
p170 RNAi

Figure 4.7. Depletion of cap-dependent protein synthesis does not affect the mitotic cell fate decision in *gld-1* loss-of-function germ cell tumors. DIC and DAPI images of *gld-1* loss-of-function control RNAi (A-B) and *ifg-1 p170* RNAi (C-D) feed worms.

dedifferentiated germ line. Phospho-Histone H3 immunostaining indicated many cells in M phase (Figure 4.8E-F).

Discussion

Changes in specific translational control in the germ line leads to the dysregulation of the stem cell populations (Francis et al., 1995a; Francis et al., 1995b; Pepper et al., 2003). LAG-2 normally stimulates the GLP-1 receptor of germ cells near the distal tip, but its signaling tapers off as cells progress beyond the mitotic region. In the *glp-1(ar202)* strain, however, GLP-1 signaling remains active beyond the wild type mitotic region and germ cells never exit mitosis (Pepper et al., 2003). Conversely, when there is a loss of function of GLD-1 germ cells initially enter meiosis, but then dedifferentiate back to mitosis (Francis et al., 1995a; Francis et al., 1995b). Similar dedifferentiation and enhanced proliferation is frequently observed in mammalian cancers. Of note, increased levels of translation initiation factors, eIF4G and eIF4E, are routinely observed in transformed cells and malignant tumors (Fukuchi-Shimogori et al., 1997; Lazaris-Karatzas et al., 1990).

In the wild type germ line the knockdown of cap-dependent translation leads to the induction of apoptosis, but does not suppress early germ cell mitosis nor differentiation into meiotic oocytes (Contreras et al., 2011; Contreras et al., 2008). The induction of apoptosis results in the cleavage of the translation initiation factor IFG-1 leading to the induction of cap-independent translation (Contreras et al., 2011). Increased proportions of cap-independent translation are correlated with enhanced expression of apoptotic and stress-related mRNAs (Morrison, 2014). We did not observe changes in standard germ cell phenotypes (other than more extensive apoptosis) that correlate with increased cap-

Figure 4.8

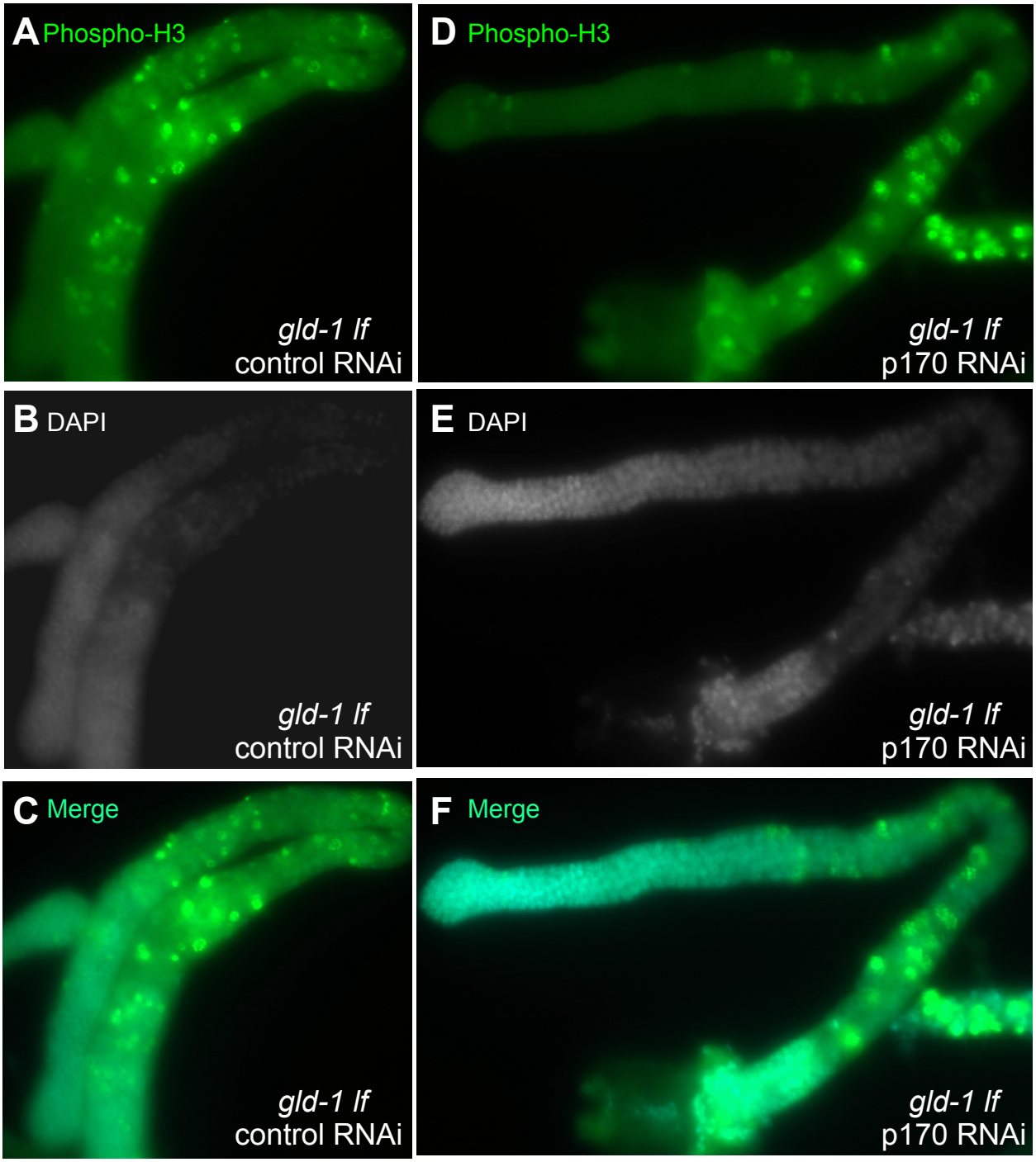
A Phospho-H3
gld-1 lf
control RNAi
D Phospho-H3
gld-1 lf
p170 RNAi
B DAPI
gld-1 lf
control RNAi
E DAPI
gld-1 lf
p170 RNAi
C Merge
gld-1 lf
control RNAi
F Merge
gld-1 lf
p170 RNAi

Figure 4.8. Population of mitotic germ cells does not change in *gld-1* loss-of-function germ cell tumors after the depletion of cap-associated IFG-1 p170. Phospho-histone immunostaining, DAPI and overlayed images of *gld-1* loss-of-function control RNAi (A-C) and *ifg-1 p170* RNAi (D-F) feed worms. DIC images confirm normal growth and differentiation of oocytes within the gonads of RNAi feed worms.

independent mRNA translation. However, since the *glp-1* and *gld-1* mutant worms have far more extensive mitotic activity, we hypothesized that suppressing cap-dependent translation might have a greater effect. Decreased cap-dependent translation results in decreased translation of cell cycle mRNAs such as cyclin D in mammals. However, we did not observe a decreased number of cells undergoing mitosis in *glp-1* or *gld-1* germ cell tumors with decreased cap-dependent translation. Additionally, we observed no change in phenotype in the germ cell tumors due to changes in translation initiation in the P0 generation.

There are several possible explanations for the absence of changes in cell fate decision due to the knockdown of IFG-1 p170 in the P0 generation. Most simply, knockdown of cap-dependent translation in the P0 generation may have not been extensive enough to fully suppress miototic protein translation. In addition, RNAi intervention in *C. elegans* has been previously observed to result in much more pronounced phenotypes in the F1 and F2 generations. Previous work from our lab indicates that meiotic chromosome condensation does not occur in the F1 generation of p170 depleted worms and infertility results (Contreras et al., 2008). However, in our germ cell tumor strains we were unable to observe changes due to knockdown of IFG-1 p170 in the F1 generation because germ cell tumor strains are themselves mostly infertile. Few, if any, worms survived into the F1 generation and those that did often had shriveled gonads that did not produce any germ cells. Alternatively, the knockdown of cap-dependent translation may result in the decreased expression of both mitotic and meiotic proteins, not changing the ratio of the two. This would prevent germ cell from properly overcoming mitotic signals as they progress into the transition zone of the gonad and enter meiosis. Previous work in our lab

indicated efficient *glp-1* mRNA translation is dependent on expression of the cap-binding initiation factor IFE-1 (Henderson et al., 2009). Additionally, recent work in the lab suggests efficient *gld-1* mRNA translation may also be dependent on IFE-1 expression (personal communication Andrew Friday). Thus, knockdown of cap-dependent translation likely decreases expression of both proteins. Finally, knockdown of cap-dependent translation may not result in overall changes in mitotic and meiotic protein expression because other translational regulators play a larger, dominant role in preventing or enhancing mRNA recruitment to ribosomes. The *C. elegans* germ line has a complex network of translational control. By simply changing the downstream step of translation initiation we may be unable to affect germ cell fate decisions without knocking down other upstream regulators of translation.

Overall, these studies revealed that disrupting the cap-dependent to independent translation activity may not be sufficient to prevent or slow germ cell tumor progression. *glp-1(ar202)* and *gld-1* worms had penetrating mitotic germ cell tumors that defy modest changes in IFG-1 activities.

CHAPTER 5: CONCLUSIONS

During normal growth, development and periods of homeostasis, cells utilize both cap-dependent and independent translation initiation to provide the necessary pool of new proteins to maintain these states (Gilbert, 2010; Komar et al., 2012; Malys and McCarthy, 2011). However, the relative contribution of cap-dependent and independent translation varies in quiescent, dividing and differentiating cells resulting in different patterns of protein expression. The ability to transition between these two mechanisms of translation initiation allows cells to adapt to changing environments and respond quickly by producing necessary proteins to change or maintain their fate decisions. Translation initiation varies both qualitatively and quantitatively in response to stress (hypoxia, cold shock, heat shock, DNA damage, UV radiation), apoptosis and viral infection (Al-Fageeh and Smales, 2009; Bornes et al., 2007; Contreras et al., 2008; Keiper and Rhoads, 1997; Tee and Proud, 2000; Tinton and Buc-Calderon, 1999; Vries et al., 1997). The contribution of cap-dependent versus independent translation is usually dictated by isoforms of eIF4G and their proteolytic cleavage (Contreras et al., 2008; Keiper and Rhoads, 1997). During stress such as heat shock, for example, mTOR signaling is inhibited leading to active 4E-BP that sequesters eIF4E preventing it from recruiting mRNA to eIF4G for ribosome association (Mamane et al., 2004). Apoptosis and viral infection, on the other hand, cleave eIF4G isoforms removing their eIF4E binding domains and preventing cap-dependent recruitment to the ribosome (Contreras et al., 2008; Keiper and Rhoads, 1997). The combined contributions of eIF4E inhibition and eIF4G cleavage alter a cell's ability to

translate mRNAs and thus alter the cell's steady state protein pool resulting in changes in cell fate.

The induction of apoptosis leads to enhanced cap-independent translation of stress and apoptotic related mRNAs.

In this study we demonstrated a physiological link between changing levels of IFG (eIF4G) isoforms and translational control of mRNAs that are involved in stress response and initiation of apoptosis. Decreased IFG-1 p170 abundance resulted in enhanced translation of cell death and chaperone mRNA in worms responding to apoptosis. Thus, these studies demonstrate the ability of the translation initiation apparatus to regulate the natural apoptotic cell fate decision in healthy, whole organisms and their natively differentiating cell lineages, such as germ cells. These studies also demonstrated that genetic depletion of a key translation initiation factor (IFG-1 p170) or its cleavage during *ced-9ts*-induced apoptosis resulted in enhanced translation of a subset of stress and apoptosis-related mRNAs. Specifically, *C. elegans hsp-3* (BiP) and *ced-9* (Bcl-2) exhibited enhanced translation after IFG-1 p170 cleavage. These data were consistent with the enhanced translation of their mammalian homologues during cap-independent conditions (Buchkovich et al., 2010; Cho et al., 2007; Sherrill et al., 2004; Yang and Sarnow, 1997). This enhanced translation is in contrast to many other cellular mRNAs (including several invoved in apoptosis) that exhibited diminished translation. Overall, this study illustrates the importance of eIF4G isoform representation in selecting mRNA for translation in response to stress. Not only did changes in dependence on the cap-independent mechanism result in increased translation of certain mRNA populations, it also resulted in changes in germ cell fate decisions.

Decreased IFG-1 p170 not only increased germ cell apoptosis, it also decreased fecundity. Thus, changes in the mode of mRNA translation are not insignificant to the entire pool of proteins available to the cell. Changes in protein expression levels were robust enough to change germ cell fate.

We propose a model that relates the mechanism of translation initiation and its ability to regulate cell fate decisions to the apoptotic pathway in normal development and physiological stress. During apoptosis, IFG-1 isoforms are targeted for cleavage by the activated caspase, CED-3. Caspase cleavage removes the cap-association domain from IFG-1 p170 preventing further cap-dependent recruitment of mRNA to the ribosome for translation. The cell must then rely primarily on cap-independent translation to respond to this apoptotic stress by either providing the cell with the means to recover from insult or succumb to cell death. Initially, translation of stress recovery and prosurvival mRNAs such as *hsp-3* and *ced-9* promote recovery by chaperoning protein folding and inhibiting apoptosis (Hengartner et al., 1992; Lee, 2005). Continued stress may then result in enhanced translation of apoptotic mRNAs such as *ced-9,* which has been also shown to also have alternative proapoptotic function (Galvin et al., 2011).

Sequential use of first anti-apoptotic and then proapoptotic IRESes for translation during progressive stress conditions has been previously demonstrated in mammalian cell culture (Holcik and Sonenberg, 2005). Using two well-established IRESes to garner this point, the authors showed that during initial stress there is first enhanced translation of XIAP mRNA to prevent cell death. However as stress continues the Apaf-1 mRNA IRES is activated to facilitate cell death (Holcik et al., 1999; King et al., 2014). Cap-independent translation of XIAP mRNA during stress results in its increased protein accumulation

(Holcik et al., 1999). XIAP binds caspases inhibiting their activity and preventing apoptotic progression (Lagace et al., 2001; Liston et al., 2003). Activation of the XIAP IRES is dependent on the presence of its ITAF, La autoantigen (Ohndorf et al., 2001). La autoantigen is dephosphorylated during Fas-induced apoptosis resulting in its migration to the cytoplasm here it can bind and activate the XIAP IRES (Ohndorf et al., 2001). During prolonged stress proapoptotic Apaf-1 is translated via its IRES due to activation by its own ITAF, PTB (King et al., 2014). Thus, our studies have begun to identify mRNA populations that allow for this initial recovery and then subsequent death in germ cells and compare these finding to those observed in mammalian cell culture. Importantly, our studies focus on the *in vivo* translation of mRNAs in whole organ systems in a living organism. This allows for cells in their homeostatic natural state to respond to one another.

Our model of stress response and cell death relies on a pathwy in which eIF4G cleavage results in changing protein expression based on the cell's ability to translate different subsets of mRNA via the cap-independent mechanism. One major criticism of this model is the idea that there is no chance for survival after caspase activation. However, evidence suggests that this is an old idea based on absolutes in the cell, and most likely is not the entire story. XIAP translational control is a prime example for why activation of caspases is not synonymous with death. XIAP and other IAP family members are able to inhibit caspase activity, preventing further cleavage of cellular components leading to cell death (Lagace et al., 2001; Liston et al., 2003). Caspase cleavage of eIF4G resulting in enhanced cap-independent translation results in increased XIAP expression and thus a reduction in caspase activity (Holcik et al., 1999). Additionally, previous studies *in C. elegans* from our lab have demonstrated that eIF4G cleavage is not just part of cellular shut

down (Contreras et al., 2011). Rather, knockdown of cap-dependent IFG-1 p170 results in a signal that induces apoptosis through other members of the apoptotic pathway (Contreras et al., 2011). Thus, the cleavage of IFG-1 p170 is not just a downstream effect of apoptotic induction, but an upstream player actively participating in the cell death decision.

Cap-independent translation initiation differs in C. elegans whole worms compared to mammalian cell culture.

Interestingly, the induction of cap-independent translation in the *C. elegans in vivo* model did not result in enhanced translation of all known orthologs of mammalian IRES-containing mRNAs. Additionally, the mRNAs identified to translate more efficiently during cap-independent conditions displayed key mechanistic and structural differences to their mammalian homologues. Thus, selective translation in this whole animal model differs from cap-independent translation observed in cultured mammalian cells responding to toxic treatments. *C. elegans* homologues of HIF-1, Apaf-1 and p53 had marked decreases in their translational efficiencies and were thus disadvantaged for initiation during cap-independent conditions. Additionally, the structure of some of these mRNAs differed from their mammalian homologues and they were found to lack sequences that have been reported to allow for cap-independent translation in mammalian cells. For example, *ced-4* (Apaf-1) was found to lack the 5' UTR IRES identified in its mammalian homologue (Coldwell et al., 2000). Even mRNAs with the conserved ability to translate cap-independently during stress do not necessarily have the same mechanism of initiation. Despite the fact that the *C. elegans* homologue of BiP, *hsp-3,* translates more efficiently during apoptosis, the majority of the message population does not contain the 5' UTR IRES

element found in mammalian BiP mRNA. *hsp-3* mRNA still translated more efficiently indicating that its can rely on an alternative mechanism of cap-independent initiation. Further studies are needed, however, to determine if the small populations of *hsp-3* mRNA with an extended 5' UTR are translated cap-independently via an IRES using a mechanism that is conserved with its mammalian counterpart. Even if the mechanism of cap-independent translation is maintained in this 5' extended mRNA population, it would not be unexpected that the purported *hsp-3* IRES sequence may behave differently in response to stress in a whole animal model or in nematodes versus humans. Thus, our data point out clear differences in the protein synthetic regulation of stress and cell death proteins in the whole animal model versus cell culture. These observations suggest that both organism and physiological context may greatly alter protein synthetic regulation particularly in response to stress.

Some differences in protein synthetic regulation are likely the result of conclusions being made in "artificial" systems including purified protein translation systems, cell free extracts and cell culture where cells are maintained in log phase growth. In cell culture protein synthesis results in a doubling of the full complement of proteins expressed about every 24 hours (Komar et al., 2012). This vastly differs from protein synthesis in multicellular organisms where cells grow at a much slower rate (Komar et al., 2012). For comparison, a human turns over about 2% of dry body weight in one day. At this rate, if a doubling of protein expression does in fact occur it would take about 50 days (Komar et al., 2012). Thus, cells in culture require far more active protein synthesis to account for the need for additional proteins during log phase growth. In cell culture (*ex vivo*), translation of cap-independent mRNAs may be outcompeted by the sheer mass of mRNAs translating. In

a whole organism model with a lower required level of overall protein synthesis for *in vivo* homeostasis, translation of this type of mRNA may become more important. Thus, these studies of cap-independent translation in a defined tissue type in the context of the whole organism are important for understanding the regulation of mRNA *in vivo* in cells in their normal homeostatic state.

The common way of determining whether mammalian 5' UTRs have IRES activities promoting cap-independnet protein synthesis is use of bicistronic plasmids. The first cistron is translated cap-dependently, however the second downstream cistron is only translated if the ribosome reinitiates using the proposed IRES sequence. Cap-independent translation has been thus far shown to be of particular importance during stress. However, most studies of using bicistronic complexes to determine IRES activity are performed under normal unstressed conditions. To properly report cap-independent character cap-independent translation should instead be characterized during conditions that promote this type of initiation. Thus, the future directions of this project include creating transgenic *C. elegans* expressing bicistronic constructs that will allow characterization of potential IRES activity in the *hsp-3* 5' UTR. These worms will allow for *in vivo* observation of cap-independent translation in a nonartificial system. Most importantly, these whole worms can then be submitted to various physiological stresses that are known to result in enhanced cap-independent translation. Here, utilization of the *hsp-3* IRES can be monitored *in vivo.* Overall, this study illustrates key differences in protein synthesis in the whole animal *C. elegans* model compared to mammalian cells in culture and highlights key advantages to studying cells in their native differentiating state.

Knockdown of cap-dependent translation does not revert the germ cell tumor phenotype.

Regulation of translation through initiation activity is an important part of regulating protein expression. However, our experiments in germ cell tumors have illustrated that this mode of regulation is likely part of a larger network of regulators and by itself may not always change cell fate. Although reduced cap-dependent translation is correlated with enhanced expression of apoptotic and stress-related mRNAs, this expression was insufficient to result in reversion of germ cell tumor phenotype. Decreased abundance of cap-dependent IFG-1 p170 did not result in reduction in mitosis, static homeostasis or a reversion to meiosis in the *glp-1* or *gld-1* germ cell tumor strains. Most likely, other translational regulators in the tight network of translational control of *glp-1, gld-1, fbf-2* and other RNAs in the *C. elegans* gonad prevented tumorous germ cell from arresting or re-entering meiosis and progressing further towards becoming mature oocytes. We cannot rule out that IFG-1 p170 RNAi may be too weak to allow for observation of altered cell fates already in the P0 generation. However, fertility issues due to both the germ cell tumor phenotype and knockdown of IFG-1 p170 make it difficult to study the subsequent F1 generation.

We should also not exclude the possibility that the inability to revert cell fate may be due to cap-independent translation of mRNAs that promote tumor progression. For example, IRES mediated translation has also been shown to be important for cell cycle transitions. ODC expression is essential for cell cycle progression during the G2/M phase of the cell cycle where protein synthesis is downregulated (Fitzgerald and Semler, 2009). To allow for this expression, ODC mRNA has been shown to translate cap-independently via an IRES sequence (Fredlund et al., 1995; Pyronnet et al., 2000). Thus, knockdown of cap-

dependent translation in germ cell tumors may result in enhanced translation of some cell cycle mRNAs that are able to translate cap-independently, while putting others at a disadvantage. Despite effectively changing the mode of translation initiation and inducing protein expression that promotes the apoptotic fate, these studies revealed that decreased IFG-1 p170 was not insufficient to prevent or slow germ cell tumor progression.

Final Comments

The work described herein illustrates the first *in vivo* demonstration of enhanced cap-independent translation resulting in alternative cell fate decisions. It made innovative use of genetic knockdown of cap-dependent translation by both direct IFG-1 p170 depletion and *ced-9ts*-induced IFG-1 cleavage. Interestingly, resulting germ cell phenotypes and mRNA translational character were not always identical. These studies linked changing proportions of eIF4G isoforms with enhanced translation of stress recovery mRNAs. This study also illuminated the importance of studying translation in *in vivo* models as opposed to "artificial" systems by demonstrating marked differences in translational regulation of key apoptotic mRNAs. Although the differences in translational control might result from a difference in organism, it is more likely that translation in natively proliferating germ cells is more physiologically representative than logarithmic growth of separated cells in *ex vivo* culture. These studies also provide important links between the induction of apoptosis and changes in the protein synthetic mechanism. Too long has it been thought that eIF4G cleavage and altered protein synthesis are just a downstream result of apoptosis. Our studies offer the first evidence that cap-independent protein synthesis is in fact an upstream effector that is actively involved in the cell death decision process. This is of

particular importance when applying translational regulation findings to cancer where there is often an upregulation of eIF4G and/or eIF4E expression. If the isoform representation of eIF4G forms could be manipulated within these cells, the therapy could promote the induction of apoptosis via a subtle protein synthetic intervention. Overall, this study successfully links a translation initiation and stress response by using the simplified genetics of the *C. elegans in vivo* model to study cell fates of cell within the undisrupted whole organism and associate them with changes in translational efficiency of mRNAs.

CHAPTER 6: EXPERIMENTAL PROCEDURES

Maintenance of C. elegans Strains

The wild type strains used in experiments were N2 variation Bristol strain or N2 crossed with the CED-1::GFP reporter (MD701, {*bcIs39* V [P_{lim-7} *ced-1::gfp* and *lin-15*(+)]}). The CED-1::GFP reporter was used to assay germ cell apoptosis as previously described (Zhou et al., 2001). The original *ifg- 1::mos* strain {*ifg-1*(cxP9279)/+, with a mos-1 transposon insertion} was made by Laurent Segalat, (CNRS) using mobilization of Mos-1 (mariner-1, *Drosophila*) by SP:Mos transposase (Bessereau, 2001; Granger et al., 2004). This line contained a stable insertion of Mos-1 transposon into *ifg-1* (M110.4) at 17,266 nt (intron 5). *ifg-1::mos*/+ males were then crossed into a strain carrying the mT1 balancer. Progeny were outcrossed five times to wild type (N2), then self crossed to homozygous *ifg-1::mos* allele in the strain, KX34. KX34 was crossed with the MD701 strain to produce an *ifg-1::mos* strain easily scored for germ line apoptosis (KX54). The *ced-9ts* {*ced-9* (n1653) *mab-5* (mu114)} and *ced-3* (n2452) strains were obtained from the *Caenorhabditis* Genetics center and were also crossed with the MD701 strain creating the resulting KX110 and KX84 strains, respectively. Germ cell tumors were studied in a *glp-1* gain of function strain (*glp-1 ar202)* (generously provided by Dr. Myon Hee Lee) and a GLD-1 loss of function strain (RAF3) (obtained from the *C. elegans* Genetics center) (Biedermann et al., 2009; Pepper et al., 2003). All strains were grown on normal growth medium (NGM) plates with E. coli strain OP50 at 20°C or 15˚C for the temperature sensitive *glp-1* germ cell tumor strain. (Brenner, 1974). Strains were shifted to 25 °C for 24 h prior to harvesting and liquid nitrogen pelleting for polysome profile experiments.

Total RNA isolation, poly(A) RNA isolation, Northern Blotting and Identification of ifg-1::mos mRNA variants

Total RNA was extracted and purified as previously described using the Trizol (Invitrogen) method (Contreras et al., 2008). Poly(A) RNA was purified using the Oligotex Direct mRNA Isolation Kit according to the manufacturer's instructions (Qiagen). Northern Blotting was performed using an antisense *ifg-1* riboprobe complementary to the 5′ half of the *ifg-1* cDNA or to the *gpd-3* cDNA. Northern Blotting of *act-1* was performed using a probe derived from the pT7T3 18-103 *act-1* plasmid that had been linearized with EcoRI. This formed a 210 T3 antisense *act-1* probe. The pCRII *ced-4 1003s/591a* plasmid constructed during the systematic *ced-4* PCR experiments was used to create a *ced-4* antisense probe. The plasmid was linearized by digestion with XhoI leading to the creation of an SP6 antisense *ced-4* probe of 1106 bp. Northern blot imaging was performed on a Typhoon 9410 (GE Health Care) and quantification of mRNAs was done with ImageQuant TL 2003 software (GE Health Care). *ifg-1* mRNA signal was normalized to *gpd-3* signal to account for total RNA loading. Sequences for the *ifg-1* mRNAs containing Mos insertions were amplified using SuperScript II (Invitrogen) with internal and external primers (5′-ACCAAACTGGGCAAACAAAG-3′, 5′-GCTCAATTCGCGCCAAACTATG-3′, 5′-ACATCGACTGCTCGACCGAA-3′, 5′-GCCGTCGCTAGCTACACATTT-3′, and 5′-GCGCATCGTTGGAGGATACA-3′) and subcloned into pCRII using TOPO cloning (Invitrogen).

Systematic ced-4 PCR experiments

Systematic RT-PCR experiments were carried out on *C. elegans* total RNA using the RT-PCR SuperScript III One-Step PCR kit (invitrogen). RT-PCR of *ced-4* mRNA was carried out using three combinations of PCR primers: *ced-4 886s/ced-4 1175a, ced-4 1003s/ced-4 1175a, and ced-4 886s/ced-4 591a* (Table 6.1). *SL1/SL2* PCR amplification was conducted using the RT-PCR SuperScript III One-Step PCR kit and the *SL1 Splice Leader s* or *SL2 Splice Leader s* primer in conjunction first with the *ced-4 288a* and then nested with the *ced-4 92a* primer. cRT-PCR was performed as previously described using primary ced-4 primers, forward *ced-4 1668s* and reverse *ced-4 288a* and nested ced-4 primers, forward *ced-4 1694s* and reverse *ced-4 92a* (Contreras et al., 2011).

Construction of Plasmids

ced-4 short RPA plasmid construction. The RT-PCR SuperScript III One-Stop RT-PCR product from amplification using the *ced-4* 886s and 1175a system was TOPO TA cloned into the pCRII vector (invitrogen) (Table 6.1). The plasmid was then digested with XhoI and relegated with T4 ligase forming a pCRII plasmid with 186 bp of the *ced-4* upstream intergenic region with the first 56 bp of *ced-4* coding sequence. This plasmid was then linearized using PvuII and then served as a template to create the *ced-4* short RPA probe.

ced-4 long RPA plasmid construction. The *ced-4* long RPA probe sequence was amplified by GoTaq Green (Promega) from *C. elegans* DNA using *ced-4 430s* and *ced-4 200a* primers (Table 6.1). The amplified sequence was then TOPO TA cloned into the pCRII vector. The resulting vector was lineralized using XbaI and served as a template to create the *ced-4* long RPA probe.

Table 6.1. Primers for systematic *ced-4* PCR experiments.

Systematic *ced-4* PCR Primers	Sequence (5'→3')
ced-4 430s	TTACAGGGTTGGGATTCTCG
ced-4 886s	ACATTTCGGGCTTGGAGA
ced-4 1003s	TCGAAAACATCACCTAGCA
ced-4 92a	TGGTTCAAAGTCGTGGATGA
ced-4 200a	TCGAAGAAAATTGGCGATCC
ced-4 288a	CTTCGAGGAAATCAGCAAGG
ced-4 1175a	AAAGTCGAGGATTAGTCGGT
ced-4 1694s	GCACCAGAAATTCTATGACTCCCT
ced-4 1668s	GAAGACTTCCCAAAGTTCATGCA
SL1 Splice Leader s	GGTTTAATTACCCAAGTTTGAG
SL2 Splice Leader s	GGTTTTAACCCAGTTACTCAAG

Table 6.1 Primers for systematic *ced-4* PCR experiments. This table includes the primer sets involved in systematic *ced-4* PCR experiments to determine alternative *ced-4* 5' endpoints.

pCRII *ced-4 886s-591a control RNA plasmid construction. ced-4* mRNA genomic sequence was amplified using the *ced-4 886s* and *ced-4 591a* primers. This amplification product was TOPO TA cloned into the pCRII vector and the vector was sequenced. The resulting vector was linearized with ClaI.

pSKifg-1 p130 and pSKifg-1 p130 d830-1114 plasmid construction. Templates for in vitro transcription and translation of IFG-1 p130 protein and truncation were in pBlueScript SK (Stratagene). cDNA encoding IFG-1 115–1156 (nt 366–3494) was obtained from Dr. Yugi Kohara (National Institute of Genetics, Japan). pSKifg-1 p130mvti was generated by PCR amplification of nt 1194–1264 and subcloning via BamHI and NheI. Upon sequencing a single base mutation was discovered in the third codon (ACT to ATT) that caused a missense substitution of Thr for Ile. This change did not prevent CED-3 cleavage. Template plasmids for *in vitro* translated IFG-1 substrates for caspase cleavage assays were constructed from pSKifg-1 p130mvti. Restriction digestion and re-ligation of pSKifg-1 p130 generated the IFG p130 d830-1114 (nt 1194-2510, 3366-3494) truncation construct. The mutation was not present in pSKifg-1 p130 d830–1114. All constructs were transformed into TOP 10 F' bacteria, grown up as large preparations, purified using Qiagen HiSpeed Maxiprep Kits (Qiagen) and were verified by DNA sequencing (Iowa State DNA Sequencing Facility).

hsp-3 RPA plasmid construction. hsp-3 upstream purported IRES sequence was amplified by primers *hsp-3fIRESstarts* and *hsp-3 52a* (Table 6.2) from the *C. elegans* cDNA clone,

yk1249d06 using GoTaq Green Master Mix (Promega). The amplification product was then TOPO TA cloned into pCRII and sequenced (Iowa State DNA sequencing facility). The resulting vector was linearlized by PvuII.

MosSCI plasmid construction and transgenic strain construction

pCRII mcherry::hsp-3fIRES::gfp and DONR mcherry::hsp-3fIRES::gfp plasmid construction. gfp sequence was amplified from the Pmyo3::RFP-24ES(285 bp)-GFP::let858.3 (a gift from the Wang lab) using GoTaq Green and the *gfpL3786starts/gfpL2786enda* primer set (Table 6.2) (Li and Wang, 2012). Primary PCR was also conducted using the pCRII*fhsp-3 (hsp-3fIRESstarts/hsp-3 52a) (hsp-3* RPA construct) and *hsp-3fIRESstarts* and *hsp-3* 52a primers. These two PCR products were then combined in an overlapping PCR amplification reaction using the *hsp-3fIRESstarts* and *gfpL3786a* primer set. The resulting *hsp-3fIRES::gfp* amplification product was then subcloned into the pCRII vector and sequenced. *mcherry* sequence was then reverse transcribed using Superscript III One-Step RT-PCR with platinum Taq (invitrogen) from RNA extracted from a *C. elegans* strain expressing mcherry {[pPie-1+Vab-1::GFP+unc-119(+)] [pPie-1-mCherry::PH(pLC 1.0 + unc 119(+)] tnls 13;ltls 44 V} (DG2160) (obtained from the *C. elegans* Genetics Center) using the *mcherrystarts/mcherryenda* primer set. The resulting *mcherry* product was then subcloned into the pCRII vector and was sequenced. Both the pCRII*hsp-3fIRES::gfp* and pCRII *mcherry* plasmid insertion sequences were amplified using the aforementioned primer set for *mcherry* (*mcherrystarts/mcherryenda*) and the *mchhesp-3fIRESs/gfpL3786enda* set for *hsp-3fIRES::gfp*. These amplification products were combined and an overlapping PCR was performed using GoTaq Green and the *mcherrystarts/gfpL3786enda* primer set. This

Table 6.2. PCR primers for construction of pDEST *pie::mcherry::fhsp-3IRES::gfp::unc-54 3' UTR* and pDEST *pie::mcherry::control::gfp::unc-54 3' UTR* plasmids.

***mcherry::hsp-3/control::gfp* Gateway Cloning Primers**	**Sequence (5'→3')**
mcherrystarts	ATGGTCTCAAAGGGTGAAGAAGA
mcherryenda	CTACTTATACAATTCATCCATGCC
gfpL3786starts	ATGAGTAAAGGAGAAGAACTTTTCA
gfpL3786enda	TTACTTGTATGGCCGGCTAGCGAAT
Hsp-3fIRESstarts	GTGCTGACGTTGCCTTGTCCTA
Hsp-3 52a	ACTGCGAGGAAGAGGAAAAA
mchhsp-3fIRESs	GGCATGGATGAATTGTATAAGTAGGTGCTGACGGTTGCCTTGTCCTATCG
Hsp-3IRESgfpa	GAAAAGTTCTTCTCCTTTACTCATGCCCAACAAGAATAAGGTCTTCATA
mchIRESControls	GGCATGGATGAATTGTATAAGTAGTACGCTCCTAAGGCAGCCAGGA
gwmcherryAUGs	GGGGACAAGTTTGTACAAAAAAGCAGGCTATGGTCTCAAAGGGTGAAGAAG
gfpgwa	GGGGACCACTTTGTACAAGAAAGCTGGGTTTACTTGTATGGCCGGCTAGCGAAT

Table 6.2. PCR primers for construction of pDEST *pie::mcherry::fhsp-3IRES::gfp::unc-54 3' UTR* and pDEST *pie::mcherry::control::gfp::unc-54 3' UTR* plasmids. This table includes the primer sets involved in constructing MosSCI *mcherry::fIRES::gfp* and *mcherry::control::gfp* constructs for creation of stable transgenic strains.

product was TOPO TA cloned and sequenced. The resulting pCRII *mcherry::fIRES::gfp* plasmid sequence was then amplified using gateway primers, *gwmcherryAUGs* and *gfpgwa.* This PCR product has *att*B1 and *att*B2 sites allowing for it to be gateway cloned. The PCR amplification product was then combined with the pDONR 221 gateway vector and BP clonase in a BP reaction per the manufacturer's instructions resulting in the creation of the pDONR 221 *mcherry::fIRES::gfp* plasmid (invitrogen).

pCRII mcherry::control::gfp and DONR mcherry::control::gfp plasmid construction. The control bicistronic construct was created with the *Hemonchus contortus* 24-kDa excretory/secretory protein (24ES; accession no. U64793.1, GenBank) sequence instead of the *hsp-3* 5' UTR. The *mchIRESControls/gfpL3786enda* primer set was used to amplify the *control::gfp* sequence from the Pmyo3::RFP-24ES(285 bp)-GFP::let858.3 plasmid (Table 6.2). Overlapping PCR was then performed by combining the *control::gfp* and aforementioned *mcherry* PCR products and using the *mcherrystarts* and *gfpL3786enda* primer set. The resulting product was then TOPO TA cloned into the pCRII vector and sequenced. pCRII *mcherry::control::gfp* plasmid sequence was then amplified using gateway primers, *gwmcherryAUGs* and *gfpgwa,* and the resulting PCR product was combined with the pDONR 221 gateway vector and BP clonase in a BP reaction. The reaction was performed per the manufacturer's instructions resulting in the creation of the pDONR 221 *mcherry::control::gfp* plasmid (invitrogen).

DONR IFG-1 p130 and DONR IFG-1 p170 plasmid construction. A pPie170 plasmid containing *ifg-1 p170* cDNA sequence fused to *flg* sequence was used as a template for *ifg-1 p170*

Expand Long Template PCR amplification using the *pPie4s* and *pPie5113a* primers (Table 6.3) (Roche). Nested PCR was then performed on the resulting PCR product using *ifg-1 p170* gateway primers (*gwifg-1p170starts* and *gwifg-1enda*) and the Expand Long Template PCR System (Roche). This product was added to a BP reaction per the manufacturer's instructs and resulted in the creation of the pDONR 221 *ifg-1 p170::flg* plasmid. *ifg-1 p130* cDNA sequence was amplified from the pF130MVTI plasmid, which contains *ifg-1 p130* cDNA with a 3' fused *flg* sequence, using the *ifgPr -758s/letUTRa* primer set. This PCR product was also gateway cloned into the DONR 221 vector creating the pDONR *ifg-1 p130::flg* plasmid.

MultiSite Gateway Three-Fragment Vector Construction of Bicistronic and IFG-1 plasmids. pDONR *mcherry::fIRES::gfp,* pDONR *mcherry::control::gfp*, pDONR *ifg-1 p170::flg* and pDONR *ifg-1 p130::flg* plasmids were combined each in turn with other plasmids in the LR clonase recombination reaction per the manufacturer's instructions (invitrogen). The pDONR 221 derived plasmids make up slot 2 of the resulting pDEST plasmid. Slot 1 is occupied by the pCG142 plasmid, which contains the *pie-1 intron::pie-1 promoter.* Slot 3 is comprised of the insert from the pCM5.37 plasmid, which contains the *unc-54 3' UTR.* All three plasmids are combined into the pDEST vector, pCFJ212 (pDESTR4-R3(cxTi10816, IV)), which contains *mos* transpose recombination sites that allows for recombination onto *C. elegans* exon IV.

Miniprep protocol for injection plasmids. Individual colonies were picked from TOP 10 cell transformations of pDEST plasmids and were grown in 2 mL cultures of LB with 100 μg/μl

Table 6.3. PCR primers for construction of pDEST *pie::ifg-1 p170::unc-54 3' UTR* and pDEST *pie::ifg-1 p130::unc-54 3' UTR* plasmids.

IFG-1 p170 and p130 Gateway Cloning Primers	Sequence (5'➔3')
pPie4s	GCTCAAACAAAGCCGATTGC
pPie5113a	GCCTGTGAACCTCATCTTCAGG
ifgPr -758s	ATGAGGGAGAAATAGCGTGCAA
letUTRa	CAGTATTTAAAATTTGAAAATTCAACGA
gwifg-1p170starts	GGGGACAAGTTTGTACAAAAAAGCAGG CTATGTCAAACGCTGTTAGTAGGG
gwifg-1p130starts	GGGGACAAGTTTGTACAAAAAAGCAGG CTATGGTTACTATTCGCGAAATTG
gwifg-1enda	GGGGACCACTTTGTACAAGAAAGCTGG GTCTACTCGAGTTTATCATCATCATC

Table 6.3. PCR primers for construction of pDEST *pie::ifg-1 p170::unc-54 3' UTR* and pDEST *pie::ifg-1 p130::unc-54 3' UTR* plasmids. This table includes the primer sets involved in constructing MosSCI IFG-1 p170 and p130 constructs for creation of stable transgenic strains.

ampicillin. 1 mL of the culture was then spun down at 8000 rpm for 1 minute and the supernatant was discarded. The pellet was then resuspended in Buffer P1 (250 μl of 50 mM Tris-HCl pH 8.0, 10 mM EDTA) followed by an addition of 250 μl Buffer P2 (0.2 M NaOH, 1% SDS). The resulting solution was then suspended in 350 μl of Buffer N3 (4M Guanidine Hydrochloride, 05M Potassium acetate, pH 4.2). The cell suspension was centrifuged for 10 minutes at 12,000 rpm. The supernatant was transferred to a filter tub (EconoSpin Spin Column for DNA, Cat. No. 1920-250) and centrifuged for 1 minute at 12,000 rpm. Flow through was discarded and centrifugation was repeated with 750 μl of 1X Buffer PE (5X PE (100 mM NaCl, 10 mM Tris-HCl pH 7.5), diluted to 1X in 100% ethanol) to wash the bound DNA. Centrifugation was repeated to dry the filter. The filter was then transferred to a new eppendorff tube. 50 μl of water was added to elute the DNA and was allowed to sit for 1 minute before a final centrifugation for 1 minute at 12,000 rpm. Note that in this process no RNase was used.

MosSCI strain construction using Bicistronic and IFG-1 plasmids. The designed plasmids of interest were injected in conjunction with the *mos1* transposase containing plasmid (pCFJ601), and *Prab-3::mCHerry::unc-54UTR* (pGH8), *Pmyo-2::mCherry::unc-54UTR* (pCFJ90) and *Pmyo-3::mCherry::unc-54UTR* (pCFJ104) negative selection plasmids into the EG6703 strains, which allows for single copy insertions on chromosome IV (plasmids obtained from Addgene, strain obtained from the *C. elegans* genetic center). Plasmids were injected at both high and low concentration as indicated by the Jorgensen Lab protocol (Frokjaer-Jensen et al., 2012; Frokjaer-Jensen et al., 2008). The high concentration injection mix was composed of: pCFJ601 (50 ng/μl), pGH8 (5-10 ng/μl), pCFJ90 (2-2.5 ng/μl),

pCFJ104 (5-10 ng/μl) and targeting vector (10-50 ng/μl) (Frokjaer-Jensen et al., 2012; Frokjaer-Jensen et al., 2008). Additonally, 10 ng/μl pMA122 was included or excluded from the high concentration injection mix. pMA122 expresses the *peel-1* negative selection marker that makes worms carrying the extrachromosomal array sensitive to heat shock. The low concentration injection mix was composed of: pCFJ104 (5 ng/μl), pGH8 (5 ng/μl), pCFJ90 (2.5 ng/μl), pCFJ601 (10 ng/μl) and targeting vector (1-10 ng/μl). The pMA122 selection vector was excluded from all low concentration injection mixes. The injection protocol was carefully followed as per instruction of the Jorgensen lab protocol (Frokjaer-Jensen et al., 2012; Frokjaer-Jensen et al., 2008).

RNase Protection Assays and Control RNA expression

RNase Protection Assays. For RNase Protection assay of *ced-4* mRNA, an antisense RNA probe uniformly labeled with [^{32}P]UTP was used extending from 156 bp into exon 1 and containing 186 bp of the 5′ UTR. A second *ced-4 long* mRNA probe extended from 176 bp into exon 1 and contained 644 bp of the intergenic region and upstream gene. The *hsp-3* mRNA probe extended from 72 bp into exon 1 of the *hsp-3* gene to the end of the longest 5′ UTR detected by ESTs (268 bp upstream of the ATG). This probe was designed using the *hsp-3* EST and thus did not contain the intron reported in the 5′ UTR. The assay was performed as previously described with the exception that the products were resolved on an 8% polyacrylamide/ urea/TBE gel (Contreras et al., 2008).

Control RNA expression. ced-4 control RNA was transcribed from the pCRII *ced-4 886s-591a* plasmid linearized with HindIII. The control *ced-4* RNA was uniformly labeled with

[^{32}P]UTP by creating a reaction mix of 4 μl 5X transcription buffer, 2 μl 100 mM DTT, 20 U RNasin, 2 μl 5 mM rdTP mix (rGTP, rCTP and rATP), 10 μl 1 mM rUTP and 20 U T7 polymerase that was incubated at 37˚C for 30 minutes. 40U of RNasin and 1 U of RNA quality DNaseI were added before an additional 15 minute incubation. The reaction was then quenched with 8 μl 250 mM EDTA, 10 μl 10% SDS, 20 μg tRNA and was brought to a total volume of 202 μl with 160 μl TE. The resulting RNA was phenol-chloroform and chloroform extracted before an ethanol precipitation. The resulting purified RNA was run on a 1% agarose gel to test quality.

Sucrose gradient fractionation of polysomes, EDTA-release and RNA-seq experiments

Sucrose gradient fractionation. Sucrose gradient fractionation was performed as detailed previously with the exception that gradient fractions were isolated in 4 volumes Trizol. (Henderson et al., 2009). RNA was prepared from half of the 1 mL fractions, storing the duplicate halves at -80˚C. For EDTA treatment, 330μL of 0.25M EDTA was added to the lysates immediately before overlaying the lysates on the gradients and cycloheximide was excluded from Buffer C.

RNA-seq. For RNA-seq experiments the entire 1 mL fraction was purified and an additional three chloroform extractions were performed for a final clean-up of the pooled fractions. Fractions 1-2 were then combined into a nonpolysomal fraction and fractions 4-11 were combined to form a polysomal fraction. RNA-seq amplification and quantification was performed by Beckman. Cufflinks software was then used to assign reads into transcripts and to estimate the abundance of these transcripts. The transcripts were then matched

back to the *C. elegans* transcriptome. The outcomes of these experiments were measurements of transcript abundances in fragments per kilobase of exon per million fragments (FPKM) (Mortazavi et al., 2008). R values for the wild type samples were then derived by dividing the polysomal FPKM value by the addition of the polysomal and nonpolysomal FPKM value for a specific biological replicate. R fold change was then derived by dividing the WT A R value by the WT B R value. Total fold change was derived by dividing the added nonpolysomal and polysomal FPKM values of the WT A sample by that of the WT B sample for a specific biological replicate. Polysomal fold change was derived by dividing the polysomal FPKM of WT A by that of WT B for a particular biological replicate. Average R fold, total fold and polysomal fold changes were then derived from the three biological replicates. Standard deviation was determined for these averaged fold changes and data was culled with over 100% standard deviation and excluded from further follow-up experiments. Additionally, a t test was used to identify targets with a significant difference in fold change between the wild type samples. Only data with a p value of less than 0.1 was used for follow-up target analysis. Finally, follow-up qPCR experiments were only conducted on targets with an R or polysomal fold change greater than 1.5. Additionally, inverted (WT A divided by WT B) R, total and polysomal fold changes were used to determine significant decreases in fold change values.

cDNA synthesis and qPCR Analysis

0.25 µg of RNA from each fraction or 1 µg total RNA was synthesized into cDNA using the iScript cDNA Synthesis Kit (BioRad) or Verso cDNA Synthesis Kit (Thermo Scientific) for RNA-seq follow-up. Real-time PCR was performed in triplicates using the iQ SYBR Green

supermix (BioRad) or SsoFast EvaGreen Supermix, for RNA-seq follow-up experiments, in an iCycler iQ5 Real-time PCR machine according the manufacture's protocol. Primer pairs used for qPCR amplification can be found in Table 6.4. Arbitrary target mRNA mass was determined in each gradient fraction by using a standard curve derived from total cDNA. The percentage of the total arbitrary mass was then determined within each gradient fraction.

Expression and Purification of rCED-3

E. coli DH5α cells were used to express recombinant *C. elegans* CED-3 as previously described (Taylor et al., 2007). CED-3 sequence subcloned into pGEX4T-1 (GE Healthcare) to generate pGSTH6CED-3221–503 was used to generate rCED-3 protein (Contreras et al., 2011). The expressed protein was then affinity purified on a Ni-NTA sepharose column (Invitrogen). CED-3 reaction buffer (50 mM HEPES, pH7.4, 150 mM NaCl, 0.5 mM sucrose, 5% glycerol) with 250 mM imidazole was then used to elute the recombinant protein from the column. The elutions were then supplemented with DTT to a final concentration of 2 mM and glycerol to a final concentration of 20%. Bradford assays with a bovine serum albumin (BSA) standard curve were then used to determine the protein concentrations in the elution fractions. Western blotting with an anti-His6 monoclonal antibody (Genscript) was used to verify recombinant H_6CED-$3^{221-503}$. The activity of the recombinant CED-3 caspase was then confirmed using the colorimetric substrate Ac-DEVD-pNA (Promega) using the protocol described by the manufacturer. In this assay we pooled 10 μl of pooled peak fractions and incubated them with the substrate (0.2 mM) for 4 hours at 37˚C. The absorbance was monitored at 405 nm and the activity was calculated using a pNA standard

Table 6.4. qPCR primers.

qPCR Primer	Sequence (5'→3')
ced-4S s	GCTGATGCTAAAAAGCGAAGA
ced-4S a	TACTTTATTCGTATTTGATGACGTAG
ced-4 SL2 s	AACCCAGTTACTCAAGATGCT
ced-4 SL2 a	GAAGGCAAAAACATTTTCA
ced-4 Total s	GACAAATGCTCGATAGGAAA
ced-4 Total a	GCCGTGTAGAAACAGAAAAA
ced-9s	CGTTTGATAGGTCTAATCTCGT
ced-9a	ATTGTGTTCCTTCCAGTTGT
cep-1s	TTCGTTTAGAACGCTCACTC
cep-1a	GTATCTGGGAACTTTTGCTTC
gnrr-7s	CAGTCAGGAAACCACAACTC
gnrr-7a	ACATTTTGCACCATAATGAAC
gpd-3s	GATCTCAGCTGGGTCTCTT
gpd-3a	TCCAGTACGATTCCACTCAC
hif-1s	GACATCATACGGACGAAGAG
hif-1a	CAAGTGGCGAGTAGTTGG
hlh-17s	GCTGTAATTCCATATGCTCAC
hlh-17a	CCAATATACTCAGCTCCTCAA
hsp-3s	GAGGATGACAAGAAGGTCAA
hsp-3a	TCTTCAATCTGGTTTTTCAGG
hsp-4s	TGCCTCTACTGAAGAAAACAA
hsp-4a	CGAGTAAAGTTTGGAGACGA
ife-5s	ATCAGCGTCTGGACTAAAAA
ife-5a	ACAGTGGCTTCGAGTGTG
mesp-1s	ATGTTTGTGCCGGATTACA
mesp-1a	TTCAGCGGGAAGAGTGAG
rpl-39s	CATGAAGTACAATGCCAAGA
rpl-39a	AACAACAGATAAGGCGAAAG

Table 6.1. PCR primer sequences. PCR primer sequences used for systematic 5' characterization of *ced-4* mRNA. (s) sense primer (a) antisense primer.

curve.

IFG-1 p130 and p170 cleavage assays and immunoblotting

The recombinant CED-3 protein (rCED-3) was preincubated at 37˚C for 30 minutes to 1 hour prior to the cleavage assay. TNT T3 coupled reticulocyte lysate system (Promega) was used to generate IFG-1 p170 and p130 protein substrates that were labeled with [^{35}S] methionine (Perkin Elmer Life Sciences). pSKifg-1 Long, pSKifg-1 p130, and pSKifg-1 p130 d830–1114 plasmids were used to generate *in vitro* IFG-1 proteins (Contreras et al., 2011). 10 μl TNT T3 coupled reactions were prepared with 0.5 μg of IFG-1 p130, p130 (d830-114) or p170 plasmid DNA and 0.8 μl of [^{35}S] methionine (10 mCi/mL). One microliter of the *in vitro* synthesized IFG-1 p130 or p170 protein was then incubated for 2 hours at 37˚C with 10 μl of rCED-3 protein. Negative control reactions were performed using 10 μl of non-catalytic BSA prepared in the CED-3 reaction buffer in place of rCED-3. Cleavage reactions were quenched by adding equal volumes of 4X SDS buffer. The radioactive proteins were then resolved via electrophoresis on a Novex 4-20% Tris-Glycine Midi Gel (Invitrogen). The gel was then dried and radioactively analyzed by phosphorimaging using the Typhoon 9410 scanner.

Western Blot Analysis

Western blots were performed using the central IFG-1 antibody that detects both the p130 and p170 protein isoforms as previously described (Contreras et al., 2008). 30 μl of protein lysates isolated from *ifg-1::mos* worms was resolved on an 8% polyacrylamide gel (37.5:1) at 70-100 volts. Protein transfer was then conducted overnight at 7.5 mA. Actin was

detected using an anti-chicken actin antibody (Sigma). Blot imaging was done using ECL+ Detection System (GE Health Care) on a Typhoon 9410 and protein quantification was done with ImageQuant TL 2003 software (GE Health Care). IFG-1 p130 and p170 signals were normalized to actin to account for total protein loading.

Fed RNAi treatment, Heat Shock, Microscopy and Determination of the Extent of Apoptosis

RNAi. RNAi experiments were performed as previously described (Contreras et al., 2008). L3 worms were transferred to RNAi plates and grown at 25°C. Their F1 adult progeny were analyzed unless otherwise indicated. Germ cell tumor RNAi experiments comparing wild type, *glp-1* and *gld-1* strains were performed by scoring the F0 generation of eggs plated on RNAi and grown at 25°C. *p170* RNAi was carried out using *ifg-1* cDNA subcloned into the pL4440 plasmid (pT72ifgN1 containing 301 bp (nt 1115-1508)) (Contreras et al., 2008). *ced-9* RNAi was performed using *ced-9* cDNA subcloned into the pL4440 plasmid (pT72ced-9 containing 436 bp (nt 195-630). Control pL4440 vector dsRNA (187bp) was used to express control RNAi, which was feed to F1 adult worms as a nontarget control. Microscopy was performed on a Zeiss Axiovert 200M as previously described on unfixed RNAi fed worms (Contreras et al., 2011).

Heat Shock and the Extent of Apoptosis. Corpses were also monitored in unfixed worms from KX110 {ced-9ts(n1653), CED-1::GFP}, MD701 (CED-1::GFP), and KX54 (ifg-1::mos, CED-1::GFP) strains after a temperature shift of L3 worms to 25 °C for 0, 12, 24, 36, and 48 h for the time course experiment. Worms frozen for RNA isolation were grown on mixed population egg plates that were shifted to 25 °C 24 h prior to liquid nitrogen pelleting.

Corpses were monitored in these worms via microscopy before freeze down. For heat shock experiments MD701 worms were stressed at 32˚C for 6 hours. Heat shock was confirmed using qPCR detecting *hsp-4* mRNA, whose transcription is upregulated during heat shock (Table 6.4). Corpses were counted in the heat shocked worms as previously described. All worms visualized for microscopy were immobilized with 0.5 μM levamisole in M9 for time course experiments and 30 nM Sodium Azide in M9 for all other experiments. Fertility assays on wild type and ifg-1::mos strains were conducted at 25 °C. The visual morphology of the worms was determined at 24-h intervals.

DAPI and Phospho-histone H3 Immunostaining. DAPI staining was performed on whole worm fixed in 3% paraformaldehyde for 30-60 minutes. Worms were then washed 2X in PTW buffer (0.1% v/v Tween 20 in PBS) before storing them in 300 μL of 100% methanol for 10 minutes to 1 week. After methanol treatment, the worms were spun down and methanol was decanted before add 200 μl of M9 with 1 μg/mL DAPI. Worms were incubate at room temperature for 15 minutes and then the solution was spun down and decanted. Two drops of Vectashield was then added and the worms were incubated at 4˚C overnight. Worms were spun down, decanted and mounted on 1.5% agarose in sterile water slides. The worms were then imaged at 40X using fluorescence microscopy. Phospho-Histone H3 staining was performed on dissected gonads that were fixed in 3% paraformaldhyde and stored in methanol. After methanol treatment the gonads were spun down and the supernatant was removed. The gonads were washed 2X in 300 μl of PTW. Blocking with 500 μl PTW with 0.5% BSA was performed overnight at 4˚C on a rotor. Primary antibody staining was then performed with a 1:00 dilution of anti-phosphohistone H3 polyclonal

antibody in PTW with 0.5% BSA for 2 hours at room temperature. The gonads were then washed 2X before secondary antibody incubation (1:400 dilution of Anti-Rabbit in PTW with 0.5% BSA) for 1 hour at room temperature. Gonads were then washed and then mounted on a 1.5% agarose sterile water pad for microscopy.

REFERENCES

Al-Fageeh, M.B., and Smales, C.M. (2009). Cold-inducible RNA binding protein (CIRP) expression is modulated by alternative mRNAs. RNA *15*, 1164-1176.

Aldabe, R., Feduchi, E., Novoa, I., and Carrasco, L. (1995). Expression of poliovirus 2Apro in mammalian cells: effects on translation. FEBS Lett *377*, 1-5.

Alnemri, E.S. (1997). Mammalian cell death proteases: a family of highly conserved aspartate specific cysteine proteases. J Cell Biochem *64*, 33-42.

Alnemri, E.S., Fernandes-Alnemri, T., and Litwack, G. (1995). Cloning and expression of four novel isoforms of human interleukin-1 beta converting enzyme with different apoptotic activities. J Biol Chem *270*, 4312-4317.

Alvarez, E., Menendez-Arias, L., and Carrasco, L. (2003). The eukaryotic translation initiation factor 4GI is cleaved by different retroviral proteases. J Virol *77*, 12392-12400.

Amiri, A., Keiper, B.D., Kawasaki, I., Fan, Y., Kohara, Y., Rhoads, R.E., and Strome, S. (2001). An isoform of eIF4E is a component of germ granules and is required for spermatogenesis in C. elegans. Development *128*, 3899-3912.

Annis, M.G., Soucie, E.L., Dlugosz, P.J., Cruz-Aguado, J.A., Penn, L.Z., Leber, B., and Andrews, D.W. (2005). Bax forms multispanning monomers that oligomerize to permeabilize membranes during apoptosis. EMBO J *24*, 2096-2103.

Backer, J.M., Myers, M.G., Jr., Shoelson, S.E., Chin, D.J., Sun, X.J., Miralpeix, M., Hu, P., Margolis, B., Skolnik, E.Y., Schlessinger, J.*, et al.* (1992). Phosphatidylinositol 3'-kinase is activated by association with IRS-1 during insulin stimulation. EMBO J *11*, 3469-3479.

Bauer, C., Brass, N., Diesinger, I., Kayser, K., Grasser, F.A., and Meese, E. (2002). Overexpression of the eukaryotic translation initiation factor 4G (eIF4G-1) in squamous cell lung carcinoma. Int J Cancer *98*, 181-185.

Belsham, G.J., McInerney, G.M., and Ross-Smith, N. (2000). Foot-and-mouth disease virus 3C protease induces cleavage of translation initiation factors eIF4A and eIF4G within infected cells. J Virol *74*, 272-280.

Benedict, M.A., Hu, Y., Inohara, N., and Nunez, G. (2000). Expression and functional analysis of Apaf-1 isoforms. Extra Wd-40 repeat is required for cytochrome c binding and regulated activation of procaspase-9. J Biol Chem *275*, 8461-8468.

Bernstein, D., Hook, B., Hajarnavis, A., Opperman, L., and Wickens, M. (2005). Binding specificity and mRNA targets of a C. elegans PUF protein, FBF-1. RNA *11*, 447-458.

Bessereau, J.L., Wright, Al, Williams, D.C., Schuske, K., Davis, M.W., Jorgensen, E.M. (2001). Mobilization of a Drosophila transposon in the Caenorhabditis elegans germ line. Nature *413*, 70-74.

Biedermann, B., Wright, J., Senften, M., Kalchhauser, I., Sarathy, G., Lee, M.H., and Ciosk, R. (2009). Translational repression of cyclin E prevents precocious mitosis and embryonic gene activation during C. elegans meiosis. Dev Cell *17*, 355-364.

Blumenthal, T., Evans, D., Link, C.D., Guffanti, A., Lawson, D., Thierry-Mieg, J., Thierry-Mieg, D., Chiu, W.L., Duke, K., Kiraly, M.*, et al.* (2002). A global analysis of Caenorhabditis elegans operons. Nature *417*, 851-854.

Blumenthal, T., and Spieth, J. (1996). Gene structure and organization in Caenorhabditis elegans. Current opinion in genetics & development *6*, 692-698.

Boise, L.H., Gonzalez-Garcia, M., Postema, C.E., Ding, L., Lindsten, T., Turka, L.A., Mao, X., Nunez, G., and Thompson, C.B. (1993). bcl-x, a bcl-2-related gene that functions as a dominant regulator of apoptotic cell death. Cell *74*, 597-608.

Boonstra, J. (2003). Progression through the G1-phase of the on-going cell cycle. J Cell Biochem *90*, 244-252.

Borman, A., and Jackson, R.J. (1992). Initiation of translation of human rhinovirus RNA: mapping the internal ribosome entry site. Virology *188*, 685-696.

Bornes, S., Prado-Lourenco, L., Bastide, A., Zanibellato, C., Iacovoni, J.S., Lacazette, E., Prats, A.C., Touriol, C., and Prats, H. (2007). Translational induction of VEGF internal ribosome entry site elements during the early response to ischemic stress. Circulation research *100*, 305-308.

Brenner, S. (1974). The genetics of Caenorhabditis elegans. Genetics *77*, 71-94.

Buchkovich, N.J., Yu, Y., Pierciey, F.J., Jr., and Alwine, J.C. (2010). Human cytomegalovirus induces the endoplasmic reticulum chaperone BiP through increased transcription and activation of translation by using the BiP internal ribosome entry site. J Virol *84*, 11479-11486.

Bushell, M., McKendrick, L., Janicke, R.U., Clemens, M.J., and Morley, S.J. (1999). Caspase-3 is necessary and sufficient for cleavage of protein synthesis eukaryotic initiation factor 4G during apoptosis. FEBS Lett *451*, 332-336.

Byrnes, K., White, S., Chu, Q., Meschonat, C., Yu, H., Johnson, L.W., Debenedetti, A., Abreo, F., Turnage, R.H., McDonald, J.C.*, et al.* (2006). High eIF4E, VEGF, and microvessel density in stage I to III breast cancer. Annals of surgery *243*, 684-690; discussion 691-682.

Cascino, I., Fiucci, G., Papoff, G., and Ruberti, G. (1995). Three functional soluble forms of the human apoptosis-inducing Fas molecule are produced by alternative splicing. J Immunol *154*, 2706-2713.

Chinnaiyan, A.M., Chaudhary, D., O'Rourke, K., Koonin, E.V., and Dixit, V.M. (1997a). Role of CED-4 in the activation of CED-3. Nature *388*, 728-729.

Chinnaiyan, A.M., O'Rourke, K., Lane, B.R., and Dixit, V.M. (1997b). Interaction of CED-4 with CED-3 and CED-9: a molecular framework for cell death. Science *275*, 1122-1126.

Chipuk, J.E., Bouchier-Hayes, L., Kuwana, T., Newmeyer, D.D., and Green, D.R. (2005). PUMA couples the nuclear and cytoplasmic proapoptotic function of p53. Science *309*, 1732-1735.

Cho, S., Park, S.M., Kim, T.D., Kim, J.H., Kim, K.T., and Jang, S.K. (2007). BiP internal ribosomal entry site activity is controlled by heat-induced interaction of NSAP1. Molecular and cellular biology *27*, 368-383.

Christensen, S., Kodoyianni, V., Bosenberg, M., Friedman, L., and Kimble, J. (1996). lag-1, a gene required for lin-12 and glp-1 signaling in Caenorhabditis elegans, is homologous to human CBF1 and Drosophila Su(H). Development *122*, 1373-1383.

Ciosk, R., DePalma, M., and Priess, J.R. (2006). Translational regulators maintain totipotency in the Caenorhabditis elegans germline. Science *311*, 851-853.

Coldwell, M.J., deSchoolmeester, M.L., Fraser, G.A., Pickering, B.M., Packham, G., and Willis, A.E. (2001). The p36 isoform of BAG-1 is translated by internal ribosome entry following heat shock. Oncogene *20*, 4095-4100.

Coldwell, M.J., Mitchell, S.A., Stoneley, M., MacFarlane, M., and Willis, A.E. (2000). Initiation of Apaf-1 translation by internal ribosome entry. Oncogene *19*, 899-905.

Coleman, L.J., Peter, M.B., Teall, T.J., Brannan, R.A., Hanby, A.M., Honarpisheh, H., Shaaban, A.M., Smith, L., Speirs, V., Verghese, E.T.*, et al.* (2009). Combined analysis of eIF4E and 4E-binding protein expression predicts breast cancer survival and estimates eIF4E activity. Br J Cancer *100*, 1393-1399.

Contreras, V., Friday, A.J., Morrison, J.K., Hao, E., and Keiper, B.D. (2011). Cap-independent translation promotes C. elegans germ cell apoptosis through Apaf-1/CED-4 in a caspase-dependent mechanism. PLoS ONE *6*, e24444.

Contreras, V., Richardson, M.A., Hao, E., and Keiper, B.D. (2008). Depletion of the cap-associated isoform of translation factor eIF4G induces germline apoptosis in C. elegans. Cell Death Differ *15*, 1232-1242.

Crittenden, S.L., Bernstein, D.S., Bachorik, J.L., Thompson, B.E., Gallegos, M., Petcherski, A.G., Moulder, G., Barstead, R., Wickens, M., and Kimble, J. (2002). A conserved RNA-binding protein controls germline stem cells in Caenorhabditis elegans. Nature *417*, 660-663.

Crittenden, S.L., Troemel, E.R., Evans, T.C., and Kimble, J. (1994). GLP-1 is localized to the mitotic region of the C. elegans germ line. Development *120*, 2901-2911.

Danial, N.N. (2007). BCL-2 family proteins: critical checkpoints of apoptotic cell death. Clin Cancer Res *13*, 7254-7263.

Datta, S.R., Katsov, A., Hu, L., Petros, A., Fesik, S.W., Yaffe, M.B., and Greenberg, M.E. (2000). 14-3-3 proteins and survival kinases cooperate to inactivate BAD by BH3 domain phosphorylation. Mol Cell *6*, 41-51.

Day, C.L., Chen, L., Richardson, S.J., Harrison, P.J., Huang, D.C., and Hinds, M.G. (2005). Solution structure of prosurvival Mcl-1 and characterization of its binding by proapoptotic BH3-only ligands. J Biol Chem *280*, 4738-4744.

De Benedetti, A., and Graff, J.R. (2004). eIF-4E expression and its role in malignancies and metastases. Oncogene *23*, 3189-3199.

De Gregorio, E., Preiss, T., and Hentze, M.W. (1999). Translation driven by an eIF4G core domain in vivo. EMBO J *18*, 4865-4874.

Denault, J.B., Bekes, M., Scott, F.L., Sexton, K.M., Bogyo, M., and Salvesen, G.S. (2006). Engineered hybrid dimers: tracking the activation pathway of caspase-7. Mol Cell *23*, 523-533.

Desagher, S., Osen-Sand, A., Nichols, A., Eskes, R., Montessuit, S., Lauper, S., Maundrell, K., Antonsson, B., and Martinou, J.C. (1999). Bid-induced conformational change of Bax is responsible for mitochondrial cytochrome c release during apoptosis. J Cell Biol *144*, 891-901.

Dinkova, T.D., Keiper, B.D., Korneeva, N.L., Aamodt, E.J., and Rhoads, R.E. (2005). Translation of a small subset of Caenorhabditis elegans mRNAs is dependent on a specific eukaryotic translation initiation factor 4E isoform. Mol Cell Biol *25*, 100-113.

Dlugosz, P.J., Billen, L.P., Annis, M.G., Zhu, W., Zhang, Z., Lin, J., Leber, B., and Andrews, D.W. (2006). Bcl-2 changes conformation to inhibit Bax oligomerization. EMBO J *25*, 2287-2296.

Dobbyn, H.C., Hill, K., Hamilton, T.L., Spriggs, K.A., Pickering, B.M., Coldwell, M.J., de Moor, C.H., Bushell, M., and Willis, A.E. (2008). Regulation of BAG-1 IRES-mediated translation following chemotoxic stress. Oncogene *27*, 1167-1174.

Dole, M.G., Clarke, M.F., Holman, P., Benedict, M., Lu, J., Jasty, R., Eipers, P., Thompson, C.B., Rode, C., Bloch, C., *et al.* (1996). Bcl-xS enhances adenoviral vector-induced apoptosis in neuroblastoma cells. Cancer Res *56*, 5734-5740.

Du, Y.C., Lewis, B.C., Hanahan, D., and Varmus, H. (2007). Assessing tumor progression factors by somatic gene transfer into a mouse model: Bcl-xL promotes islet tumor cell invasion. PLoS Biol *5*, e276.

Eckmann, C.R., Crittenden, S.L., Suh, N., and Kimble, J. (2004). GLD-3 and control of the mitosis/meiosis decision in the germline of Caenorhabditis elegans. Genetics *168*, 147-160.

Eckmann, C.R., Kraemer, B., Wickens, M., and Kimble, J. (2002). GLD-3, a bicaudal-C homolog that inhibits FBF to control germline sex determination in C. elegans. Dev Cell *3*, 697-710.

Etchison, D., Milburn, S.C., Edery, I., Sonenberg, N., and Hershey, J.W. (1982). Inhibition of HeLa cell protein synthesis following poliovirus infection correlates with the proteolysis of a 220,000-dalton polypeptide associated with eucaryotic initiation factor 3 and a cap binding protein complex. J Biol Chem *257*, 14806-14810.

Farley, B.M., and Ryder, S.P. (2012). POS-1 and GLD-1 repress glp-1 translation through a conserved binding-site cluster. Mol Biol Cell *23*, 4473-4483.

Fernandes-Alnemri, T., Litwack, G., and Alnemri, E.S. (1995a). Mch2, a new member of the apoptotic Ced-3/Ice cysteine protease gene family. Cancer Res *55*, 2737-2742.

Fernandes-Alnemri, T., Takahashi, A., Armstrong, R., Krebs, J., Fritz, L., Tomaselli, K.J., Wang, L., Yu, Z., Croce, C.M., Salveson, G., *et al.* (1995b). Mch3, a novel human apoptotic cysteine protease highly related to CPP32. Cancer Res *55*, 6045-6052.

Filbin, M.E., and Kieft, J.S. (2009). Toward a structural understanding of IRES RNA function. Current opinion in structural biology *19*, 267-276.

Filipenko, N.R., MacLeod, T.J., Yoon, C.S., and Waisman, D.M. (2004). Annexin A2 is a novel RNA-binding protein. J Biol Chem *279*, 8723-8731.

Fitzgerald, K.D., and Semler, B.L. (2009). Bridging IRES elements in mRNAs to the eukaryotic translation apparatus. Biochim Biophys Acta *1789*, 518-528.

Flowers, A., Chu, Q.D., Panu, L., Meschonat, C., Caldito, G., Lowery-Nordberg, M., and Li, B.D. (2009). Eukaryotic initiation factor 4E overexpression in triple-negative breast cancer predicts a worse outcome. Surgery *146*, 220-226.

Francis, R., Barton, M.K., Kimble, J., and Schedl, T. (1995a). gld-1, a tumor suppressor gene required for oocyte development in Caenorhabditis elegans. Genetics *139*, 579-606.

Francis, R., Maine, E., and Schedl, T. (1995b). Analysis of the multiple roles of gld-1 in germline development: interactions with the sex determination cascade and the glp-1 signaling pathway. Genetics *139*, 607-630.

Fredlund, J.O., Johansson, M.C., Dahlberg, E., and Oredsson, S.M. (1995). Ornithine decarboxylase and S-adenosylmethionine decarboxylase expression during the cell cycle of Chinese hamster ovary cells. Experimental cell research *216*, 86-92.

Frokjaer-Jensen, C., Davis, M.W., Ailion, M., and Jorgensen, E.M. (2012). Improved Mos1-mediated transgenesis in C. elegans. Nat Methods *9*, 117-118.

Frokjaer-Jensen, C., Davis, M.W., Hopkins, C.E., Newman, B.J., Thummel, J.M., Olesen, S.P., Grunnet, M., and Jorgensen, E.M. (2008). Single-copy insertion of transgenes in Caenorhabditis elegans. Nature genetics *40*, 1375-1383.

Fukuchi-Shimogori, T., Ishii, I., Kashiwagi, K., Mashiba, H., Ekimoto, H., and Igarashi, K. (1997). Malignant transformation by overproduction of translation initiation factor eIF4G. Cancer Res *57*, 5041-5044.

Furuichi, Y., LaFiandra, A., and Shatkin, A.J. (1977). 5'-Terminal structure and mRNA stability. Nature *266*, 235-239.

Galvin, B.D., Denning, D.P., and Horvitz, H.R. (2011). SPK-1, an SR protein kinase, inhibits programmed cell death in Caenorhabditis elegans. Proceedings of the National Academy of Sciences of the United States of America *108*, 1998-2003.

Gao, X., and Pan, D. (2001). TSC1 and TSC2 tumor suppressors antagonize insulin signaling in cell growth. Genes Dev *15*, 1383-1392.

Garami, A., Zwartkruis, F.J., Nobukuni, T., Joaquin, M., Roccio, M., Stocker, H., Kozma, S.C., Hafen, E., Bos, J.L., and Thomas, G. (2003). Insulin activation of Rheb, a mediator of mTOR/S6K/4E-BP signaling, is inhibited by TSC1 and 2. Mol Cell *11*, 1457-1466.

Gibson, L., Holmgreen, S.P., Huang, D.C., Bernard, O., Copeland, N.G., Jenkins, N.A., Sutherland, G.R., Baker, E., Adams, J.M., and Cory, S. (1996). bcl-w, a novel member of the bcl-2 family, promotes cell survival. Oncogene *13*, 665-675.

Gilbert, W.V. (2010). Alternative ways to think about cellular internal ribosome entry. The Journal of biological chemistry *285*, 29033-29038.

Gilbert, W.V., Zhou, K., Butler, T.K., and Doudna, J.A. (2007). Cap-independent translation is required for starvation-induced differentiation in yeast. Science *317*, 1224-1227.

Gradi, A., Imataka, H., Svitkin, Y.V., Rom, E., Raught, B., Morino, S., and Sonenberg, N. (1998). A novel functional human eukaryotic translation initiation factor 4G. Molecular and cellular biology *18*, 334-342.

Graff, J.R., Konicek, B.W., Carter, J.H., and Marcusson, E.G. (2008). Targeting the eukaryotic translation initiation factor 4E for cancer therapy. Cancer Res *68*, 631-634.

Granger, L., Martin, E., and Segalat, L. (2004). Mos as a tool for genome-wide insertional mutagenesis in Caenorhabditis elegans: results of a pilot study. Nucleic acids research *32*, e117.

Grespi, F., Soratroi, C., Krumschnabel, G., Sohm, B., Ploner, C., Geley, S., Hengst, L., Hacker, G., and Villunger, A. BH3-only protein Bmf mediates apoptosis upon inhibition of CAP-dependent protein synthesis. Cell Death Differ *17*, 1672-1683.

Grover, R., Ray, P.S., and Das, S. (2008). Polypyrimidine tract binding protein regulates IRES-mediated translation of p53 isoforms. Cell Cycle *7*, 2189-2198.

Gu, L., Zhu, N., Zhang, H., Durden, D.L., Feng, Y., and Zhou, M. (2009). Regulation of XIAP translation and induction by MDM2 following irradiation. Cancer Cell *15*, 363-375.

Gumienny, T.L., Lambie, E., Hartwieg, E., Horvitz, H.R., and Hengartner, M.O. (1999). Genetic control of programmed cell death in the Caenorhabditis elegans hermaphrodite germline. Development *126*, 1011-1022.

Haghighat, A., Svitkin, Y., Novoa, I., Kuechler, E., Skern, T., and Sonenberg, N. (1996). The eIF4G-eIF4E complex is the target for direct cleavage by the rhinovirus 2A proteinase. J Virol *70*, 8444-8450.

Hansen, D., Hubbard, E.J., and Schedl, T. (2004). Multi-pathway control of the proliferation versus meiotic development decision in the Caenorhabditis elegans germline. Dev Biol *268*, 342-357.

Heikkinen, T., Korpela, T., Fagerholm, R., Khan, S., Aittomaki, K., Heikkila, P., Blomqvist, C., Carpen, O., and Nevanlinna, H. (2013). Eukaryotic translation initiation factor 4E (eIF4E) expression is associated with breast cancer tumor phenotype and predicts survival after anthracycline chemotherapy treatment. Breast cancer research and treatment *141*, 79-88.

Henderson, M.A., Cronland, E., Dunkelbarger, S., Contreras, V., Strome, S., and Keiper, B.D. (2009). A germline-specific isoform of eIF4E (IFE-1) is required for efficient translation of stored mRNAs and maturation of both oocytes and sperm. J Cell Sci *122*, 1529-1539.

Henderson, S.T., Gao, D., Lambie, E.J., and Kimble, J. (1994). lag-2 may encode a signaling ligand for the GLP-1 and LIN-12 receptors of C. elegans. Development *120*, 2913-2924.

Hengartner, M.O., Ellis, R.E., and Horvitz, H.R. (1992). Caenorhabditis elegans gene ced-9 protects cells from programmed cell death. Nature *356*, 494-499.

Hengartner, M.O., and Horvitz, H.R. (1994). C. elegans cell survival gene ced-9 encodes a functional homolog of the mammalian proto-oncogene bcl-2. Cell *76*, 665-676.

Henis-Korenblit, S., Strumpf, N.L., Goldstaub, D., and Kimchi, A. (2000). A novel form of DAP5 protein accumulates in apoptotic cells as a result of caspase cleavage and internal ribosome entry site-mediated translation. Mol Cell Biol *20*, 496-506.

Heschl, M.F., and Baillie, D.L. (1989). Characterization of the hsp70 multigene family of Caenorhabditis elegans. DNA *8*, 233-243.

Heschl, M.F., and Baillie, D.L. (1990). The HSP70 multigene family of Caenorhabditis elegans. Comp Biochem Physiol B *96*, 633-637.

Hinds, M.G., Lackmann, M., Skea, G.L., Harrison, P.J., Huang, D.C., and Day, C.L. (2003). The structure of Bcl-w reveals a role for the C-terminal residues in modulating biological activity. EMBO J *22*, 1497-1507.

Holcik, M., Lefebvre, C., Yeh, C., Chow, T., and Korneluk, R.G. (1999). A new internal-ribosome-entry-site motif potentiates XIAP-mediated cytoprotection. Nat Cell Biol *1*, 190-192.

Holcik, M., and Sonenberg, N. (2005). Translational control in stress and apoptosis. Nat Rev Mol Cell Biol *6*, 318-327.

Holcik, M., Yeh, C., Korneluk, R.G., and Chow, T. (2000). Translational upregulation of X-linked inhibitor of apoptosis (XIAP) increases resistance to radiation induced cell death. Oncogene *19*, 4174-4177.

Holm, N., Byrnes, K., Johnson, L., Abreo, F., Sehon, K., Alley, J., Meschonat, C., Md, Q.C., and Li, B.D. (2008). A prospective trial on initiation factor 4E (eIF4E) overexpression and cancer recurrence in node-negative breast cancer. Annals of surgical oncology *15*, 3207-3215.

Hu, Y., Benedict, M.A., Wu, D., Inohara, N., and Nunez, G. (1998). Bcl-XL interacts with Apaf-1 and inhibits Apaf-1-dependent caspase-9 activation. Proc Natl Acad Sci U S A *95*, 4386-4391.

Huang, D.C., and Strasser, A. (2000). BH3-Only proteins-essential initiators of apoptotic cell death. Cell *103*, 839-842.

Imataka, H., Gradi, A., and Sonenberg, N. (1998). A newly identified N-terminal amino acid sequence of human eIF4G binds poly(A)-binding protein and functions in poly(A)-dependent translation. The EMBO journal *17*, 7480-7489.

Imataka, H., Olsen, H.S., and Sonenberg, N. (1997). A new translational regulator with homology to eukaryotic translation initiation factor 4G. EMBO J *16*, 817-825.

Imataka, H., and Sonenberg, N. (1997). Human eukaryotic translation initiation factor 4G (eIF4G) possesses two separate and independent binding sites for eIF4A. Mol Cell Biol *17*, 6940-6947.

Jackson, R.J., Hellen, C.U., and Pestova, T.V. (2010). The mechanism of eukaryotic translation initiation and principles of its regulation. Nat Rev Mol Cell Biol *11*, 113-127.

Jan, E., Kinzy, T.G., and Sarnow, P. (2003). Divergent tRNA-like element supports initiation, elongation, and termination of protein biosynthesis. Proc Natl Acad Sci U S A *100*, 15410-15415.

Jan, E., and Sarnow, P. (2002). Factorless ribosome assembly on the internal ribosome entry site of cricket paralysis virus. J Mol Biol *324*, 889-902.

Jang, S.K., Pestova, T.V., Hellen, C.U., Witherell, G.W., and Wimmer, E. (1990). Cap-independent translation of picornavirus RNAs: structure and function of the internal ribosomal entry site. Enzyme *44*, 292-309.

Jang, S.K., and Wimmer, E. (1990). Cap-independent translation of encephalomyocarditis virus RNA: structural elements of the internal ribosomal entry site and involvement of a cellular 57-kD RNA-binding protein. Genes Dev *4*, 1560-1572.

Jennings, M.D., Zhou, Y., Mohammad-Qureshi, S.S., Bennett, D., and Pavitt, G.D. (2013). eIF2B promotes eIF5 dissociation from eIF2*GDP to facilitate guanine nucleotide exchange for translation initiation. Genes Dev *27*, 2696-2707.

Johannes, G., Carter, M.S., Eisen, M.B., Brown, P.O., and Sarnow, P. (1999). Identification of eukaryotic mRNAs that are translated at reduced cap binding complex eIF4F concentrations using a cDNA microarray. Proc Natl Acad Sci U S A *96*, 13118-13123.

Jones, A.R., and Schedl, T. (1995). Mutations in gld-1, a female germ cell-specific tumor suppressor gene in Caenorhabditis elegans, affect a conserved domain also found in Src-associated protein Sam68. Genes Dev *9*, 1491-1504.

Joshi-Barve, S., De Benedetti, A., and Rhoads, R.E. (1992). Preferential translation of heat shock mRNAs in HeLa cells deficient in protein synthesis initiation factors eIF-4E and eIF-4 gamma. The Journal of biological chemistry *267*, 21038-21043.

Karbowski, M., Norris, K.L., Cleland, M.M., Jeong, S.Y., and Youle, R.J. (2006). Role of Bax and Bak in mitochondrial morphogenesis. Nature *443*, 658-662.

Keiper, B.D., Gan, W., and Rhoads, R.E. (1999). Protein synthesis initiation factor 4G. Int J Biochem Cell Biol *31*, 37-41.

Keiper, B.D., Lamphear, B.J., Deshpande, A.M., Jankowska-Anyszka, M., Aamodt, E.J., Blumenthal, T., and Rhoads, R.E. (2000). Functional characterization of five eIF4E isoforms in Caenorhabditis elegans. J Biol Chem *275*, 10590-10596.

Keiper, B.D., and Rhoads, R.E. (1997). Cap-independent translation initiation in Xenopus oocytes. Nucleic acids research *25*, 395-402.

Keith, B., and Simon, M.C. (2007). Hypoxia-inducible factors, stem cells, and cancer. Cell *129*, 465-472.

Kieft, J.S. (2008). Viral IRES RNA structures and ribosome interactions. Trends in biochemical sciences *33*, 274-283.

Kim, Y.K., Back, S.H., Rho, J., Lee, S.H., and Jang, S.K. (2001). La autoantigen enhances translation of BiP mRNA. Nucleic acids research *29*, 5009-5016.

Kimble, J., and Crittenden, S.L. (2007). Controls of germline stem cells, entry into meiosis, and the sperm/oocyte decision in Caenorhabditis elegans. Annu Rev Cell Dev Biol *23*, 405-433.

King, H.A., Cobbold, L.C., Pichon, X., Poyry, T., Wilson, L.A., Booden, H., Jukes-Jones, R., Cain, K., Lilley, K.S., Bushell, M.*, et al.* (2014). Remodelling of a polypyrimidine tract-binding protein complex during apoptosis activates cellular IRESs. Cell Death Differ *21*, 161-171.

Kirienko, N.V., Mani, K., and Fay, D.S. (2010). Cancer models in Caenorhabditis elegans. Developmental dynamics : an official publication of the American Association of Anatomists *239*, 1413-1448.

Komar, A.A., and Hatzoglou, M. (2011). Cellular IRES-mediated translation: the war of ITAFs in pathophysiological states. Cell Cycle *10*, 229-240.

Komar, A.A., Mazumder, B., and Merrick, W.C. (2012). A new framework for understanding IRES-mediated translation. Gene *502*, 75-86.

Koong, A.C., Auger, E.A., Chen, E.Y., and Giaccia, A.J. (1994). The regulation of GRP78 and messenger RNA levels by hypoxia is modulated by protein kinase C activators and inhibitors. Radiat Res *138*, S60-63.

Korneeva, N.L., Lamphear, B.J., Hennigan, F.L., and Rhoads, R.E. (2000). Mutually cooperative binding of eukaryotic translation initiation factor (eIF) 3 and eIF4A to human eIF4G-1. The Journal of biological chemistry *275*, 41369-41376.

Kovall, R.A. (2008). More complicated than it looks: assembly of Notch pathway transcription complexes. Oncogene *27*, 5099-5109.

Kraemer, B., Crittenden, S., Gallegos, M., Moulder, G., Barstead, R., Kimble, J., and Wickens, M. (1999). NANOS-3 and FBF proteins physically interact to control the sperm-oocyte switch in Caenorhabditis elegans. Curr Biol *9*, 1009-1018.

Krausslich, H.G., Nicklin, M.J., Toyoda, H., Etchison, D., and Wimmer, E. (1987). Poliovirus proteinase 2A induces cleavage of eucaryotic initiation factor 4F polypeptide p220. J Virol *61*, 2711-2718.

Kuwana, T., Bouchier-Hayes, L., Chipuk, J.E., Bonzon, C., Sullivan, B.A., Green, D.R., and Newmeyer, D.D. (2005). BH3 domains of BH3-only proteins differentially regulate Bax-mediated mitochondrial membrane permeabilization both directly and indirectly. Mol Cell *17*, 525-535.

Kuwana, T., Mackey, M.R., Perkins, G., Ellisman, M.H., Latterich, M., Schneiter, R., Green, D.R., and Newmeyer, D.D. (2002). Bid, Bax, and lipids cooperate to form supramolecular openings in the outer mitochondrial membrane. Cell *111*, 331-342.

Lagace, M., Xuan, J.Y., Young, S.S., McRoberts, C., Maier, J., Rajcan-Separovic, E., and Korneluk, R.G. (2001). Genomic organization of the X-linked inhibitor of apoptosis and identification of a novel testis-specific transcript. Genomics *77*, 181-188.

Lamont, L.B., Crittenden, S.L., Bernstein, D., Wickens, M., and Kimble, J. (2004). FBF-1 and FBF-2 regulate the size of the mitotic region in the C. elegans germline. Dev Cell *7*, 697-707.

Lamphear, B.J., Kirchweger, R., Skern, T., and Rhoads, R.E. (1995). Mapping of functional domains in eukaryotic protein synthesis initiation factor 4G (eIF4G) with picornaviral proteases. Implications for cap-dependent and cap-independent translational initiation. The Journal of biological chemistry *270*, 21975-21983.

Lang, K.J., Kappel, A., and Goodall, G.J. (2002). Hypoxia-inducible factor-1alpha mRNA contains an internal ribosome entry site that allows efficient translation during normoxia and hypoxia. Mol Biol Cell *13*, 1792-1801.

Lazaris-Karatzas, A., Montine, K.S., and Sonenberg, N. (1990). Malignant transformation by a eukaryotic initiation factor subunit that binds to mRNA 5' cap. Nature *345*, 544-547.

Lee, A.S. (2005). The ER chaperone and signaling regulator GRP78/BiP as a monitor of endoplasmic reticulum stress. Methods *35*, 373-381.

Lee, H.C., Gu, W., Shirayama, M., Youngman, E., Conte, D., Jr., and Mello, C.C. (2012). C. elegans piRNAs mediate the genome-wide surveillance of germline transcripts. Cell *150*, 78-87.

Lee, J.H., Pestova, T.V., Shin, B.S., Cao, C., Choi, S.K., and Dever, T.E. (2002). Initiation factor eIF5B catalyzes second GTP-dependent step in eukaryotic translation initiation. Proc Natl Acad Sci U S A *99*, 16689-16694.

Lee, M.H., and Schedl, T. (2001). Identification of in vivo mRNA targets of GLD-1, a maxi-KH motif containing protein required for C. elegans germ cell development. Genes Dev *15*, 2408-2420.

Leibowitz, R., and Penman, S. (1971). Regulation of protein synthesis in HeLa cells. 3. Inhibition during poliovirus infection. J Virol *8*, 661-668.

Li, B.D., McDonald, J.C., Nassar, R., and De Benedetti, A. (1998a). Clinical outcome in stage I to III breast carcinoma and eIF4E overexpression. Annals of surgery *227*, 756-756l; discussion 761-753.

Li, D., and Wang, M. (2012). Construction of a bicistronic vector for the co-expression of two genes in Caenorhabditis elegans using a newly identified IRES. Biotechniques *52*, 173-176.

Li, H., Zhu, H., Xu, C.J., and Yuan, J. (1998b). Cleavage of BID by caspase 8 mediates the mitochondrial damage in the Fas pathway of apoptosis. Cell *94*, 491-501.

Li, P., Nijhawan, D., Budihardjo, I., Srinivasula, S.M., Ahmad, M., Alnemri, E.S., and Wang, X. (1997). Cytochrome c and dATP-dependent formation of Apaf-1/caspase-9 complex initiates an apoptotic protease cascade. Cell *91*, 479-489.

Lin, J.H., Li, H., Yasumura, D., Cohen, H.R., Zhang, C., Panning, B., Shokat, K.M., Lavail, M.M., and Walter, P. (2007). IRE1 signaling affects cell fate during the unfolded protein response. Science *318*, 944-949.

Lindquist, S., and Petersen, R. (1990). Selective translation and degradation of heat-shock messenger RNAs in Drosophila. Enzyme *44*, 147-166.

Liston, P., Fong, W.G., Kelly, N.L., Toji, S., Miyazaki, T., Conte, D., Tamai, K., Craig, C.G., McBurney, M.W., and Korneluk, R.G. (2001). Identification of XAF1 as an antagonist of XIAP anti-Caspase activity. Nat Cell Biol *3*, 128-133.

Liston, P., Fong, W.G., and Korneluk, R.G. (2003). The inhibitors of apoptosis: there is more to life than Bcl2. Oncogene *22*, 8568-8580.

Liu, Y., Kuersten, S., Huang, T., Larsen, A., MacMorris, M., and Blumenthal, T. (2003). An uncapped RNA suggests a model for Caenorhabditis elegans polycistronic pre-mRNA processing. RNA *9*, 677-687.

Lodish, H.F. (1974). Model for the regulation of mRNA translation applied to haemoglobin synthesis. Nature *251*, 385-388.

Long, X., Lin, Y., Ortiz-Vega, S., Yonezawa, K., and Avruch, J. (2005). Rheb binds and regulates the mTOR kinase. Curr Biol *15*, 702-713.

Ma, X.M., and Blenis, J. (2009). Molecular mechanisms of mTOR-mediated translational control. Nat Rev Mol Cell Biol *10*, 307-318.

Maduro, M. (2011). Omission of RNase and addition of ethanol precipitation improve transgenesis using spin column-purified DNA. The Worm Breeder's Gazette *19*, 10-11.

Malys, N., and McCarthy, J.E. (2011). Translation initiation: variations in the mechanism can be anticipated. Cell Mol Life Sci *68*, 991-1003.

Mamane, Y., Petroulakis, E., Rong, L., Yoshida, K., Ler, L.W., and Sonenberg, N. (2004). eIF4E--from translation to transformation. Oncogene *23*, 3172-3179.

Marissen, W.E., Gradi, A., Sonenberg, N., and Lloyd, R.E. (2000). Cleavage of eukaryotic translation initiation factor 4GII correlates with translation inhibition during apoptosis. Cell Death Differ *7*, 1234-1243.

Marissen, W.E., and Lloyd, R.E. (1998). Eukaryotic translation initiation factor 4G is targeted for proteolytic cleavage by caspase 3 during inhibition of translation in apoptotic cells. Mol Cell Biol *18*, 7565-7574.

Matsuura, H., Shinmyo, A., and Kato, K. (2008). Preferential translation mediated by Hsp81-3 5'-UTR during heat shock involves ribosome entry at the 5'-end rather than an internal site in Arabidopsis suspension cells. Journal of bioscience and bioengineering *105*, 39-47.

McClusky, D.R., Chu, Q., Yu, H., Debenedetti, A., Johnson, L.W., Meschonat, C., Turnage, R., McDonald, J.C., Abreo, F., and Li, B.D. (2005). A prospective trial on initiation factor 4E (eIF4E) overexpression and cancer recurrence in node-positive breast cancer. Annals of surgery *242*, 584-590; discussion 590-582.

Mitchell, S.A., Brown, E.C., Coldwell, M.J., Jackson, R.J., and Willis, A.E. (2001). Protein factor requirements of the Apaf-1 internal ribosome entry segment: roles of polypyrimidine tract binding protein and upstream of N-ras. Molecular and cellular biology *21*, 3364-3374.

Mitchell, S.A., Spriggs, K.A., Coldwell, M.J., Jackson, R.J., and Willis, A.E. (2003). The Apaf-1 internal ribosome entry segment attains the correct structural conformation for function via interactions with PTB and unr. Molecular Cell *11*, 757-771.

Mori, C., Nakamura, N., Kimura, S., Irie, H., Takigawa, T., and Shiota, K. (1995). Programmed cell death in the interdigital tissue of the fetal mouse limb is apoptosis with DNA fragmentation. Anat Rec *242*, 103-110.

Morino, S., Imataka, H., Svitkin, Y.V., Pestova, T.V., and Sonenberg, N. (2000). Eukaryotic translation initiation factor 4E (eIF4E) binding site and the middle one-third of eIF4GI constitute the core domain for cap-dependent translation, and the C-terminal one-third functions as a modulatory region. Mol Cell Biol *20*, 468-477.

Morrison, J.K., Friday, A.J., Henderson, M.A., Hao E., Keiper, B.D. (2014). Induction of cap-independent BiP (hsp-3) and Bcl-2 (ced-9) translation in response to eIF4G (IFG-1) depletion in C. elegans. Translation, 2:e28935.

Mortazavi, A., Williams, B.A., McCue, K., Schaeffer, L., and Wold, B. (2008). Mapping and quantifying mammalian transcriptomes by RNA-Seq. Nat Methods *5*, 621-628.

Muchmore, S.W., Sattler, M., Liang, H., Meadows, R.P., Harlan, J.E., Yoon, H.S., Nettesheim, D., Chang, B.S., Thompson, C.B., Wong, S.L.*, et al.* (1996). X-ray and NMR structure of human Bcl-xL, an inhibitor of programmed cell death. Nature *381*, 335-341.

Murray, A.W. (2004). Recycling the cell cycle: cyclins revisited. Cell *116*, 221-234.

Myers, M.G., Jr., Backer, J.M., Sun, X.J., Shoelson, S., Hu, P., Schlessinger, J., Yoakim, M., Schaffhausen, B., and White, M.F. (1992). IRS-1 activates phosphatidylinositol 3'-kinase by associating with src homology 2 domains of p85. Proc Natl Acad Sci U S A *89*, 10350-10354.

Nanda, J.S., Saini, A.K., Munoz, A.M., Hinnebusch, A.G., and Lorsch, J.R. (2013). Coordinated movements of eukaryotic translation initiation factors eIF1, eIF1A, and eIF5 trigger phosphate release from eIF2 in response to start codon recognition by the ribosomal preinitiation complex. J Biol Chem *288*, 5316-5329.

Nevins, T.A., Harder, Z.M., Korneluk, R.G., and Holcik, M. (2003). Distinct regulation of internal ribosome entry site-mediated translation following cellular stress is mediated by apoptotic fragments of eIF4G translation initiation factor family members eIF4GI and p97/DAP5/NAT1. J Biol Chem *278*, 3572-3579.

Nicholson, D.W., Ali, A., Thornberry, N.A., Vaillancourt, J.P., Ding, C.K., Gallant, M., Gareau, Y., Griffin, P.R., Labelle, M., Lazebnik, Y.A.*, et al.* (1995). Identification and inhibition of the ICE/CED-3 protease necessary for mammalian apoptosis. Nature *376*, 37-43.

Nomoto, A., Lee, Y.F., and Wimmer, E. (1976). The 5' end of poliovirus mRNA is not capped with m7G(5')ppp(5')Np. Proc Natl Acad Sci U S A *73*, 375-380.

O'Connor, L., Strasser, A., O'Reilly, L.A., Hausmann, G., Adams, J.M., Cory, S., and Huang, D.C. (1998). Bim: a novel member of the Bcl-2 family that promotes apoptosis. The EMBO journal *17*, 384-395.

Ohndorf, U.M., Steegborn, C., Knijff, R., and Sondermann, P. (2001). Contributions of the individual domains in human La protein to its RNA 3'-end binding activity. J Biol Chem *276*, 27188-27196.

Olsen, D.S., Savner, E.M., Mathew, A., Zhang, F., Krishnamoorthy, T., Phan, L., and Hinnebusch, A.G. (2003). Domains of eIF1A that mediate binding to eIF2, eIF3 and eIF5B and promote ternary complex recruitment in vivo. EMBO J *22*, 193-204.

Oltvai, Z.N., Milliman, C.L., and Korsmeyer, S.J. (1993). Bcl-2 heterodimerizes in vivo with a conserved homolog, Bax, that accelerates programmed cell death. Cell *74*, 609-619.

Pandolfi, P.P. (2004). Aberrant mRNA translation in cancer pathogenesis: an old concept revisited comes finally of age. Oncogene *23*, 3134-3137.

Passmore, L.A., Schmeing, T.M., Maag, D., Applefield, D.J., Acker, M.G., Algire, M.A., Lorsch, J.R., and Ramakrishnan, V. (2007). The eukaryotic translation initiation factors eIF1 and eIF1A induce an open conformation of the 40S ribosome. Mol Cell *26*, 41-50.

Pelletier, J., and Sonenberg, N. (1988). Internal initiation of translation of eukaryotic mRNA directed by a sequence derived from poliovirus RNA. Nature *334*, 320-325.

Peng, J., Tan, C., Roberts, G.J., Nikolaeva, O., Zhang, Z., Lapolla, S.M., Primorac, S., Andrews, D.W., and Lin, J. (2006). tBid elicits a conformational alteration in membrane-bound Bcl-2 such that it inhibits Bax pore formation. J Biol Chem *281*, 35802-35811.

Pepper, A.S., Killian, D.J., and Hubbard, E.J. (2003). Genetic analysis of Caenorhabditis elegans glp-1 mutants suggests receptor interaction or competition. Genetics *163*, 115-132.

Pestova, T.V., and Hellen, C.U. (2003). Translation elongation after assembly of ribosomes on the Cricket paralysis virus internal ribosomal entry site without initiation factors or initiator tRNA. Genes Dev *17*, 181-186.

Pestova, T.V., Lomakin, I.B., and Hellen, C.U. (2004). Position of the CrPV IRES on the 40S subunit and factor dependence of IRES/80S ribosome assembly. EMBO Rep *5*, 906-913.

Pestova, T.V., Shatsky, I.N., and Hellen, C.U. (1996). Functional dissection of eukaryotic initiation factor 4F: the 4A subunit and the central domain of the 4G subunit are sufficient to mediate internal entry of 43S preinitiation complexes. Mol Cell Biol *16*, 6870-6878.

Petros, A.M., Medek, A., Nettesheim, D.G., Kim, D.H., Yoon, H.S., Swift, K., Matayoshi, E.D., Oltersdorf, T., and Fesik, S.W. (2001). Solution structure of the antiapoptotic protein bcl-2. Proc Natl Acad Sci U S A *98*, 3012-3017.

Pisarev, A.V., Chard, L.S., Kaku, Y., Johns, H.L., Shatsky, I.N., and Belsham, G.J. (2004). Functional and structural similarities between the internal ribosome entry sites of hepatitis C virus and porcine teschovirus, a picornavirus. J Virol *78*, 4487-4497.

Pisarev, A.V., Shirokikh, N.E., and Hellen, C.U. (2005). Translation initiation by factor-independent binding of eukaryotic ribosomes to internal ribosomal entry sites. Comptes rendus biologies *328*, 589-605.

Potter, C.J., Huang, H., and Xu, T. (2001). Drosophila Tsc1 functions with Tsc2 to antagonize insulin signaling in regulating cell growth, cell proliferation, and organ size. Cell *105*, 357-368.

Pourkarimi, E., Greiss, S., and Gartner, A. (2012). Evidence that CED-9/Bcl2 and CED-4/Apaf-1 localization is not consistent with the current model for C. elegans apoptosis induction. Cell Death and Differentiation *19*, 406-415.

Praitis, V., Casey, E., Collar, D., and Austin, J. (2001). Creation of low-copy integrated transgenic lines in Caenorhabditis elegans. Genetics *157*, 1217-1226.

Pyronnet, S., Imataka, H., Gingras, A.C., Fukunaga, R., Hunter, T., and Sonenberg, N. (1999). Human eukaryotic translation initiation factor 4G (eIF4G) recruits mnk1 to phosphorylate eIF4E. EMBO J *18*, 270-279.

Pyronnet, S., Pradayrol, L., and Sonenberg, N. (2000). A cell cycle-dependent internal ribosome entry site. Mol Cell *5*, 607-616.

Raught, B., Gingras, A.C., Gygi, S.P., Imataka, H., Morino, S., Gradi, A., Aebersold, R., and Sonenberg, N. (2000). Serum-stimulated, rapamycin-sensitive phosphorylation sites in the eukaryotic translation initiation factor 4GI. EMBO J *19*, 434-444.

Renatus, M., Stennicke, H.R., Scott, F.L., Liddington, R.C., and Salvesen, G.S. (2001). Dimer formation drives the activation of the cell death protease caspase 9. Proceedings of the National Academy of Sciences of the United States of America *98*, 14250-14255.

Revil, T., Toutant, J., Shkreta, L., Garneau, D., Cloutier, P., and Chabot, B. (2007). Protein kinase C-dependent control of Bcl-x alternative splicing. Mol Cell Biol *27*, 8431-8441.

Rhoads, R.E. (1993). Regulation of eukaryotic protein synthesis by initiation factors. J Biol Chem *268*, 3017-3020.

Rhoads, R.E., and Lamphear, B.J. (1995). Cap-independent translation of heat shock messenger RNAs. Curr Top Microbiol Immunol *203*, 131-153.

Rijnbrand, R., van der Straaten, T., van Rijn, P.A., Spaan, W.J., and Bredenbeek, P.J. (1997). Internal entry of ribosomes is directed by the 5' noncoding region of classical swine fever virus and is dependent on the presence of an RNA pseudoknot upstream of the initiation codon. J Virol *71*, 451-457.

Rosenwald, I.B., Lazaris-Karatzas, A., Sonenberg, N., and Schmidt, E.V. (1993). Elevated levels of cyclin D1 protein in response to increased expression of eukaryotic initiation factor 4E. Mol Cell Biol *13*, 7358-7363.

Ruggero, D., Montanaro, L., Ma, L., Xu, W., Londei, P., Cordon-Cardo, C., and Pandolfi, P.P. (2004). The translation factor eIF-4E promotes tumor formation and cooperates with c-Myc in lymphomagenesis. Nat Med *10*, 484-486.

Saleh, A., Srinivasula, S.M., Acharya, S., Fishel, R., and Alnemri, E.S. (1999). Cytochrome c and dATP-mediated oligomerization of Apaf-1 is a prerequisite for procaspase-9 activation. J Biol Chem *274*, 17941-17945.

Sattler, M., Liang, H., Nettesheim, D., Meadows, R.P., Harlan, J.E., Eberstadt, M., Yoon, H.S., Shuker, S.B., Chang, B.S., Minn, A.J.*, et al.* (1997). Structure of Bcl-xL-Bak peptide complex: recognition between regulators of apoptosis. Science *275*, 983-986.

Schafer, K.A. (1998). The cell cycle: a review. Veterinary pathology *35*, 461-478.

Schmelzle, T., and Hall, M.N. (2000). TOR, a central controller of cell growth. Cell *103*, 253-262.

Schmid, M., Kuchler, B., and Eckmann, C.R. (2009). Two conserved regulatory cytoplasmic poly(A) polymerases, GLD-4 and GLD-2, regulate meiotic progression in C. elegans. Genes Dev *23*, 824-836.

Schneider, R.J. (1995). Cap-independent translation in adenovirus infected cells. Curr Top Microbiol Immunol *203*, 117-129.

Schuler, M., Connell, S.R., Lescoute, A., Giesebrecht, J., Dabrowski, M., Schroeer, B., Mielke, T., Penczek, P.A., Westhof, E., and Spahn, C.M. (2006). Structure of the ribosome-bound cricket paralysis virus IRES RNA. Nature structural & molecular biology *13*, 1092-1096.

Seydoux, G., Mello, C.C., Pettitt, J., Wood, W.B., Priess, J.R., and Fire, A. (1996). Repression of gene expression in the embryonic germ lineage of C. elegans. Nature *382*, 713-716.

Shaham, S., and Horvitz, H.R. (1996). An alternatively spliced C. elegans ced-4 RNA encodes a novel cell death inhibitor. Cell *86*, 201-208.

Shatkin, A.J. (1976). Capping of eucaryotic mRNAs. Cell *9*, 645-653.

Sherrill, K.W., Byrd, M.P., Van Eden, M.E., and Lloyd, R.E. (2004). BCL-2 translation is mediated via internal ribosome entry during cell stress. The Journal of biological chemistry *279*, 29066-29074.

Shirayama, M., Seth, M., Lee, H.C., Gu, W., Ishidate, T., Conte, D., Jr., and Mello, C.C. (2012). piRNAs initiate an epigenetic memory of nonself RNA in the C. elegans germline. Cell *150*, 65-77.

Shkreta, L., Froehlich, U., Paquet, E.R., Toutant, J., Elela, S.A., and Chabot, B. (2008). Anticancer drugs affect the alternative splicing of Bcl-x and other human apoptotic genes. Mol Cancer Ther *7*, 1398-1409.

Shkreta, L., Michelle, L., Toutant, J., Tremblay, M.L., and Chabot, B. The DNA damage response pathway regulates the alternative splicing of the apoptotic mediator Bcl-x. J Biol Chem *286*, 331-340.

Siridechadilok, B., Fraser, C.S., Hall, R.J., Doudna, J.A., and Nogales, E. (2005). Structural roles for human translation factor eIF3 in initiation of protein synthesis. Science *310*, 1513-1515.

Sonenberg, N., Morgan, M.A., Merrick, W.C., and Shatkin, A.J. (1978). A polypeptide in eukaryotic initiation factors that crosslinks specifically to the 5'-terminal cap in mRNA. Proc Natl Acad Sci U S A *75*, 4843-4847.

Spahn, C.M., Jan, E., Mulder, A., Grassucci, R.A., Sarnow, P., and Frank, J. (2004). Cryo-EM visualization of a viral internal ribosome entry site bound to human ribosomes: the IRES functions as an RNA-based translation factor. Cell *118*, 465-475.

Spieth, J., Brooke, G., Kuersten, S., Lea, K., and Blumenthal, T. (1993). Operons in C. elegans: polycistronic mRNA precursors are processed by trans-splicing of SL2 to downstream coding regions. Cell *73*, 521-532.

Spriggs, K.A., Bushell, M., and Willis, A.E. (2010). Translational regulation of gene expression during conditions of cell stress. Mol Cell *40*, 228-237.

Stower, H. (2012). Small RNAs: piRNA surveillance in the C. elegans germline. Nature reviews Genetics *13*, 518-519.

Sulston, J.E., and Horvitz, H.R. (1977). Post-embryonic cell lineages of the nematode, Caenorhabditis elegans. Dev Biol *56*, 110-156.

Sulston, J.E., Schierenberg, E., White, J.G., and Thomson, J.N. (1983). The embryonic cell lineage of the nematode Caenorhabditis elegans. Dev Biol *100*, 64-119.

Szalai, G., Krishnamurthy, R., and Hajnoczky, G. (1999). Apoptosis driven by IP(3)-linked mitochondrial calcium signals. EMBO J *18*, 6349-6361.

Tax, F.E., Yeargers, J.J., and Thomas, J.H. (1994). Sequence of C. elegans lag-2 reveals a cell-signalling domain shared with Delta and Serrate of Drosophila. Nature *368*, 150-154.

Taylor, R.C., Brumatti, G., Ito, S., Hengartner, M.O., Derry, W.B., and Martin, S.J. (2007). Establishing a blueprint for CED-3-dependent killing through identification of multiple substrates for this protease. The Journal of biological chemistry *282*, 15011-15021.

Tee, A.R., and Proud, C.G. (2000). DNA-damaging agents cause inactivation of translational regulators linked to mTOR signalling. Oncogene *19*, 3021-3031.

Thoma, C., Bergamini, G., Galy, B., Hundsdoerfer, P., and Hentze, M.W. (2004). Enhancement of IRES-mediated translation of the c-myc and BiP mRNAs by the poly(A) tail is independent of intact eIF4G and PABP. Molecular Cell *15*, 925-935.

Thornberry, N.A. (1997). The caspase family of cysteine proteases. Br Med Bull *53*, 478-490.

Tinton, S.A., and Buc-Calderon, P.M. (1999). Hypoxia increases the association of 4E-binding protein 1 with the initiation factor 4E in isolated rat hepatocytes. FEBS letters *446*, 55-59.

Tsujimoto, Y., Cossman, J., Jaffe, E., and Croce, C.M. (1985). Involvement of the bcl-2 gene in human follicular lymphoma. Science *228*, 1440-1443.

Tsujimoto, Y., and Croce, C.M. (1986). Analysis of the structure, transcripts, and protein products of bcl-2, the gene involved in human follicular lymphoma. Proc Natl Acad Sci U S A *83*, 5214-5218.

Tsukiyama-Kohara, K., Iizuka, N., Kohara, M., and Nomoto, A. (1992). Internal ribosome entry site within hepatitis C virus RNA. J Virol *66*, 1476-1483.

Uren, R.T., Dewson, G., Chen, L., Coyne, S.C., Huang, D.C., Adams, J.M., and Kluck, R.M. (2007). Mitochondrial permeabilization relies on BH3 ligands engaging multiple prosurvival Bcl-2 relatives, not Bak. J Cell Biol *177*, 277-287.

Vaux, D.L. (1999). Caspases and apoptosis - biology and terminology. Cell Death Differ *6*, 493-494.

Vries, R.G., Flynn, A., Patel, J.C., Wang, X., Denton, R.M., and Proud, C.G. (1997). Heat shock increases the association of binding protein-1 with initiation factor 4E. The Journal of biological chemistry *272*, 32779-32784.

Wang, E.T., Sandberg, R., Luo, S., Khrebtukova, I., Zhang, L., Mayr, C., Kingsmore, S.F., Schroth, G.P., and Burge, C.B. (2008). Alternative isoform regulation in human tissue transcriptomes. Nature *456*, 470-476.

Wang, L., Miura, M., Bergeron, L., Zhu, H., and Yuan, J. (1994). Ich-1, an Ice/ced-3-related gene, encodes both positive and negative regulators of programmed cell death. Cell *78*, 739-750.

Waskiewicz, A.J., Johnson, J.C., Penn, B., Mahalingam, M., Kimball, S.R., and Cooper, J.A. (1999). Phosphorylation of the cap-binding protein eukaryotic translation initiation factor 4E by protein kinase Mnk1 in vivo. Mol Cell Biol *19*, 1871-1880.

Wei, M.C., Lindsten, T., Mootha, V.K., Weiler, S., Gross, A., Ashiya, M., Thompson, C.B., and Korsmeyer, S.J. (2000). tBID, a membrane-targeted death ligand, oligomerizes BAK to release cytochrome c. Genes & development *14*, 2060-2071.

Wei, M.C., Zong, W.X., Cheng, E.H., Lindsten, T., Panoutsakopoulou, V., Ross, A.J., Roth, K.A., MacGregor, G.R., Thompson, C.B., and Korsmeyer, S.J. (2001). Proapoptotic BAX and BAK: a requisite gateway to mitochondrial dysfunction and death. Science *292*, 727-730.

Weingarten-Gabbay, S., Khan, D., Liberman, N., Yoffe, Y., Bialik, S., Das, S., Oren, M., and Kimchi, A. (2013). The translation initiation factor DAP5 promotes IRES-driven translation of p53 mRNA. Oncogene.

Williams, C., Xu, L., and Blumenthal, T. (1999). SL1 trans splicing and 3'-end formation in a novel class of Caenorhabditis elegans operon. Mol Cell Biol *19*, 376-383.

Willis, S.N., Chen, L., Dewson, G., Wei, A., Naik, E., Fletcher, J.I., Adams, J.M., and Huang, D.C. (2005). Proapoptotic Bak is sequestered by Mcl-1 and Bcl-xL, but not Bcl-2, until displaced by BH3-only proteins. Genes Dev *19*, 1294-1305.

Willis, S.N., Fletcher, J.I., Kaufmann, T., van Delft, M.F., Chen, L., Czabotar, P.E., Ierino, H., Lee, E.F., Fairlie, W.D., Bouillet, P.*, et al.* (2007). Apoptosis initiated when BH3 ligands engage multiple Bcl-2 homologs, not Bax or Bak. Science *315*, 856-859.

Wilson, J.E., Powell, M.J., Hoover, S.E., and Sarnow, P. (2000). Naturally occurring dicistronic cricket paralysis virus RNA is regulated by two internal ribosome entry sites. Mol Cell Biol *20*, 4990-4999.

Wolter, K.G., Hsu, Y.T., Smith, C.L., Nechushtan, A., Xi, X.G., and Youle, R.J. (1997). Movement of Bax from the cytosol to mitochondria during apoptosis. J Cell Biol *139*, 1281-1292.

WormBase (2007). hsp-3. In WormBase: C elegans online database, J.S. R. Durbin, L. Stein and P. Sternberg, ed.

WormBase (2014). WormBase: C elegans online database.

Xue, D., Shaham, S., and Horvitz, H.R. (1996). The Caenorhabditis elegans cell-death protein CED-3 is a cysteine protease with substrate specificities similar to those of the human CPP32 protease. Genes Dev *10*, 1073-1083.

Yamamoto, K., Ichijo, H., and Korsmeyer, S.J. (1999). BCL-2 is phosphorylated and inactivated by an ASK1/Jun N-terminal protein kinase pathway normally activated at G(2)/M. Molecular and cellular biology *19*, 8469-8478.

Yang, Q., and Sarnow, P. (1997). Location of the internal ribosome entry site in the 5' non-coding region of the immunoglobulin heavy-chain binding protein (BiP) mRNA: evidence for specific RNA-protein interactions. Nucleic acids research *25*, 2800-2807.

Yang, X., Chang, H.Y., and Baltimore, D. (1998). Essential role of CED-4 oligomerization in CED-3 activation and apoptosis. Science *281*, 1355-1357.

Yu, C., Minemoto, Y., Zhang, J., Liu, J., Tang, F., Bui, T.N., Xiang, J., and Lin, A. (2004). JNK suppresses apoptosis via phosphorylation of the proapoptotic Bcl-2 family protein BAD. Molecular Cell *13*, 329-340.

Yuan, J., Shaham, S., Ledoux, S., Ellis, H.M., and Horvitz, H.R. (1993). The C. elegans cell death gene ced-3 encodes a protein similar to mammalian interleukin-1 beta-converting enzyme. Cell *75*, 641-652.

Zhou, Z., Hartwieg, E., and Horvitz, H.R. (2001). CED-1 is a transmembrane receptor that mediates cell corpse engulfment in C. elegans. Cell *104*, 43-56.

Zou, H., Henzel, W.J., Liu, X., Lutschg, A., and Wang, X. (1997). Apaf-1, a human protein homologous to C. elegans CED-4, participates in cytochrome c-dependent activation of caspase-3. Cell *90*, 405-413.

Zou, H., Li, Y., Liu, X., and Wang, X. (1999). An APAF-1.cytochrome c multimeric complex is a functional apoptosome that activates procaspase-9. J Biol Chem *274*, 11549-11556.

APPENDIX A: CAP-INDEPENDENT IFG-1 p130 IS A SUBSTRATE FOR CED-3 DURING APOPTOSIS*

*** Contreras V, Friday AJ, Morrison JK, Friday AJ, Hao E, Keiper BD. Cap-Independent Translation Promotes C. elegans Apoptosis through Apaf-1/CED-4 in a Caspase-Dependent Mechanism. 2011; 10.1371/journal.pone.0024444.**

Introduction

The induction of apoptosis leads to changes in the ability of the translation initiation apparatus to select mRNAs for translation. Cap-dependent translation is based on the ability of eIF4G isoforms to provide a scaffolding complex that allows for the active recruitment of mRNA to the ribosome for translation (Lamphear et al., 1995; Sonenberg et al., 1978). eIF4GI and eIF4GII have domains that bind the ribosome, the cap-binding protein, eIF4E, and PABP (Imataka et al., 1998) (Lamphear et al., 1995; Morino et al., 2000). During apoptosis, activated caspase-3 cleaves the eIF4G isoforms: eIF4GI, eIF4GII and p97 (Bushell et al., 1999; Marissen et al., 2000). Cleavage removes the eIF4E and PABP domains from eIF4GI preventing cap-dependent mRNA recruitment to the ribosome (Morino et al., 2000). eIF4GII is degraded and plays no further known role in the initiation of translation (Nevins et al., 2003). The constitutively cap-independent eIF4G isoform, p97, is also a target for caspase-3 cleavage during apoptosis (Henis-Korenblit et al., 2000). Cleaved eIF4GI and p97 are still able to initiate translation of a select subset of mRNAs cap-independently (Henis-Korenblit et al., 2000; Marissen and Lloyd, 1998; Nevins et al., 2003). This change in initiation mechanism results in decreased translation of mRNAs that rely on cap-recruitment for their initiation, while allowing for the enhanced translation of mRNAs that can initiate translation cap-independently.

Similar changes in the initiation of translation occur after the induction of apoptosis within *C. elegans*. *C. elegans* have two eIF4G homologues, IFG-1 p170 and IFG-1 p130 (Contreras et al., 2008). IFG-1 p170 is the cap-dependent eIF4G homologue and contains domains that associate with the eIF4E homologues, IFEs, and the PABP (Contreras et al., 2008). Much like in mammals, caspase-cleavage of IFG-1 p170 results in the removal of the cap and poly(A) binding domains preventing cap-dependent mRNA recruitment for translation (Contreras et al., 2011). The *C. elegans* caspase, CED-3, is a highly specific protease that cleaves proteins at a tetrapeptide recognition sequence and requires an aspartate residue in the P1 position (Taylor et al., 2007). In the case of IFG-1 p170 the defined caspase cleavage site is at TTTD456 (Contreras et al., 2011). The other eIF4G homologue, IFG-1 p130, does not contain the IFE and PABP domains (Contreras et al., 2008). Thus, IFG-1 p130 is constitutively cap-independent, much like mammalian p97 (Contreras et al., 2011; Henis-Korenblit et al., 2000). The known CED-3 cleavage site is 65 amino acids downstream of the proposed initiating methionine of IFG-1 p130. This study focuses on determining whether IFG-1 p130 is similarly cleaved by CED-3 during apoptosis, producing a 65 amino acid smaller fragment that may still support cap-independent protein synthesis.

Results

IFG-1 p130 is also a substrate for CED-3. To determine if IFG-1 p130 is cleaved by direct substrate cleavage by *C. elegans* caspase CED-3, as opposed to indirect or secondary proteolytic activity that may be observed *in vivo* and in whole worm extracts, we used recombinant IFG-1 p170, IFG-1 p130 and CED-3 to determine specific cleavage events. We

generated active recombinant *C. elegans* CED-3 (rCED-3) using previously described purification conditions (Taylor et al., 2007). CED-3 is synthesized as a catalytically inactive proenzyme of approximately 32 kDa (Thornberry, 1997). Upon activation it is autoprocessed to form a heterotetramer composed of large subunit, p17 and small subunit p15/p13. Sequences encoding catalytic portion (amino acids 221-503) were fused to N-terminal GST and 6X His tags and were expressed in E. coli. Expression of the protein in bacteria revealed robust autocatalytic processing into well-defined subunits. Western blotting of bacterial lysate showed very little full length GST-His6-CED-3201-503, but considerable accumulation of processed intermediates (data not shown). Similar rCED-3 intermediates, which include the p17 and p13 subunits required for activity, were co-purified upon Ni-NTA affinity chromatography. Proteolytic activity was confirmed in the partially purified rCED-3 using the synthetic tetrapeptide substrate Ac-DEVD-pNA, revealing a 53-fold increase in activity above the background (Figure A.1). These data demonstrate that rCED-3 displays similar autocatalytic activity and substrate specificity to other purified effector caspases (Thornberry, 1997).

Mapping of the *ifg-1* mRNA 5' ends shows that the proposed initiating methionine (M391) for IFG-1 p130 is just 65 amino acids upstream of the CED-3 (caspase) cleavage site that was identified for IFG-1 p170 (TTTD456). Given the proximity of the proposed IFG-1 p130 translation start (MVTI) and CED-3 cleavage site, we attempted to determine if IFG-1 p130 was still cleaved by rCED-3 to remove this 65 amino acid leader. This cleavage was then compared to IFG-1 p170 cleavage by rCED-3 (Figure A.2A). We subcloned and expressed a [35S] methionine-labeled IFG-1 p130 (391-1156) in rabbit reticulocyte lysate. [35S]-labeled IFG-1 p170 (1-1156) (unmodified migrates at 150 kDa) was also synthesized

Figure A.1

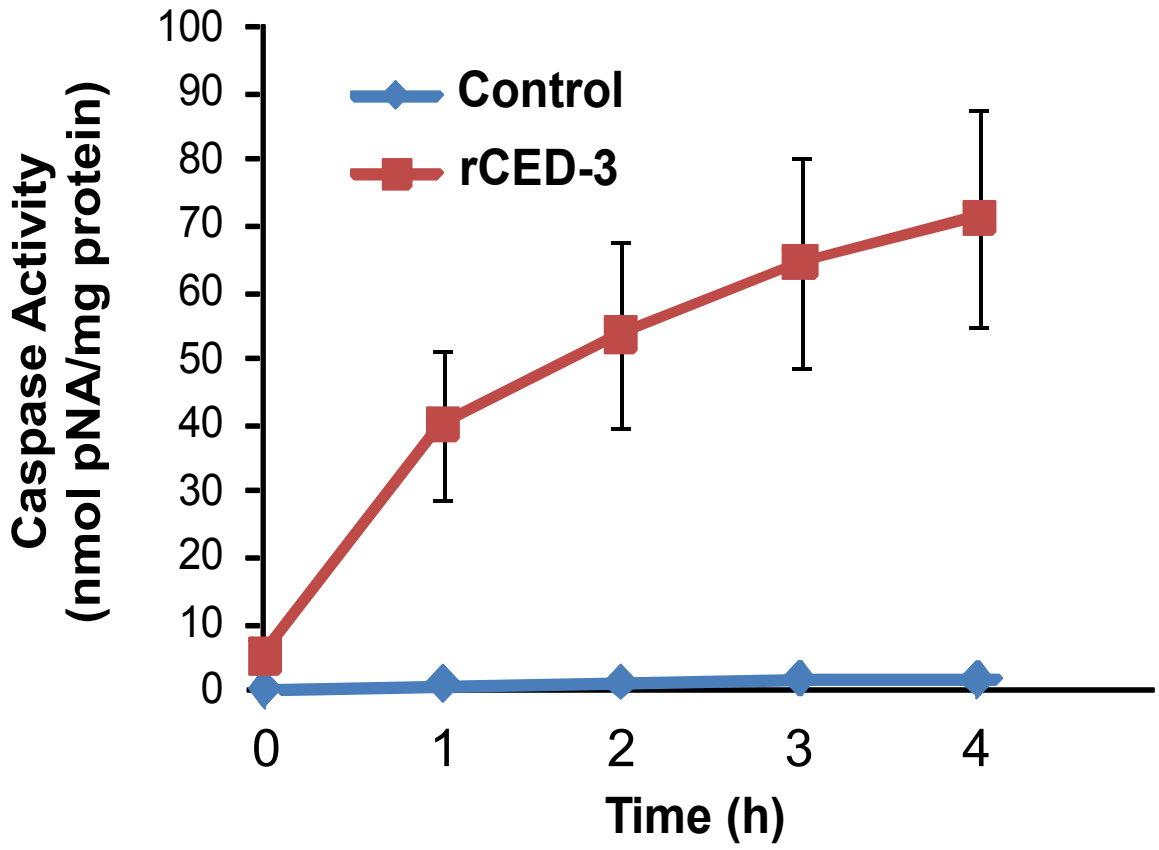
Caspase Activity
(nmol pNA/mg protein)
100
90
80
70
60
50
40
30
20
10
0
Control
rCED-3
0
1
2
3
4
Time (h)

Figure A.1. Generating catalytically active *C. elegans* recombinant CED-3. Caspase activity for rCED-3 was determined using chromogenic substrate Ac-DEVD-pNA (Promega) and measured at a wavelength of 405 nm. Partially purified enzyme (10 µl; 133–196 µg total protein) was added to the substrate (0.2 mM) and the rate of proteolysis monitored over a 4 h period. Activity (U) is expressed as nmoles pNA released per milligram protein per hour. Caspase activity (35 U/h) was compared to control reactions containing equivalent amounts of a bovine serum albumin (0.78 U/h), showing a 44-fold increase in rate. Data is representative of three independent preparations of rCED-3. Error bars are S.E.M.

in rabbit reticulocyte lysate from a full-length cDNA as previously described (Contreras et al., 2011). The radiolabeled IFG-1 p130 and p170 were then treated with rCED-3. p130 cleavage gave rise to a very closely migrating smaller product that could just be resolved by SDS gel electrophoresis (Figure A.2B). This cleavage product was compared to IFG-1 p170 cleavage, which migrated similarly. However, because there is a frequently observed closely migrating smaller product in untreated p130 due to a second translation start (personal communication Dr. Vince Contreras), we could not definitively demonstrate cleavage by rCED-3. To conclusively show that this site in p130 was recognized and cleaved, we generated an internal deletion construct (IFG-1 p130 d830-1114) that maintains the site but is smaller in size for better gel resolution. The deletion construct's cleavage product could be clearly resolved migrating several kDa smaller than the parent peptide (55 kDa), consistent with loss of the N-terminal 65 amino acids (Figure A.2C). Thus, although not apparent from western blots of native protein, *C. elegans* IFG-1 p130 is also processed by CED-3.

Discussion

During apoptosis there is an activation of caspases due to their self-proteolytic cleavage resulting from close proximity of procaspases within the apoptosome (Renatus et al., 2001). Caspases then cleave cellular machinery, including the protein synthetic apparatus, resulting in cell death. One of the targets of caspase cleavage is the translation initiation factors eIF4G (IFG-1 p170) and p97 (IFG-1 p130), which are involved in cap-dependent and cap-independnet protein synthesis respectively. In this study we demonstrated that the cap-independent IFG-1 isoform, IFG-1 p130, is also a substrate for cleavage by CED-3 during apoptosis removing the N-terminal

Figure A.2

A

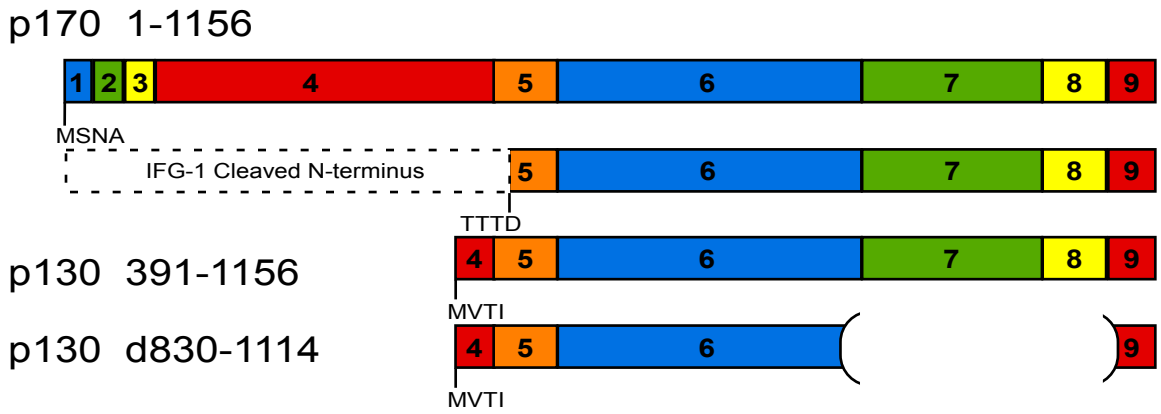
p170 1-1156
1
2
3
4
5
6
7
8
9
MSNA
IFG-1 Cleaved N-terminus
TTTD
p130 391-1156
MVTI
p130 d830-1114
MVTI

B

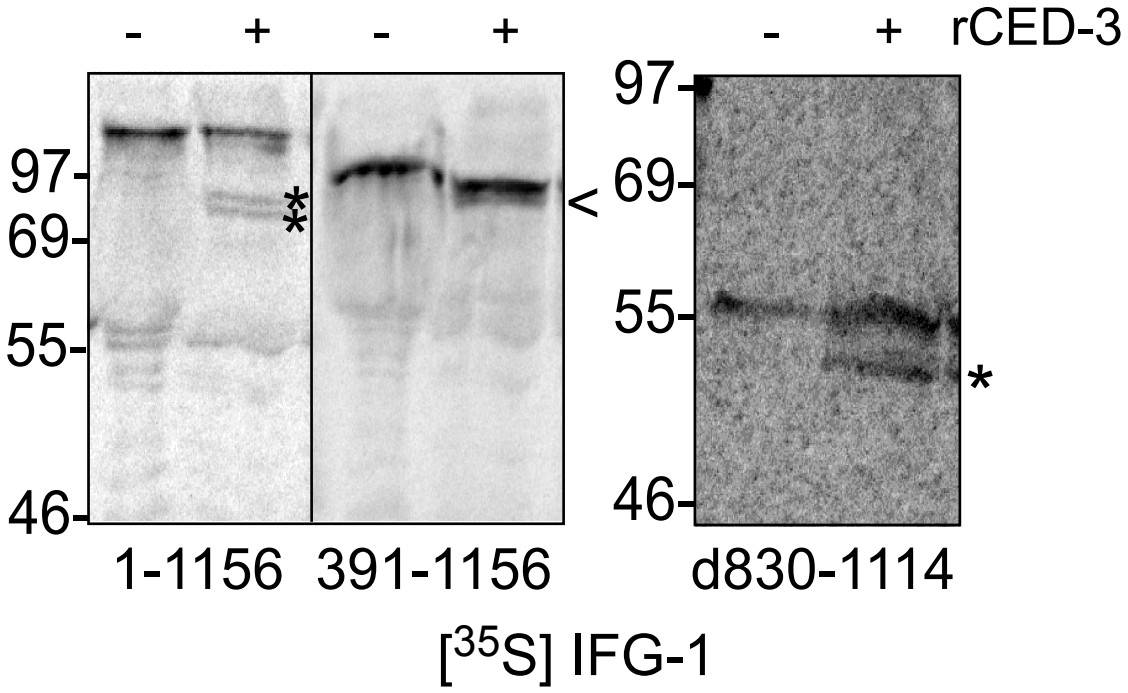
- + - + - + rCED-3
97
69
55
46
**
<
*
1-1156
391-1156
d830-1114
[35S] IFG-1

Figure A.2. CED-3 cleaves IFG-1 p130 *in vitro*. (A) Schematic diagram depicting the mapped CED-3 cleavage site and translation starts in full length IFG-1 p170 (1–1156), p130 (391–1156) and an internally truncated version of p130 (d830–1114). Numbered boxes correspond to protein encoding exons. (B) Radiolabeled IFG 1–1156, 391–1156 and d830–1114 proteins were incubated with rCED-3 (+) as described above, resolved by 12% or 4-20% SDS-PAGE, and visualized by phosphorimaging. Control reactions (–) were incubated with bovine serum albumin. Cleaved fragments are represented by asterisks (*). A product migrating just under IFG p130 (391–1156; <) was indistinguishable from an internal start site product, preventing conclusive determination of cleavage. However, cleavage of an internally truncated IFG p130 (d830–1114) produced a product that was better resolved and was conclusive.

65 amino acids. Despite the fact that the smaller proposed band migrates closely to full-length IFG-1 p130, we demonstrated that IFG-1 p130 native protein cleavage should not be attributed to a second translation start, but rather to N-terminal processing *in vivo*. Cleavage was confirmed by generating a recombinant internal deletion construct whose cleavage product could be easily resolved. After cleavage we were able to confirm a stable cleaved product that should maintain continued cap-independent translation within the cell (Figure A.2). This continued cap-independent translation during apoptosis may allow for the selective translation of cell death and stress related mRNAs allowing for either cellular recovery or the initiation of cellular suicide.

APPENDIX B. CONFIRMATION OF TRANSLATIONAL REGULATION OF CELL DEATH AND APOPTOSIS-RELATED mRNAs DURING CAP-INDEPENDENT TRANSLATION.

Introduction

Certain mRNAs have the propensity to be translated cap-independently allowing them to be translated more efficiently during apoptosis (Coldwell et al., 2000). In order to determine the mRNAs in *C. elegans* that translate cap-independently, we use sucrose gradient fractionation to resolve polyribosomal complexes. However, other RNA binding proteins (RBP), besides ribosomes, have been previously observed to change gradient localization of target mRNAs (Filipenko et al., 2004). Annexin A2 (ANXA2) cosediments with messenger ribonucleoprotein complexes (mRNPs) in heavier gradient fractions after sucrose gradient fractionation (Filipenko et al., 2004). This sedimentation was not maintained after RNase treatment demonstrating that it is dependent on RNA binding (Filipenko et al., 2004). Additionally, it was confirmed that ANXA2 associates with mRNP complexes, not polyribosomes (Filipenko et al., 2004). When the ANXA2-RNP complex was immunoprecipitated from each gradient fraction c-Myc RNA was identified as one of the target mRNA for ANXA2 binding (Filipenko et al., 2004). Thus, c-Myc localization in these gradient fractions is partially attributed to ANXA2 binding (Filipenko et al., 2004).

In this study we optimize sucrose gradient fractionation and confirmed the validity of our polysomal complex resolution results. To initiate cap-independent translation, we used two strains: a strain with increased cap-independent translation due to a splicing defect, *ifg-1::mos* and a strain with increased apoptosis leading to IFG-1 p170 cleavage, *ced-9ts* (Contreras et al., 2011; Morrison, 2014). We confirmed that the observed increases in

translational efficiency, with the exception of *ced-4* mRNA, did not result from RBP as opposed to ribosome binding. *ced-4* mRNA was found to associate with some other, thus far unidentified, RBP complicating interpretations of *ced-4* mRNA gradient localization. Additionally we confirmed increased target mRNA quantity resulting in increased target mRNA availability for ribosome translation was not responsible for the observed increase in translational efficiency. These results confirmed previous finding that while *hsp-3* mRNA is translated cap-independently other *C. elegans* mRNAs are no longer translated efficiently including *hif-1, cep-1* and *ced-4*.

Results

Optimization of gradient conditions allowing for determination of changes in mRNA translational efficiency. To determine changes in mRNA translational efficiency, worm lysates from wild type, *ifg-1::mos* and *ced-9ts* strains were fractionated on sucrose gradients to resolve polyribosomal complexes. The mRNAs of interest were then quantified across the gradient by qPCR, allowing us to monitor differences in mRNA distribution. These changes in distribution reflect variations in bound ribosomes allowing us to determine increases/decreases in translational efficiency. To observe differences in translational efficiency via qPCR, RNA must be isolated from each gradient fraction and be reverse transcribed into cDNA. The RNA quantity in each fraction is directly proportional to the quantity of worms ground to prepare lysate and ultracentrifuged on the sucrose gradient. The amount of material ultracentrifuged on the gradient had to be optimized to allow for maximized RNA quantity yields without overloading the gradient and destroying resolution of ribosomal complexes. For this and other biochemical procedures, populations

Figure B.1

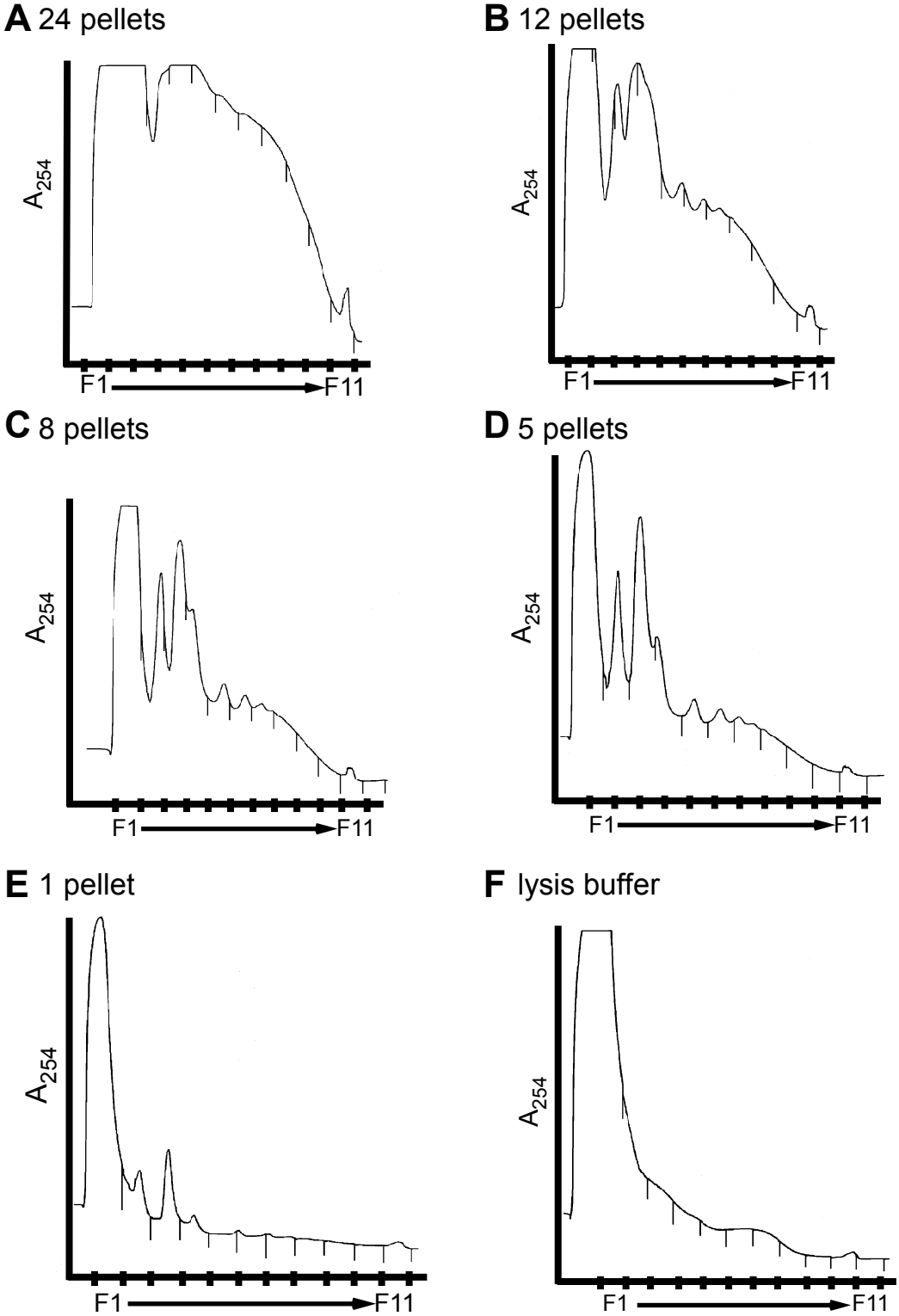
A 24 pellets
B 12 pellets
C 8 pellets
D 5 pellets
E 1 pellet
F lysis buffer
A254
F1
F11

Figure B.1. Optimization of *C. elegans* lysate loading on sucrose gradients. During sucrose gradient fractionation of worm lysates from *ced-9ts* (A-F) strains absorbance was measured at 254nm. Optimization of lysate loading by decreasing number of worm pellets. (A) 24 pellets (B) 12 pellets (C) 8 pellets (D) 5 pellets (E) 1 pellet (F) lysis buffer alone.

of worms were sedimented and then suspended in an equal volume water or dilute buffers containing RNase inhibitors. Worms were subsequently frozen by dropping them in into liquid nitrogen and were then stored at -80˚C. For polysome gradient resolution, decreasing numbers of worm pellets were ground and ultracentrifuged on the gradient (Figure B.1A-F). We determined that eight pellets (50% packed worms) could be maximally run on the gradient without overloading (Figure B.1C). Thus, RNA quantities were maximized by running lysates of 8 pellets over sucrose gradients, without overloading the gradient making interpretation of RNA quality via absorbance difficult.

Changes in mRNA translation efficiency did not result from gross changes in total mRNA quantity. Vast changes in the total amount of target mRNAs can potentially result in false interpretations of increases or decreases in mRNA translational efficiency. Increased amounts of mRNA present may result in increased availability of the specific mRNA to the translation initiation machinery and to ribosomes. In this case the mRNA might change its competitive advantage relative to the rest of the message population, resulting in apparent increases in mRNA translational efficiency. To confirm that changes observed were not due to greatly increased mRNA quantity, but instead an increased ability of the translation initiation complex to recruit the mRNA for translation, we determined the total amount of target mRNAs in total RNA samples extracted directly from worm pellets under each test condition. Total amounts of *hsp-3, hsp-4, ced-9, cep-1* and *hif-1* mRNAs were quantified and normalized to *gpd-3* in wild type, *ced-9ts* and *ifg-1::mos* worms (Figure B.2). We observed no significant change in *hsp-3, hsp-4, ced-9, cep-1* and *hif-1* mRNAs in either the *ced-9ts* or

Figure B.2

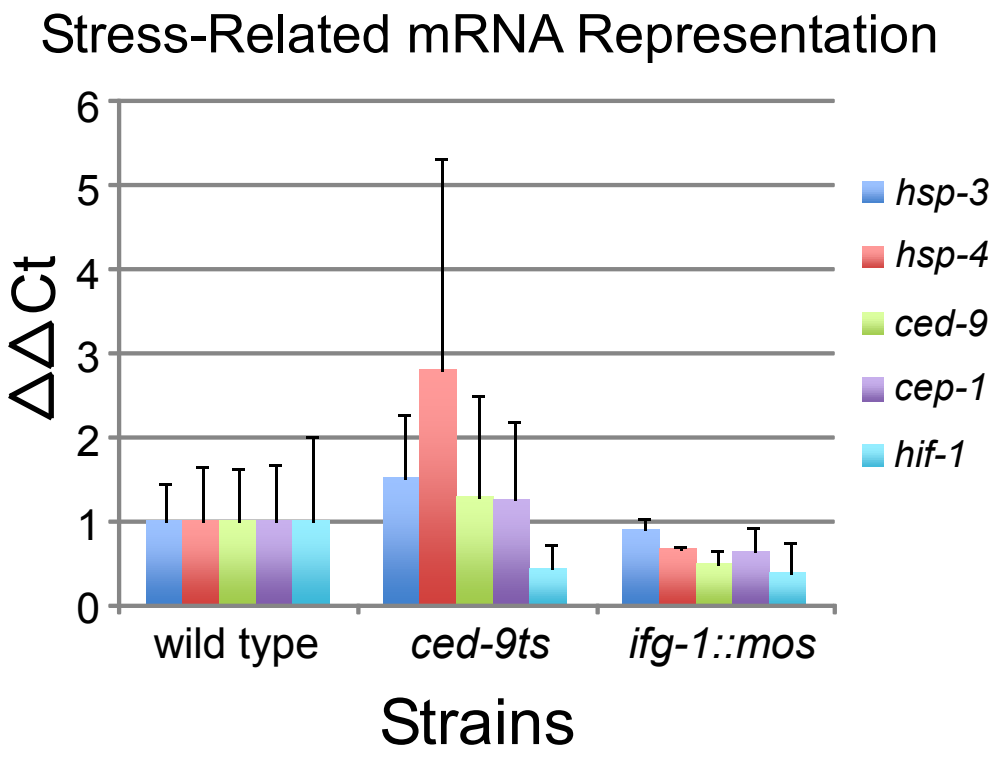
Stress-Related mRNA Representation
6
5
4
3
2
1
0
ΔΔCt
hsp-3
hsp-4
ced-9
cep-1
hif-1
wild type
ced-9ts
ifg-1::mos
Strains

Figure B.2. mRNA abundance is not responsible for increased polysome loading of stress and apoptosis related mRNAs. qPCR amplification of *hsp-3, hsp4, ced-9, cep-1* and *hif-1* from total RNA extracts from wild type, *ced-9ts* and *ifg-1::mos* strains. There is no significant change in mRNA representation in the *ced-9ts* and *ifg-1::mos* strains.

ifg-1::mos strains when compared to wild type. Thus, any variations observed in translational efficiency were not due to large changes in mRNA availability to the ribosome.

Changes in *hsp-3* mRNA distribution result from increases in bound ribosomes. Shifts in the gradient are due to changes in weight of mRNAs, presumably due to bound ribosomes. However, these shifts in mRNA distribution within the gradient may not be solely due to changes in the number of bound ribosomes, but can be influenced by other factors such as RBPs (Filipenko et al., 2004). We compared the sedimentation of mRNAs within the gradient with or without bound ribosomes. Ribosomes, unlike many RBPs require divalent magnesium to bind mRNA. To determine if shifts of mRNAs in the gradient were due to changes in the number of bound ribosomes, gradients were treated with EDTA to chelate magnesium, resulting in ribosome dissociation. Wild type and *ced-9ts* worm lysates were fractionated on sucrose gradients before (Figure B.3A and B.3B) and after (Figure B.3C and B.3D) EDTA addition. EDTA treatment lead to the loss of *gpd-3* mRNA from the heavy, actively translating fractions of the gradient, and its appearance in the lighter fractions representing nontranslating RNAs, as ribosomes were dissociated in wild type (Figure B.4A) and *ced-9ts* (Figure B.4B) strains. Similar changes in *hsp-3* mRNA distribution also resulted from the release of bound ribosomes. *hsp-3* mRNA transitioned into the nontranslating and lightly translating region of the gradient after EDTA treatment in both the wild type (Figure B.4C) and *ced-9ts* (Figure B.4D) strains. From these control experiments conducted in parallel to those in Chapter 2, we can conclude that the observed increase in *hsp-3* mRNA translational efficiency in the *ced-9ts* strain when compared to wild type must be attributed to an increased number of bound ribosomes.

Figure B.3

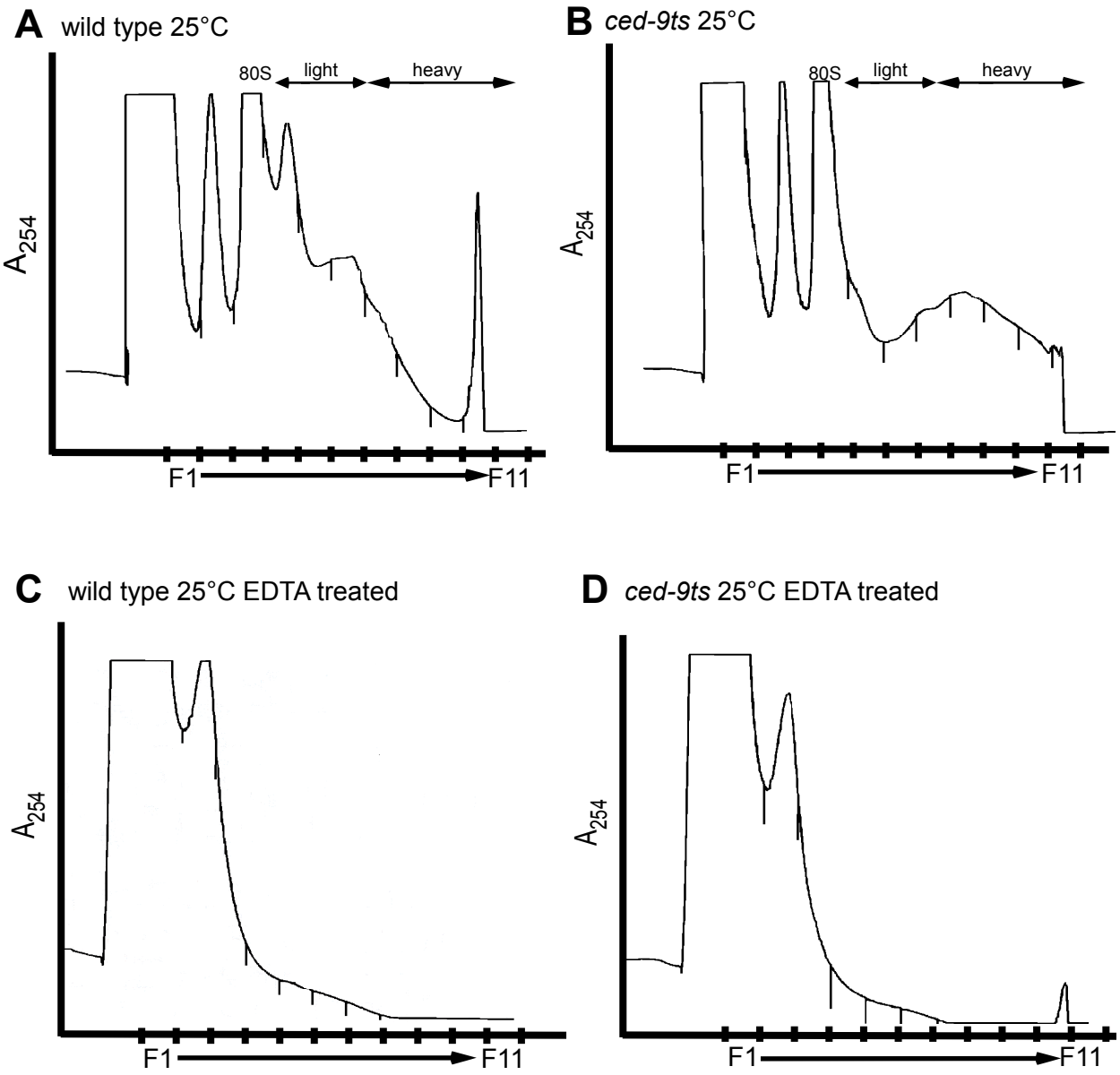
A wild type 25°C
80S
light
heavy
A254
F1
F11
B ced-9ts 25°C
80S
light
heavy
A254
F1
F11
C wild type 25°C EDTA treated
A254
F1
F11
D ced-9ts 25°C EDTA treated
A254
F1
F11

Figure B.3. EDTA is used to release ribosomes in order to verify that changes in gradient localization are due to changes in mRNA translational efficiency. Polysome profiles depicting the continuous density gradient fractionation of total RNA in wild type (A), *ced-9ts* (B) strains. To determine if the position of mRNAs in the gradient is due to bound ribosomes cycloheximide was removed from the gradients and EDTA was added to chelate magnesium ions in the wild type (C) and *ced-9ts* (D) strains. These gradients represent 1 of 2 biological replicates of wild type and *ced-9ts* strains.

***ced-4* mRNA is bound by other unidentified RNA binding proteins complicating interpretations of its translational efficiency.** EDTA treatment led to the transition of *gpd-3* mRNA from the heavy fractions of the gradient into the lighter fractions as ribosomes were dissociated. However, we did not observe a similar release of *ced-4* mRNA into the lighter gradient fractions after ribosome dissociation. Instead, in the wild type strain *ced-4* mRNA transitioned into the middle of the gradient (fraction 6) in the presence of EDTA, indicating that the mRNA was still bound by some other large mRNA binding protein or large structure (Figure B.4E). Interestingly, in the *ced-9ts* strain *ced-4* mRNA was retained in even heavier gradient fractions after release of ribosomes, fractions 9 through 11 (Figure B.4F). This indicates that the unknown factor that binds *ced-4* mRNA changes in the *ced-9ts* strain (Figure B.4G).

Increased temperature leads to changes in polyadenylation site usage of *act-1* mRNA. *act-1* mRNA was used a as control mRNA for RPAs to determine equal loading and RNA quality. A probe was designed that extended through the entire 3' UTR of *act-1* mRNA (Figure B.5A). RPAs were performed on RNA isolated from wild type worms grown at normal growth conditions (20˚C) and temperature stressed conditions (25˚C 25 hours) (Figure B.5B). It is important to note that this temperature treatment is not suffienct to induce strandard heat shock in *C. elegans.* During both growth conditions, there were two protected fragments of approximately 90 and 145 nts, indicative of two different polyadenylation sites. These sites shifted downstream by about 10 nucleotides during

Figure B.4

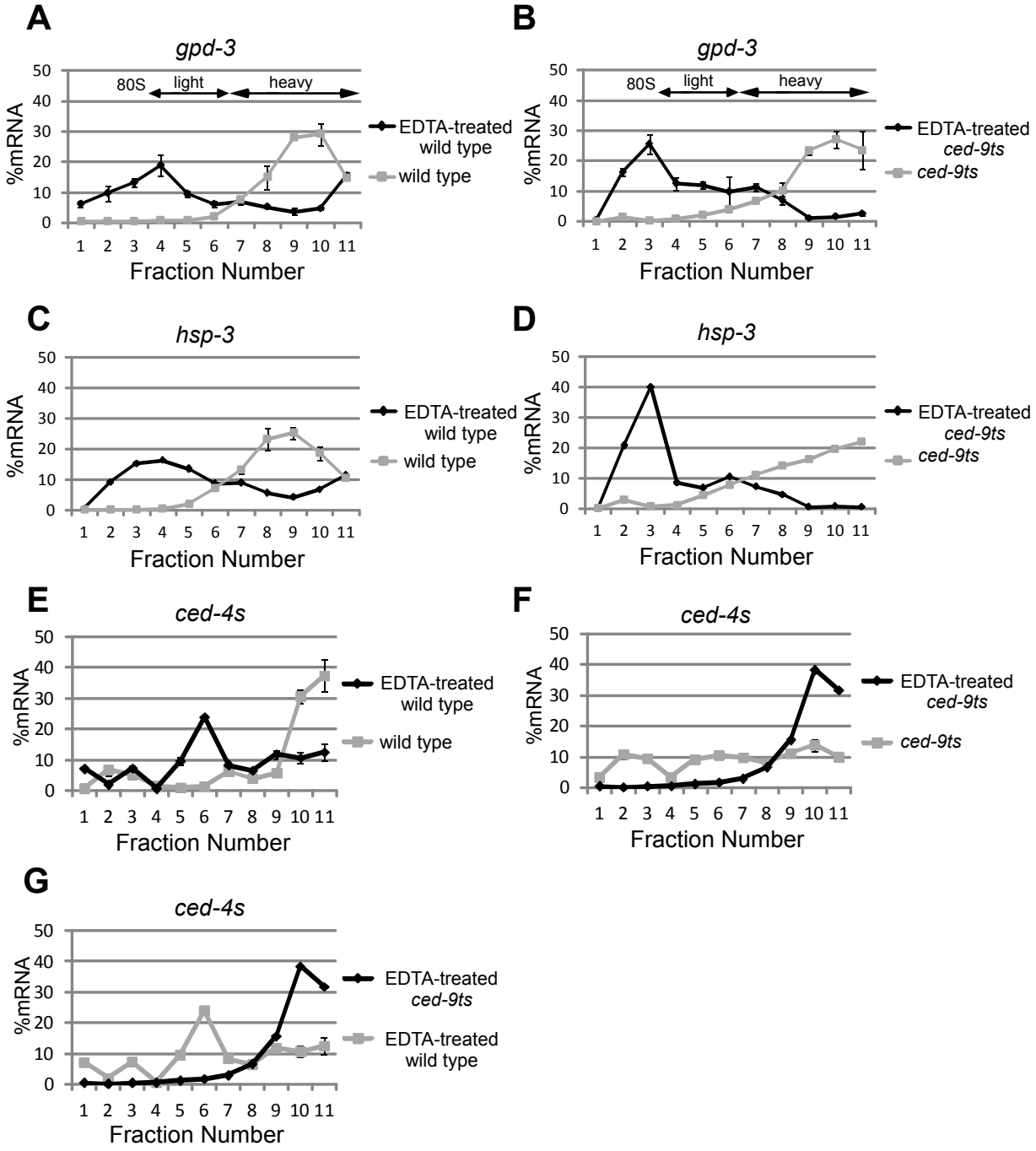
A
gpd-3
80S
light
heavy
%mRNA
Fraction Number
EDTA-treated wild type
wild type
B
gpd-3
80S
light
heavy
%mRNA
Fraction Number
EDTA-treated ced-9ts
ced-9ts
C
hsp-3
%mRNA
Fraction Number
EDTA-treated wild type
wild type
D
hsp-3
%mRNA
Fraction Number
EDTA-treated ced-9ts
ced-9ts
E
ced-4s
%mRNA
Fraction Number
EDTA-treated wild type
wild type
F
ced-4s
%mRNA
Fraction Number
EDTA-treated ced-9ts
ced-9ts
G
ced-4s
%mRNA
Fraction Number
EDTA-treated ced-9ts
EDTA-treated wild type

Figure B.4. *hsp-3* localization in the gradient is dependent on ribosome association, but interpretations of *ced-4* mRNA localization are more complicated. *hsp-3* mRNA sedimentation correlates bound ribosomes. Shifts in *gpd-3* position in the gradient after EDTA treatment are depicted in wild type (A) and *ced-9ts* (B) strains. The position of *hsp-3* also shifts in the gradient after EDTA treatment in the wild type (C) and *ced-9ts* (D) strains. *ced-4s* remains bound by heavy complexes after EDTA in the wild type (E) and *ced-9ts* (F) strains. The weight of the complex differs in the wild type and *ced-9ts* strains (G).

temperature stressed conditions. This shift suggests use of the downstream AU-rich cleavage site.

Discussion

Studies in Chapter 2 and 3 address changes in translation initaiton efficiency of mRNAs during apoptosis. This results in increased dependence on cap-independent translation as the cap-dependent translation initiation complex is inactivated (Contreras et al., 2011). To determine the specific mRNAs that can still be translated cap-independently we use sucrose gradient resolution of polyribosomal complexes. However, interpretations of these data can be difficult without proper controls to determine if shifts within the gradient are actually dependent on changes in bound ribosomes. In this study we ruled out other factors that may have resulted in false interpretations. Vastly increased target mRNA abundance, due to increased transcription or mRNA stability, may also increase the probability that mRNA is recruited to the ribosome by changes in competition rather than initiation potential. In our cap-independent, *ifg-1::mos,* and apoptotic strain, *ced-9ts,* we observed no dramatic change in the abundance of any of our target mRNAs. Thus, increased transcription or mRNA stability did not result in the increased translational efficiency of *hsp-3* and *ced-9* mRNA*.* On the same note, the decreased translational efficiency of *hif-1, hsp-4, ced-4* and *cep-1* mRNAs did not result from a decrease in RNA quantity leading to a decreased probability of ribosome association.

Sucrose gradients resolution of polyribosomes is based on weight (sedimention rate) of the entire translating complex. However, an mRNA's sedimentation may be increased by RBPs other than ribosomes, if they are sufficiently large (Filipenko et al.,

Figure B.5

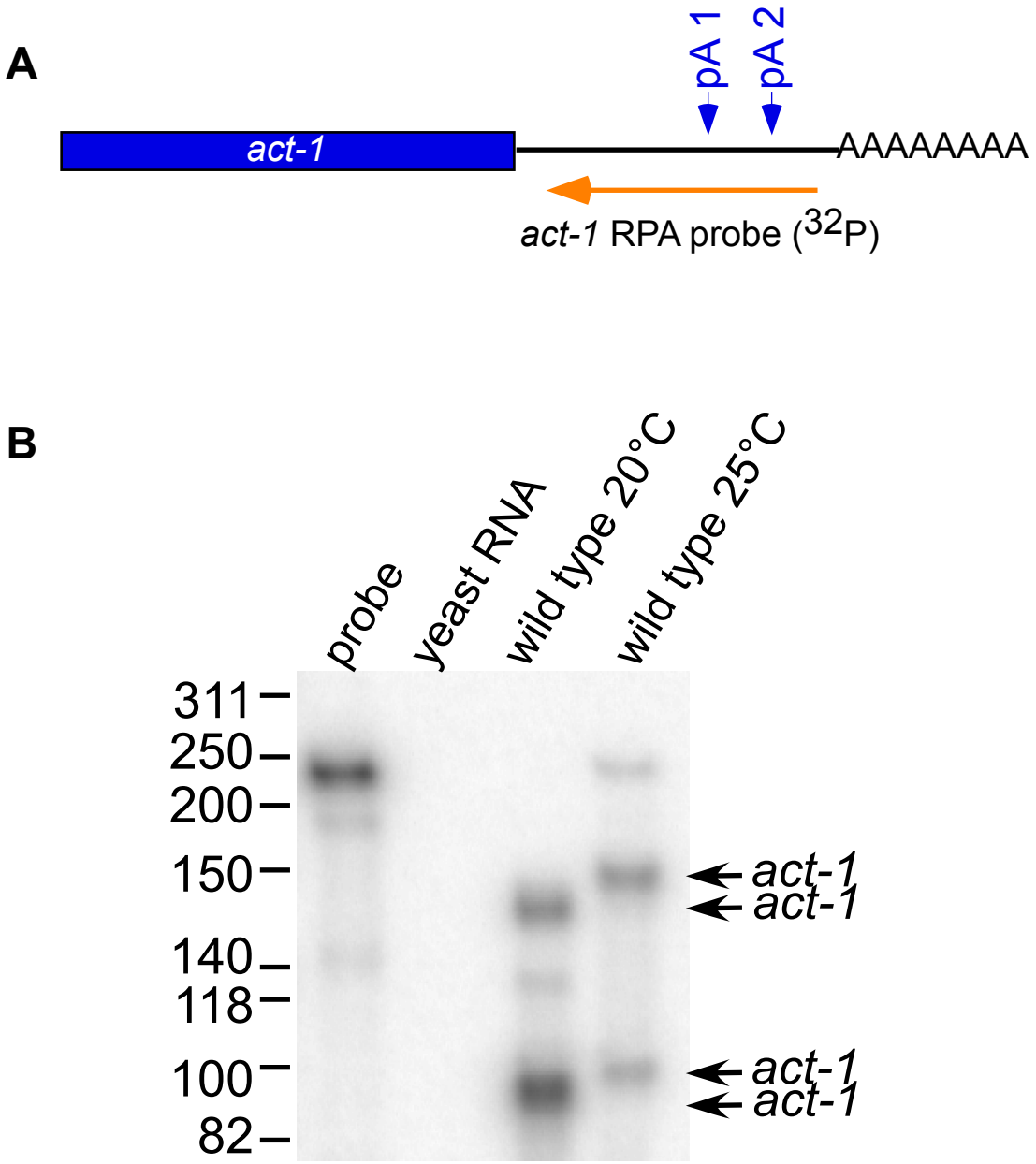
A
pA 1
pA 2
act-1
AAAAAAAA
act-1 RPA probe (32P)
B
probe
yeast RNA
wild type 20°C
wild type 25°C
311
250
200
150
140
118
100
82
act-1
act-1
act-1
act-1

Figure B.5. Polyadenylation site cleavage of *act-1* mRNA differs during temperature stressed conditions. (A) Schematic shows *act-1* RPA probe (orange arrow) coverage of *act-1* 3' UTR. Polyadenylation sites are indicated by blue arrows. (B) RPAs were performed using the *act-1* probe on wild type and wild type temperature stressed worms. 3′ UTR endpoints of *act-1* are indicated by the specified arrows.

2004). Thus, to attribute the shifts within the sucrose gradient solely to bound ribosomes we used EDTA to chelate magnesium and release the ribosomes. Thus, if the sedimentation position within the gradient was dependent on bound ribosomes, then the mRNA should no longer be found in the heavy regions of the gradient, but instead remain near the top where it was loaded. We confirmed that the sedimentation in *hsp-3* mRNA within the gradient resulted exclusively from bound ribosomes. Therefore, changes in its sedimenation upon apoptosis or IFG-1 p170 depletion must be due to more ribosome subunits bound. By contrast, the *ced-4* mRNA has decreased translational efficiency in the *ced-9ts* strain. However, this interpretation is complicated by the fact that other factors apparently bind *ced-4* mRNA leading to positional changes in the sucrose gradients. However, this effect does not affect the overall interpretation due to the fact that in the *ced-9ts* strain *ced-4* mRNA translational efficiency decreases despite the binding of factors that cause *ced-4* mRNA to sediment in the heavier fractions of the gradient when no ribosomes are bound. Although factors bind *ced-4* mRNA in the wild type strain as well, *ced-4* mRNA in this case is only maintained in the middle region of the gradient after magnesium chelation.

These experiments to optimize resolution, quantify mRNA representation and characterize ribosomal complexes allow us to confirm our results that *hsp-3* and *ced-9* mRNA are translated more efficiently. The findings also confirm the decreased translational efficiency of *hif-1, cep-1* and *ced-4* mRNAs. Thus, our methods to elucidate the interplay between cap-dependent and –independent translation during development represent a valid assessment of how this interplay results in selective mRNA translation and thus influences cell fate decisions.

APPENDIX C. DESIGN OF CAP-INDEPENDENT IFG-1 p130 AND CAP-DEPENDENT IFG-1 p170 OVEREXPRESSING STRAINS

Introduction

mRNAs have differing abilities to be initiated for translation via the cap-dependent and cap-independent mechanisms. Cap-independent mRNAs are often associated with stress response and apoptosis whereas cap-dependent mRNAs are associated with grow and cell cycle progression (Morrison, 2014; Rosenwald et al., 1993). Balance of the relative contribution of cap-dependent versus independent translation might enable cells to react to environmental queues and respond with protein expression patterns that allow them to adapt to a changing environment. *C. elegans* have two eIF4G homologues, IFG-1 p170 and IFG-1 p130 (Contreras et al., 2008). IFG-1 p170 is the cap-dependent eIF4G homologue and contains domains that associate with the eIF4E homologues, IFEs, and the PABP and thus actively recruits mRNA to the ribosome via recognition of the mRNA cap (Contreras et al., 2008). IFG-1 p130, on the other hand, is constitutively cap-independent and does not bind IFEs that allow for active cap-based recruitment of mRNA (Contreras et al., 2008). This study focuses on determining the entire mRNA subpopulations that may be translated cap-dependently and cap-independently by developing transgenic *C. elegans* strains that express a single IFG isoform, p130 or p170, in the absence of the other. Developing these transgenic lines additionally allows for the delineation of the developmental defects that would result from the loss of cap-dependent or cap-independent translation and the production of the proteins dependent on these processes.

Results

Flag-tagged *ifg-1* p170 and p130 *mos* plasmids were created for MosSCI transgenic development. *ifg-1* p170 and p130 were PCR amplified from the previously described pSK IFG-1 p170 and p130 plasmids (Appendix A) using primers with att sites allowing for gateway cloning. Note that *ifg-1* p170 and p130 sequences were fully spliced cDNAs preventing alternative splicing that might occur if the *ifg-1* gene sequences were used. The *ifg-1* sequences were also fused to a single Flag tagged sequence to allow for affinity chromatography, identification of recombinant protein and isolation of protein complexes. The isolation of protein complexes would allow us to identify the initiation factors and IRES trans-acting factors necessary for the initiation of cap-dependent or cap-independent translation. The amplified *ifg-1* p130 or p170 was then gateway cloned into a DONR vector (DONR221) using BP clonase (invitrogen). The resulting DONR gateway vector was then three-way gateway cloned using LR clonase into a Destination vector containing the *mos* transposon recombination sites (Figure C.1). Three-way gateway cloning allowed from the insertion of sequences flanking the 5' and 3' ends of the *ifg-1* sequence. The 5' sequence flanking sequence is the *pie-1* promoter that allows for germ line expression of the transgene. The *unc-54* 3' UTR sequence was the inserted 3' flanking sequence. This allowed for resulting transgenic *ifg-1* p170 or p130 to have an unregulated 3' UTR. Additionally, the Destination plasmids contained a *C. briggsae unc-119* rescue gene. Thus, by injecting into a *C. elegans* strain lacking *unc-119* that is unable to swim normally, we can detect worms expressing our destination plasmids by their ability to properly swim. The resulting destination plasmids for *ifg-1* p170 and *ifg-1* p130 were individually injected into an *unc-119* deletion strain (EG6703) containing the *mos* transposon at a known site in

Figure C.1

A

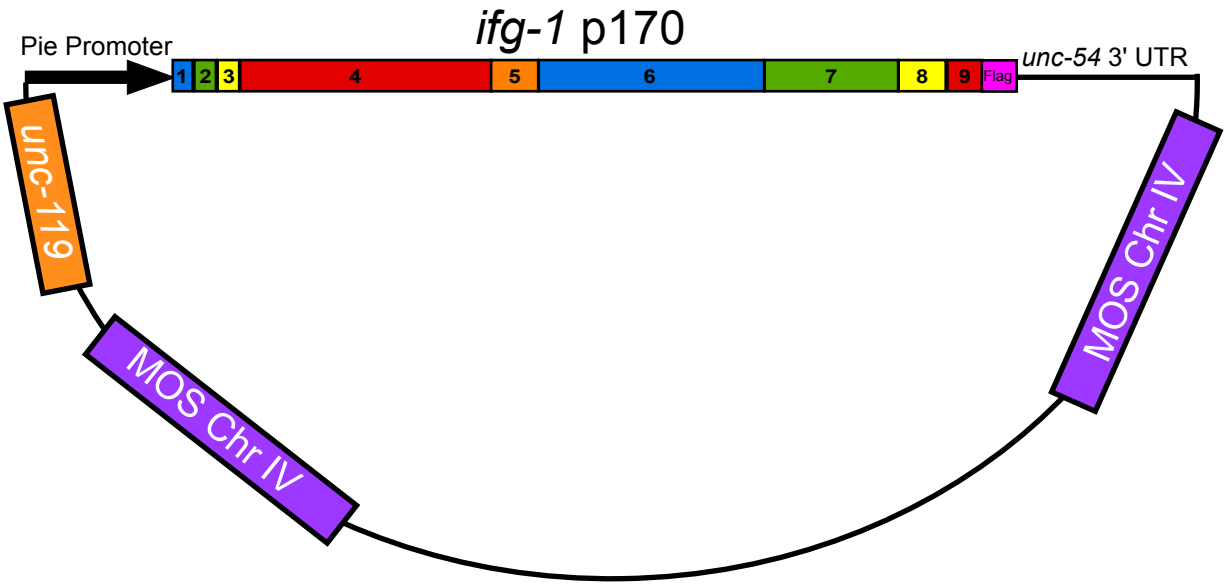
ifg-1 p170
Pie Promoter
1
2
3
4
5
6
7
8
9
Flag
unc-54 3' UTR
unc-119
MOS Chr IV
MOS Chr IV

B

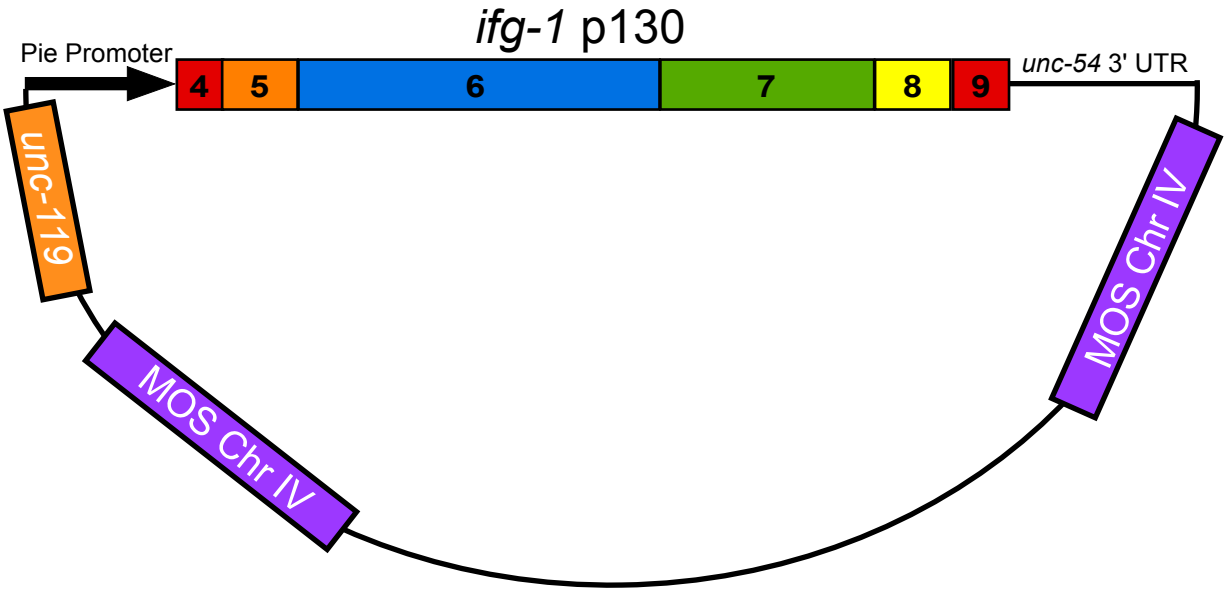
ifg-1 p130
Pie Promoter
4
5
6
7
8
9
unc-54 3' UTR
unc-119
MOS Chr IV
MOS Chr IV

Figure C.1. MosSCI plasmids for creation of IFG-1 p170 and p130 overexpressing transgenic strains. (A) MosSCI plasmid designed to create *ifg-1* p170 overexpressing strains. Mos recombination sites are indicated in purple. *C. briggase unc-119* gene rescue to indicate extrachromosomal arrays or integration events with the MosSCI IFG-1 p170 plasmid (orange). Bold arrow indicates the *pie-1* promoter to allow for germ line expression of IFG-1 p170. 3' UTR contained in this plasmid is *unc-54.* (B) MosSCI plasmid designed to create *ifg-1* p130 overexpressing strains.

chromosome IV. The *mos* transposon allows for a single-site insertion of the *ifg-1* p170 or p130 flag-tagged cDNA into the genome. A plasmid containing mos transposase was co-injected allowing for the mobilization of the *ifg-1* p170 or p130 cDNA from the injected plasmid to chromosome IV. Three other plasmids (pGH8, pCFJ90, pCFJ104) with mCherry fused to proteins expressed in the neurons, body wall or pharynx were co-injected as well. These plasmids provided a negative selection against isolation of transgenic strains containing only an extrachromosomal array expressing IFG-1 p170 or p130 as opposed to a chromosome-integrated transgene. Injections to date have resulted in extrachromosomal expression of all co-injection plasmids. However, we have thus far been unable to identify worms expressing integrated IFG-1 p170 or p130 or to demonstrate stable rescue for their *unc-119* deficiency. Other labs have reported that contaminating RNases in plasmid preparations of injection plasmids can result in inefficient transgenic line creation (Maduro, 2011). Thus, we prepared plasmid preparations without the use of RNase A. While this improved the ratio of worms expressing the co-injection plasmids, it did not result in the creation of transgenic flag tagged IFG-1 p170 or p130 strains.

Discussion

Transgenic line creation, particularly involving germ line expression, can often be problematic. Although recent MosSCI methods can result in specific integration events, initially injections must first lead to extrachromosomal arrays, which can often be toxic due to high transgene expression. Other techniques can be used to generate transgenic strains such as micropartical gene bombardments. Gene bombardments use DNA coated gold

particles that are projected into the gonad. Higher numbers of integrated strains often occur due to the DNA entering the nucleus of germ cells (Praitis et al., 2001).

APPENDIX D. IRES-MEDIATED CAP-INDEPENDENT *hsp-3* (BiP) mRNA TRANSLATION DURING STRESS

Introduction

Cap-independent translation can be enhanced due to a number of stressors in mammalian cell culture. Previous studies have illuminated a variety of stressors including heat shock, cold shock, apoptosis, DNA damage and hypoxia that have resulted in the enhanced cap-independent translation of target mRNAs (reviewed in (Spriggs et al., 2010)). One such cap-independent mRNA is BiP (Thoma et al., 2004; Yang and Sarnow, 1997). BiP mRNA encodes a chaperone protein involved in heat shock recovery. BiP has been shown to translate cap-independently via an IRES during heat shock (Cho et al., 2007). We desired to determine if the *C. elegans* homologue, *hsp-3* mRNA, is also translated cap-independently via an IRES sequence at the 5' end. Li, et al. identified an IRES in the 5' UTR of extended transcripts of the *C. elegans hsp-3* mRNA (Li and Wang, 2012). However, when Li et al. designed their constructs to test this putative IRES in bicistronic reporters, their putative IRES sequence contained an intron sequence that is spliced out of the extended *hsp-3* mRNA variant, based on all identified catalogued *hsp-3* ESTs (WormBase, 2007). This intron contains enhancer elements and a TATA box that appear to be capable of promoting transcription of shorter *hsp-3* variants lacking the purported IRES (Heschl and Baillie, 1989, 1990). Thus, we sought to construct a bicistronic reporter construct with a fully spliced putative *hsp-3* IRES leader to confirm or refute IRES-driven HSP-3 protein expression. Our previous studies have demonstrated that *hsp-3* mRNA is translated cap-independently. However, this translation is apparently not dependent on an IRES sequence

(Morrison, 2014). Thus, *hsp-3* mRNA could translate cap-independently, but not via the purported IRES. Previous studies have demonstrated that heat shock mRNAs may be translated cap-independently in the absence of an IRES in stressed mammalian and plant cells, and in virus infected cells (Dinkova et al., 2005; Joshi-Barve et al., 1992; Rhoads and Lamphear, 1995; Schneider, 1995).

The *C. elegans* gonad provides the ideal animal model system for the *in vivo* study of cap-independent translation IRES-mediated translation during stress using this *hsp-3* bicistronic construct containing dual fluorescent (mCherry and GFP) reporters. As the germ cells enter meiosis, their chromosomes are condensed resulting in suppressed transcription. Therefore, changes in protein expression, leading to oocyte maturation or apoptosis result from the regulation of translation of stored maternal mRNAs. Using this bicistronic construct we can study the changes in the ratio of cap-dependent and –independent translation in different regions of the gonad simply by comparing relative red versus green fluorescence. Specifically, we will be able to observe whether there is an increase in *hsp-3* IRES-driven mRNA translation in the apoptotic region of the gonad, where IFG-1 p170 caspase cleavage is proposed to result in enhanced cap-independent translation. Additionally we will be able to more generally determine *hsp-3* IRES-driven mRNA translation in the gonad in response to mild or prolonged heat shock (Contreras et al., 2008). It is important to note that single germ cell resolution fluorescence microscopy will allow the assay of *hsp-3* IRES utilization in every individual cell of every stage of development in the gonad. Due to the semitransparency of *C. elegans* this microscopy may be performed on live worms.

In this study we were able to design a more authentic *hsp-3* mRNA bicistronic construct to test for IRES-mediated translation and to optimize its expression under stress conditions. The plasmids and preliminary work here provides the basis for future studies in which to elucidate the validity of an *hsp-3* IRES and to determine the cap-independent conditions that promote the enhanced translational efficiency of *hsp-3* mRNA via this purported IRES.

Results

Construction of Bicistronic *hsp-3* Plasmids and MosSCI. The *hsp-3* 5' UTR region sequence, from the single known authentic extended *hsp-3* variant identified using ESTs, was PCR amplified directly from the EST (WormBase, 2007). By amplifying directly from the EST, we were able to exclude the intron present in the 5' UTR that had been included in previous experiments done by other labs trying to determine whether the *hsp-3* 5' UTR had IRES activity (Li and Wang, 2012). The amplified sequence included the partial sequence (52 bp) of exon 1 and the 317 bp *hsp-3* 5' UTR. Overlapping PCR amplification resulted in 3' fusion GFP gene sequence (from Pmyo3::RFP-24ES(285 bp)-GFP::let858.3) and 5' fusion of mCherry cDNA sequence (from pCRII mcherry) to *hsp-3* 5' UTR. This amplification effectively created a bicistronic *hsp-3* construct. The *mcherry::hsp-3::gfp* fused construct was then PCR amplified using primers with att sites allowing for gateway cloning into a DONR (DONR221) and then Destination vector ((pDESTR4-R3(cxTi10816, IV)) (as previously described (Appendix C)). The final destination vector included *mos* recombination sites flanking the transgene of interest, the *pie-1* promoter (allowing for germ line expression) and the *unc-54* 3' UTR (preventing transgene expression regulation

via the 3' UTR) (Figure D.1A-B). The same procedure was followed to create a control bicistronic plasmid with *Hemonchus contortus* 24-kDa excretory/secretory protein (24ES; accession no. U64793.1, GenBank) sequence instead of the *hsp-3* 5' UTR. The resulting *hsp-3* and control bicistronic Destination plasmids also contained a *C. briggsae unc-119* rescue gene. Mutation of *unc-119* results in worms that are unable to swim normally. By injecting into the *unc-119* deficient strain we detected worms swimming normally and thus expressing our destination plasmids. The bicistronic Destination plasmids were individually injected into an *unc-119* mutant strain (EG6703) containing the *mos* transposon at a known site in chromosome IV. The *mos* transposon allows for a single-site insertion on chromosome IV of the bicistronic plasmids. Co-injection plasmids allowed for the mobilization of the mos transposon (pCFJ601) and negative selection against extrachromosomal array instead of integrated expression (pCFJ90, pCFJ104, pGH8). We identified worms rescued for *unc-119* (swimming worms) and expressing the negative selection plasmids, indicating that they received the *mos* transgenic plasmids in an extrachromosomal array. However, *unc-119* expression was soon lost and rescue was not found in subsequent progeny. This could result from a lack of transgene integration in germ line cells. However, high levels of toxic genes in extrachromosomal arrays might also result in worm death and an inability to produce progeny. Thus, we injected lower concentrations of transgenic plasmids (Frokjaer-Jensen et al., 2012). This resulted in an increased number of swimming worms expressing the co-injection plasmids, but did not result in stable transgenic integration or rescued progeny. Additonally, as the result of other labs reporting contaminating RNases in plasmid preparations of injection plasmids resulting in inefficient transgenic line creation we prepared plasmid preparation without

Figure D.1

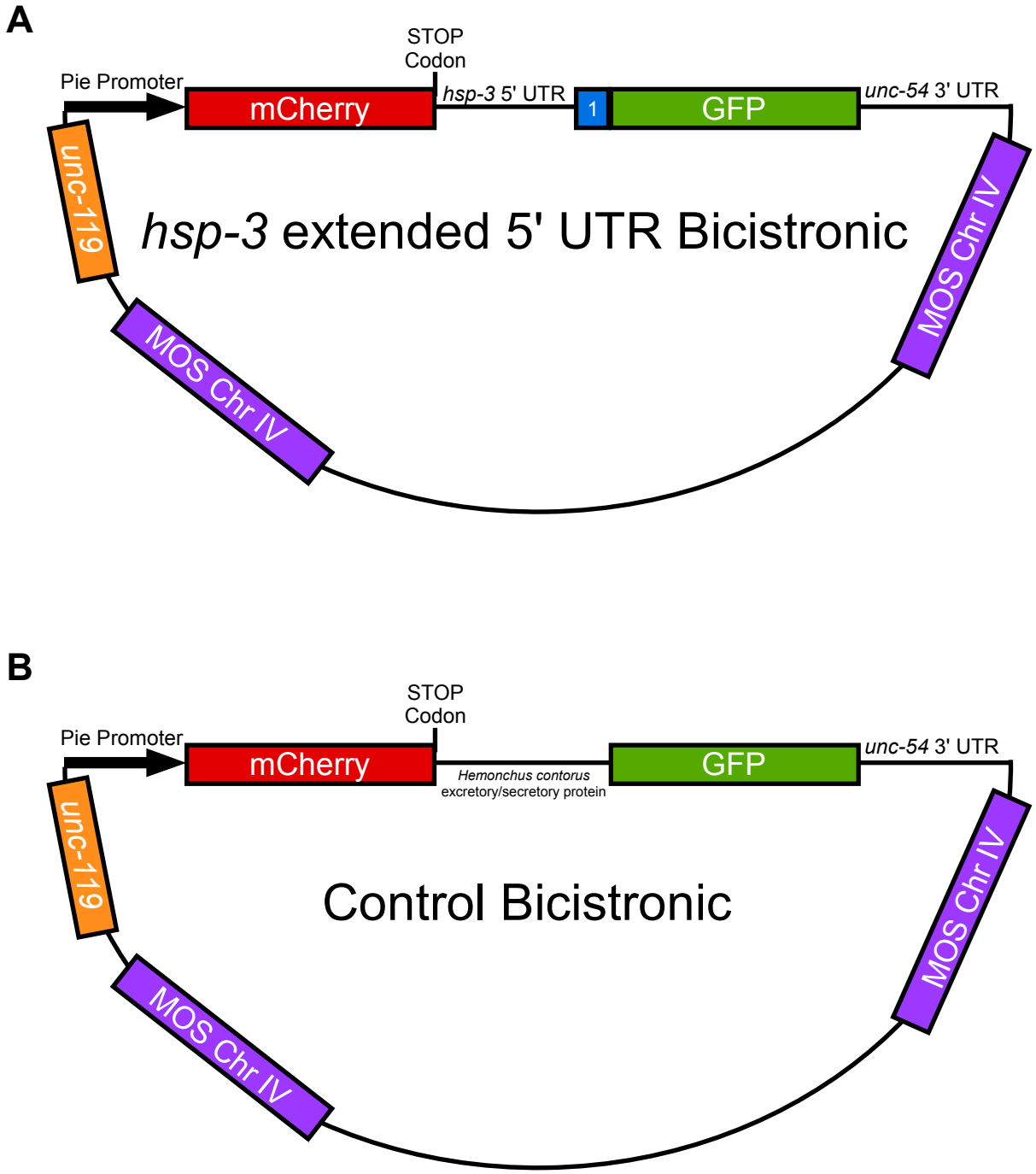
A
STOP
Codon
Pie Promoter
mCherry
hsp-3 5' UTR
1
GFP
unc-54 3' UTR
unc-119
hsp-3 extended 5' UTR Bicistronic
MOS Chr IV
MOS Chr IV
B
STOP
Codon
Pie Promoter
mCherry
Hemonchus contorus
excretory/secretory protein
GFP
unc-54 3' UTR
unc-119
Control Bicistronic
MOS Chr IV
MOS Chr IV

Figure D.1. MosSCI plasmids for creation of *hsp-3* and control bicistronic transgenic strains. (A) MosSCI plasmid designed to create *mcherry::hsp-3::gfp* transgenic strain. Mos recombination sites are indicated in purple. *C. briggsae unc-119* gene rescue to indicate extrachromosomal arrays or integration events with the MosSCI *mcherry::hsp-3::gfp* plasmid (orange). Bold arrow indicates the *pie-1* promoter to allow for germ line expression of *mcherry::hsp-3::gfp*. The *mcherry* coding region does not contain any introns and is followed by a stop codon. The stop codon is followed by the *hsp-3* 5' UTR and partial exon 1 fused to the GFP coding region with introns. 3' UTR contained in this plasmid is *unc-54.* (B) MosSCI plasmid designed to create *mcherry::control::gfp* transgenic strains. The plasmid is the same as above except it contains the *Hemonchus contours* excretory/secretory protein sequence, which has no IRES activity, instead of the proposed *hsp-3* IRES sequence.

the use of RNase A (Maduro, 2011). This also improved the ratio of worms expressing the co-injection plasmids, but also did not result in the creation of transgenic strains.

Optimization of Proposed Apoptotic Cap-Independent Conditions. We have previously demonstrated that enhanced cap-independent translation of specific mRNAs results from a decreased proportion of the cap-dependent IFG-1 p170 isoform in comparison to the cap-independent p130 isoform (Morrison, 2014). These observation were made in the *ced-9ts* and *ifg-1::mos* transgenic strains. In these strains there is a reduction in full-length IFG-1 p170 expression due to a splicing mediated *ifg-1* mRNA deficiency or *ced-9ts*-mediated IFG-1 protein cleavage. Additionally, our lab has previously demonstrated that RNAi targeted against IFG-1 p170 results in its depletion while not reducing IFG-1 p130 expression (Contreras et al., 2008). Here we wished to demonstrate that knockdown of CED-9 expression using targeted *ced-9* RNAi is sufficient to induce a similar level of apoptosis.

In wild type, CED-1::GFP expressing, worms *ced-9* RNAi (Figure D.2G-I) induced a visible increase in the number of germ cell corpses within the *C. elegans* gonad in comparison to control RNAi fed worms (Figure D.2A-C). CED-1::GFP is expressed by gonad sheath cells that engulf apoptosing germ cells (Zhou et al., 2001). Thus, CED-1::GFP decoration of apoptotic germ cells allows live visualization of the apoptotic process. The level of apoptosis was visibly comparable to the number of germ cell corpses observed after the knockdown of IFG-1 p170 (Figure D.2D-F). Knockdown of CED-9 did not result in morphological changes in the gonad that had been previously observed upon IFG-1 p170 knockdown, suggesting there were less detrimental effects (Contreras et al., 2008). Quantification of the corpses shows that there is a significant increase in germ cell corpses

Figure D.2

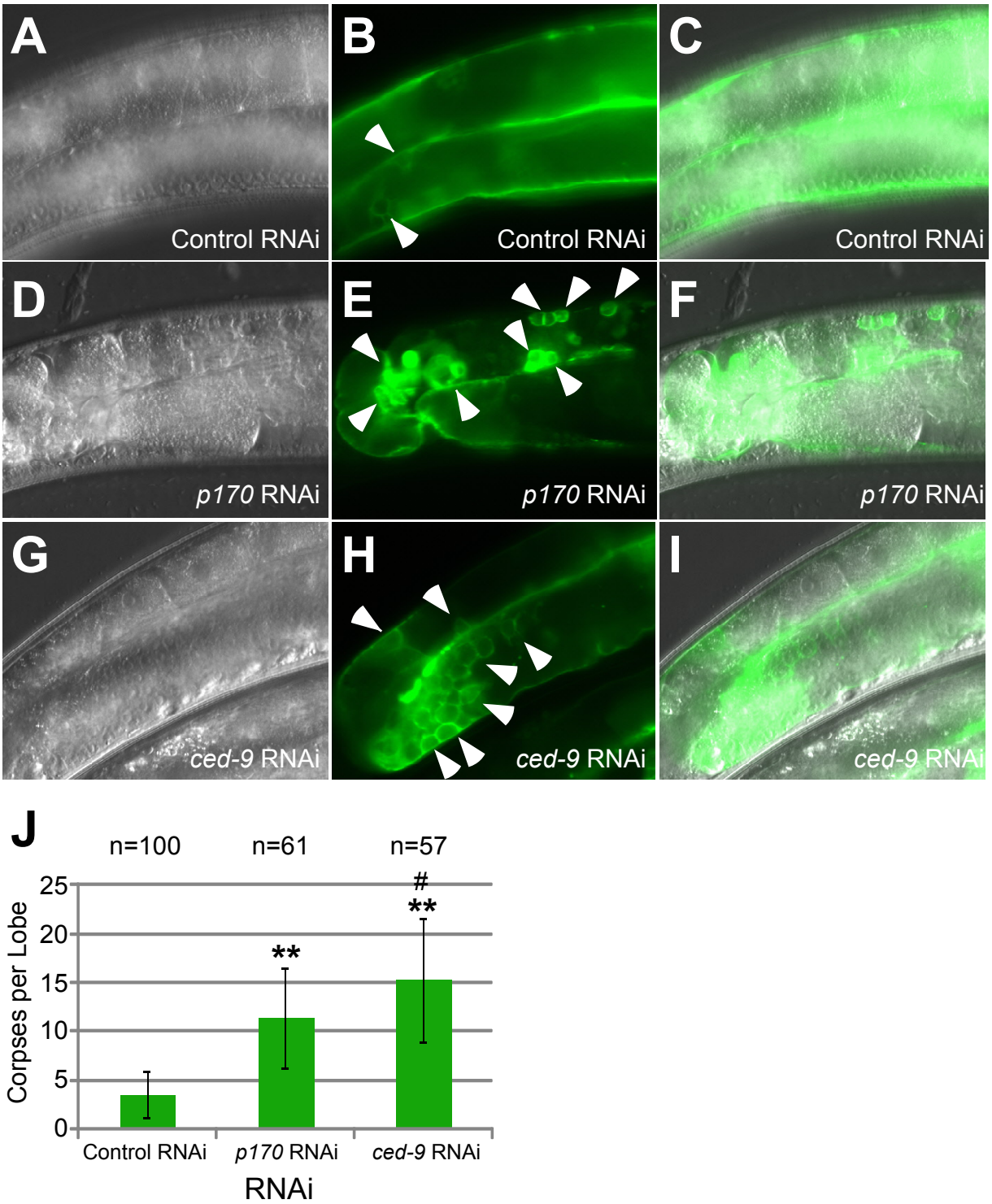
A
Control RNAi
B
Control RNAi
C
Control RNAi
D
p170 RNAi
E
p170 RNAi
F
p170 RNAi
G
ced-9 RNAi
H
ced-9 RNAi
I
ced-9 RNAi
J
n=100
n=61
n=57
#
**
**
Corpses per Lobe
25
20
15
10
5
0
Control RNAi
p170 RNAi
ced-9 RNAi
RNAi

Figure D.2. *ced-9* RNAi induces germ cell apoptosis. Fluorescence, DIC and overlayed images of wild type, CED-1::GFP, expressing worms feed control (A-C), *ifg-1 p170* (D-F) and *ced-9* (G-I) RNAi. DIC images confirm normal growth and differentiation of oocytes within the gonads of RNAi feed worms. (J) A graph depicting counts of CED-1::GFP decorated corpses in worms feed control, *ifg-1 p170* and *ced-9* RNAi. ** $p<0.001$ *ifg-1 p170* and *ced-9* RNAi significantly different from control RNAi, # $p<0.018$ *ifg-1 p170* significantly different from *ced-9* RNAi strain.

due to the knockdown of CED-9 (Figure D.2J). CED-9 knockdown also resulted in a significant increase in corpses in comparison to the knockdown of IFG-1 p170 demonstrating that direct perturbation of the apoptotic pathway results in the largest apoptotic induction. This apoptotic induction due to the knockdown of CED-9 was dependent on caspase CED-3 activation (Figure D.3). There was no observed increased in apoptotic corpses due to CED-9 knockdown in the *ced-3* deletion strain in comparison to the wild type strain (Figure D.3A-B,D) or *ced-3* deletion strain fed control RNAi (Figure D.3C-D). Quantification of corpses indicated that there was no significant increase in germ cell corpses in the *ced-3* deletion strain due to knockdown of CED-9 protein (Figure D.3E).

Optimization of heat shock conditions. Heat shock has been previously shown to result in cap-independent IRES-mediated translation of mammalian BiP mRNA (Cho et al., 2007). Thus, we wanted to investigate whether we observed a similar increase in the *C. elegans hsp-3* (BiP) IRES-mediated translation during heat shock conditions. There are no previous reports in *C. elegans* whether heat shock results in the induction of apoptosis within the gonad. Therefore we submitted wild type worms to a 6 hour authentic heat shock at 32˚C and looked for visible increases in germ cell corpses (Figure D.4D-F) in comparison to normal growth conditions (Figure D.4A-C). As a positive control for germ cell apoptosis, a strain with high levels of constitutive apoptosis, *ced-9ts,* was monitored (Figure D.4G-I). Remarkedly, there was no visibly apparent increase in germ cell apoptosis due to heat shock. Quantification of corpses revealed that there was no significant change in germ cell corpses due to heat shock (Figure D.4J).

Figure D.3

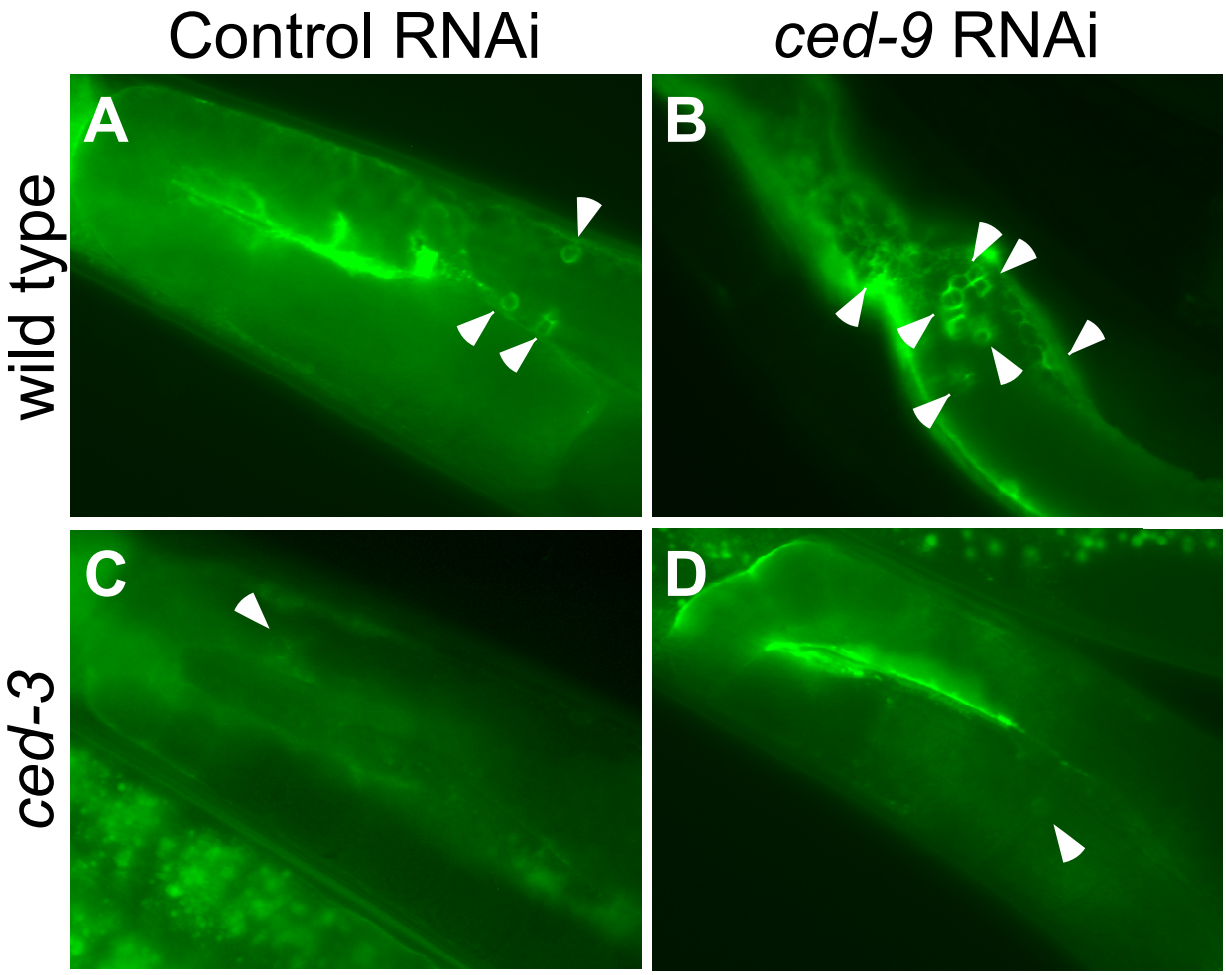
Control RNAi
ced-9 RNAi
wild type
ced-3
A
B
C
D

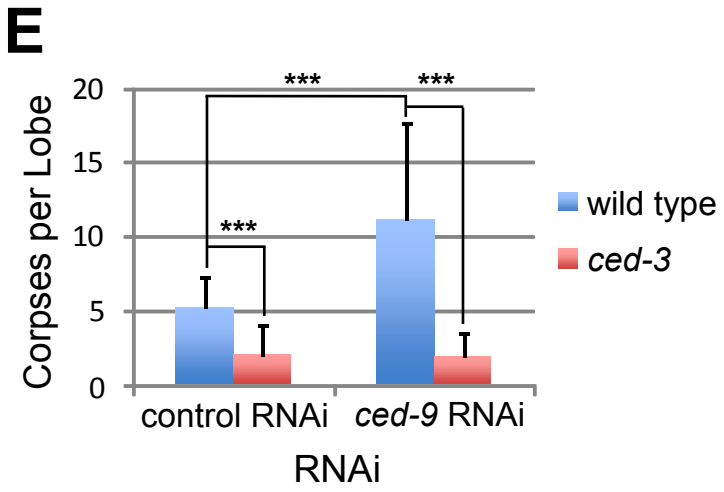
E
Corpses per Lobe
20
15
10
5
0
***
***
***
control RNAi
ced-9 RNAi
RNAi
wild type
ced-3

Figure D.3. Induction of germ cell apoptosis by *ced-9* RNAi is dependent on CED-3 expression. Fluorescent image of CED-1::gfp expressing illuminated corpses in wild type worms fed control (A) and *ced-9* (B) RNAi compared to *ced-3* worms fed control (C) and *ced-9* (D) RNAi. (E) Graph depicting corpse counts per lobe of the gonad in wild type worms fed control and *ced-9* RNAi compared to *ced-3* worms fed control and *ced-9* RNAi. *** indicate p=0.0001.

Discussion

Creation of transgenic lines, particularly involving germ line expression, often can be problematic due to toxicity resulting from high expression of extrachromosomal arrays. Transgenic expression of genes in such arrays or multicopy insertions is also often silenced. Interestingly, even the creation of MosSCI transgenic lines has elucidated a process referred to as RNA-induced epigenetic silencing, in which there is a silencing of transgenes (RNA*e*) (Lee et al., 2012; Shirayama et al., 2012). piRNAs are able to recognize nonself RNAs leading to their active and heritable silencing (Lee et al., 2012; Shirayama et al., 2012; Stower, 2012). GFP and other foreign genes can lead to targeted silencing via targeted piRNAs (Lee et al., 2012; Shirayama et al., 2012; Stower, 2012). This silencing becomes more prevalent when foreign genes are fused to the 5' end of the transgene injected (Lee et al., 2012; Shirayama et al., 2012; Stower, 2012). For example, when *gfp* was fused to the 5' end of *cdk-1* 0% of transgenes were expressed. *gfp* fused to the 3' end of *cdk-1* resulted in 100% of worms with germ line expression (Lee et al., 2012; Shirayama et al., 2012). In our experiments, we used mcherry fused to the 5' end of our constructs. Potentially this may result in the silencing of our transgene, which was heritable, thus resulting in no observed swimming offspring. Other techniques can be used to generate transgenic strains such as gene microparticle bombardments. Gene bombardments use DNA coated gold particles that are projected into the gonad. Higher numbers of integrated strains often occur due to the DNA entering the nucleus of the germ cells (Praitis et al., 2001). RNases present in plasmid preparations of injection plasmids can result in inefficient transgenic line creation (Maduro, 2011). To prevent the resulting decrease in transgenic animals resulting from injections with RNase contamination, we prepared

Figure D.4

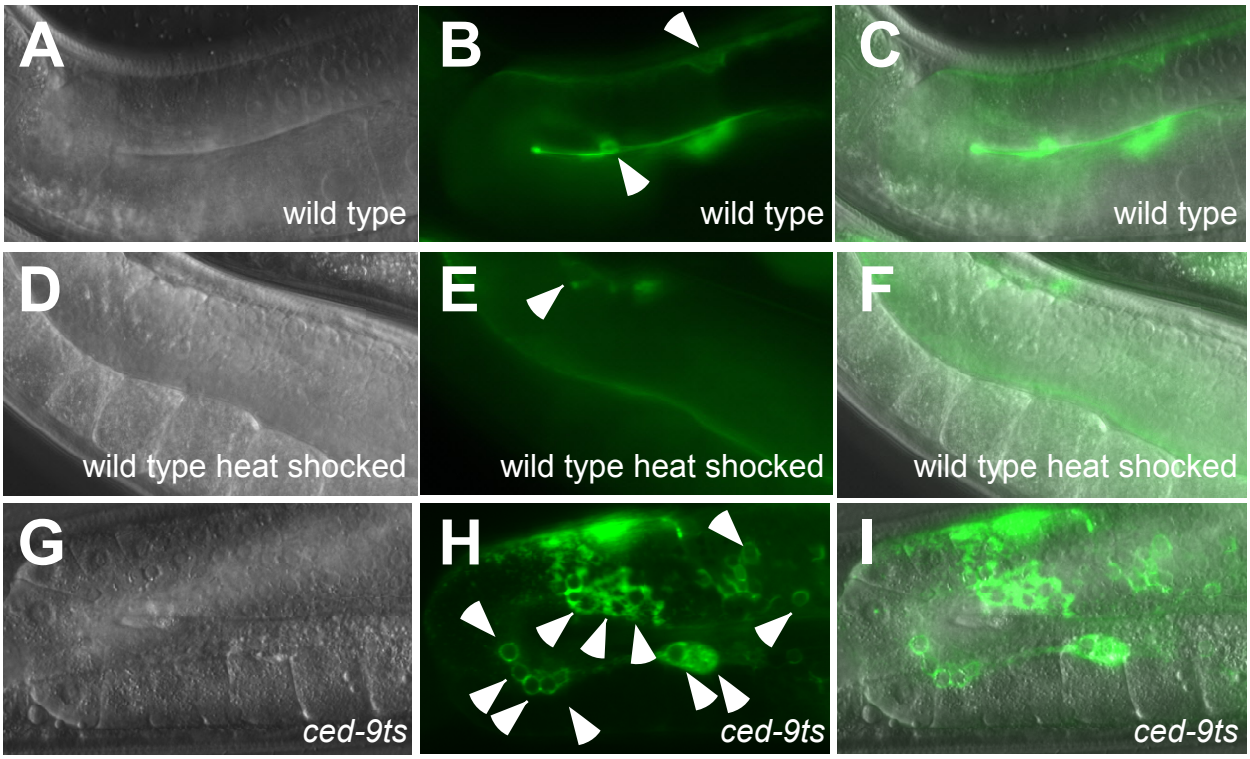
A
wild type
B
wild type
C
wild type
D
wild type heat shocked
E
wild type heat shocked
F
wild type heat shocked
G
ced-9ts
H
ced-9ts
I
ced-9ts

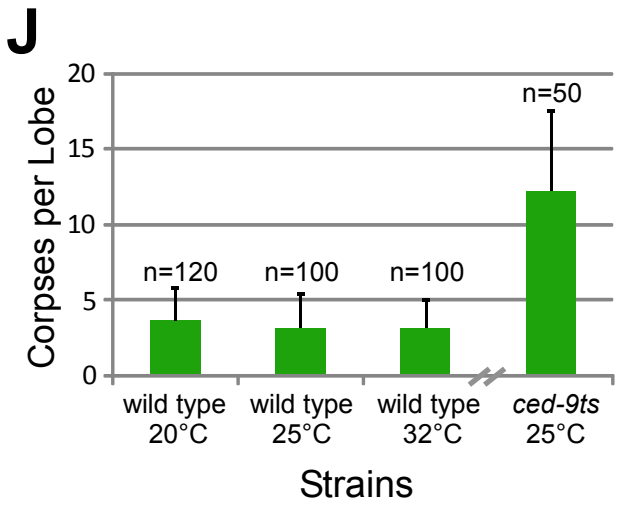
J
Corpses per Lobe
20
15
10
5
0
n=120
n=100
n=100
n=50
wild type 20°C
wild type 25°C
wild type 32°C
ced-9ts 25°C
Strains

Figure D.4. Heat shock does not induce germ cell apoptosis in *C. elegans*. Fluorescence, DIC and overlayed images of wild type, CED-1::GFP, expressing worms (A-C) and heat shocked (D-F) worms. DIC images confirm normal growth and differentiation of oocytes within the gonads of RNAi feed worms. (G-I) Fluorescence, DIC and overlayed images of *ced-9ts,* CED-1::GFP, expressing worms included as a comparison to illustrate a gonad full of apoptotic corpses. (J) A graph depicting counts of CED-1::GFP decorated corpses in wild type worms, wild type temperature stressed worms (25˚C) and wild type heat shocked worms (32˚C). *ced-9ts* strain corpse counts were lobe from a different experiment included to indicate the number of corpses expected per lobe of the gonad during the induction of apoptosis.

plasmid preparations without the use of RNase A. These plasmid preparations lead to higher success rates of co-injection plasmid expression, but did not result in the creation of transgenic lines. We confirmed *ced-9* RNAi was sufficient to induced apoptosis through CED-3 activation and thus may be used to observe changes in bicistronic activity during apoptosis. While such useful transgenic worm strains have so far eluded us, current attempts and ancillary optimizations described here have provided the basis for future studies once successful creation of transgenic bicistronic lines are achieved.

APPENDIX E: GENOMIC APPROACH TO mRNA TRANSLATION BY RNA-SEQ ANALYSIS OF RESOLVED POLYSOMES

Introduction

We have previously demonstrated the importance of cap-independent initiation to the enhanced translation of stress and apoptosis-related *hsp-3* (BiP) and *ced-9* (Bcl-2) mRNAs. However, stress and apoptosis are only two examples of the importance of different mechanisms of translation initiation to cell fate decisions. Additional work in our lab has highlighted the importance of alternative modes of translation initiation to oocyte and sperm development (Contreras et al., 2008; Henderson et al., 2009; Morrison, 2014). In wild type worms there is a linear progression of germ cells from mitosis through meiosis in the *C. elegans* gonad producing fully grown oocytes. However, the loss of most late oocytes and proximal germ line deterioration after IFG-1 p170 depletion suggests an additional essential role for cap-dependent translation in germ line oocyte development (Contreras et al., 2008; Morrison, 2014). Furthermore, depletion of cap binding *C. elegans* eIF4E isoform, IFE-1, demonstrates IFE-1 is essential for the efficient cap-dependent translation of many germ line development and/or maturation mRNAs (Henderson et al., 2009). mRNAs, such as *oma-1* (oocyte maturation defective), *mex-1* (muscle excess), *pos-1* (posterior segregation), *pal-1* (posterior alae in males), *glp-1* (abnormal germ line proliferation), *gld-1* (defective in germ line development) and *vab-1* (variable abnormal morphology) are no longer translated efficiently in the absence of IFE-1 (personal communication Andrew Friday) (Henderson et al., 2009). These examples highlight the importance of cap-dependent translation in the additional cell fate decision of germ line development.

Our findings also suggest that cap-independent initiation differs in the natively differentiating *C. elegans* germ line in comparison to cultured mammalian cells undergoing stress (Morrison, 2014). Our studies highlighted that *cep-1* (p53), *ced-4* (Apaf-1) and *hif-1* (Hif-1) mRNAs were unable to translate cap-independently during germ cell apoptosis or enhanced cap-independent conditions (Morrison, 2014). Such observations led us to question what were the identities of all mRNAs whose translation is either markedly cap-dependent or –independent and which of these mRNAs are essential for natively differentiating germ line development. In the process of identifying such mRNAs, we may elucidate additional key biological differences from stressed, cultured mammalian cells.

Previous experiments in other labs have highlighted the significance of assaying cap-independent translation on a global level (Johannes et al., 1999). In the Sarnow lab, knockdown of cap-dependent translation was assayed by viral infection in which eIF4G isoforms were cleaved thereby removing their cap-binding domains (Johannes et al., 1999). Microarray analysis was then performed on polysomal fractions of sucrose gradient fractionation experiments to determine mRNAs that were still associated with polyribosomes after eIF4G depletion (Johannes et al., 1999). They were able to demonstrate Pim-1 and Cyr61 mRNAs were translated more efficiently during viral infection (Johannes et al., 1999). Furthermore, bicistronic reporters demonstrated that these mRNAs were translated via IRES sequences (Johannes et al., 1999). Overall, their data illustrates the ability to detect changes in translational efficiency on a global level. In this study we aimed at determining similar global changes in translation initiation during cap-independent conditions. This study develops a methodology to interpret those changes in translation initiation using RNA-seq as a quantification and gene identification tool.

Results

In this study, we intended to focus on determining the entire populations of mRNAs in *C. elegans* that are either highly cap-dependent or highly cap-independent in their translational ability. We intended to use the *ifg-1::mos* strain expressing a *ced-1::gfp* transgene (KX54) to monitor germ cell apoptotic events while simultaneously observing changes in the translational efficiency of target mRNAs (Morrison, 2014). With a temperature sensitive *ifg-1* splicing defect, *ifg-1::mos* worms have decreased p170-driven cap-dependent and increased p130-driven cap-independent translation relative to the wild type CED-1::GFP expressing strain (MD701) (Morrison, 2014). Thus, the approach was to assess translational efficiency of *ifg-1::mos* and wild type *C. elegans* mRNAs using RNA-seq analysis of pooled RNAs from the polysomal and nonpolysomal regions of sucrose gradients. However, in growing the large mass of worms for preparation from polysomes, the wild type strain was inadvertently substituted for the *ifg-1::mos* (Figure E.1). Thus, instead of comparing translational efficiencies of wild type and *ifg-1::mos* worms, we developed a method for interpreting these proposed changes in translational efficiency in a transcriptome-wide manner using RNA-seq as our quantification and gene identification tool. By comparing wild type (WT A) versus wild type (WT B) in triplicates we were able to optimize data analysis for future experiments in which we would compare wild type versus experimental conditions. Furthermore, we identified key points where additional statistical rigor is required to exclude biological variation within the wild type strain itself.

Figure E.1

A

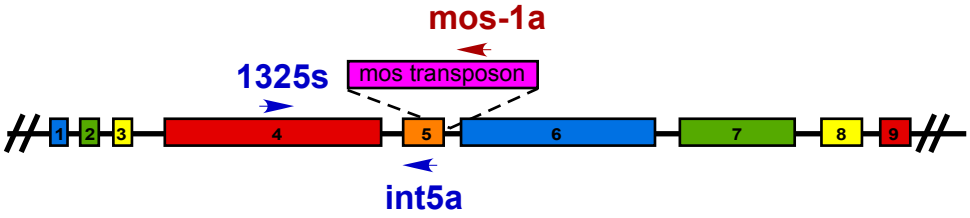
mos-1a
1325s
mos transposon
1
2
3
4
5
6
7
8
9
int5a

B

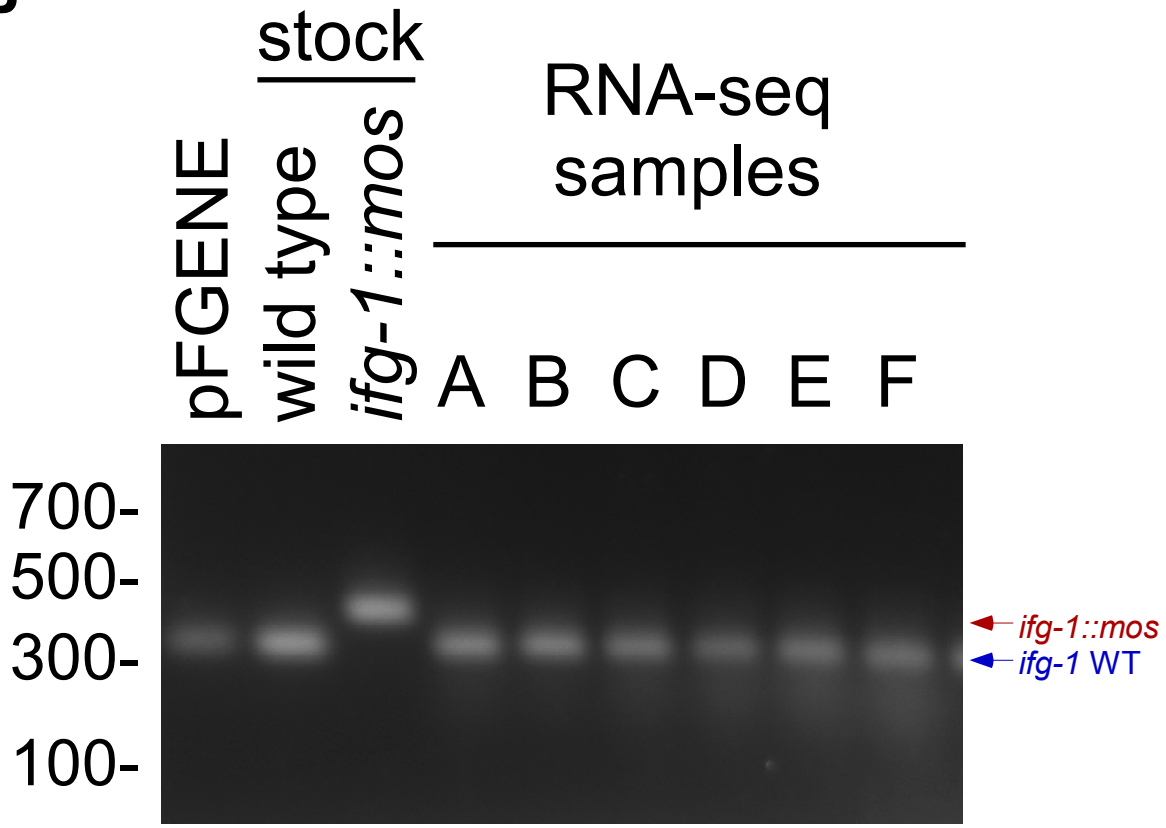
stock
pFGENE
wild type
ifg-1::mos
RNA-seq samples
A
B
C
D
E
F
700-
500-
300-
100-
ifg-1::mos
ifg-1 WT

Figure E.1. Genotype analysis of worm pellets submitted for RNA-seq analysis. (A) PCR analysis using primers to detect a *mos* insertion in the *ifg-1* gene was performed to determine the genotype of strains submitted for RNA-seq analysis. An increased PCR fragment size is indicative of a *mos* insertion in the *ifg-1* gene. Positions of primers for amplification are marked. Note that heterozygous worm strains show simultaneous amplification of both fractions (not shown). (B) RNA-seq samples were compared to stock samples of wild type and *ifg-1::mos* worms. They were also compared to PCR amplification of the *ifg-1* gene in a pF plasmid. These PCR results demonstrate that all samples sent for RNA-seq analysis had wild type *ifg-1* gene without the *mos* insertion. A= WT B biological replicate #1, B= WT A biological replicate #1, C= WT B biological replicate #2, D= WT A biological replicate #2, E= WT B biological replicate #3 and F= WT A biological replicate #3.

RNA-seq Analysis to determine global changes in the efficiency of translation. In this study we focused on changes in translation initiation for the entire population of mRNAs. Sucrose gradient centrifugation was used to resolve mRNAs that are actively translated on polysomes in the wild type strain group A (WT A) in comparison to wild type strain group B (WT B) (Figure E.2A-B). RNA was extracted from each gradient fraction. The nonpolysomal fractions (fractions 1 and 2) were then combined into a "nontranslating" fraction. The 80S fraction (fraction 3) was excluded from further analysis and this fraction served as a buffer between the nontranslating and translating regions of the gradient. Fractions 4-11 were combined into a "translating" region fraction. RNA-seq was then performed by Beckman Coulter Genomics using biological triplicates of "nontranslating" and "translating" fractions from WT A and WT B worms. Cufflinks software was used by Beckman Coulter Genomics to assign reads, assemble reads into transcripts and to estimate the abundance of these transcripts. The transcripts were then matched back to the *C. elegans* transcriptome (WS240). The outcomes of these experiments were measurements of mRNA abundances in fragments per kilobase of exon per million fragments (FPKM) (Mortazavi et al., 2008).

The FPKM values are generally used to assay changes in the transcriptome when determined from cellular total RNA samples (Mortazavi et al., 2008). However, in this study our interest was primarily regulation of mRNA translation. In order to focus on these changes in mRNA translation, we determined changes in the proportion of mRNA in the nontranslating and translating regions of the gradient in WT A and WT B (Figure E.3). Nonpolysomal and polysomal mRNA quantities were derived from their respective FPKM outputs from RNA-seq analysis. We then approximated the total RNA content across the

Figure E.2

A WT A 25°C

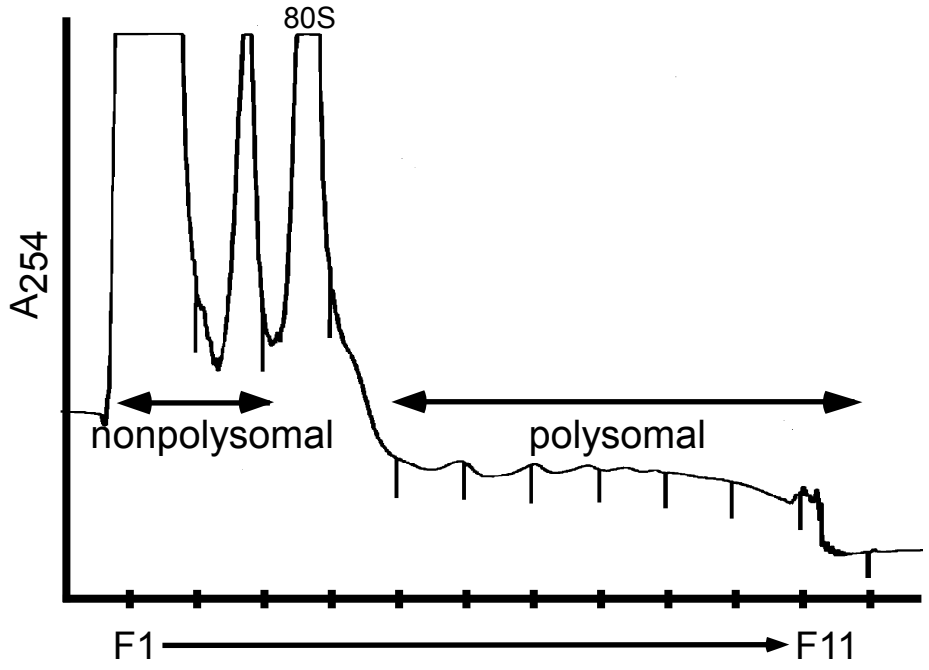

B WT B 25°C

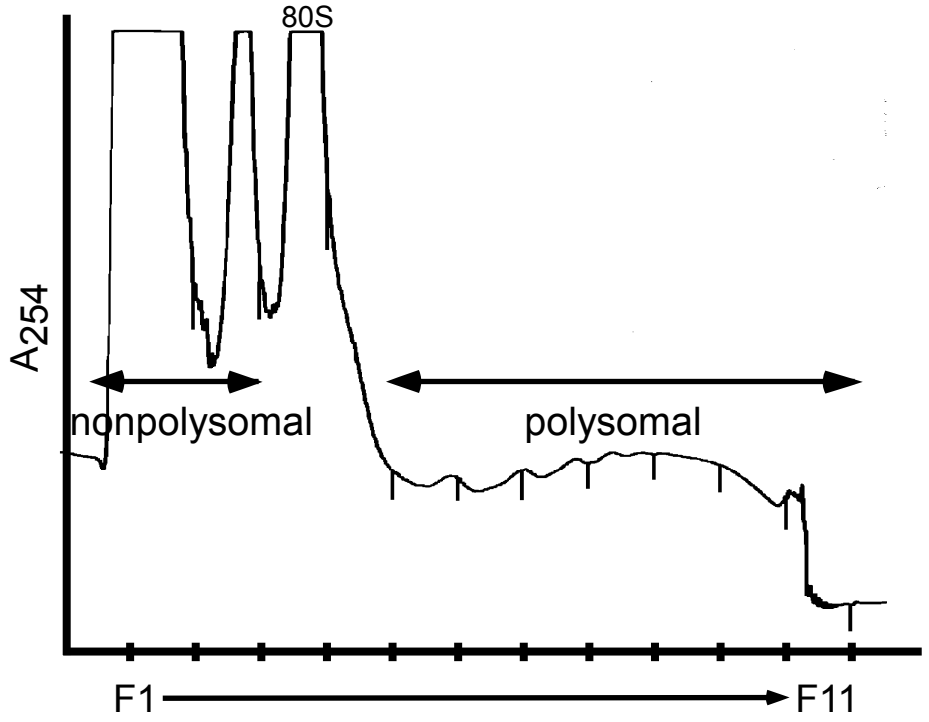

Figure E.2. Polysome profiles from sucrose gradients fractionated with continuous monitoring of absorbance at 254 nm of WT A and WT B fractionated gradients used for RNA-seq. During sucrose gradient fractionation of worm lysates from WT A (A) and WT B (B) strains absorbance was measured at 254nm. These gradients represent 1 of 3 biological replicates of each wild set. The profiles of biological replicates closely resemble one another. Fraction 1-2 (nonpolysomal) and 4-11 (polysomal) were pooled for RNA-seq experiments.

gradient by adding the FPKM values from the polysomal and nonpolysomal regions. "R" values were then derived to represent polysomal mRNA content normalized to total mRNA content in the samples (Figure E.4A). R_A is defined as the quantity of a specific WT A polysomal mRNA normalized to the total amount of that particular WT A mRNA, meaning the quantity in the nonpolysomal and polysomal region combined. Similarly, R_B is equivalent to the quantity of a target mRNA in the polysomal region normalized to the total amount of that mRNA across the gradient in a particular WT B biological replicate. We next derived a term "R fold Change" to denote changes in the relative representation of a specific message in the polysomal/translating region of the gradient between the two test groups (Figure E.4A) (derivation of the terms and equations for R_A, R_B and R fold, personal communication Andrew Friday). The R fold term was derived by dividing WT A R value (R_A) by WT B R value (R_B). The normalization of the WT A and WT B target polysomal mRNA to their total target mRNA quantity (T) prevents changes in relative transcription or mRNA stability from complicating interpretations of increased translational efficiency. For example, increased mRNA levels due to altered gene transcription or enhanced mRNA stability may mean increased availability of that mRNA to the ribosomes. These changes would be mistakenly perceived as increased in translational efficiency. Thus, normalization prevented these perceived increases in translational efficiency due to increased total target mRNA quantity. We did note changes in transcription/mRNA stability in WT A versus WT B by deriving a total fold change value (Figure E.4B). We first derived T_A and T_B as the summation of the FPKMs from the polysomal and nonpolysomal samples of their respective strains. The ratio of T_A to T_B is referred to as the total fold change. Additionally, we evaluated changes in the amount of mRNA in the polysomal region without

Figure E.3

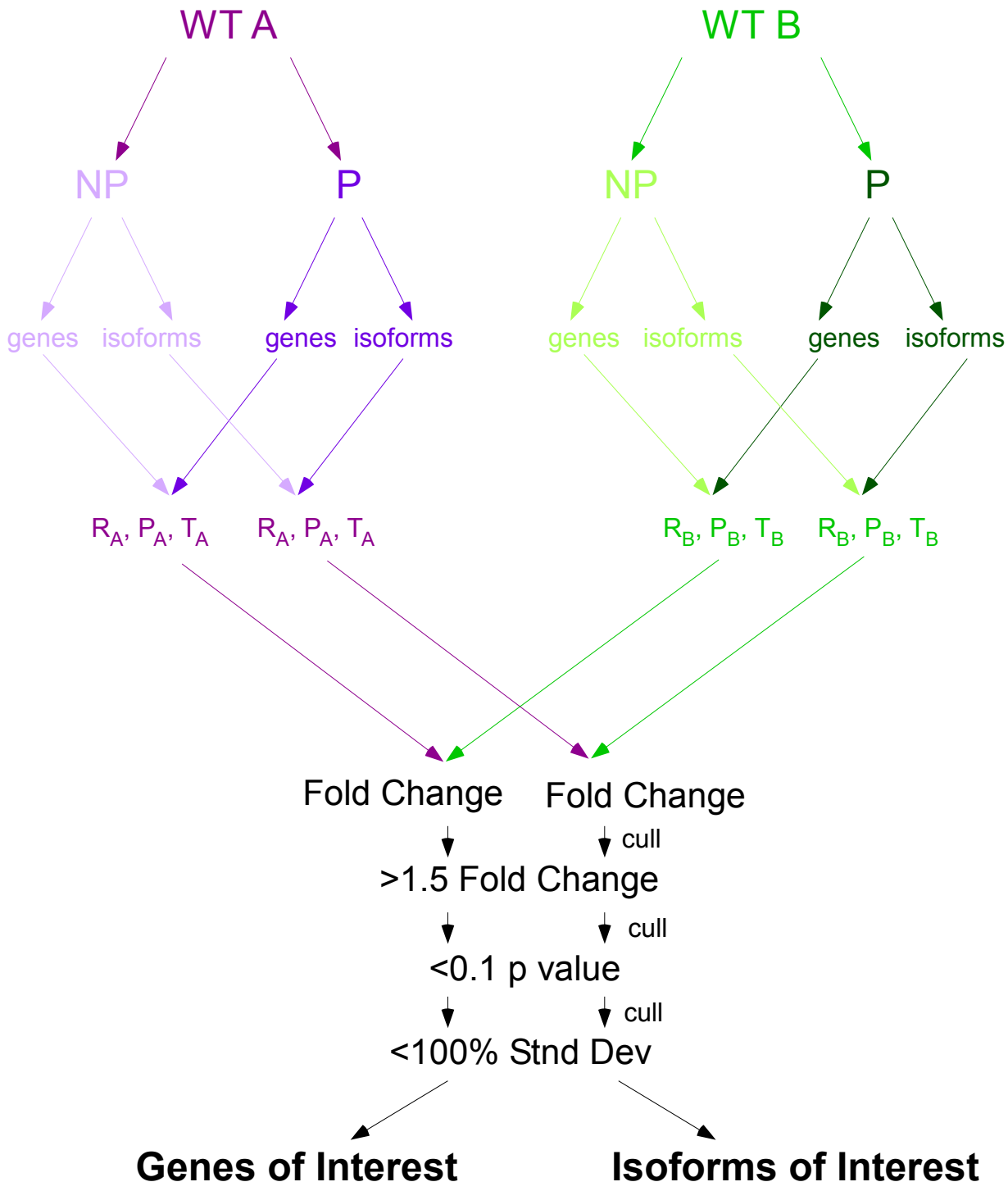
WT A
WT B
NP
P
NP
P
genes
isoforms
genes
isoforms
genes
isoforms
genes
isoforms
R_A, P_A, T_A
R_A, P_A, T_A
R_B, P_B, T_B
R_B, P_B, T_B
Fold Change
Fold Change
cull
>1.5 Fold Change
cull
<0.1 p value
cull
<100% Stnd Dev
Genes of Interest
Isoforms of Interest

Figure E.3. Schematic of RNA-seq experiments and analysis. This schematic represents the steps taken in the RNA-seq analysis. Nonpolysomal (NP) and polysomal (P) RNA from WT A and WT B worms were analyzed via RNA-seq. Cufflinks was then used to assign reads into transcripts from the *C. elegans* transcriptome and to estimate the abundance of these transcripts. The outcomes of these experiments were measurements of transcript abundances in FPKM. FPKM values were then used to derived polysomal RNA normalized to total RNA (Rw and Ri), polysomal RNA (Pw and Pi) and total RNA (Tw and Ti) in each strain. These values were then used to determine fold changes. Data was then culled at a 1.5 fold or greater change in R fold change value, p value less than 0.1 and percent standard deviation of less than 100 percent.

normalization to total mRNA quantities, defined as polysomal fold change (Figure E.4C). For this calculation P_A is equivalent to the FPKM of WT A polysomal samples and P_B is equivalent to the FPKM of WT B polysomal samples. The ratio of P_A to P_B is referred to as the polysomal fold change. These three ratios (R fold, total fold and polysomal fold) were determined for gene products and isoform products by calculating separate ratios for each (See Figure E.3 and E.4).

RNA-seq based quantification of R fold change of gene products. The resulting R fold output of these calculations was then used to determine if there were authentic, detectable changes in the translational efficiency of all detected *C. elegans* mRNAs. This allows detection of mRNAs that are translated more or less efficiently between our replicates A and B. The expectation of these results would be no detected difference in R fold change as a result of these two test groups both containing wild type worms. Surprisingly, we were able to observe many transcripts via our current analysis that were determined to be significantly increased despite the fact that we were comparing like samples. R fold values of greater than 1.5 or inverse R fold values of greater than 1.5 were then further analyzed. Inverse R fold is defined as R_B divided by R_A or an indicated decrease in translational efficiency when comparing WT A to WT B. A 1.5 fold change was chosen as the cut off for further analysis based upon previous experience in our lab working with R fold changes derived from microarray analysis for *ife-1*-deficient versus wild type worms (personal communication Andrew Friday). T tests were performed to determine the specific mRNAs with a significant difference in R fold change. mRNAs with a p value < 0.1 were selected for further analysis. These t tests compared R_A and R_B values in order to

Figure E.4

A

$$R_A = \frac{\text{polysomal WT A FPKM}}{\text{polysomal FPKM + nonpolysomal FPKM WT A}}$$

$$R_B = \frac{\text{polysomal WT B FPKM}}{\text{polysomal FPKM + nonpolysomal FPKM WT B}}$$

$$\text{Rfold} = \frac{R_A}{R_B}$$

B

$$T_A = \text{polysomal FPKM + nonpolysomal FPKM WT A}$$

$$T_B = \text{polysomal FPKM + nonpolysomal FPKM WT B}$$

$$\text{Total fold} = \frac{T_A}{T_B}$$

C

$$T_A = \text{polysomal WT A FPKM}$$

$$T_B = \text{polysomal WT B FPKM}$$

$$\text{Polysomal Fold} = \frac{P_A}{P_B}$$

Figure E.4. Equations for determination of fold changes of RNA-seq results. (A) Derivation of R fold change. R_A=WT A R fold value, R_B=WT B R fold value. (B) Derivation of total fold change. (C) Derivation of polysomal fold change. Inverse or inverted functions indicated fold changes comparing WT B to WT A instead of vise versa.

determine if they were significantly different from one another. The distribution of R_A versus R_B was analyzed for each biological replicate and significant p values and R fold changes were noted (Figure E.5A). There was a linear correlation of y=x between the majority of R_A and R_B values illustrating that most RNAs had no substantial change in translational efficiency in WT A when compared to WT B, as expected. However, not all gene products resulted in a linear correlation. Instead, many genes were demonstrated to have significant R fold increases of greater than 1.5. *C. elegans* GAPDH (*gpd-3*) had no change in ribosome loading indicating no change in the general translation of housekeeping mRNAs and substantiating that the observed differences were not due to differences in gradient resolution.

A subset of genes correspond to identified mRNAs suspected to translate with increased or decreased translational efficiency. The gene subset with increased mRNA translational efficiency (increased R fold), is indicative of mRNAs that are translated more efficiently during test conditions. However, when comparing wild type strain replicates, we would not expect to find differences in mRNA translational efficiency. The subset of mRNAs found to have a significantly different R fold value in the WT A are represented in Figure E.5B. A large number of transcripts were determined by our current analysis to have a significant R fold values close to 1. This indicates that despite the fact that the t test determines these points to be significantly different, our data culling at an R fold change value of 1.5 would eliminate most of these false positive results. However, a large number of gene products were still found to have a significant R fold increase of greater than 1.5. When looking at the individual R fold comparisons for each biological replicate, we found that many of the gene products had highly variable R fold changes. For example, the mRNA

Figure E.5

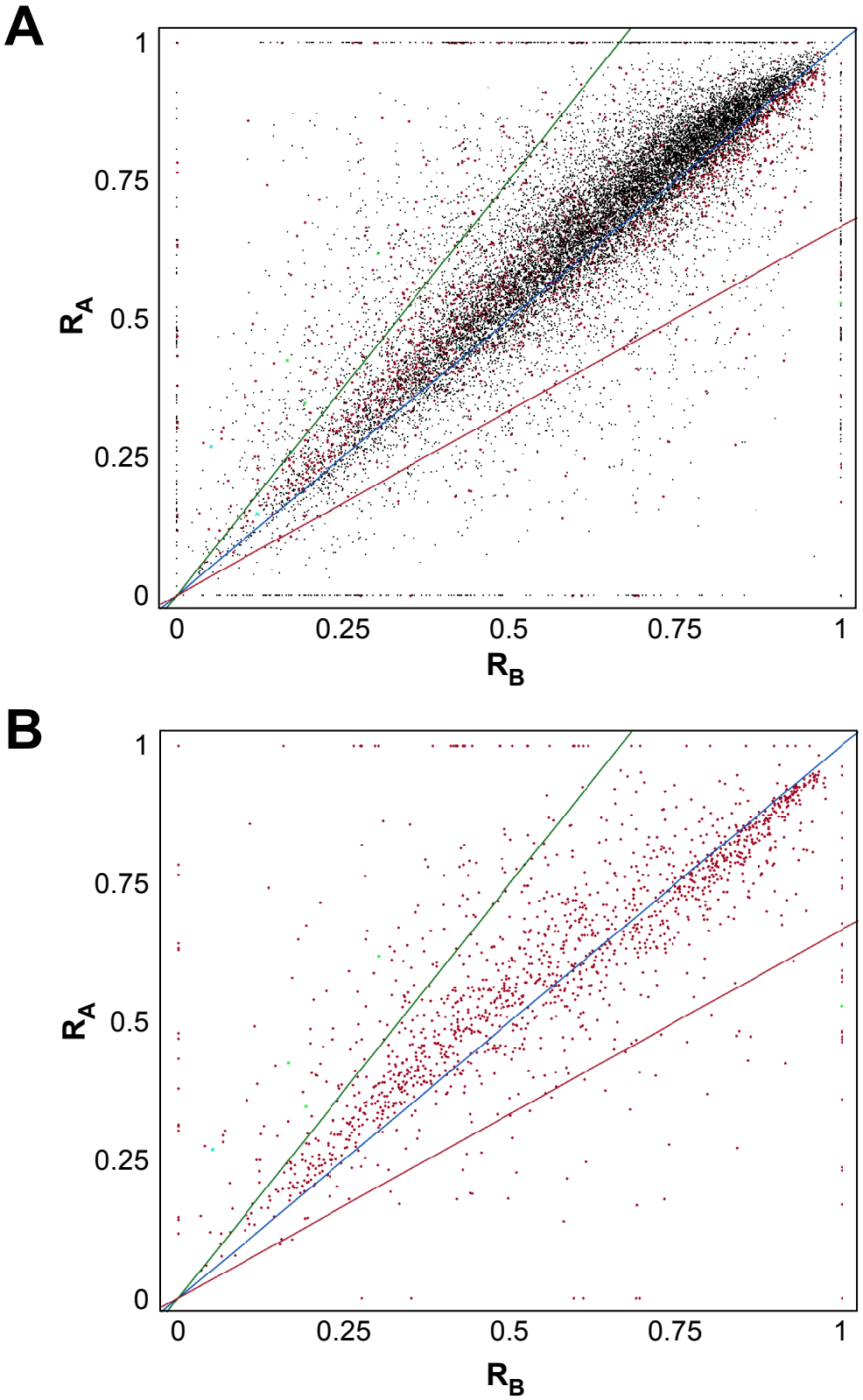
A
1
0.75
0.5
0.25
0
R_A
0
0.25
0.5
0.75
1
R_B
B
1
0.75
0.5
0.25
0
R_A
0
0.25
0.5
0.75
1
R_B

Figure E.5. Representation of R Fold Change RNA-seq gene results. (A) Graph depicting gene R values in WT B versus WT A worms (R_B vs. R_A). This graph depicts one biological replicate, but is representative of the other two biological replicates. Highlighted in pink are the significant data points (p value<0.1). Blue line depicts y=x or no fold change. Green line depicts y=1.5x or a 1.5 R fold change increase. Red line depicts y=0.67x or 1.5 R fold change decrease (B) Graph depicting only significant R fold change (p value<0.1). In future experiments, similar graphs comparing wild type R values to *ifg-1::mos* R values will enable us to observe changes in normalized polysomal mRNA loading due to IFG-1 depletion and the induction of cap-independent translation. The data in these graphs are derived from transcripts matched to the *C. elegans* gene database.

with the largest R fold change increase, *fbxc-17* mRNA, had R fold changes that ranged from 1.77 to 7.84. In the *fbxc-17* mRNA R fold change example, all R fold values were above 1.5-fold threshold for analyzing significant R fold data. Looking at the raw data to try to determine how a false positive may be culled in future experiments, we observed that the raw FPKM values for the polysomal and nonpolysomal regions of the gradients of WT A and WT B were very small. The confidence interval of *fbxc-17* FPKM values approached 0. This mRNA was not the only transcript to be found to have a significant R fold change by our current analysis that was most likely deemed significant due to an inability to detect the message in all biological replicates. When graphing R_A versus R_B many R values are located on the x or y axis, indicating R_A or R_B is equal to zero. Additionally, many points are found to have an R_A or R_B value (x or y value) of 1. An R_A or R_B value of 1 means that the nonpolysomal FPKM value was equal to 0 in the sample of interest. A nonpolysomal FPKM value of 0 indicates that the message is either very efficiently translated or more likely that the mRNA detected is near the detection limit and thus is not consistently detected. Thus, for analysis in future experiments, these data would indicate that an additional cull must be made using the raw FPKM values. This cull should remove mRNAs with FPKM values close to the detection limit of RNA-seq quantification to avoid false positives from further analysis. The recommendation for such a data cull would be to exclude further analysis of mRNAs in which all three or two of the three biological replicates have an FPKM confidence interval that converges on zero for its nonpolysomal or polysomal samples.

Aberrant significant R fold values, however, were not only detected for gene products with low FPKM values. Additionally, we observed aberrant significant R fold changes of biological replicates that were highly variable. *srz-60* mRNA, for example, has R

fold changes of 2.05, 0.96 and 2.94 in our biological replicates. In this example, only 2 of the 3 individual R fold change values from our biological replicates meet the 1.5 fold increase criteria for further analysis. The final replicate was actually demonstrated to have a decreased R fold change value. Thus, with our current method of statistical analysis we picked targets for follow-up work that did not consistently have a positive fold change among their biological replicates. This one example was not an anomaly, but part of a much larger group of targets deemed significant despite this biological variability. Therefore, it may be useful in future RNA-seq experiments to have a data cull removing inconsistent increases in R fold value or to decrease the p value deemed to be significant.

Likewise target mRNAs with a statistically significant R fold change decrease (increased inverse R fold change) of greater than 1.5-fold were determined. These mRNAs have increased polysomal loading in WT B when normalized to total mRNA content. The overall quantity of identified targets and their fold change values (both increased or decreased) are represented in Figure E.6A. Many gene products from the *C. elegans* transcriptome were not detected via the RNA-seq amplification and are highlighted in blue. Only a small portion of the mRNAs (988 messages of 46454 total messages) were found to have an R fold change of more than 1.5 (increase or decrease). However, the identified mRNAs with an R fold increase or decrease of 1.5-fold was much larger than expected for mRNAs isolated from biological replicates of the same strain. Of these messages, 533 had a 1.5-2.5 fold increase, 86 had a fold increase of greater than 2.5, 308 had a fold decrease of 1.5-2.5 fold and 61 had a fold decrease of greater than 2.5. Statistically significant changes are outlined, illustrating the proportion of targets culled by 1.5 fold change and a p value of less than 0.1. Only a small portion of the messages with R fold changes of greater than 1.5

Figure E.6

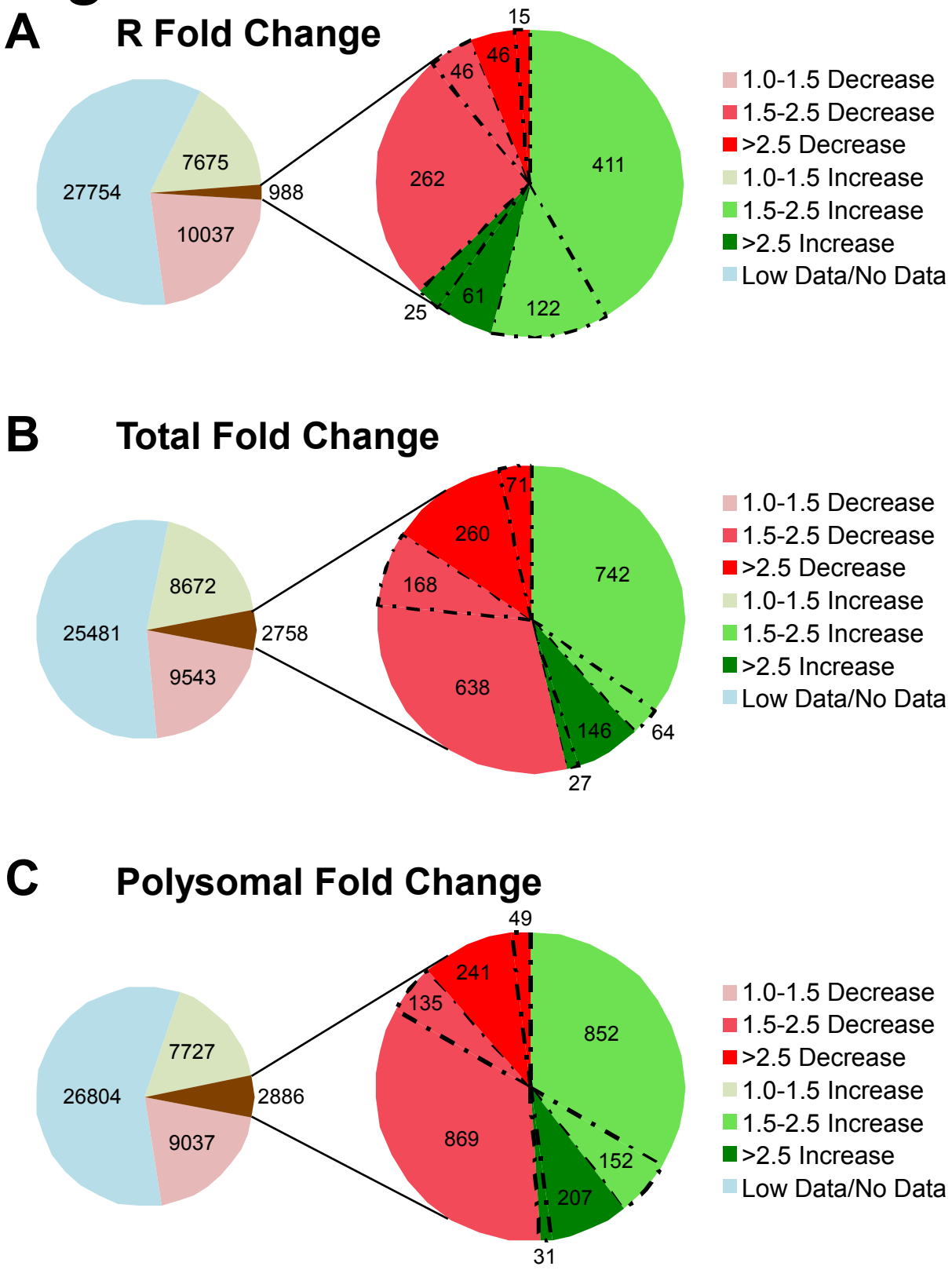
A
R Fold Change
27754
7675
988
10037
15
46
46
262
411
25
61
122
B
Total Fold Change
25481
8672
2758
9543
71
260
168
742
638
146
64
27
C
Polysomal Fold Change
26804
7727
2886
9037
49
241
135
852
869
152
207
31
1.0-1.5 Decrease
1.5-2.5 Decrease
>2.5 Decrease
1.0-1.5 Increase
1.5-2.5 Increase
>2.5 Increase
Low Data/No Data

Figure E.6. Pie charts illustrating the percent of the genes undergoing a specific fold change value. (A) R fold change. Aberrant significant R fold change ($p<0.1$) of greater than 1.5 are outlined with dotted lines. These outlined sectors denote the statistically relevant changes. (B) Total fold change. Aberrant significant total fold change ($p<0.1$) of great than 1.5 are outlined with dotted lines. These outlined sectors denote the statistically relevant changes. (C) Polysomal fold change. Aberrant significant polysomal fold change ($p<0.1$) of greater than 1.5 are outlined with dotted lines. These outlined sectors denote the statistically relevant changes. The data in these graphs are derived from transcripts matched to the *C. elegans* gene database.

were found to be statistically significant differences from their WT A representation. This demonstrates our ability to cull that data relatively successfully. However, additional criteria must be derived to prevent other aberrant R fold decreases from being referred to as significant changes. These mRNAs had reproducible increases or decreases in R fold values that were consistent within the biological replicates and thus statically significant.

RNA-seq based quantification of total gene product abundance (total fold change). We desired to determine mRNAs with an indicated increase in transcription or stability when comparing WT A and WT B. Changes in mRNA abundance were quantified as a total fold change (Figure E.4B). In these experiments we were comparing wild type samples to wild type samples and thus we anticipated no change in total RNA representation. Total RNA quantity of individual mRNAs in WT A (T_A) was compared to those in WT B (T_B) and was shown to have a y=x linear correlation (Figure E.7A). This indicates that the majority of messages have no substantial change in mRNA abundance, as expected. This also demonstrates that our current analysis process is effectively able to cull most of the biological variation within the wild type strain. However, a subset of messages was found to have an increased or decreased total fold change of greater than 1.5-fold. The percentage of mRNA targets that have significant increases or decreases in translational efficiency are depicted in Figure E.6B. A larger number of mRNA targets had quantifiable total fold changes than R fold changes as a result of how these fold changes were calculated. When total fold changes were calculated, they only required the nonpolysomal or polysomal region of WT A and WT B to have a quantifiable FPKM value. However, when calculating R fold, quantifiable mRNA abundances must be present in the polysomal region

of both the WT A and its matched biological replicate of WT B to derive an R fold ratio. The difference in the number of genes with identified R fold and total fold changes, indicates that some mRNAs were only present in the nonpolysomal region of the gradient. For future analysis to successfully depict actual total fold change increases, these data must also be culled by FPKM values that approach undetectable levels.

A larger number of targets (2758 of 46454) were identified to have a fold change of greater than or less than 1.5-fold. Thus, a larger number of mRNAs were found to have apparent changes in their transcription and/or mRNA stability than their weighted translational efficiency. These differences in the total amount of mRNAs may be due to biological differences in the level of transcription or more likely may be due to a need for more stringent perimeters to determine significant differences in total fold change. Therefore, in future experiments more stringent perimeters such as a smaller p value must be applied in order to exclude false positive total fold changes.

RNA-seq based quantification of polysomal fold change of gene products. Apparent changes in polysomal loading were also determined in the WT A compared to WT B. In this case, we did not normalize polysomal loading to total mRNA content. Instead the polysome FPKM of WT A was compared to the polysome FPKM of WT B. Looking at polysomal fold changes allows for observation of differences in polysomal loading not accounting for changes in total mRNA quantity. It thus depicts outcomes where there is enhanced translation resulting from either increased mRNA representation or increased translation initiation ability. A large number of targets (1886 of 46454) were found to have increased polysome mRNA content in WT A (Figure 4.6C). Overall, most WT A polysomal

Figure E.7

A

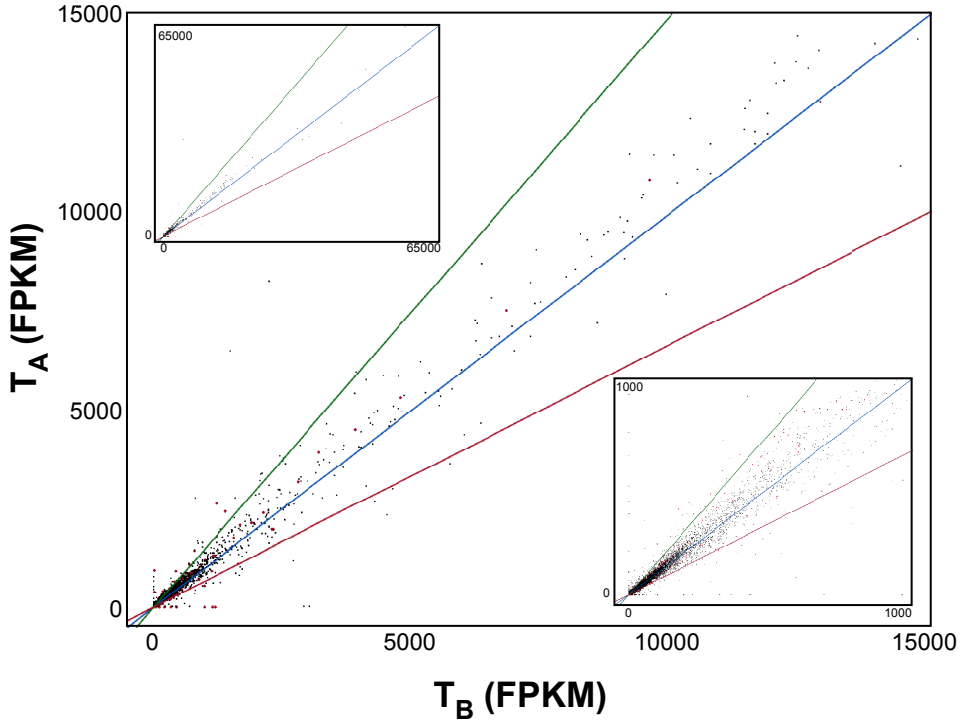
15000
10000
5000
0
0
5000
10000
15000
T_A (FPKM)
T_B (FPKM)
65000
0
0
65000
1000
0
0
1000

B

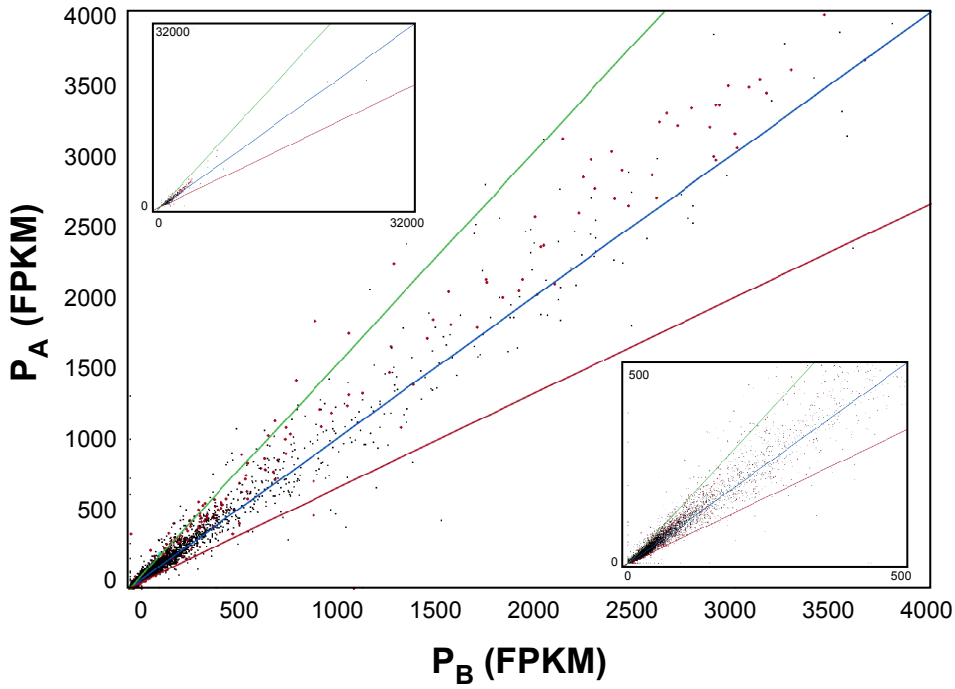
4000
3500
3000
2500
2000
1500
1000
500
0
0
500
1000
1500
2000
2500
3000
3500
4000
P_A (FPKM)
P_B (FPKM)
32000
0
0
32000
500
0
0
500

Figure E.7. Representation of Total Fold Change and Polysomal Fold Change RNA-seq gene results. (A) Graph depicting gene total changes in WT B versus WT A worms (T_B vs. T_A). This graph depicts one biological replicate, but is representative of the other two biological replicates. Highlighted in pink are the significant data points (p value<0.1). Inset graphs represent zoomed in and zoomed out versions of the total fold change graph. Blue line depicts y=x or no fold change. Green line depicts y=1.5x or a 1.5 total fold change increase. Red line depicts y=0.67x or 1.5 total fold change decrease. During future experiments, similar graphs comparing wild type total to *ifg-1::mos* total will enable us to observe changes in total mRNA representation due to IFG-1 depletion. (B) Graph depicting gene polysomal fold changes in WT B versus WT A worms (P_A vs. P_B). This graph depicts one biological replicate, but is representative of the other two biological replicates. Highlighted in pink are the significant data points (p value<0.1). Inset graphs represent zoomed in and zoomed out versions of the polysomal fold change graph. Blue line depicts y=x or no fold change. Green line depicts y=1.5x or a 1.5 polysomal fold change increase. Red line depicts y=0.67x or 1.5 polysomal fold change decrease. In future experiments, similar graphs comparing wild type polysomal to *ifg-1::mos* polysomal will enable us to observe changes in polysomal mRNA loading due to IFG-1 depletion and the induction of cap-independent translation. The data in these graphs are derived from transcripts matched to the *C. elegans* gene database.

content (P_A) values were found to have a y=x linear correlation with WT B polysomal content (P_B) values. This once again demonstrates that the majority of mRNAs do not have a change in their polysomal loading as would be expected when comparing wild type groups (Figure 4.7B). This correlation of P_A and P_B clearly demonstrates the good reproducibility of our gradients. Many mRNAs with significant R fold changes were additionally found to have significant polysomal fold changes. For example, *bath-22, srg-49, skr-11* and *his-8* were preliminarily found to have significant R fold and polysomal fold changes. Similarly, many R fold decreases were associated with polysomal fold decreases, such as *sri-22, ceh-21* and *col-132.* This indicates that by simply comparing R fold changes and polysomal fold changes to determine their consistency we are unable to detect aberrant fold change increases or decreases. Therefore, a consistent significant R Fold and Polysomal Fold change is not necessarily an indicator for the validity of these detected changes in translational efficiency. It also indicates that aberrant increases in polysomal loading are still detected after normalization. Many of the polysomal FPKM values were very small, as previously observed for mRNAs with significant R fold changes. Once again, this may have resulted in aberrant increases in polysomal loading as a result of mRNA quantities being near the detection limit of RNA-seq experiments.

RNA-seq Analysis to determine global changes in the efficiency of translation of specific isoforms. Thus far our analysis was performed on gene products, however we also wanted to determine changes in the translational efficiency of isoform products that result from alternative start site utilization or alternative splicing of *C. elegans* genes. The data were derived from the same RNA-seq experiment, but instead of Beckman Coulter

Figure E.8

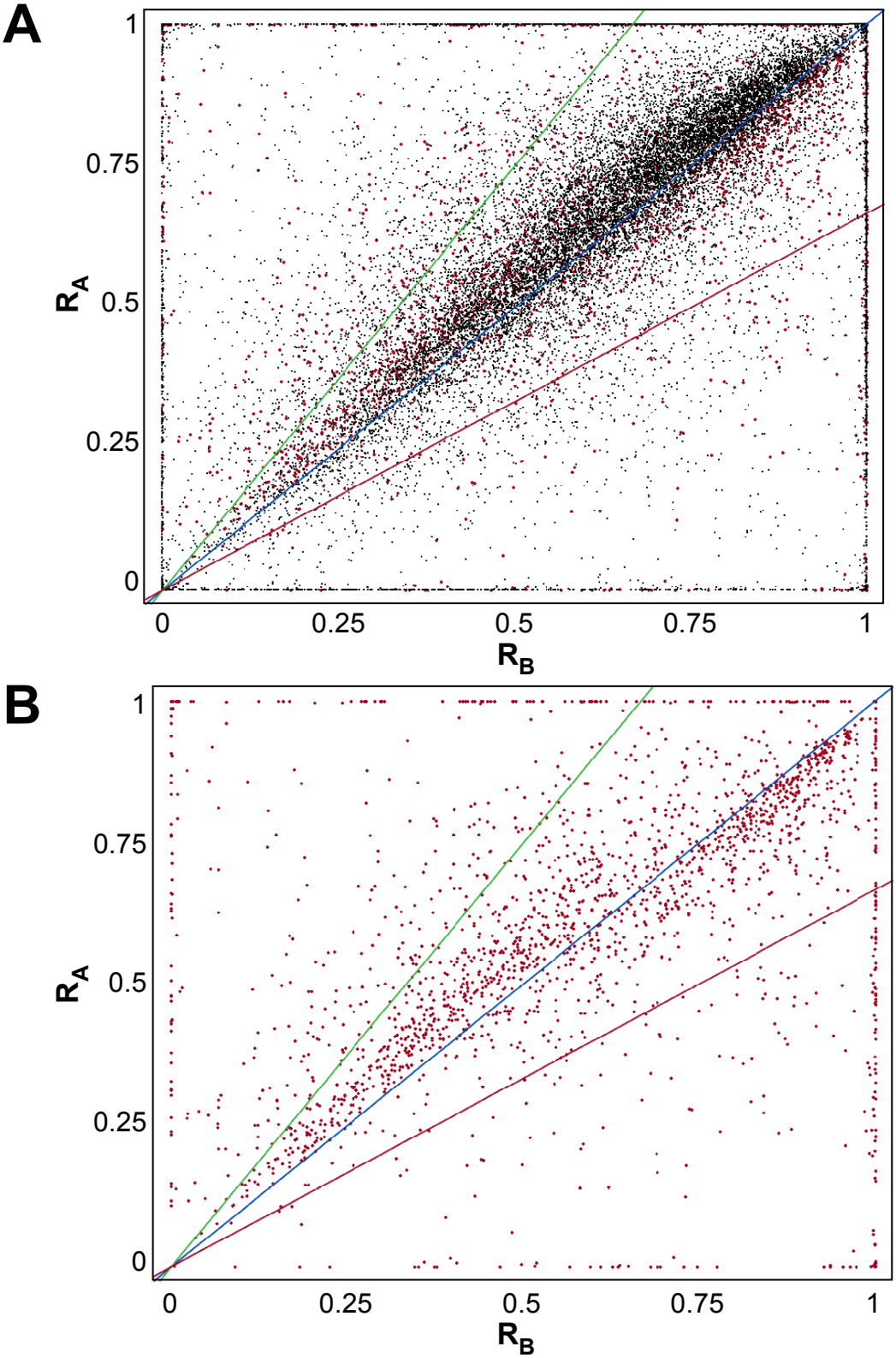
A
1
0.75
0.5
0.25
0
R_A
0
0.25
0.5
0.75
1
R_B
B
1
0.75
0.5
0.25
0
R_A
0
0.25
0.5
0.75
1
R_B

Figure E.8. Representation of R Fold Change Fold Change RNA-seq isoform results. (A) Graph depicting isoform R changes in WT B versus WT B worms (R_B vs. R_A). This graph depicts one biological replicate, but is representative of the other two biological replicates. Highlighted in pink are the significant data points (p value<0.1). Blue line depicts y=x or no fold change. Green line depicts y=1.5x or a 1.5 R fold change increase. Red line depicts y=0.67x or 1.5 R fold change decrease. (B) Graph depicting only significant R fold change (p value<0.1). The data in these graphs are derived from transcripts matched to the *C. elegans* isoform database.

Genomics aligning sequences to the *C. elegans* gene database, sequences were aligned to *C. elegans* isoforms database using Cufflinks. Paired-end RNA-seq was performed to allow for estimation of mRNA variant (isoform) abundance (Wang et al., 2008). In paired-end experiments, RNA fragments are sequenced from both ends by Beckman Coulter Genomics resulting in two reads for each fragment. Two reads per fragment provides sufficient sequence knowledge to estimate isoform abundances via alignments to individual transcripts (Wang et al., 2008). However, sequence fragments may align to more than one isoform of the same gene. Cufflinks software thus uses a statistical model to perform a minimum cost maximum matching analysis based on the "percent spliced in" score (Wang et al., 2008). The "percent spliced in" is an estimate of the fraction of inclusion reads of a particular isoform to the total amount of inclusion and exclusion reads for a particular isoform (Wang et al., 2008).

We similarly determined R_A and R_B values for mRNA splice variants and compared their distributions and found a linear y=x correlation. This illustrated that the majority of mRNA splice variants, like the majority of compiled gene mRNAs analyzed, had no change in translational efficiency as would be expected when comparing like samples (Figure E.8A). A subset of mRNAs had a significant R fold value change once again illustrating a need for additional parameters to prevent false positive R Fold changes from being further analyzed (Figure E.8B). 5758 mRNA variants of 56273 total variants in the *C. elegans* transcriptome were found to have an R fold change of greater than 1.5 (Figure E.9A). Interestingly, many of these mRNAs are found in certain classes, such as long intervening non-coding RNAs and antisense non-coding RNAs. Many isoform FPKM values were very low. Apparently, these are only minor mRNA variants that are nearly undetectable. These

Figure E.9

A R Fold Change

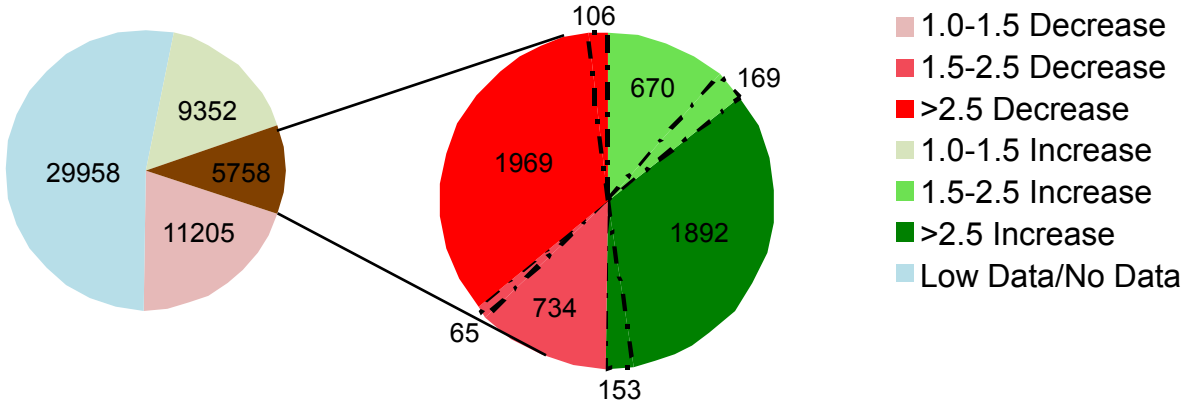

B Total Fold Change

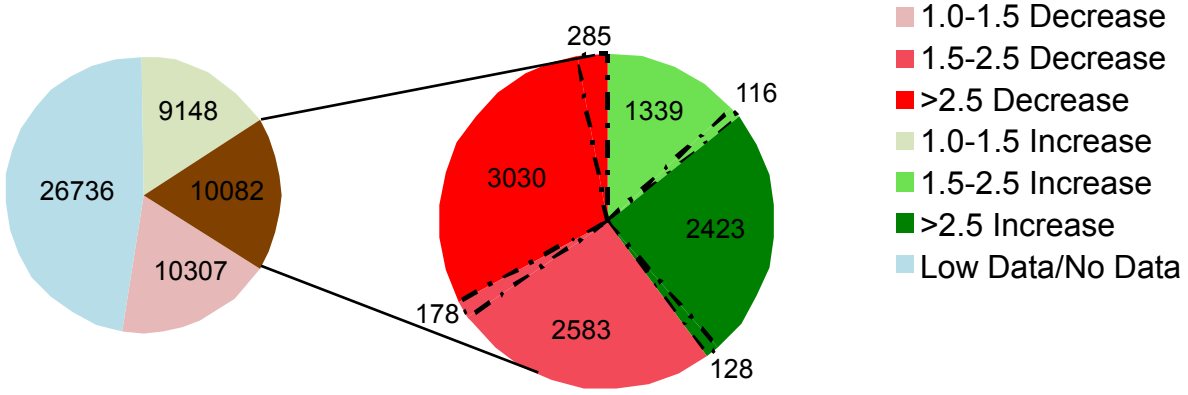

C Polysomal Fold Change

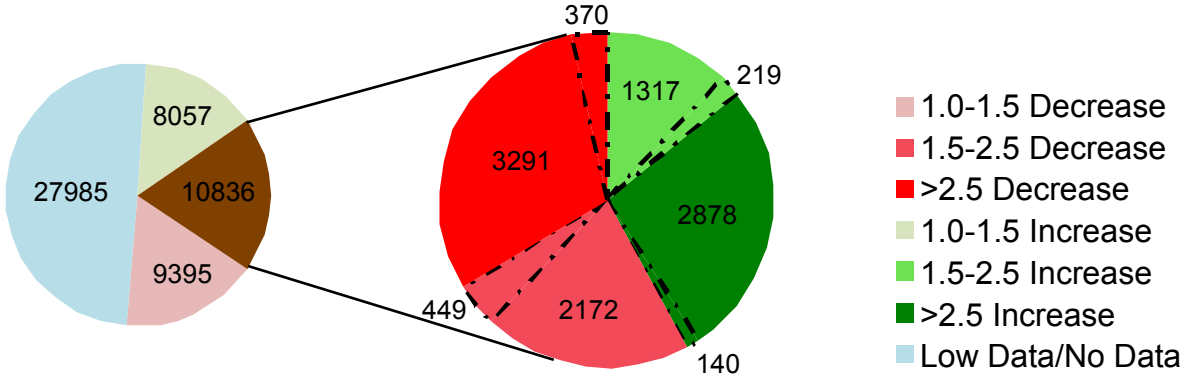

Figure E.9. Pie charts illustrating the percent of the isoforms undergoing a specific fold change value. (A) R fold change. Aberrant significant R fold change ($p<0.1$) of greater than 1.5 are outlined with dotted lines. These outlined sectors denote the statistically relevant changes. (B) Total fold change. Aberrant significant total fold change ($p<0.1$) of great than 1.5 are outlined with dotted lines. These outlined sectors denote the statistically relevant changes. (C) Polysomal fold change. Aberrant significant polysomal fold change ($p<0.1$) of greater than 1.5 are outlined with dotted lines. These outlined sectors denote the statistically relevant changes. The data in these graphs are derived from transcripts matched to the *C. elegans* isoform database.

low FPKM values, when used as divisors, led to aberrantly large fold change values. As a result, most of these values were deemed insignificant via the T test. However, the presence of other R fold changes being deemed as significant despite comparing like samples indicates the need to once again cull the data by low FPKM values to prevent these aberrantly large fold changes from being deemed significant. The majority of messages with an increased or decreased R fold change of genes were also found to have a significant isoform R fold change for one or more of its isoforms. However, several genes did not have an increased R fold change despite the significant increased R fold of one of its isoforms including *btb-4* and *hmg-12.*

RNA-seq based quantification of total mRNA variant, isoform, abundance. To determine mRNAs with increased transcription or stability in WT A, which might lead to aberrant increases in polysomal loading, we quantified the total RNA fold change of mRNA splice variants from WT A to WT B. When we compared these values via a scatter plot we found a y=x linear correlation illustrating that the majority of mRNA variants had no substantial change in total mRNA quantity as would be expected when comparing like samples (Figure E.10A). Overall, over 10,000 isoforms were found to have a total fold change greater than 1.5 fold (Figure E.9B). Of those 10,000 identified changes, however, only 707 isoforms were found to have a statistically significant ($p<0.1$) increase or decrease in total mRNA content. Although a p value of less than 0.1 was able to substantially cull the data, 707 false aberrant increases in total fold change were still detected. This indicates further statistical stringency must be applied to future analyses with mutant strain to eliminate this large number of false positive results. The majority of

Figure E.10

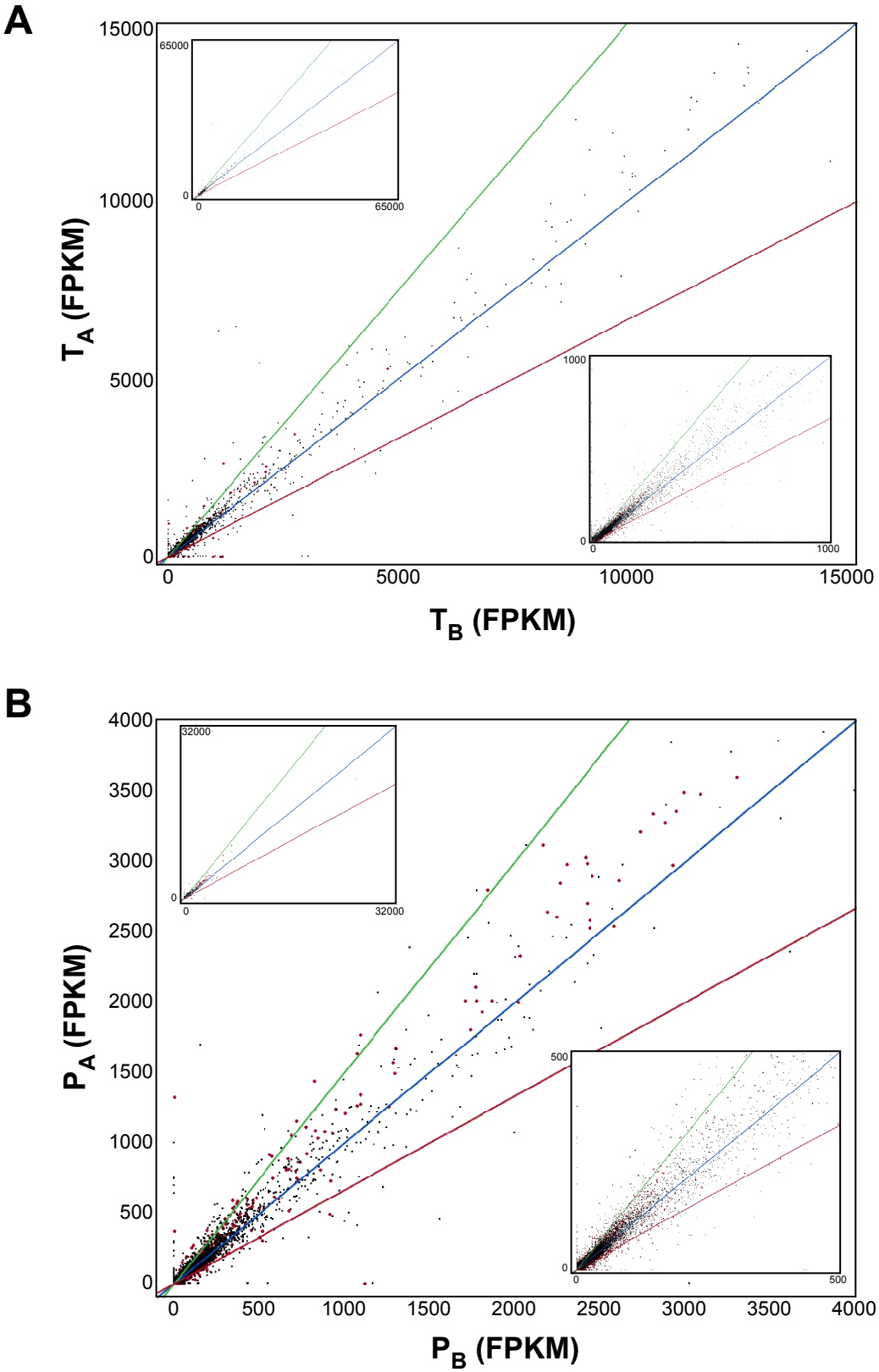
A
15000
10000
5000
0
0
5000
10000
15000
T_A (FPKM)
T_B (FPKM)
65000
0
0
65000
1000
0
0
1000
B
4000
3500
3000
2500
2000
1500
1000
500
0
0
500
1000
1500
2000
2500
3000
3500
4000
P_A (FPKM)
P_B (FPKM)
32000
0
0
32000
500
0
0
500

Figure E.10. Representation of Polysomal and Total Fold Change RNA-seq isoform results. (A) Graph depicting isoform total changes in WT B versus WT A worms concentrating on the lower total fold change values to better observe the majority of the data points (T_B vs. T_A). This graph depicts one biological replicate, but is representative of the other two biological replicates. Highlighted in pink are the significant data points (p value<0.1). Inset graphs represent zoomed in and zoomed out versions of the total fold change graph. Blue line depicts y=x or no fold change. Green line depicts y=1.5x or a 1.5 total fold change increase. Red line depicts y=0.67x or 1.5 total fold change decrease. (B) Graph depicting isoform polysomal changes in WT B versus WT A worms (P_B vs. P_A). This graph depicts one biological replicate, but is representative of the other two biological replicates. Highlighted in pink are the significant data points (p value<0.1). Inset graphs represent zoomed in and zoomed out versions of the polysomal fold change graph. Blue line depicts y=x or no fold change. Green line depicts y=1.5x or a 1.5 polysomal fold change increase. Red line depicts y=0.67x or 1.5 polysomal fold change decrease. The data in these graphs are derived from transcripts matched to the *C. elegans* isoform database.

genes isoform messages with a significant total fold change had one or more isoform with a significant total fold change, as expected.

RNA-seq based quantification of polysomal mRNA variant, isoform, abundance. Changes in polysomal loading were also determined in WT A compared to WT B to determine aberrant changes in translational efficiency of isoforms via our current analysis. In this case, as previously indicated with gene product analysis, we did not normalize polysomal loading to total mRNA content. Instead the polysome FPKM of WT A was compared to the polysome FPKM of WT B. We once again observed a linear (y=x) correlation between WT A and WT B polysomal FPKM values illustrating that most mRNA splice variants had no change in polysomal loading as would be expected when comparing like samples (Figure E.10B). Isoforms with a significant polysomal fold increase and decrease were identified. As previously observed with the gene polysomal fold change values, polysomal fold change values were typically correlated with either increased total RNA or were found to have a significant increase in R fold change. Additionally, a significant number of genes undergoing a polysomal fold change increase or decrease were identified to have one or more isoforms with a significant increase or decrease. However, not all isoforms were found to have a corresponding gene increase or decrease in translational efficiency. In total, over 10,000 isoforms were found to have a fold change of greater than 1.5, 1178 of which were significant (Figure 4.8C). This once again indicates that despite our current statistical analysis culling a large number of aberrant polysomal fold increases that the culling was not sufficient to remove all aberrant polysomal increases. Instead, there are

Figure E.11

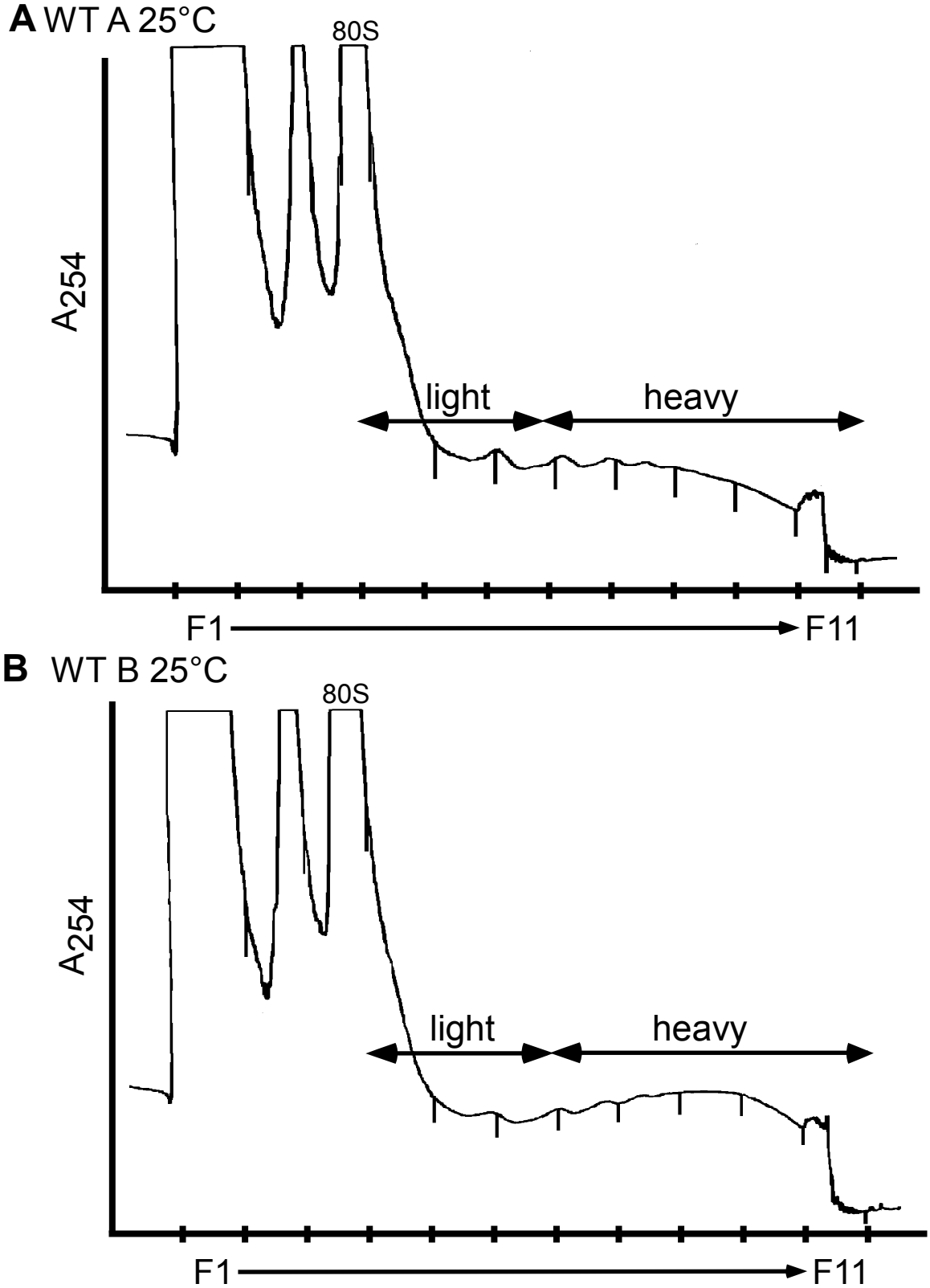
A WT A 25°C
80S
A254
light
heavy
F1
F11
B WT B 25°C
80S
A254
light
heavy
F1
F11

Figure E.11. Polysome profiles from sucrose gradients fractionated with continuous monitoring of absorbance at 254 nm of WT A and WT B lysates used for RNA-seq follow-up analysis. During sucrose gradient fractionation of worm lysates from WT B (A) and WT A (B) strains absorbance was measured at 254nm. These gradients represent 1 of 2 biological replicates of wild type groupings.

still a large number of isoforms that are determined to be significant despite the fact that we not expect to observe differences in like samples.

Confirmation analysis using independent, complete gradient resolution. Putatively translation altered in mRNAs from RNA-seq were confirmed and characterized more discretely by qPCR amplification of target mRNAs across the gradient. We desired to determine whether the differences in translational efficiency within our WT A and WT B samples were the result of true biological variation in our target messages or more likely the result of less stringent statistical analysis resulting in us defining these RNAs as having significant increase/decrease in translation. Worm lysates were fractionated on sucrose gradients to resolve polyribosome complexes as previously performed when preparing samples from RNA-seq experiments (Figure E.11A-B). The worm pellets used to create protein lysates for follow-up analyses were from the same freeze downs as those used for RNA-seq analysis. This allowed us to more directly compare RNA-seq results to qPCR amplification across the gradient. Sucrose gradient fractions were not combined and instead mRNA content was quantified across each gradient fraction by qPCR. Translational efficiencies of target mRNAs were calculated by determining the percentage of target represented in each gradient fraction. *gpd-3* mRNA translational efficiency was used as an indicator of efficient global translation. *gpd-3* mRNA was translated efficiently and almost identically in WT A and WT B samples (Figure E.12A). When comparing the percent RNA per fraction in WT A and WT B to determine the similarity in the curves and thus the reproducibility of *gpd-3* mRNA fractionation, we determined a coefficient of determination or the proportion of the variance of WT A that is predictable from WT B to be 93% (Figure

Figure E.12

A

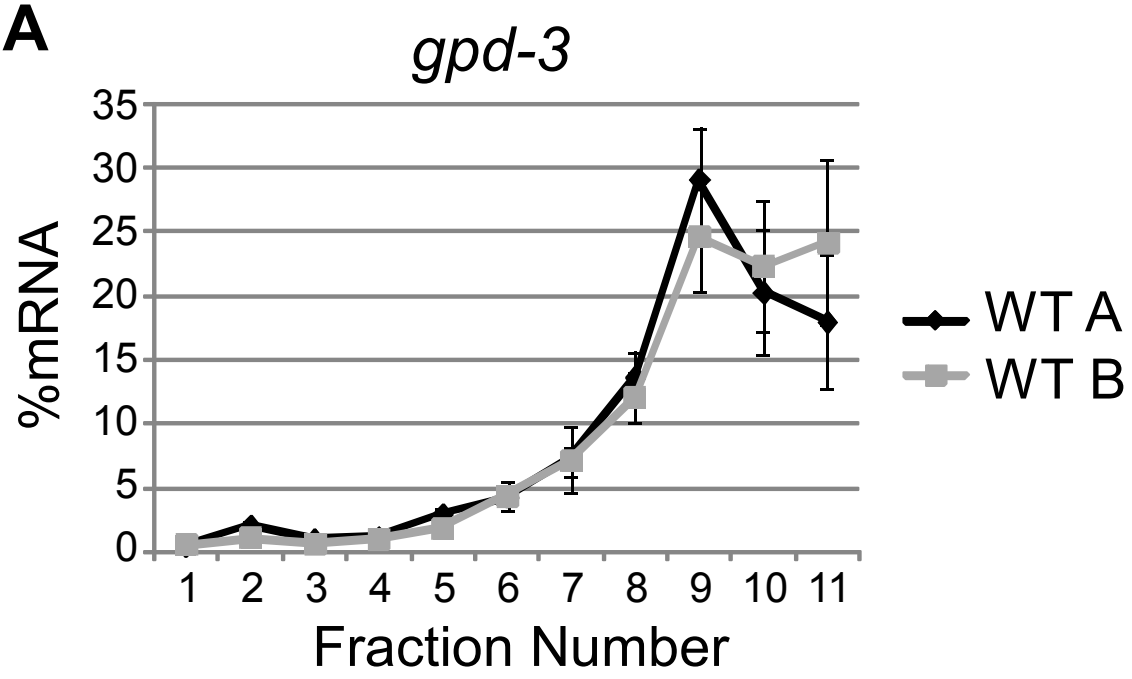

B

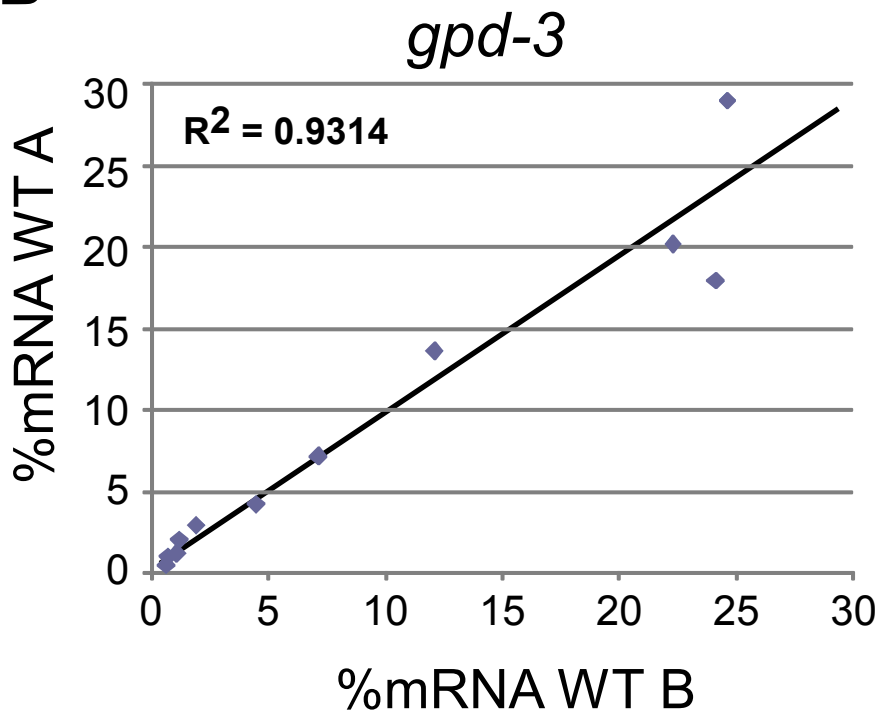

Figure E.12. No change in global mRNA translation or gradient fractionation. RNA distributions were quantified by qPCR in WT A and WT B from polysome profiles depicted in Figure 4.10. These gradients represent 1 of 2 biological replicates of WT A and WT B worms. (A) *gpd-3* mRNA translational efficiency was determined in WT A and WT B strains. (B) Comparison of percent *gpd-3* mRNA per fraction in WT A and WT B samples indicating the correlation of a single mRNA with gradient resolution.

E.12B). Thus, sucrose gradient fractionation or biological variation within the wild type strain did not result in differences in global translation.

hlh-17, fbxb-111, fezf-1 and gnrr-7 mRNAs have no change in translational efficiency quantified by full gradient polysome resolution, despite a predicted increase or decrease via R fold change RNA-seq results. *hlh-17* was identified as a target of interest via RNA-seq with an R fold change of 1.62 (Table E.1). *hlh-17* encodes a transcription factor that is important for larval development, egg laying and chemotaxis and thus provided an interesting candidate for the developmental and fertility defects that we had previously observed after IFG-1 depletion. As a result of being involved in these processes, *hlh-17* would be an interesting target if detected in future experimental analysis, but our current analysis may indicate that biological variation may result in it having a false positive increased R fold change. Despite the identified increase in polysomal content when normalized to total RNA content in the WT B RNA-seq results, qPCR analysis was not able to confirm increased translational efficiency (Figure 4.13A). Instead the percent representation of *hlh-17* mRNA in each gradient fraction did not change substantially. Thus, we were unable to confirm any change in translational efficiency. This indicates that the increased translational efficiency that we detected by RNA-seq analysis results from low stringency in the RNA-seq analysis rather than true biological variation. Additionally, preliminary results indicate that other mRNAs identified by R fold change as becoming translationally enhanced in WT A, *fbxb-111* and *fezf-1* mRNAs, were also not found to have altered translation when quantified by full gradient polysome resolution (Figure 4.13B-C). We also noted a 1.55 inverse R fold change value, for *gnrr-7* mRNA quantified by RNA-seq

Table E.1. Identified mRNA targets for qPCR follow-up studies.

Gene Name	Gene Description	Mean R Fold Change	Stnd. Dev	p value
hlh-17	Helix-loop-helix (bHLH) transcription factor, essential for larval development, egg-laying, and chemotaxis to potassium and sodium ions	1.62	0.37	0.023
Fbxb-111	Encodes a protein containing an F-box, a motif predicted to mediate protein-protein interactions either with homologs of yeast Skp-1p or with other proteins.	2.02	0.72	0.076
fezf-1	homolog of the human gene ZNF195 (or p57KIP2), mutation leads to Beckwith-Wiedemann syndrome (OMIM:130650).	1.77*	0.44	0.029
Gene Name	**Gene Description**	**Mean Inverted R Fold Change**	**Stnd. Dev**	**p value**
Gnrr-7	Human GoNadotropin- Releasing hormone Receptor (GnRHR) related	1.55	0.30	0.005
Gene Name	**Gene Description**	**Mean Polysomal Fold Change**	**Stnd. Dev**	**p value**
ife-5	Initiation Factor 4E (eIF4E), expressed in the germ line	1.53	0.35	0.069
rpl-39	Large ribosomal subunit L39 protein.	1.57	0.50	0.098
mesp-1	Meiotic Spindle	1.60	0.08	0.056

Table E.1. Identified mRNA targets for qPCR follow-up studies. This table includes the gene products that were identified as targets for increased or decreased translational efficiency as identified by RNA-seq. * indicates *fezf-1* mRNA was identified as a target via both its R fold change and polysomal fold change. Gene descriptions were derived from Wormbase Version WS242 (WormBase, 2014).

and attempted to confirm these results. However, we were unable to confirm decreased translational efficiency of *gnrr-7* mRNA (Figure 4.13D). The translational activity of *gnrr-7* mRNA in WT A was almost identically to *gnrr-7* mRNA in the WT B when determined via full gradient analysis. These data confirm that the indicated increase or decrease in translational efficiency determined by R fold change increases/decreases of RNA-seq analysis was not the result of true biological variation.

ife-5, rpl-39 and mesp-1 mRNAs have little change in translational efficiency quantified by full gradient polysome resolution, despite a predicted increase via polysomal fold change RNA-seq results. We then attempted to confirm increased translational efficiency of other mRNAs of interest that were identified by a significant increased polysomal fold change quantified by RNA-seq. However, the very modest changes in translational efficiency for these mRNA seen by full resolution sucrose gradient qPCR again were inconsistent with substantial changes quantified by RNA-seq. *ife-5* mRNA was predicted to have a 1.53 fold increase in polysomal loading. However, there was no substantial change in polysome loading of *ife-5* mRNA (Figure 4.13E). On the same note, we attempted to confirm the enhanced translation of the large ribosome subunit protein's mRNA, *rpl-39* (WormBase, 2014). *rpl-39* mRNA was translated nearly identically in one of the biological replicates of WT A and WT B when quantified by full gradient qPCR (Figure 4.13F). However, the second biological replicate depicts a slight decrease in translational efficiency, which is contrary to our predictions. This decrease in translational efficiency indicates that *rpl-39* mRNA has a somewhat variable translational activity within the wild type strain. Finally, we assessed the translational efficiency of *mesp-1* mRNA via full

Figure E.13

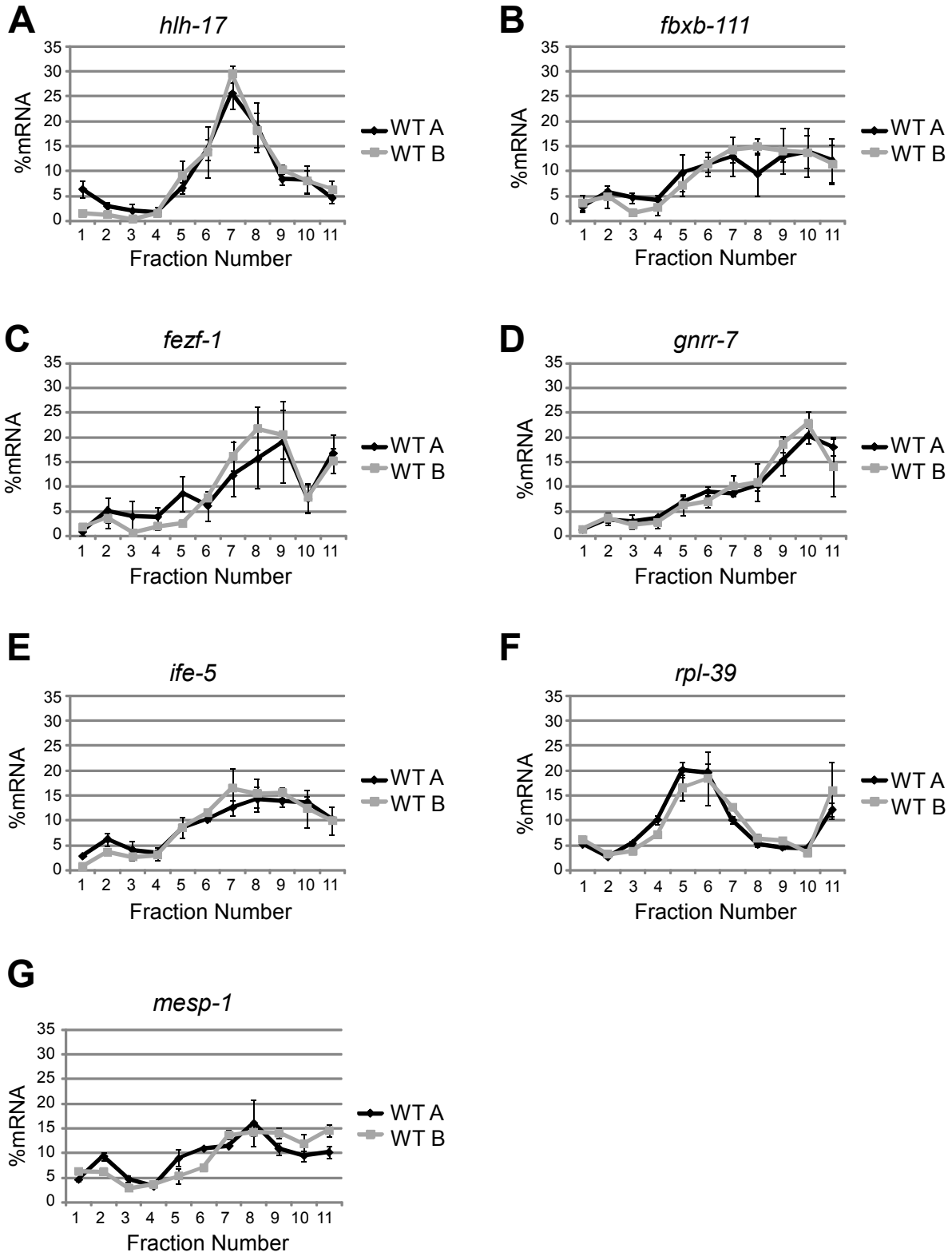
A
hlh-17
B
fbxb-111
C
fezf-1
D
gnrr-7
E
ife-5
F
rpl-39
G
mesp-1
%mRNA
Fraction Number
WT A
WT B
0
5
10
15
20
25
30
35
1 2 3 4 5 6 7 8 9 10 11

Figure E.13. Discrepancies in RNA-seq results and changes in translational efficiency determined by qPCR analysis. (A) *hlh-17* mRNA translational efficiency was determined in WT A and WT B worms. (B) *fbxb-111* mRNA translational efficiency was determined in WT A and WT B worms (this determination is preliminary as a result of primer dimer formation in qPCR reactions). (D) *fezf-1* mRNA translational efficiency was determined in WT A and WT B worms (this determination is preliminary as a result of primer dimer formation in qPCR reactions). (E) *gnrr-7* mRNA translation efficiency was determined in WT A and WT B worms. (A) *ife-5* mRNA translation efficiency was determined in WT A and WT B worms. (B) *rpl-39* mRNA translation efficiency was determined in WT A and WT B worms. (G) *mesp-1* mRNA translation efficiency was determined in WT A and WT B worms. All qPCR data was confirmed in biological duplicates.

gradient qPCR (Figure 4.13G). *mesp-1* mRNA translational efficiency quantified by full gradient qPCR did not change in WT A when compared to WT B in the first biological replicate. However, like *rpl-39, mesp-1* mRNA also displayed a slight decrease in translational efficiency in the second biological replicate contrary to expectations. Once again, these data indicate some biological variability in translational activity of certain mRNAs within the wild type strain. Together these data indicate that the increases in translational efficiency determined via RNA-seq analysis were not due to true biological increases in translation, but rather the result of less stringent statistical analysis deeming them significant changes.

Discussion

In this study we desired to develop a method to analyze global changes in translational efficiency using RNA-seq as a quantification and gene identification tool. In doing so, we developed an analysis tool to interpret organism wide changes in translational efficiency by quantifying and comparing nonpolysomal and polysomal mRNA content in wild type worms. When comparing wild type samples to one another, RNA-seq analysis elucidated a wide variety of targets with increased translational efficiency based on R fold or polysomal fold change. This indicated the need for increased stringency in determining whether or not fold changes were significant and should be followed-up with additional analysis. However, development and optimization of this RNA-seq analysis has resulted in a methodology, which may help to better understand how changes in translational efficiency effect cell fate decisions. Varying cell fate decisions may result during periods in which protein expression patterns change due to increased reliance on the cap-independent

mechanism. For example, during apoptosis and viral infection there is increased reliance on cap-independent translation due to eIF4G cleavage.

As analysis continues with test samples there are several more calculations to note that may require additional optimization. We developed the R fold term to determine changes in polysome content while normalizing to total RNA content in the respective strain. However, this term may not have been the best indicator for changes in translational efficiency. If polysomal content of an mRNA was initially very low and there was a lot of nonpolysomal mRNA, small changes in the quantity of polysomal mRNA are amplified by the R fold change equation. This leads to an increased number aberrant changes in polysome loading that are determined to be significant via our current analysis. Conversely, equivalent changes in the nonpolysomal region, if most of the message is polysomal, are deemed insignficant. The experimental sampling was designed by dividing the nonpolysomal and polysomal regions and excluding the 80S fraction to more readily detect changes in the nonpolysomal region as mRNAs are no longer translated efficiently. Thus, our R fold value should more easily account for changes in the nonpolysomal region. An alternative way to calculate changes in gradient mRNA distribution is to compare a pure ratio of polysomal content to nonpolysomal content. In this way, normalization to total RNA content would not be relevant and changes in the distribution in the gradient could be readily observed. Additionally, thus far the documented changes in translational efficiency that have been previously observed in the *ifg-1::mos* strain are primarily found within the polysomal region. *hsp-3* mRNA, for example, transitions from lighter to heavier polysomes, but might remain relatively constant in the overall pooled polysomal fraction subjected to RNA-seq analysis (Morrison, 2014). These changes would not be observed by RNA-seq

unless samples were subdivided and quantified in each gradient fraction. It may be feasible in the future RNA-seq anlyses, that the gradient could be divided and pooled into nonpolysomal, light polysomes and heavy polysomes. Transitions between the light and heavy polysomes might then be more readily elucidated and we could more likely detect the subtle decreases translational efficiency of messages that we had previously studied such as *hif-1* and *ced-4* mRNA (Morrison, 2014).

Overall, in this study we began to develop and optimize a method for delineation of changes in the translational efficiency of all expressed mRNAs within a living, whole organism, *C. elegans.* The discovery of subsets of highly cap-dependent and independent mRNAs in future studies will help to determine the importance of each mechanism of translation initiation and the processes that are dependent in changing the proportions of these mechanisms. Development of this assay would result in determination of mRNAs that are translated cap-independently allowing for prosurival or proapoptotic fate decisions during apoptosis, heat shock, viral infection or other stressors that result in the induction of cap-independent translation. Additionally, mRNAs required for development, many of which have been observed to translate cap-dependently, may be determined in a natively differentiating cell lineage. Although additional work must be completed to determine the subsets of highly cap-dependent and –independent mRNAs, this study provided the foundation for such determinations.

Procedures to complete RNA-seq analysis of cap-independent translational control in *C. elegans.*

In order to complete additional experiments with the *ifg-1::mos* strain, the methodology used in these experiments must be replicated precisely. The need for precise replication is due to the desire to compare *ifg-1::mos* RNA-seq results to the aforementioned complete analysis of the wild type strain. Thus, here the experimental procedures and analysis steps are carefully delineated for future follow-up experiments and analysis.

Preparation of egg plates for growth and harvesting of worms for RNA-seq experiments. A single OP50 colony was picked and grown up in 90 mL 2XYT broth overnight. The next day, eight to ten egg yolks were isolated into a sterile beaker. The smaller the egg yolks, the more egg yolks that were used. 90 mL of 2XYT broth was heated to 60˚C in a sterile beaker. Egg yolks were then mixed with the preheated 2XYT broth and the mixture was heated to 60˚C for 10 minutes. The mixture was then cooled to 30˚C and the OP50 culture was added. The OP50 culture egg mixture was then incubated at 37˚C for 60 minutes. 5 mL of egg bacteria mixture was added per 10 cm 5X Peptone plate. The 5X Peptone plates had been pre-dried at 37˚C for a couple of hours. The plates were then incubated for 1-2 nights at 37˚C with their lids cracked. Once the egg mixture had dried, but before the 5X Peptone plates were cracked, the plates were removed from the 37˚C incubator and were stored at 4˚C until they were used for growth and harvesting experiments. Egg plates were never stored for more than 1 month before use.

Growth and harvesting of worms for RNA-seq experiments. Wild type (MD701) and *ifg-1::mos* (KX54) strains were grown on NGM plates with OP50 until the plates were almost starved. One plate of wild type worms and 3-5 plates of *ifg-1::mos* worms were

transferred to their respective egg plates (1 each) on the same day. These worms were grown on egg plates for about one week, no long than two weeks, until the egg plate was covered with the respective strains. The egg plates had a monolayer of worms, but these worms were not close to being starved (a lot of egg remained). The worms were then washed off their respective egg plates, washed three times with M9 and transferred to a fresh egg plate before temperature shifting the worms to 25˚C for 24 hours. If a large number of worms were washed off the initial plate and there was fear of starvation on a second plate then the worms were divided into 2 egg plates for the final incubation period.

After the 24 hour incubation at 25˚C, worms were washed from egg plates using M9 and washed an additional 2-3 times in order to remove the majority of egg that was washed off the egg plates with the worms. After the final wash, worms were resuspended in 10 mL of M9 solution with 0.1% tween 20. These worms were then transferred to an empty 10 cm plate and were perturbed on the shaker at 125 rpm for 1 hour. Perturbation allowed the worms to clear their digestive tract of additional egg and OP50 bacteria. After 1 hour the worms were collected and the 10 cm plate was washed with an additional 5 mL of M9 to collect the remaining worms. Worms were then washed once with M9 before being resuspended in an equal volume of 70% sucrose and sterol water (7 mL of each). Worms were then spun down for at least 5 minutes at high speed. Floating worms were removed from the top of the sucrose and water mix. M9 solution with 0.1% tween was additionally used to carefully perturb worms from the sides of the 15 mL conical used for floating. These worms were also collected for additional washes and freeze down.

The collected worms were then washed one time with M9. After the M9 wash the supernatant was removed and the packed worms were resuspended in an equal volume of

sterol water with 1% vanadyl RNC. Worms were then dropped into liquid nitrogen using a 2 mL disposable pipet for freezing. The resulting worm pellets were stored at -80˚C. Worm pellets were not stored more than 6 months because after a 6 month time period we started to observe changes in the polysome profiles from worm lysates using these pellets. After freeze down a single worm pellet should be used for PCR analysis using primers to guarantee the proper genotyping of the frozen down strains. Additionally, during the pelleting process one worm pellet was not dripped into liquid nitrogen, but was instead dripped onto an OP50 plate. These worms were then washed off the OP50 plates and were resuspended in M9 with 1 mM levamisole to immobilize the worms. The worms were used for microscopy to note the extent of apoptosis in the gonad and to guarantee that gonad morphology was not too compromised. Vast changes in gonad morphology are correlated with a decreased polysomal message content being observed during sucrose gradient fractionation.

Preparation of gradients for sucrose gradient fractionation. Gradeints were prepared as previously described (Dinkova et al., 2005). A 45% sucrose in 1X Gradient Buffer was prepared using 15.75 g sucrose, 7 mL 5X Gradient Buffer (1.5 M KCl, 250 mM HEPES, 10 mM $MgCl_2$; pHed to 8.0 with KOH) and 35 µL 1M DTT. The resulting solution was brought up to a total volume of 35 mL with DEPC-treated water (Dinkova et al., 2005). A second 10% sucrose solution in 1X gradient buffer was then made by combining 3.5 g sucrose, 7 mL 5X Gradient Buffer, 35 µL 1M DTT and enough DEPC-treated water to bring the final solution volume to 35 mL (Dinkova et al., 2005). If six gradients were made the above reaction mixes of 45% and 10% sucrose were doubled. Both sucrose solutions were

equilibrated on ice. SW-41 tubes were added to the Seton rotating gradient maker rack and the tubes were marked with a sharpie to indicate a volume of 5 mL. 6 mL of 10% sucrose solution was added to each SW-41 tube. A syringe and needle was then used to add 5 mL (to the pre-marked sharkie line) of 45% sucrose solution to the bottom of the tube containing the 10% sucrose solution. A cap was carefully added to each SW-41 tube being careful not to disturb the sucrose solutions and making sure that no bubbles are left within the SW-41 tube. The seton gradient maker was then run for 4.06 minutes, with an angle of 80˚C and a speed of 8. The resulting gradients were then stored at 4˚C overnight.

Worm lysate preparation and sucrose gradient fractionation. Worm lysates were prepared as previously described (Dinkova et al., 2005). 4 mL of lysis buffer (for 6 samples) was made fresh on the day of fractionation by combining 800 µL 5X Lysis Buffer Stock (250 mM Tris HCl (pH 8.0), 1500 mM NaCl, 50 mM $MgCl_2$, 5 mM EGTA), 20 µL 50 mg/mL heparin, 80 µL 40,000 U/mL RNasin, 80 µL 200 mM Vanadyl RNC, 80 µL 250 mM PMSF, 162 µL 9.8 mg/mL cycloheximide (made fresh), 8 µL DTT and 400 µL 10% Triton X, and bringing the solution to a total volume of 4 mL with DEPC-treated water (Dinkova et al., 2005). The Beckman centrifuge and SW-41 rotor were pre-chilled to 4˚C. 8 worm pellets were then ground, using a mortar and pestle, in 2 drops of lysis buffer per pellet ground and liquid nitrogen. Once the pellets were thoroughly homogenized and ground into a find powder, the powder was transferred to a 50 mL canonical tube and placed on ice. The powder was then allowed to melt slowly with additional, occasional, gentle warming using body heat. When the lysate was fully melted, the 50 mL conical tube was quickly centrifuged and the lysate was removed into a 1.7 mL microcentrifuge tube. The

microcentrifuge tubes were then spun at 10,000 rpm and 4˚C for 15 minutes. Supernatant was then removed from each microcentrifuge tube, being sure to avoid the lipid layer floating at the surface of the lysate. Lysates were transferred to a clean microcentrifuge tube while gradients were removed from 4˚C storage and prepared for lysate overlay. Caps were removed from SW-41 sucrose gradients and 0.5 mL of sucrose was removed off the top of the gradients using a pipet. Lysates were then carefully overlayed on their individual gradients. Additional lysis buffer was added to samples if it was necessary to balance gradient samples for centrifugation.

Gradients were then centrifuged under vacuum for 1 hour and 45 minutes at 38,000 rpm and 4˚C. Additionally, deceleration was set to zero to prevent perturbation of the gradients after centrifugation. Sucrose gradient fractionation was performed as detailed previously (Henderson et al., 2009). Sucrose gradient fractionation was performed on an Isco Density Fractionation System collecting 1 mL fractions. The Isco Fractionation System was set with the following perimeters in Program 1: type= simple, rack type= micro tubes, last tube= 12, fractionation= by time, Time= 1 minute. The pump speed was set to 40. UV absorbance was monitored using a sensitivity of 1.0 and a chart speed of 150. Sucrose gradient fractions were divided into 2 500 µL aliquots and stored at -80˚C.

RNA extraction from gradient fractions. . RNA isolation was performed as detailed previously with the exception that gradient fractions were isolated in 4 volumes Trizol. (Henderson et al., 2009). 500 µL frozen gradient fractions were defrosted on ice and then divided into 250 µL aliquots. 1 mL of TRIzol was added to each aliquot and the samples were incubated at room temperature for 5 minutes. 200 µL of chloroform was then added

to each sample. The samples were then shacked vigorously for 15 seconds and were incubated at room temperature for 2 minutes. The samples were centrifuged at 12K, 4˚C for 15 minutes. The aqueous layer was removed and precipitated in 1 mL isopropyl alcohol for 10 minutes at room temperature. After precipitation, the samples were centrifuged for 10 minutes at 12K and 4˚C. The isopropyl alcohol supernatant was removed and discarded. The RNA pellet was then washed with 70% ethanol (in DEPC-treated water). The pellet was then centrifuged for an additional 5 minutes at 7.5K and 4˚C. The supernatant was once again discarded first using a 200 µL pipet and then using a gel loading pipet. The pellet was then dried in the speed vacuum for 2 minutes without heat and excess liquid was removed with a gel loading pipet. The pellet was then resuspended in 100 µL of DEPC-treated water. All like pellets (all 4 aliquots) were then recombined results in 400 µL of RNA sample per gradient fraction. 20 µg of glycogen was then added to each gradient fraction. The samples were then phenol:chloroform extracted one time, followed by 3 chloroform:isoamyl alcohol extractions. The RNA was then precipitated in 1 mL ethanol and 20 µL sodium acetate overnight at 4˚C. The next morning, the RNA samples were centrifuged at 10K and 4˚C for 20 minutes. The pellets were then washed with 70% ethanol (in DEPC-treated water). Excess liquid was removed using a gel loading pipet tip and the samples were dried in the speed vacuum for 2 minutes. Once again, any additional ethanol was removed using a gel loading pipet. The pellets were then resuspended in 30 µL of DEPC-treated water for RNA-seq experiments or 10 µL of DEPC-treated water for qPCR follow-up experiments and the concentration was quantified using the nanodrop.

Preparation of samples for RNA-seq analysis. For RNA-seq experiments an additional three chloroform extractions were performed for a final clean-up of the pooled fractions. Fractions 1-2 (25 μL of each) were then combined into a nonpolysomal fraction and fractions 4-11 (25 μL of each) were combined to form a polysomal fraction. The pooled fractions were diluted to a total volume of 400 μL. The additional chloroform extractions were then performed on these pooled fractions. The pooled fractions were then ethanol precipitated and resuspended in 30 μL of DEPC-treated water. The pooled fractions were then nanodropped to determine their concentrations and were diluted to 0.1 μg/μL (see excel spreadsheet: RNA fraction quantifications 03-13-14.xls for sample calculation). 20 μL of sample were submitted to Beckman Coulter in a 96 well plate for RNA-seq analysis.

RNA-seq amplification and quantification was performed by Beckman. Cufflinks software was then used to assign reads into transcripts and to estimate the abundance of these transcripts. The transcripts were then matched back to the *C. elegans* transcriptome (Wormbase version: WS240). The outcomes of these experiments were measurements of transcript abundances in fragments per kilobase of exon per million fragments (FPKM) (Mortazavi et al., 2008).

RNA-seq analysis using excel spreadsheets. Spread sheets designed for gene analysis and isoform analysis are called "RNAseq gene analysis cull 1 w deleted empty columns 06-03-14" and "RNAseq data calc-1 06-03-14.xlsx" respectively. The calculations performed in the spreadsheets are identical. The only differences in spreadsheets values are the additional columns denoting length and coverage of isoforms. Columns denoting coverage (for isoform output only), FPKM, FPKM hi confidence intervals, FPKM low

confidence intervals and FPKM status were copied in pasted into this master spreadsheet from each cufflinks data output sheet from Beckman Coulter RNA-seq experiments. All data was sorted by tracking id prior to copying and pasting to preserve gene or isoform order for comparisons. The data was input in a specific order: *ifg-1::mos* polysomal #1, *ifg-1::mos* nonpolysomal #1, wild type polysomal #1, wild type nonpolysomal #1, *ifg-1::mos* polysomal #2, *ifg-1::mos* nonpolysomal #2, wild type polysomal #2, wild type nonpolysomal #2, *ifg-1::mos* polysomal #3, *ifg-1::mos* nonpolysomal #3, wild type polysomal #3 and wild type nonpolysomal #3. After each data set of paired *ifg-1::mos* and wild type polysomal and nonpolysomal values, intermediate calculations were performed. First, wild type total RNA quantity was calculated by adding the FPKM values of wild type nonpolysomal and polysomal for the individual biological replicate (Figure E.4). Next, Rw was calculated (Figure E.4) by dividing the wild type polysomal FPKM value by the wild type total FPKM quantity. However, if the wild type total value (Tw) was equal to 0 then Rw was defined as not applicable. *ifg-1::mos* total (Ti) and Ri were then calculated similarly using the *ifg-1::mos* FPKM values. Once again, if *ifg-1::mos* total (Ti) was equal to 0, Ri was defined as not applicable. R fold change was then calculated by dividing Ri by Rw (Figure E.4). However, if the sum of Tw and Ti was equal to 0, this value was defined as not applicable. Similarly, inverted R fold change was calculated by dividing Rw by Ri. Similarly, if the sum of Tw and Ti was equal to 0 then the inverted R fold change was defined as not applicable. Total fold change was then calculated by dividing Ti by Tw. If the sum of Tw and Ti was equal to 0 this value was defined as not applicable. The inverse total fold change was calculated by dividing Tw by Ti and once again the value was defined as not applicable if the sum of Tw and Ti was equal to 0. Finally for each biological replicate the polysomal fold

change and inverse polysome fold change was calculated. Polysomal fold change was calculated by dividing *ifg-1::mos* polysomal FPKM by wild type polysomal FPKM. If the sum of the polysomal FPKM values was equal to 0 this value was defined as not applicable. The inverse polysomal fold change was calculated by dividing wild type polysomal FPKM by *ifg-1::mos* polysomal FPKM. Once again, if the sum of polysomal FPKM values was equal to 0 the polysomal fold change was defined as not applicable. These calculations were performed for each biological replicate. If, however, future RNA-seq experiments are performed with *ifg-1::mos* samples and compared to the wild type samples in this experiment then these calculations should not be carried out on each biological replicate. These calculations are only valid when comparing matched biological replicates. The calculations should be carried out using all biological replicates at once instead of determining the average fold changes based on individual biological replicates. Thus instead of calculating individual R fold values for each biological replicate one R fold value would be calculated (R fold change=[Ri(1)+Ri(2)+Ri(3)]/[Rw(1)+Rw(2)+Rw(3)]).

The mean R fold change, inverted R fold change, total fold change, inverted total fold change, polysomal fold change and inverted polysomal fold change and their standard deviations were then calculated using the three biological replicates. The difference between the mean and standard deviation as well as the percent of standard deviation of the mean was also calculated for each fold change. The percent standard deviation of the mean is equivalent to the standard deviation divided by the mean. A column was then added to the spreadsheet to denote if any of the biological replicates of wild type or *ifg-1::mos* had an FPKM value denoted as lowdata. The next three columns in the spreadsheet denote whether or not an FPKM value was recorded for the nonpolysomal or polysomal

region of wild type or *ifg-1::mos* samples for a particular biological replicate (1-3). The presence of at least one FPKM value was indicated by DATA and NO DATA denoted the absence of an FPKM value for all samples in the biological replicate. These values were then translated into numerical values where 1 indicates the presence of data and 0 indicates its absence. These values were then added and the sum was recorded in the No Data Total column. Thus, a value of 3 in the no data column would indicate that at least 1 FPKM value was recorded in each pair of biological replicates, whereas a 0 value would indicate no recorded FPKM values for the gene or isoform of interest. We then determined if the mean fold change and inverted mean fold change minus their respective standard deviations was greater than 1. This was used as an indicator of whether the fold change was actually an increase or decrease when considering its standard deviation. The next column on the spreadsheet was used to indicate genes or isoforms that were not present and thus had 0 FPKM values for nonpolysomal or polysomal samples in both the wild type and *ifg-1::mos* worms in all biological replicates. Therefore, if the sum of all FPKM values was equal to 0 then the value in this column was 0. If the FPKM value of any of the samples was greater than 0 then the value in this column was equal to 1. For culling zero values, the column can be sorted to group gene/isoforms with 0 or greater than 0 total summed FPKM values.

The three R fold changes from the 3 biological replicates then appear on the spreadsheet once again. The column that follows these R fold changes indicates the ascension order of the R fold change values. The ascension order must be determined in order to determine if there are any high or low outlier R fold changes within the three biological replicates. The ascension order where biological replicate 1>2>3 was recorded as 1; 1>3>2 was recorded as 2; 2>1>3 was recorded as 3; 2>3>1 was recorded as 4; 3>1>2

was recorded as 5; 3>2>1 was recorded as 6. A Q test was then used to determine outliers. To determine the experimental Q value for high outliers the difference between the largest R fold change and its next closest R fold change were divided by the range of the R fold change values. For example, if the ascension order was 1>2>3 then the Q experimental value to determine high outliers would be (R fold change #1 – R fold change #2)/(R fold change #1 – R fold change #3). If Q experimental is greater then Q critical, which is equal to 0.97 for a 95% confidence interval, then the largest biological replicate R fold change value would be considered a high outlier. Similarly a Q experimental value was used to determine low outliers. If Q experimental was greater than Q critical (0.97) then the biological replicate with the smallest R fold change value was determined to be a low outlier. High outliers and low outliers may be therefore taken into consideration when analyzing the data and decisions may be made as to whether to include or exclude the biological replicate outlier from further analysis.

The spreadsheet then contains columns with the aforementioned Rw and Ri values for each biological replicate. These values are duplicated in order to determine p values to indicate whether there is a significant difference between wild type and *ifg-1::mos* R values (Rw vs. Ri). Of note, Rw 1 and Ri 1 appear twice; once before biological replicate 2 and once after biological replicate 3. This duplication is required for the grouping of values to ensure proper p value calculations using excel. A two tailed unpaired t test with unequal variance was then performed using excel to compare Rw and Ri values and determine when there was a significant difference between the two. The same duplication of values and t test calculations were performed for Tw and Ti, and Pw and Pi.

The next column indicates whether all biological replicates had at least 1 recorded FPKM value for wild type or *ifg-1::mos.* "All Pass" indicates that all biological replicates have at least 1 recorded FPKM value in the nonpolysomal or polysomal region of wild type or *ifg-1::mos* strains. "Rep 1" indicates that biological replicate 1 had no recorded FPKM values. "Rep 2" indicates that biological replicate 2 had no recorded FPKM values. "Rep 3" indicates that biological replicate 3 had no recorded FPKM values. Finally, "no data" indicates that more than 1 biological replicate lacked a single recorded FPKM value. Mean R fold change, inverted R fold change, total fold change, inverted total fold change, polysomal fold change, inverted polysomal fold change and their standard deviations were then determined excluding the biological in which there were no recorded FPKM values. However, in light of the current control analysis, I would suggest these calculations are no longer applicable. The control experiments delineated in this appendix indicate that low FPKM values should be excluded from further analysis. Therefore, when one or more of the biological replicates does not have a recorded FPKM value in the nonpolysomal or polysomal samples of wild type or *ifg-1::mos* worms, the target gene or isoform should be excluded from further analysis.

Preparation of cDNA for qPCR follow-up experiments and qPCR analysis. 0.25 μg of RNA from each fraction was synthesized into cDNA using Verso cDNA Synthesis Kit (Thermo Scientific) for RNA-seq follow-up. As a result of only using 0.25 μg of RNA, the reaction mix used was ¼ of the manufacturer's protocol's recommended volumes resulting in the total volume of the reaction mix being 5 μL. Thus per reaction a reaction mix 1 μL of 5X cDNA synthesis buffer, 0.5 μL of dNTP mix, 0.25 μL of RNA primer (50:50 mix of

Anchored Oligo-dT and random hexamers) and 0.25 μL of Verso enzyme mix was combined. The reaction mix was made in bulk for all gradient fractions, so 2 μL of this resulting reaction mix was added to each gradient fraction 0.25 μg RNA aliquot. The final volume was brought up to 5 μL. After cDNA synthesis the total volume of cDNA was diluted to 50 μL. Real-time PCR was performed in triplicates using SsoFast EvaGreen Supermix, for RNA-seq follow-up experiments, in an iCycler iQ5 Real-time PCR machine according the manufacture's protocol. Per reaction (25 μL total volume) 12.5 μL of SsoFast EvaGreen supermix was combined with 1 μL of the primer set (10 μM), 1 μL of cDNA preparation and 10.5 μL of nuclease-free water. Each qPCR plate was run with a standard curve run in duplicates for the primer set used on the plate. 10 ng, 3.3 ng, 1.1 ng, 0.37 ng, 0.123 ng and 0 ng total cDNA quantities were used to develop the standard curve. iCycler iQ5 software was used to calculate the standard curve. The resulting output equation is Ct=m*log(starting quantity)+b. Arbitrary target mRNA mass was determined in each gradient fraction by using a standard curve derived from total cDNA and using the fraction specific Ct values (spreadsheet gpd-3 qPCR.xls shows an example calculation). Thus, each fraction's arbitrary mass was calculated by using the equation "starting quantity"=10^[(Ct-b)/m] where m and b values are defined using the standard curve. The percentage of the total arbitrary mass was then determined within each gradient fraction by dividing the arbitrary mass within a particular fraction by the sum of all arbitrary masses across the gradient and multiplying it by 100.